

Copyright is owned by the Author of the thesis. Permission is given for a copy to be downloaded by an individual for the purpose of research and private study only. The thesis may not be reproduced elsewhere without the permission of the Author.

# Predicting horse limb responses to surface variations with a 3D musculoskeletal model

A thesis presented in partial fulfilment of the requirements for the degree of

**Doctor of Philosophy**

**In**

**Biomechanics**

At Massey University, Manawatu,

New Zealand

**Aliénor Bardin**

**2020**

## Abstract

Thoroughbred racehorses are often affected by musculoskeletal injuries, leading to involuntary rest periods, early retirement or death. A number of studies have focused on identifying risk factors. A major focus of research has been track surface properties because it should be possible to modify these so that the risk of musculoskeletal injury is minimised. Among all the track surface properties studied to date, consistency of the surface is reported to be one of the main injury risk factors.

The aim of this study was to develop a preliminary 3D musculoskeletal model of the whole equine forelimb based on data published in the literature and derived from anatomical measurements; and to determine the effects of the perturbations by the ground surface on the limb response with the musculoskeletal model developed and to assess whether the response occurs acutely in the perturbed stance phase or in the next stance phase.

To answer these questions, gait data were collected from ridden Thoroughbreds passing through a perturbation area, where the surface hardness was changed by adding wood or foam under the baseline sand surface.

The horses changed their joint flexion/extension patterns in response to changes in hardness. In response to the hard perturbation, the proximal limb spring was more compliant, evidenced by increased shoulder flexion. The elbow and carpal joints were more flexed in the intervening swing phase. In response to the soft perturbation, more coffin joint flexion was observed during both the perturbed and the following stance phase.

The preliminary musculoskeletal model of the equine forelimb developed in this thesis allow the observation and study of the forelimb reaction to hardness perturbation through the joint excursions and tendon and ligament strains.

## Acknowledgements

First, I would like to thank Dr Bob Colborne, my main supervisor, for everything he did for me; for offering me the PhD position, for helping me with all the administrative tasks on my arrival in New Zealand, for helping me to find an accommodation, for teaching me the locomotion system of horses, for helping me to collect data, and for reading and correcting all I wrote.

Thanks to Dr Chris Rogers, who helped me with writing, introduced me to other scientists at the ICEEP 2018 conference and allowed me to discover the NZ yearling parade.

Thanks to my other two PhD committee members, Luca Panizzi, who gave good advice on my writing and to Dr Liqiong Tang, for her practical advice.

I would like to express all my gratitude for the funding of this project and my PhD scholarship to the New Zealand Equine Trust. The Massey University Foundation and the Ron Kilgour Memorial Trust provided funding for my participation in the ICEEP 2018 conference in Australia.

Many thanks to all the riders, horses and their owners who participated in the study and without whom it would not have been possible to run this study.

I am grateful to all those who helped to collect data. Julie Huat and Astrid Meuly helped with the Thoroughbred limb dissection, Kylie Legg tested the ligament properties reported in the Appendix and Nila Taylor worked with us on an Equine Trust Summer Scholarship collecting and processing gait data. Finally, many thanks to my family, friends and acquaintances who supported me.

## Table of contents

Abstract.....	i
Acknowledgements .....	ii
Table of contents.....	iii
List of figures .....	viii
List of tables .....	xiii
List of abbreviations .....	xvi
<b>Chapter 1 Introduction and literature review .....</b>	<b>1</b>
I. Introduction.....	1
II. Context.....	2
II.A. Racing industry.....	2
II.B. Injuries in horse races.....	2
II.C. Modelling in biomechanics.....	5
III. Hoof-track interaction .....	7
III.A. Risk factors.....	7
III.B. Surface properties.....	7
III.B.1. Impactors .....	8
III.B.2. Force plates and hoof-mounted devices .....	10
III.B.3. Comparison of surface properties .....	12
III.B.4. Best properties? .....	16
IV. Equine modelling .....	19
IV.A. The spring model.....	19
IV.B. Musculoskeletal model.....	23
IV.B.1. The different approaches.....	23
IV.B.2. Reasons .....	23
IV.B.3. Equine musculoskeletal models .....	25
IV.B.4. Modelling challenges.....	27

V.	Conclusion.....	27
VI.	References.....	29
<b>PART 1 CREATING THE MUSCULOSKELETAL MODEL .....</b>		<b>40</b>
<b>Chapter 2 Collecting Ligament and tendon properties.....</b>		<b>41</b>
I.	Introduction.....	41
II.	Segment properties .....	41
III.	Muscle-tendon properties.....	42
III.A.	Muscle-tendon properties required for modelling .....	42
III.B.	Muscle-tendon data .....	43
IV.	Ligament properties.....	46
V.	Conclusion and discussion.....	48
VI.	References.....	50
<b>Chapter 3 Development of the musculoskeletal model .....</b>		<b>51</b>
I.	Introduction.....	51
II.	Materials and methods.....	51
II.A.	Limb components.....	51
II.B.	The Anybody Modeling System™ .....	53
III.	Development of the model .....	54
III.A.	Segments and initial positions .....	54
III.B.	Joints, markers and kinematics.....	56
III.C.	Scaling functions .....	57
III.D.	Changing the segment definitions .....	61
III.E.	Kinetic study.....	62
III.F.	Final version.....	64
IV.	Conclusion & Discussion.....	65
V.	References.....	67
<b>Chapter 4 Testing the preliminary model with gait data .....</b>		<b>69</b>

## Predicting horse limb responses to surface variations

I.	Introduction.....	69
II.	Method & Material .....	69
II.A.	Experimental setup .....	69
II.B.	Markers.....	70
III.	Results .....	71
III.A.	Kinematic files.....	72
III.A.1.	Trot files .....	72
III.A.2.	Right lead canter files .....	72
III.A.3.	Left lead canter files .....	73
III.B.	Sagittal plane joint movements .....	73
III.B.1.	Coffin joint excursion.....	74
III.B.2.	Fetlock joint excursion .....	75
III.B.3.	Carpal joint excursion .....	78
III.B.4.	Elbow joint excursion.....	80
III.B.5.	Shoulder joint excursion .....	83
III.C.	Tendon and ligament strains .....	84
IV.	Conclusion & Discussion.....	85
V.	References.....	89

## **PART 2 STUDY OF THE HORSE LIMB RESPONSE TO GROUND HARDNESS**

### **PERTURBATION ..... 90**

#### **Chapter 5 Gait data collection with perturbations ..... 91**

I.	Introduction.....	91
II.	Material & Method .....	91
II.A.	Experimental set-up .....	91
II.B.	Perturbation pit.....	92
II.C.	Horses.....	92
II.D.	Qualisys software .....	94

III.	Results .....	96
III.A.	Trot files.....	96
III.B.	Canter files.....	98
IV.	Discussion & Conclusion.....	99
V.	References.....	102
<b>Chapter 6 Limb response to perturbations.....</b>		<b>103</b>
I.	Introduction.....	103
II.	Material & Methods.....	103
III.	Results .....	104
III.A.	Statistical results of the joint excursions .....	104
III.A.1.	Coffin joint: sagittal angle .....	104
III.A.2.	Fetlock joint: sagittal angle .....	110
III.A.3.	Carpal joint: sagittal angle.....	114
III.A.4.	Elbow joint: sagittal angle .....	118
III.A.5.	Shoulder joint: sagittal angle.....	122
III.B.	Statistical results of the ligament and tendon strains.....	127
III.B.1.	Ligament and tendon strains during stance at trot.....	128
III.B.2.	Ligament and tendon strains during stance at canter.....	129
IV.	Summary of joint excursions and soft tissue strains.....	131
V.	Conclusion.....	133
V.A.	Response to perturbations at trot .....	134
V.B.	Response to perturbations at right lead canter.....	135
VI.	Discussion .....	136
VII.	References.....	139
<b>Chapter 7 Conclusions .....</b>		<b>140</b>
I.	Introduction.....	140
II.	Effect of the perturbation .....	140

## Predicting horse limb responses to surface variations

II.A.	Statistical model.....	140
II.B.	Responses to perturbations.....	141
II.C.	Comparison to literature .....	144
III.	Musculoskeletal model .....	145
III.A.	Segments .....	145
III.B.	Ligament and muscle-tendon units.....	145
III.C.	Joints.....	146
III.D.	Scaling.....	147
III.E.	Model validation .....	147
IV.	Conclusion .....	148
IV.A.	Hardness perturbation in racetrack .....	148
IV.B.	Improving the musculoskeletal model .....	149
V.	References.....	151
<b>Appendix: Ligament, muscle and tendon properties .....</b>		<b>153</b>
I.	Ligament properties.....	153
II.	Muscle-tendon data.....	154
II.A.	Muscle-tendon properties.....	154
II.B.	Muscle-tendon origin and insertion sites.....	155
II.B.1.	Lateral digital extensor (LDE) .....	155
II.B.2.	Common digital extensor (CDE) .....	155
II.B.3.	Extensor carpi obliquus (ECO).....	156
II.B.4.	Extensor carpi radialis (ECR).....	157
II.B.5.	Ulnaris lateralis (UL).....	158
II.B.6.	Flexor carpi radialis (FCR).....	159
II.B.7.	Flexor carpi ulnaris (FCU).....	160
II.B.8.	Deep digital flexor (DDF).....	161
II.B.9.	Superficial digital flexor (SDF) .....	161

## List of figures

Figure 1 Distribution of the reported events with number of cases (Perkins et al., 2004b) (MSI = Musculoskeletal Injuries).....	3
Figure 2 CT derived image of the Scapula segment with its local reference frame on the estimated centre of mass. Lateral view on the left, cranial view on the right.....	55
Figure 3 Position of markers (green points) and antebrachiocarpal joint point (red point) on the antebrachium segment. Lateral (on the left) and cranial (on the right) views of the radius-ulna 3D image. All three points are superimposed on the lateral view.....	56
Figure 4 Dorsal (A), ventro-caudal (B) and medial (C) views of the elbow with the brachium and antebrachium scaled with the first scaling function. ....	58
Figure 5 Lateral (A) and dorso-caudal (B) views of the distal phalanx scaled by the second scaling function.....	58
Figure 6 Dorsal (A), ventro-caudal (B) and medial (C) views of the elbow and lateral (D) and dorso-caudal (E) views of the distal phalanx with all segments scaled by the third scaling function..	59
Figure 7 Problem of joint geometry due to scaling. Medial views of the elbow of the CT-scanned bones (on the left) and of the scaled segments (on the right) .....	60
Figure 8 Medial view of the elbow with the segments and joint geometries scaled by the final scaling function.....	61
Figure 9 Lateral (on the left) and cranial (on the right) of the distal phalanx with the contact points (red points) .....	63
Figure 10 Diagram of the model .....	64
Figure 11 Picture of the camera set-up used to collect gait data (on top) and diagram of the camera set-up (on bottom). The horse forelimb was aimed to land in the “forelimb landing zone” represented on the diagram, which match the zone just after the poles on the ground.....	70
Figure 12 Picture of a horse equipped with the whole set of markers used to collect the Initialization data.....	71
Figure 13 Example of coffin angles. Joint angle is defined as the angle between the long axis of the metacarpus segment and the long axis of the pastern segment, as indicated. The positive sign corresponds to a flexed position and the negative sign to an extended position. ....	74
Figure 14 Right forelimb coffin joint excursions at trot (A), right lead canter (B) and left lead canter (C). The graphs present the average and standard deviation computed from all the gait data files (n=53 files for trot, n=23 for right lead canter and n=21 files for left lead canter). The data were time-normalized from -1 to 0 as stance phase and from 0 to 1 as swing phase.....	74

Figure 15 Example of fetlock angles. Joint angle is defined as the angle between the long axis of the metacarpus segment and the long axis of the pastern segment, as indicated. The positive sign corresponds to a flexed position and the negative sign to an extended position. .... 75

Figure 16 Right forelimb fetlock joint excursions at trot (A), right lead canter (B) and left lead canter (C). The graphs present the average and standard deviation computed from all the gait data files (n=53 files for trot, n=23 for right lead canter and n=21 files for left lead canter). The data were time-normalized from -1 to 0 as stance phase and from 0 to 1 as swing phase..... 76

Figure 17 Example of carpal angles. Joint angle is defined as the angle between the long axis of the antebrachium segment and the long axis of the metacarpus segment, as indicated. The positive sign corresponds to a flexed position..... 78

Figure 18 Right forelimb carpal joint excursions at trot (A), right lead canter (B) and left lead canter (C). The graphs present the average and standard deviation computed from all the gait data files (n=53 files for trot, n=23 for right lead canter and n=21 files for left lead canter). The data were time-normalized from -1 to 0 as stance phase and from 0 to 1 as swing phase..... 78

Figure 19 Example of elbow joint angles. Joint angle is defined as the angle between the long axis of the brachium segment and the long axis of the antebrachium segment, as indicated. The positive sign corresponds to a flexed position..... 80

Figure 20 Right forelimb elbow joint excursions at trot (A), right lead canter (B) and left lead canter (C). The graphs present the average and standard deviation computed from all the gait data files (n=53 files for trot, n=23 for right lead canter and n=21 files for left lead canter). The data were time-normalized from -1 to 0 as stance phase and from 0 to 1 as swing phase..... 81

Figure 21 Example of shoulder joint angles. Joint angle is defined as the angle between the long axis of the scapula segment and the long axis of the brachium segment, as indicated. The positive sign corresponds to a flexed position..... 83

Figure 22 Right forelimb shoulder joint excursions at trot (A), right lead canter (B) and left lead canter (C). The graphs present the average and standard deviation computed from all the gait data files (n=53 files for trot, n=23 for right lead canter and n=21 files for left lead canter). The data were time-normalized from -1 to 0 as stance phase and from 0 to 1 as swing phase. .... 83

Figure 23 Diagram illustrating the filling of the perturbation pit to create the perturbation. The hole is filled with 12cm of wood and covered with 6cm of sand for the baseline (on the left); with 5cm of sand in the bottom and 12cm of wood and covered with 1cm of sand for the hard perturbation (in the middle); and with 12cm of wood covered with 5cm of foam and 1cm of sand for the soft perturbation (on the right). .... 92

## Predicting horse limb responses to surface variations

Figure 24 Horse forelimb equipped with the segmental and joint markers to collect the Initialization file. Cranio-lateral view (on the left) and lateral view (in the middle) of the whole forelimb and cranio-lateral view of the distal forelimb (from carpus to hoof) on the right .....	93
Figure 25 Snapshot of the marker positions on the whole forelimb at the beginning of the stance phase for a trial at trot with Qualisys Track Manager software .....	94
Figure 26 Example of trajectory with gaps to fill (on the left) and zoom on one gap being filled (on the right) using the Qualisys interface .....	95
Figure 27 Coffin joint excursion at trot over the baseline (BL, on top), over the hard perturbation (HP, in the middle) and over the soft perturbation (SP, on bottom). The curves represent the averages (plain lines) and the standard error of mean (dotted lines) of the coffin joint excursion at trot computed for all the files (n=32 files for BL; n=27 files for HP and n=24 files for SP). Time was normalized from -1 to 0 as the perturbed stance phase, from 0 to 1 as the swing phase and from 1 to 2 as the second stance phase. ....	105
Figure 28 Coffin joint excursion at right lead canter over the baseline (BL, on top), over the hard perturbation (HP, in the middle) and over the soft perturbation (SP, on bottom). The curves represent the averages (plain lines) and the standard error of mean (dotted lines) of the coffin joint excursion at canter computed for all the files (n=24 files for BL; n=28 files for HP and n=24 files for SP). Time was normalized from -1 to 0 as the perturbed stance phase, from 0 to 1 as the swing phase and from 1 to 2 as the second stance phase. ....	108
Figure 29 Fetlock joint excursion at trot over the baseline (BL, on top), over the hard perturbation (HP, in the middle) and over the soft perturbation (SP, on bottom). The curves represent the averages (plain lines) and the standard error of mean (dotted lines) of the fetlock joint excursion at trot computed for all the files (n=32 files for BL; n=27 files for HP and n=24 files for SP). Time was normalized from -1 to 0 as the perturbed stance phase, from 0 to 1 as the swing phase and from 1 to 2 as the second stance phase. ....	111
Figure 30 Fetlock joint excursion at right lead canter over the baseline (BL, on top), over the hard perturbation (HP, in the middle) and over the soft perturbation (SP, on bottom). The curves represent the averages (plain lines) and the standard error of mean (dotted lines) of the fetlock joint excursion at canter computed for all the files (n=24 files for BL; n=28 files for HP and n=24 files for SP). Time was normalized from -1 to 0 as the perturbed stance phase, from 0 to 1 as the swing phase and from 1 to 2 as the second stance phase. ....	113
Figure 31 Carpal joint excursion at trot over the baseline (BL, on top), over the hard perturbation (HP, in the middle) and over the soft perturbation (SP, on bottom). The curves represent the averages (plain lines) and the standard error of mean (dotted lines) of the carpal joint excursion at	

trot computed for all the files (n=32 files for BL; n=27 files for HP and n=24 files for SP). Time was normalized from -1 to 0 as the perturbed stance phase, from 0 to 1 as the swing phase and from 1 to 2 as the second stance phase. .... 115

Figure 32 Carpal joint excursion at right lead canter over the baseline (BL, on top), over the hard perturbation (HP, in the middle) and over the soft perturbation (SP, on bottom). The curves represent the averages (plain lines) and the standard error of mean (dotted lines) of the carpal joint excursion at canter computed for all the files (n=24 files for BL; n=28 files for HP and n=24 files for SP). Time was normalized from -1 to 0 as the perturbed stance phase, from 0 to 1 as the swing phase and from 1 to 2 as the second stance phase. .... 117

Figure 33 Elbow joint excursion at trot over the baseline (BL, on top), over the hard perturbation (HP, in the middle) and over the soft perturbation (SP, on bottom). The curves represent the averages (plain lines) and the standard error of mean (dotted lines) of the elbow joint excursion at trot computed for all the files (n=32 files for BL; n=27 files for HP and n=24 files for SP). Time was normalized from -1 to 0 as the perturbed stance phase, from 0 to 1 as the swing phase and from 1 to 2 as the second stance phase. .... 119

Figure 34 Elbow joint excursion at right lead canter over the baseline (BL, on top), over the hard perturbation (HP, in the middle) and over the soft perturbation (SP, on bottom). The curves represent the averages (plain lines) and the standard error of mean (dotted lines) of the elbow joint excursion at canter computed for all the files (n=24 files for BL; n=28 files for HP and n=24 files for SP). Time was normalized from -1 to 0 as the perturbed stance phase, from 0 to 1 as the swing phase and from 1 to 2 as the second stance phase. .... 121

Figure 35 Shoulder joint excursion at trot over the baseline (BL, on top), over the hard perturbation (HP, in the middle) and over the soft perturbation (SP, on bottom). The curves represent the averages (plain lines) and the standard error of mean (dotted lines) of the shoulder joint excursion at trot computed for all the files (n=32 files for BL; n=27 files for HP and n=24 files for SP). Time was normalized from -1 to 0 as the perturbed stance phase, from 0 to 1 as the swing phase and from 1 to 2 as the second stance phase. .... 123

Figure 36 Shoulder joint excursion at right lead canter over the baseline (BL, on top), over the hard perturbation (HP, in the middle) and over the soft perturbation (SP, on bottom). The curves represent the averages (plain lines) and the standard error of mean (dotted lines) of the shoulder joint excursion at canter computed for all the files (n=24 files for BL; n=28 files for HP and n=24 files for SP). Time was normalized from -1 to 0 as the perturbed stance phase, from 0 to 1 as the swing phase and from 1 to 2 as the second stance phase. .... 126

Figure 37 Lateral view of the radius/ulna. Radial origin sites of the LDE ..... 155

Predicting horse limb responses to surface variations

Figure 38 Lateral view of the distal part of the humerus. Humeral origin site of the CDE..... 156

Figure 39 Lateral view of the proximal part of the radius/ulna. Radial origin of the CDE..... 156

Figure 40 Lateral view of the radius/ulna. Origin site of the ECO..... 156

Figure 41 Cranial view of the distal part of the radius. Origin site of the ECO ..... 156

Figure 42 Lateral view of the proximal part of the metacarpus. Insertion site of the ECO..... 157

Figure 43 Lateral view of the distal part of the humerus. Humeral origin of the ECR ..... 157

Figure 44 Drawing of the UL and the sites of samples used to measure the UL properties (in orange)  
..... 158

Figure 45 Lateral view of the distal part of the humerus. Origin site of the UL ..... 159

Figure 46 Lateral view of the carpus. Insertion sites of the UL..... 159

Figure 47 Caudal view of the carpus. Insertion sites of the UL..... 159

Figure 48 Medial view of the distal part of the humerus. Origin site of the FCR..... 160

Figure 49 Caudal view of the carpus. Insertion site of the FCR ..... 160

Figure 50 Medial view of the distal part of the humerus. Origin site of the FCU ..... 160

Figure 51 Caudal view of the carpus. Insertion site of the FCU ..... 160

Figure 52 Medial view of the radius/ulna. Radial and ulnar insertion sites of the DDF..... 161

Figure 53 Medial view of the distal part of the humerus. Humeral origin site of the DDF ..... 161

Figure 54 Medial view of the distal part of radius/ulna. Radial origin of the SDF ..... 162

## List of tables

Table 1 Muscle properties that are required or that can be added for each muscle model.....	43
Table 2 Muscle data used for the AnyBody Thoroughbred forelimb model, obtained from published literature (1-5) and from laboratory dissection data (6) .....	46
Table 3 Ligament data used for modelling which was obtained from published literature.....	48
Table 4 Summary of the models published in the literature, the model used in this study and the key differences between these models .....	52
Table 5 Trot data files, details per horse: number of files, velocity, stance phase duration and swing phase duration (average $\pm$ standard deviation).....	72
Table 6 Right lead canter data files, details per horse: number of files, velocity, stance phase duration and swing phase duration (average $\pm$ standard deviation). .....	73
Table 7 Left lead canter data files, details per horse: number of files, velocity, stance phase duration and swing phase duration (average $\pm$ standard deviation). .....	73
Table 8 Right forelimb coffin flexion and extension peaks at trot. Amplitude and time of occurrence reported in the literature and computed in the model (average $\pm$ standard deviation). The data were time-normalized from -1 to 0 as stance phase and from 0 to 1 as swing phase. ....	75
Table 9 Right forelimb fetlock flexion and extension peaks at trot. Amplitude and time of occurrence reported in the literature and computed in the model (average $\pm$ standard deviation). The data were time-normalized from -1 to 0 as stance phase and from 0 to 1 as swing phase. ....	76
Table 10 Right forelimb fetlock flexion and extension peaks at right lead canter. Amplitude and time of occurrence reported in the literature and computed in the model (average $\pm$ standard deviation). The data were time-normalized from -1 to 0 as stance phase and from 0 to 1 as swing phase. ....	77
Table 11 Right forelimb fetlock flexion and extension peaks at left lead canter. Amplitude and time of occurrence reported in the literature and computed in the model (average $\pm$ standard deviation). The data were time-normalized from -1 to 0 as stance phase and from 0 to 1 as swing phase. ....	77
Table 12 Right forelimb carpal flexion and extension peaks at trot. Amplitude and time of occurrence reported in the literature and computed in the model (average $\pm$ standard deviation). The data were time-normalized from -1 to 0 as stance phase and from 0 to 1 as swing phase. ....	79
Table 13 Right forelimb carpal flexion and extension peaks at right lead canter. Amplitude and time of occurrence reported in the literature and computed in the model (average $\pm$ standard deviation). The data were time-normalized from -1 to 0 as stance phase and from 0 to 1 as swing phase. ....	79
Table 14 Right forelimb carpal flexion and extension peaks at left lead canter. Amplitude and time of occurrence reported in the literature and computed in the model (average $\pm$ standard deviation). The data were time-normalized from -1 to 0 as stance phase and from 0 to 1 as swing phase. ....	80

## Predicting horse limb responses to surface variations

Table 15 Right forelimb elbow flexion and extension peaks at trot. Amplitude and time of occurrence reported in the literature and computed in the model (average $\pm$ standard deviation). The data were time-normalized from -1 to 0 as stance phase and from 0 to 1 as swing phase. ....	81
Table 16 Right forelimb elbow flexion and extension peaks at right lead canter. Amplitude and time of occurrence reported in the literature and computed in the model (average $\pm$ standard deviation). The data were time-normalized from -1 to 0 as stance phase and from 0 to 1 as swing phase. ....	82
Table 17 Right forelimb elbow flexion and extension peaks at left lead canter. Amplitude and time of occurrence reported in the literature and computed in the model (average $\pm$ standard deviation). The data were time-normalized from -1 to 0 as stance phase and from 0 to 1 as swing phase. ....	82
Table 18 Trot data files, details per horse: number of files, velocity, 1 <sup>st</sup> and 2 <sup>nd</sup> stance phase durations and swing phase duration (average $\pm$ standard deviation) for each perturbation condition .....	97
Table 19 Right lead canter data files, details per horse: number of files, velocity, 1 <sup>st</sup> and 2 <sup>nd</sup> stance phase durations and swing phase duration (average $\pm$ standard deviation) for each perturbation condition .....	99
Table 20 Coffin joint excursion at trot: peak values and their time of occurrence over the baseline, the hard and the soft perturbation conditions (average $\pm$ SEM). ....	106
Table 21 Coffin joint excursion at right lead canter: peak values and their time of occurrence over the baseline, the hard and the soft perturbation conditions (average $\pm$ SEM). ....	109
Table 22 Fetlock joint excursion at trot: peak values and their time of occurrence over the baseline, the hard and the soft perturbation conditions (average $\pm$ SEM). ....	112
Table 23 Fetlock joint excursion at canter: peak values and their time of occurrence over the baseline, the hard and the soft perturbation conditions (average $\pm$ SEM). ....	114
Table 24 Carpal joint excursion at trot: peak values and their time of occurrence over the baseline, the hard and the soft perturbation conditions (average $\pm$ SEM). ....	116
Table 25 Carpal joint excursion at canter: peak values and their time of occurrence over the baseline, the hard and the soft perturbation conditions (average $\pm$ SEM). ....	118
Table 26 Elbow joint excursion at trot: peak values and their time of occurrence over the baseline, the hard and the soft perturbation conditions (average $\pm$ SEM). ....	120
Table 27 Elbow joint excursion at canter: peak values and their time of occurrence over the baseline, the hard and the soft perturbation conditions (average $\pm$ SEM). ....	122
Table 28 Shoulder joint excursion at trot: peak values and their time of occurrence over the baseline, the hard and the soft perturbation conditions (average $\pm$ SEM). ....	124

## Predicting horse limb responses to surface variations

Table 29 Shoulder joint excursion at canter: peak values and their time of occurrence over the baseline, the hard and the soft perturbation conditions (average $\pm$ SEM). .....	127
Table 30 Maximal strains computed within the tendons and ligaments at trot during the perturbed stance phase and the following stance phase over the perturbation conditions (average $\pm$ SEM)...	128
Table 31 Maximal strains computed within the tendons and ligaments at canter during the perturbed stance phase and the following stance phase over the perturbation conditions (average $\pm$ SEM). Horse and velocity differences were accounted for and the effect of velocity were removed in the averages presented here .....	130
Table 32 Main effects of the hard perturbation on the joint excursions and tendon and ligament strains at trot .....	131
Table 33 Main effects of the hard perturbation on the joint excursions and tendon and ligament strains at canter .....	132
Table 34 Main effects of the soft perturbation on the joint excursions and tendon and ligament strains at trot .....	132
Table 35 Main effects of the soft perturbation on the joint excursions and tendon and ligament strains at canter .....	133
Table 36 Ligament properties .....	153
Table 37 Muscle and tendon properties.....	154

## List of abbreviations

AIC	Akaike Information Criterion
ALDDF	Accessory Ligament of the Deep Digital Flexor
ALSDF	Accessory Ligament of the Superficial Digital Flexor
ANOVA	ANalysis Of Variance
BL	BaseLine
CDE	Common Digital Extensor
CT	Computed Tomography
DDF	Deep Digital Flexor
ECO	Extensor Carpi Obliquus
ECR	Extensor Carpi Radialis
FCR	Flexor Carpi Radialis
FCU	Flexor Carpi Ulnaris
HP	Hard Perturbation
LDE	Lateral Digital Extensor
MSI	MusculoSkeletal Injuries
SDF	Superficial Digital Flexor
SDFT	Tendon of the Superficial Digital Flexor
SEM	Standard Error of the Mean
SP	Soft Perturbation
St-swing	Stance-swing phase transition
UL	Ulnaris Lateralis

# Chapter 1

## Introduction and literature review

### I. Introduction

The Thoroughbred industry has an important place in the New Zealand economy accounting for approximately 1% of New Zealand's Gross Domestic Product (Bolwell *et al.*, 2017a). However, many of the Thoroughbreds that enter race training will be affected by musculoskeletal injuries, which would lead to rest periods in the best cases, but could also lead to retirement or death. The most frequently reported location for the musculoskeletal injuries are the distal forelimb (Perkins *et al.*, 2004b).

A number of studies have focused on identifying risk factors. One of the major areas of research is track surface properties, because it should be possible to modify these so that the risk of musculoskeletal injury would be reduced (Oikawa *et al.*, 2000; Setterbo *et al.*, 2013). Among all the track surface properties examined, consistency was reported to be one of the main injury risk factors. However, to date, only epidemiological studies have focused on this property. The aim of this thesis is therefore to test how unexpected variations in surface hardness, leading to inconsistency in track surface properties, affect the motion and loading of the limb, which could lead to an increased risk of musculoskeletal injury. For that, a model is required. Different equine limb models have been developed, and the most developed is the spring-mass model (McGuigan and Wilson, 2003). However, to study the effects of inconsistency of a track on the soft tissues of the limb requires the use of a model that includes those soft tissues and therefore a musculoskeletal model is needed. Other equine musculoskeletal models have been developed, but they generally have only included the distal limb (Brown *et al.*, 2003b; Symons *et al.*, 2016).

The musculoskeletal model requires input parameters derived from gait and force plate data against which the model can be tested and developed. To obtain these data the ground hardness was altered in one discrete area of an indoor riding arena by adding wood or foam under the sand surface, to perturb the horse's gait during one stance phase. Gait data were collected from horses passing through the perturbed area and for the subsequent swing and stance phases. The main objectives of this thesis were twofold:

- To develop a preliminary 3D musculoskeletal model of the whole equine forelimb based on data published in the literature and derived from anatomical measurements (Part 1)
- To determine the effects of the perturbations by the ground surface on the limb response with the musculoskeletal model developed and to assess whether the response occurs acutely in the perturbed stance phase or in the next stance phase (Part 2)

## II. Context

### II.A. Racing industry

The history of the Thoroughbred in New Zealand began in 1840 when the first Thoroughbred stallion was imported. That same year, the first race meeting was organised in Wellington. Since then, the Thoroughbred industry has expanded and is now the most economically important part of the New Zealand equine industry, with approximately 40% of the annual Thoroughbred foal crop exported (Rogers *et al.*, 2017). Thoroughbred and Standardbred racing and the sport-horse industries generate around 2% of New Zealand's GDP (Gross Domestic Product) (Bolwell *et al.*, 2017a).

Regarding the international Thoroughbred industry, New Zealand has the 6<sup>th</sup> largest breeding industry (Gee *et al.*, 2017) and is the 11<sup>th</sup> largest racing jurisdiction based on the number of horses starting in races (Bolwell *et al.*, 2017a). Every year, around 5,500 and 300 horses start in approximately 2,900 flat races and 120 jump races respectively (Bolwell *et al.*, 2016, 2017a; Rogers *et al.*, 2017).

Within New Zealand, since the global financial crisis (2007-2008), there has been a consistent reduction of the number of Thoroughbred foals born but the number of horses exported and the proportion of horses lost from the racing industry has remained relatively unchanged (Rogers *et al.*, 2014). Horses may be lost from the racing industry because of voluntary or involuntary reasons. About one-third of Thoroughbreds that enter race training are retired prematurely, mainly because they lack talent, and another third involuntarily, in 78% of these cases because of musculoskeletal injuries (Perkins *et al.*, 2004b). Thus, musculoskeletal injury represents the most significant, potentially manageable, reason for horses being lost from training and the industry.

### II.B. Injuries in horse races

The importance of horses involuntarily retired, or that had reduced training or racing opportunities due to injury, is highlighted by the number of epidemiological studies that have been published. Some of these studies have focused on events occurring during racing. However, it has been reported that these race day events account for only a small proportion of total injuries in Thoroughbreds and that

the majority of the injuries, and the time at risk, is associated with training (Parkin, 2008; Ramzan and Palmer, 2011).

Perkins *et al.* (2004b) reported the number of events during training periods (Figure 1) that were associated with a rest period, retirement or death. Of a total of 2,652 events reported, 1,594 led to a voluntary rest period (1,234) and retirement (360). The other events reported were musculoskeletal injury (834) leading to a rest period (697), death (19) and retirement (118); respiratory disease (165) leading to a rest period (128) and retirement (37); and miscellaneous (59) leading to rest (38), death (7) and retirement (14). The musculoskeletal injuries (834 cases) involved limbs (807), vertebral column (26) and skull (1). The limb musculoskeletal injuries were localised in the distal forelimb (563), the distal hindlimb (28), the proximal forelimb (26) and the proximal hindlimb (82). Other musculoskeletal injuries were not included in the subcategories as they involved more than one region, or the region affected was not reported.

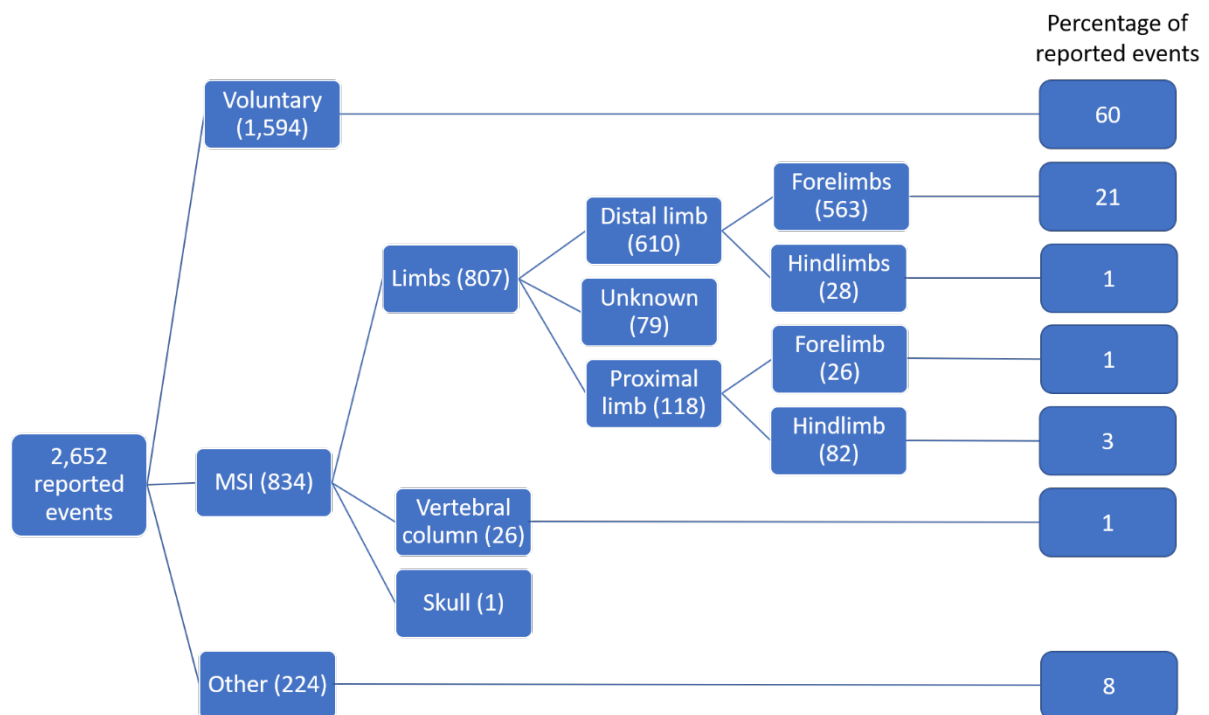


Figure 1 Distribution of the reported events with number of cases (Perkins *et al.*, 2004b)  
(MSI = Musculoskeletal Injuries)

Among all the events reported during both training and racing, the most common type was musculoskeletal injury of the distal forelimb (Bolwell *et al.*, 2017b; Parkin, 2008; Perkins *et al.*, 2004b), as illustrated in Figure 1. The soft tissue structures most frequently affected by musculoskeletal injury are the superficial digital flexor tendon and the suspensory ligament and less frequently the deep digital flexor tendon, its check ligament and the sesamoidean ligaments (Hill, 2003; Rosanowski *et al.*,

2016). Fractures are most often associated with retirement and death. The risk of a particular type of fracture varies with the type of racing. In Thoroughbreds racing at the Hong Kong Jockey Club, catastrophic fractures most frequently involved the proximal sesamoid bones followed by the carpus and proximal phalanx. Non-catastrophic fractures were observed 3.6 times more frequently than the catastrophic fractures and most often involved the carpus and proximal phalanx (Sun *et al.*, 2019). In an earlier study of racing in the UK, Clegg (2011) reported lateral condylar fractures of the third metacarpal bone to be the most common fracture reported for all forms of National Hunt racing, while in flat racing on all-weather surfaces bilateral proximal sesamoid fractures predominated. In flat turf racing, proximal phalanx fractures were the most common fatal fracture (Parkin *et al.*, 2004b).

Injuries have a direct effect on costs, through medical or surgical care, time lost from racing as well as public perception (Perkins *et al.*, 2004b). Musculoskeletal injuries are the major cause of involuntary rest days, with approximately 37% of training Thoroughbreds affected and an average rest duration of 70 days (from 1 to 460 days). Most musculoskeletal injuries require a rest period (83.6%), however they sometimes lead to premature retirement (14.1%) or death (2.3%). The musculoskeletal injuries leading most often to retirement or death are fractures, followed by tendon and ligament injuries. The risk of tendon and ligament injuries increases with the age of the horse and its gender, with the incidence rate for males is 2.5 times higher than for females (Perkins *et al.*, 2004b).

In order to reduce these losses, it is important to determine the risk factors for these injuries, which can be grouped into three categories: horse level factors, such as age and sex; race level factors, such as track condition and race distance; and management factors, such as racing load and management of previous injuries (Hitchens *et al.*, 2019). According to Perkins *et al.* (2004a, 2004b), the main risk factors for the broad category of musculoskeletal injuries are: horse age, gender, cumulative exercise intensity, hoof balance, previous injuries, age at first race, number of starts, physical contact between horses during a race, race distance and class, field size, and barrier position. Among all the identified risk factors, many are not modifiable or unrealistic to prevent, as is the case for gender (Parkin, 2008). On the other hand, Hitchens *et al.* (2019) suggest that preventing older horses from racing, limiting the number of horses in a race, and avoiding harder surfaces would reduce the risk of musculoskeletal injury.

In relation to fracture and dorsal metacarpal disease, the risk factors associated with cyclic load and surface have been the most studied. Repair and adaptation processes are important for the health of the connective tissues of the limb. Exposing a horse to continued or extreme load may overwhelm this process, and thus place the horse at risk of more serious musculoskeletal injuries (Perkins *et al.*, 2004b). Exposure of the tissues of the limb to such loads is determined by training and racing

management, which can be changed by regulation or voluntary adjustment of training regimens. A balance needs to be found between too little high-speed exercise and too much high-speed exercise. Indeed, if the exposure to cyclic load causes subchondral bone damage, the lack of high-speed exercise in training would not allow the bone to adapt to the loads experienced under racing conditions. Both scenarios increase the risk of fracture during racing (Parkin, 2008).

The role of the racetrack surface as a risk factor for musculoskeletal injury has been described in a number of studies. Different racetrack surfaces have different risk profiles for musculoskeletal injury (Parkin, 2008). This means that it could be possible to reduce the risk of injury to horses training or racing on a track by adapting its design or surface condition (Perkins *et al.*, 2004a). The first surface property studied was the surface hardness, which has been positively associated with the prevalence of lameness in a number of studies (Parkin, 2008). When evaluated in a univariate model, the odds ratio of fatal fracture increased incrementally from 1 (heavy-soft going) through 1.5 (good-soft) to 2.2 (good-firm). However, in a multivariate model including the number of runners and the course distance, odds ratio for fatal fracture increased from 1 (heavy-soft going) through 3.8 (good-soft) to 4.1 (good-firm) (Parkin *et al.*, 2004a).

Racetrack surface is still a major area of research (Parkin, 2008). However, athletic injury in racehorses is complex and related to multiple factors affecting both performance and health (Perkins *et al.*, 2004a). The relationships between surface properties and risk of injuries have not been completely established and reducing the risk of a single cause of injury could increase the risk of other injuries (Parkin, 2008). To understand the relationships between racetrack surface properties and risk of musculoskeletal injuries, it will be necessary to fully understand how the tissues of the limb respond mechanically to the surface properties, including stiffness and variability.

### II.C. Modelling in biomechanics

Biomechanical models have been developed to illustrate the mechanisms allowing animals to interact with the environment. These models can be classified under three main types: conceptual models, physical models and mathematical models (Alexander, 2003).

The conceptual models explain a mechanism by using another one that is well understood. For example, the movement of the foot on the ground during human walking has been compared to an egg rolling from one end to the other. The purpose of this type of model is to clarify and understand simply a complex mechanism without mathematical consideration. However, they are generally not realistic (Alexander, 2003).

## Chapter 1 Literature review

The physical models consist of built structures. This type of model is used to demonstrate that a proposed mechanism actually works, check the output of mathematical models, facilitate observations that would be difficult to make on real organism, explain unexpected phenomena, and determine the consequences of changes in structures. Moreover, physical models indicate why a particular structure is better than another (Alexander, 2003).

Finally, mathematical models represent a mechanical output with mathematical equations. These models are used for prediction, seeking an optimum and inverse optimization. This category can be subdivided into four sub-groups: the simple models, the more realistic models, the optimization models and the inverse optimization models. The simple models are the best for establishing general principles. They have been used in human, animal and insect locomotion, to explore effects of changing the properties of tendons and muscles or the number of joints, and to explain other phenomena that can be observed, such as the different shapes of bones or the feeding suction of fish. Some problems may require more realistic models, which are often used to explain more complicated movements, such as somersault or to calculate stresses in elaborately shaped bones. If these models are more realistic than simple models, the assumptions made to develop these models prevent their application in some environments or scenarios. For instance, a model studying the ligament strains at a joint will consider the bones as rigid bodies, and although this model can be accurate for the ligaments it will never be possible to use it to study bone fracture processes. Optimization models enable the calculation of the best structure or pattern of movement possible. For example, they have been used to predict the optimum properties of muscle-tendon units to minimize the metabolic energy costs of movements, and in plants to determine the best patterns of branching to minimize the bending moment and maximize light interception. Lastly, the inverse optimization models are used to test hypotheses, generally about the parameters to optimize, by comparing the results of modelling to actual measurements. This type of model has been used in movement studies, with different optimized parameters: acceleration, muscle power or metabolic energy costs. Another application of this method is to predict forces within the muscles. As there are more muscles than degrees of freedom at a joint, the contributory forces to a net joint moment exerted by each muscle cannot be determined. Optimization functions are needed to determine how the load is shared between the different muscles (Alexander, 2003). Different combinations of optimizations have been tested, depending on the aim of the studies. Seireg and Arvikar (1973) proposed different objectives for optimization of load sharing between muscles: the minimization of the forces in the muscles, the minimization of the work done by the muscles, the minimization of the vertical reaction forces at each joint and the minimization of the moments carried by the ligaments at the joints. Other objectives can be created by combinations of those listed. However, it seems that one optimization function may be

specific to a case. The mathematically predicted muscle forces in Herzog and Leonard's (1991) model of the feline tarsal joint did not agree well with the experimentally determined actual muscle forces. They highlighted the variation in load sharing between step cycles as a culprit, and identified that these were due to variation in force-velocity characteristics and/or to delays of onset of activation between muscles. They also indicated that changes in load sharing between speeds may be caused by changes in the magnitude of centrally controlled activation, and none of these principles were considered in their theoretical model.

To conclude, one of the main risk factors for musculoskeletal injury is the racetrack surface. However, the interaction between the surface and the horse's limb remains unclear, partly due to our current incomplete knowledge of the adaptive mechanisms of the distal limb, which can be studied using a mathematical model.

### III. Hoof-track interaction

#### III.A. Risk factors

A number of studies have reported an association of track surface and injury in both race and sport horses (Oikawa *et al.*, 2000; Robin *et al.*, 2009; Setterbo *et al.*, 2011; Setterbo *et al.*, 2013; Stover, 2003). Indeed, track surface properties affect both the forelimb hoof impact accelerations and the ground reaction forces (Gustas *et al.*, 2006b; Ratzlaff *et al.*, 2005; Rollot *et al.*, 2004; Setterbo *et al.*, 2009; Setterbo *et al.*, 2011). The most important track surface properties implicated in racehorse musculoskeletal injuries are the hardness and consistency of the surface. The consistency is influenced by the homogeneity of material composition, moisture content, compaction and cushion depth (Cheney *et al.*, 1973; Kai *et al.*, 1999; Mahaffey *et al.*, 2013; Oikawa *et al.*, 2000; Peterson and McIlwraith, 2008; Peterson *et al.*, 2010; Ratzlaff *et al.*, 1997; Setterbo *et al.*, 2013). A greater understanding of the material properties of racetracks, and optimising these might reduce the risk of musculoskeletal injury (Setterbo *et al.*, 2009; Symons *et al.*, 2014a; Symons *et al.*, 2016), and maximise horse performance.

#### III.B. Surface properties

A number of studies have explored the relationship between the track surface (dirt, turf, synthetic, sand) and the rates and type of injury (Arthur, 2010; Hill *et al.*, 1986; Rosanowski *et al.*, 2016). Due to the varying material properties of the different racetrack surfaces and their effects on shock and vibration of the hoof and distal limb, some types of track surface are associated with certain injuries, such as proximal sesamoid bone fractures on all-weather tracks and proximal phalanx fractures on turf (Parkin *et al.*, 2004b). The higher incidence of certain injuries may be associated with the inherent

material properties of the different track surfaces. However, there is some variation in the type of injury and the magnitude of the risk associated with different track surfaces reported in the literature. This inconsistency may be due to differences in experimental design, analytic approach, injury and case definition and confounding factors (Setterbo *et al.*, 2009). In addition, variation in environmental factors and surface maintenance procedures have a major impact on the relationship between track surface and injuries, and are hard to control (Setterbo *et al.*, 2011).

Rapid loading of the hoof during contact has been identified as an injury mechanism (Pratt, 1997) and track surface properties have been shown to affect the nature of the impact shock and vibrations in the distal limb. The impact shock was attenuated, and the vibration amplitude reduced on an all-weather waxed trotting track compared to a crushed sand track (Chateau *et al.*, 2009b). Vertical ground reaction forces at trot and canter are highest at midstance, and deformation of the hoof capsule, compressive forces across the joints and loading of the suspensory tendons and ligaments are highest at or after this time (Johnston and Back, 2006). These loading events are primarily associated with articular cartilage and subchondral bone degeneration (Chateau *et al.*, 2009b; Radin *et al.*, 1973; Serink *et al.*, 1977). To quantify mechanical loading at impact, tools such as impactors have been developed to replicate the ground reaction forces of a horse in terms of load and speed (Clanton *et al.*, 1991; Mahaffey *et al.*, 2013; Oikawa *et al.*, 2000; Peterson *et al.*, 2008; Peterson and McIlwraith, 2008; Pratt, 1985; Ratzlaff *et al.*, 1997; Setterbo *et al.*, 2011). The rate of loading can be described on live horses through the use of ground reaction force measuring devices or of accelerometers on the limbs (Barrey, 1990; Frederick and Henderson, 1970; Kai *et al.*, 2000; Ratzlaff *et al.*, 1990; Roepstorff and Drevemo, 1993).

### III.B.1. Impactors

Impactors seek to replicate the kinetic impact of the hoof with the surface, and measuring the properties at different locations of a same track provide an indication of the consistency of the hoof track interaction. They have been used to describe a positive linear relationship between the impact force measured and the rate of occurrence of lameness on sand racetracks (Cheney *et al.*, 1973). Using an impactor that measured both vertical force and shear force during simulated hoof landing, Peterson and McIlwraith (2008) reported a reduction in peak vertical load of 34% after harrowing of a dirt track used for Thoroughbred racing, but also that variability of the measured load increased by more than the double across the 24 locations tested. The advantages of impactors are to remove the variability between horses, and to avoid the use of live animals in research (Chateau *et al.*, 2009b; Cheney *et al.*, 1973; Peterson *et al.*, 2008; Ratzlaff *et al.*, 1997; Robin *et al.*, 2009).

There has been an increase in the sophistication of the impactors used and their ability to represent the hoof-ground interaction. Pratt (1984) tested the ability of a track to absorb kinetic energy from the hoof. However, his method was cumbersome and inadequate to measure the properties of an entire track (Oikawa *et al.*, 2000). Small loads (10kg) from small heights (under 1m) were used to study only the vertical forces, which are not representative of the triplanar equine hoof impact during racing, and thus do not allow complete characterisation of the surface properties for racing conditions (Pratt, 1985).

Clanton *et al.* (1991) used a cone penetrometer in an impactor with a load cell to measure the force applied to penetrate the soil of a Thoroughbred dirt track to carriage depth. Once again, this method did not describe the complexity of the surface properties, nor did they report their vertical impact velocities. The forces measured during penetration of the soil to 3, 6 and 9 cm only averaged 200, 450 and 1,200 N, which are substantially smaller than the typical vertical ground reaction force (Merkens and Schamhardt, 1994) under the forelimb in a walking horse (about 4,000 N). If the loading rates are not similar to those subjected to the hoof at gallop and if the loads applied are much smaller than required to test the soil to the correct depth, so as to replicate the loading patterns observed in a galloping horse, then the characterization of the surface can only be used in relative terms (Peterson *et al.*, 2008). Indeed, Clanton's (1991) study was only seeking to characterize the relative surface properties at defined locations across the width of the track and at certain points along its length.

Oikawa *et al.* (2000) combined a self-propelled racetrack hardness measurement device to an analysis system to systematically measure track hardness, and sand depth for dirt surfaces, in all locations of a track. The serial measurements for one entire track were performed across intervals of 5 meters. This device solves the cumbersome nature of the characterisation of a whole track by the devices developed previously.

Peterson *et al.* (2008) developed a mobile testing system that was able to load the track at the rate and loads applied at gallop, at first contact and during the first part of the stance phase when the superincumbent weight was transferred to the hoof. This platform allows the system to be positioned anywhere on the track for sampling the surface and was able to detect changes in the track properties caused by inconsistent surface maintenance.

The main drawback of the use of impactors is the strain-rate dependence of the racetrack properties (Ratzlaff *et al.*, 1997; Setterbo *et al.*, 2013). Moreover, studies compared either the peak vertical acceleration, which does not include any consideration of the shear strength of the surface, or used

small loads, making these tests only representative of the acute impact phase of the horse gait (Peterson *et al.*, 2008).

### III.B.2. Force plates and hoof-mounted devices

The ground reaction force is a relevant property in track surface studies to assess the interaction between the hoof and the ground surface (Robin *et al.*, 2009). In particular, analysis of impact of the hoof and limb may be useful when attempting to improve track conditions (Kai *et al.*, 2000). Two methods have been described to measure the ground reaction force: the use of a force plate or a pressure plate (Pratt and O'Connor, 1976; Robin *et al.*, 2009); or the use of hoof-mounted devices like force measuring shoes, accelerometers and strain gauges (Bjorck, 1958; Parsons *et al.*, 2011).

#### III.B.2.a. Force plates vs hoof-mounted devices

The advantages of using a force plate are the ability to measure actual ground reaction forces in three dimensions and the ease of operation. The disadvantages include expense, the inability to record forces exerted during successive strides, difficulties in obtaining simultaneous recordings of forces exerted by more than one limb, in recording forces at faster gaits and in getting horses to step on the plate, which is the main drawback of this method (Frederick and Henderson, 1970; Kai *et al.*, 2000; Parsons *et al.*, 2011; Ratzlaff *et al.*, 1990; Schamhardt *et al.*, 1993). These limitations generally mean this method is not suitable for measurements in field conditions, at high speed (Robin *et al.*, 2009). Pressure plates have been proposed as an alternative solution to force plates. Compared to force plates, they offer the advantages to allow the analysis of simultaneous and consecutive hoof strikes at once and to provide information on the loading of the different portions of the hoof (Oosterlinck *et al.*, 2010b). However, pressure plates cannot simply replace a force plate when high accuracy of force values is needed (Oosterlinck *et al.*, 2010a). If hoof-mounted devices can overcome many of the disadvantages of the use of force plates, such as measuring the ground reaction force over a large number of strides on a wide variety of surfaces (Kai *et al.*, 2000; Parsons *et al.*, 2011; Robin *et al.*, 2009; Roland *et al.*, 2005), they have other disadvantages. Their volume and weight might affect the gait of the horse. Shoes with strain gauge transducers may not be reliable due to the heavy weight of the device, which may alter the horse's motion pattern. The measures of the vertical ground reaction forces may also be distorted in devices including strain gauge transducers or piezoelectric transducers by the use of preloaded transducers or by the transducers supporting only a portion of the vertical ground reaction forces. In addition, the first hoof-mounted devices did not supply information about acceleration, which is an important component of the kinetic analysis of gait and gives information on shock and vibration during hoof impact on the ground (Barrey *et al.*, 1991; Hjerten and Drevemo, 1994).

III.B.2.b. *Development of hoof-mounted devices*

Given the advantages offered by hoof-mounted devices compared to force plates, a number of studies have focused on their development and improvement. The first hoof-mounted device was developed by Bjorck (1958). He attached strain gauges to a shoe to measure vertical and horizontal forces exerted by draft horses. The patterns of the force-time curves obtained with this device were typical, in shape, of those obtained by other methods, although the shoe was heavy and thick (Kai *et al.*, 2000). Frederick and Henderson (1970) developed and tested a force-sensitive horseshoe that incorporated three preloaded transducers and obtained the vertical ground reaction forces exerted by a horse at different gaits.

Barrey (1990) used an instrumented boot to investigate vertical ground reaction forces exerted at four parts of the hoof. Ratzlaff *et al.* (1987), Ratzlaff *et al.* (1990) and Ratzlaff *et al.* (1993) developed two types of light-weight instrumented shoes using piezoelectric transducers, which measured ground reaction forces exerted over the centre of the frog or at three points on the hoof by horses at different gaits. Roepstorff and Drevemo (1993) equipped a light horseshoe with strain gauges at the toe and at each of the quarters. This device was then used by Roepstorff *et al.* (1994) to analyse the effect of different treadmill constructions on ground reaction forces exerted by trotting horses.

Kai *et al.* (2000) developed a hoof-mounted device composed of two metal plates, two bolts, four load cells and three accelerometers. The forces recorded from the four load cells (medial and lateral heel, medial and lateral toe) were summed to yield an overall vertical force curve which closely resembled, in both amplitude and shape, the pattern of vertical force measured using a force platform reported by other studies for trot and canter (Gustas *et al.*, 2006b; Merkens *et al.*, 1993). Further the data recorded at trot and canter from two measurement sessions a week apart were not significantly different from each other.

Gustas *et al.* (2004) trotted horses across a force platform, while also collecting data from accelerometers mounted on the fore and hind hooves. The accelerometer signals for the first 50 ms after fore and hind hoof contact were temporally similar but vertical deceleration amplitudes were greater in the fore compared to the hind limbs, agreeing with earlier studies and reflecting the mechanical differences between the functions of the fore and hind limbs. Signals from the force platform likewise indicated similar temporal patterns but with greater rate of loading and larger vertical and horizontal braking forces measured under the forelimb. Roland *et al.* (2005) developed a 3D dynamometric horseshoe weighting 860 g. It was tested on a treadmill and provided force profiles similar to those reported by studies using other devices (hoof-mounted or force plates). More recently, Chateau *et al.* (2009a) developed a lighter custom-made device (490g), which was tested on

several types of ground at slow speed, and was judged to be well adapted to compare the ground reaction forces of different surfaces.

The device used by Chateau *et al.* (2009b) was sensitive enough to discriminate between the biomechanical effects of a crushed sand track and an all-weather waxed track. However, they only tested two kinds of tracks and it is unknown if the device is sufficiently sensitive to identify change of properties within a surface due to variation in moisture level or depth.

The main disadvantage of the studies using live horses is the variability between horses. For example, Chateau *et al.* (2009b) observed the pattern of hoof deceleration during landing composed of two peaks and found differences between three horses. For two of them, they observed a delay of the second peak, but not for the third horse and they were unable to explain the reason for this difference.

However, when comparing data, consideration is needed on the mechanism in which the device is used as the stiffness of the surface decreases when the angle of impact increases and when the impact velocity decreases (Setterbo *et al.*, 2011; Setterbo *et al.*, 2013). Thus, the setup of the testing device can have a large impact on the absolute properties reported for a surface.

### III.B.3. Comparison of surface properties

Racetrack surface mechanical properties have generally been compared between surface types (turf, sand, dirt, synthetic). Very few recent studies have compared the properties between traditional surfaces, but have focused on how synthetic surfaces differ to generally one of the traditional surfaces. The difficulty of such comparisons is the maintenance of the ground surface. Indeed, harrowing has been reported as significantly affecting the mechanical behaviour of the surface (Tranquille *et al.*, 2015). Within turf tracks, the turf roots and the soil moisture levels are responsible for increased hardness and resistance to shear (Ratzlaff *et al.*, 1997; Zebarth and Sheard, 1985). Epidemiological studies have identified that turf tracks were associated with a lower risk of breakdown compared to dirt surfaces (Mohammed *et al.*, 1991), however, this will vary with the state of the track. The Jockey Club's Equine Injury Database (<http://www.jockeyclub.com/default.asp?section=Resources&area=10>, data for 2019) indicates racing fatalities are lowest on synthetic surfaces (0.93 fatal injuries per 1,000 starts on synthetic compared to 1.56 on turf surfaces and 1.60 on dirt) although the interaction between surface type and age of the horse continues to be equivocal. Whereas older horses tend to be more at risk of injury on dirt surfaces, there is no significant difference in fatal injury rate between 2-year old horses and older horses on synthetic surfaces (Larkin, 2011).

### III.B.3.a. *Synthetic surfaces*

Synthetic racetracks are reported to provide improved consistency and safety compared to dirt tracks (Rezendes, 2007). The synthetic surfaces have been described as generally less stiff and softer than dirt surfaces (Setterbo *et al.*, 2011; Setterbo *et al.*, 2013), and to have better shock-absorbing properties than dirt or sand surfaces (Chateau *et al.*, 2009b; Robin *et al.*, 2009; Setterbo *et al.*, 2009; Symons *et al.*, 2014a; Symons *et al.*, 2016).

The maximum vertical forces and loading rates are reported to be lower on synthetic than on traditional surfaces (Chateau *et al.*, 2009b; Crevier-Denoix *et al.*, 2009; Robin *et al.*, 2009; Setterbo *et al.*, 2009; Setterbo *et al.*, 2011; Setterbo *et al.*, 2013). For example, Setterbo *et al.* (2009) reported peak vertical ground reaction forces of 11.5 N.kg<sup>-1</sup>, 13.8 N.kg<sup>-1</sup> and 16.1 N.kg<sup>-1</sup> for synthetic, turf and dirt racing surfaces respectively in cantering Thoroughbred horses, and loading rates of 106 N.kg<sup>-1</sup>.s<sup>-1</sup>, 193 N.kg<sup>-1</sup>.s<sup>-1</sup> and 111 N.kg<sup>-1</sup>.s<sup>-1</sup> respectively. However, as previously stated, the maintenance and hydration status will affect the surface properties at any measurement time.

The same overall pattern has been reported for the ground reaction forces, maximum impact forces, vertical force peak at impact, vertical force at mid-stance and maximum longitudinal braking force (Chateau *et al.*, 2009b; Crevier-Denoix *et al.*, 2013b; Robin *et al.*, 2009; Setterbo *et al.*, 2009; Setterbo *et al.*, 2011; Setterbo *et al.*, 2013). The peak vertical ground reaction force on the synthetic surface was 83% of the peak on a dirt surface and 71% of the peak on a turf surface (Setterbo *et al.*, 2009). The times of occurrence of the maximal longitudinal force during braking and of vertical force at mid-stance were delayed by 24% and 9% respectively on all-weather waxed surfaces compared to turf surfaces (Crevier-Denoix *et al.*, 2013b), and the time of maximal “sink” of the hoof into the surface was likewise delayed by 30%. A dirt surface, while potentially having more resistance to vertical compression (depending on its depth and maintenance state) will usually allow more horizontal sliding of the hoof, compared to a turf surface that will resist this sliding and therefore allow a greater braking effect across a shorter timespan (Pratt, 1997).

Another important parameter to characterize the interaction between the hoof and the track surface is the deceleration of the hoof at impact. On an all-weather surface, the vertical hoof velocity before impact was higher than on a turf surface but the acute hoof deceleration at impact was not significantly different between surfaces (Crevier-Denoix *et al.*, 2013b). Chateau *et al.* (2009b) recorded a shorter braking phase in trotters on a crushed sand surface (29.7 ms) than on an all-weather surface (35.5 ms) and Robin *et al.* (2009) associated this with a larger amplitude braking force on the crushed sand track (2,923 N) compared to the all-weather surface (2,392 N).

## Chapter 1 Literature review

The impact of the hoof on the ground surface creates vibrations within the hoof, which are subsequently transmitted to other tissues within the legs. In general, hoof vibrations at impact have lower amplitudes on synthetic surfaces than on traditional surfaces (Chateau *et al.*, 2009b; Robin *et al.*, 2009; Setterbo *et al.*, 2009). This is due to the fact that different surfaces have different vibration energy; for example, low frequency vibrations have higher amplitude on a turf surface compared to an all-weather surface and high frequency vibrations have higher amplitude on an all-weather surface than on a turf surface (Crevier-Denoix *et al.*, 2013b).

Stride characteristics have also been compared between the different types of surface. Slip and sink distances during braking and at maximal sink have been reported to be larger on an all-weather surface than on turf (Crevier-Denoix *et al.*, 2013b). Horizontal displacement of the heel during slide is smaller on a synthetic surface than on a dirt surface (Symons *et al.*, 2014a). Shorter stride length and higher stride frequency have been observed on all-weather tracks compared to crushed sand (Chateau *et al.*, 2009b; Robin *et al.*, 2009). The maximum fetlock angle and the heel-strike fetlock angles of the hind limb are smaller and the maximum fetlock angle is delayed on a synthetic surface compared to a dirt surface (Symons *et al.*, 2014a).

With all these observations, it seems that synthetic surfaces may mitigate the risk of musculoskeletal injuries (Symons *et al.*, 2014a). However, different results may be observed with different environment and management conditions. For example, the differences between dirt and synthetic surfaces increase as the dirt surface is compacted with repeating impacts or increasing impact velocities (Setterbo *et al.*, 2013) and decrease after harrowing the dirt surface (Setterbo *et al.*, 2011). Moreover, these studies can be affected by large inter-horse variability due to small horse sample size (Chateau *et al.*, 2009b; Crevier-Denoix *et al.*, 2009; Robin *et al.*, 2009).

The apparent “better properties” of the synthetic surfaces compared to the traditional surfaces explain the substitution of dirt racetracks with synthetic racetracks (Setterbo *et al.*, 2011). In 2006, the California Horse Racing Board declared that all major tracks in the state must install a synthetic track surface by the end of 2007 (Peterson *et al.*, 2010). With these conversions, fatality rate has been reported to be reduced (Arthur, 2010; Setterbo *et al.*, 2009). This, nevertheless, is just an interpretation as horseshoe regulation and pre-race examination practices also changed at this time (Arthur, 2010). In addition, trainers and veterinarians observed longer race times and more non-catastrophic musculoskeletal injuries. This, combined with the difficulty in managing the synthetic racetrack surface led to the reinstallation of some dirt surfaces (Symons *et al.*, 2016). The observation of greater numbers of non-catastrophic injuries may have been related to the change in surfaces, or may simply have been due to changes in data collection, which are more and more robust.

III.B.3.b. *Other comparisons*

Racetrack surfaces are generally graded according to an ordinal scale that relates to the track hardness and these vary according to the track surface type (dirt or turf). The studies that have used this classification to compare different racetrack surfaces have been epidemiologic. Mohammed *et al.* (1992) reported higher odds of breakdowns on “sloppy” and “good” tracks than on “muddy” and “firm” tracks respectively (odds ratio of 2.8 and 2.3, respectively). Zebarth and Sheard (1985) reported the odds of serious injury associated with “fast” track conditions was 3.5 times that associated with “heavy” track conditions. Harder, drier or faster race surfaces may be associated with higher risks than rain-affected softer or slower race surfaces (Reiser *et al.*, 2000).

In addition to comparison of racetrack surfaces by their class (fast, slow...), it is possible to examine their properties (hardness, shear strength, etc.). A number of studies have related the hardness of track surfaces to an increase of incidence of injuries (Cheney *et al.*, 1973; Drevemo and Hjerten, 1991; Drevemo *et al.*, 1994; Pratt, 1984). Other authors have reported that the ability of a racetrack surface to absorb impact shock reduces the number of breakdowns (Kai *et al.*, 1999; Ratzlaff *et al.*, 2005). Clanton *et al.* (1991) concluded that the high incidence of breakdowns in one area of a racetrack used for Thoroughbred racing was caused, in part, by the change in slope and compaction of the track in this area. The impact intensity and the shearing forces linked to the horizontal deceleration of the hoof are believed to be important factors in the occurrence of lameness (Cheney *et al.*, 1973; Hjerten and Drevemo, 1994). Impact intensity is related to density and composition of the track (Barrey *et al.*, 1991). Both compaction and composition of the track surface dramatically affect hoof impact deceleration (Barrey *et al.*, 1991; Pratt, 1984). Lower compaction and higher percentages of organic matter result in lower impact forces (Ratzlaff *et al.*, 1997). The compaction of the track surface may also vary broadly over different areas of the same track (Clanton *et al.*, 1991; Drevemo and Hjerten, 1991; Drevemo *et al.*, 1994; Pratt, 1984; Ratzlaff *et al.*, 1997).

Some studies on surface physical properties have also related these to mechanical properties. For example, an increase in moisture content of the surface leads to a decrease of the variation in the magnitude of vertical forces between successive strides (Ratzlaff *et al.*, 1997). However, the problem of comparing racetrack surfaces by physical properties is the interdependence of some properties. For example, an increased cushion depth reduces the dry density and hardness of the surface, which results in lower peak decelerations of the hoof at impact; and a reduced dry density leads to a reduced frequency and duration of vibrations at hoof impact (Barrey *et al.*, 1991). There are even more complex relationships between properties. Ratzlaff *et al.* (1997) reported that when the moisture content was increased up to 8%, returned energy and impact resistance decreased and when the

moisture content was increased from 8% to 14%, energy returned and impact resistance were progressively increasing. Changes in moisture content also affected the hoof-surface forces, but this relationship depended on the speed of the horses; indeed, they observed the lowest forces at 8% moisture content for horses galloping between 14.5 and 15.4 m.s<sup>-1</sup> and at 12% moisture content for horses galloping between 15.5 and 16.5 m.s<sup>-1</sup>. The hoof-surface forces are also affected by changes in the percentage of energy returned and the impact resistance of the track. For horses with a speed between 14.5 and 15.4 m.s<sup>-1</sup>, the forces exerted increased as energy returned and impact resistance increased whereas for a speed between 15.5 and 16.5 m.s<sup>-1</sup>, the forces exerted decreased as energy returned and impact resistance increased (Ratzlaff *et al.*, 1997).

### III.B.4. Best properties?

The objective when installing a new racetrack is to ensure it would have the best properties possible, which implies identifying the surface properties that would minimize the incidence of injuries and maximise the performance of the horses. It is then necessary to understand the role of the track surface in equine locomotion.

During the stance phase (the period from first impact to the end of break over) large peak decelerations, the highest vertical load, and highest shear loads are applied (Biewener, 2003; Gustas *et al.*, 2006b; Peterson *et al.*, 2008; Radin *et al.*, 1991), which is why this is the most studied period of the gait cycle. Large high-frequency decelerations in both the vertical and cranio-caudal directions in the early stance phase can have detrimental effects on the musculoskeletal system with associated subchondral bone damage and degenerative changes in the joints (Gustas *et al.*, 2004; Gustas *et al.*, 2006b; Lahm *et al.*, 2004; Lahm *et al.*, 2005; Palmer *et al.*, 1996; Parsons *et al.*, 2011; Radin *et al.*, 1973; Radin, 1999; Serink *et al.*, 1977; Wilson *et al.*, 2001). The forces associated with these large amplitude and high-frequency hoof decelerations are transmitted to more proximal musculoskeletal structures through the hoof as shockwaves (Dyrhe-Poulsen *et al.*, 1994; Gustas *et al.*, 2001; Gustas *et al.*, 2004; Gustas *et al.*, 2006b; Hjerten and Drevemo, 1994; Merkens and Schamhardt, 1994; Parsons *et al.*, 2011; Pratt and O'Connor, 1976; Symons *et al.*, 2014a; Willemen *et al.*, 1999; Wilson *et al.*, 2001). A damping effect has been described, with the attenuations occurring distal to the proximal phalanx (Dyrhe-Poulsen *et al.*, 1994) or distal to metacarpus (Gustas *et al.*, 2001; Willemen *et al.*, 1999). These attenuations have been specified in some research; Lanovaz *et al.* (1998) and Willemen *et al.* (1999) described the frequency attenuation as being mainly within the soft tissues of the hoof, while the amplitude attenuation seems to be related to the bones and interphalangeal joints at a slow trot (Gustas *et al.*, 2004).

During the impact phase, the hoof is moving at high speed downwards and requires the track to decelerate it and this is the role of the cushion of the track when compressed (Peterson *et al.*, 2008). At first contact, the loading of the limb leads to increased friction between hoof and ground. The vertical deceleration curve shows two peaks during this phase; the first low peak is attributed to heel landing and the second peak to complete landing of the hoof (Chateau *et al.*, 2009b). The horizontal deceleration curve is described as a complex of more or less prominent peaks followed by the distinct local minimum coinciding with the first maximum of the loading rates. The onset of the ground reaction force is characterized by this period (Gustas *et al.*, 2004). The ground reaction force is composed of two principal components; the force associated with acute hoof impact and the one associated with loading of the hoof by the superincumbent limb during stance (Gustas *et al.*, 2001; Gustas *et al.*, 2004; Gustas *et al.*, 2006b; Hjerten and Drevemo, 1994; Parsons *et al.*, 2011; Ratzlaff *et al.*, 2005).

The braking phase is defined as the period following impact and during which the hoof still undergoes a sliding movement before complete stabilization on the ground (Chateau *et al.*, 2009b). The forward movement of the hoof coincides with a period of fast extension of the fetlock joint and fast flexion of the coffin joint (Back *et al.*, 1995; Gustas *et al.*, 2004; Johnston *et al.*, 1995). The combination of the sliding hoof, the fast moving distal bone segments and the successive increase in load is suggested to be the cause of the coinciding second complex of vertical deceleration peaks at hoof level, which are also measured at the metacarpus (Gustas *et al.*, 2001). During this phase, there is a rapid increase in the longitudinal braking of the hoof, which appears as a single peak. This peak indicates a horizontal velocity change at the hoof, and shows a large variation in amplitude and timing. The next longitudinal hoof braking peak appears at the time of the second distinct increase in the horizontal hoof braking and metacarpal deceleration (Gustas *et al.*, 2001). The end of this phase is characterized by a more gradual longitudinal deceleration of the hoof. The time period of the horizontal braking of the hoof is also an important factor in the attenuation of the impact (Gustas *et al.*, 2001). Gustas *et al.* (2006b) concluded that the qualities of the ground surface have an effect on the hoof-braking pattern. The role of the surface during this phase is to help the hoof decelerate, which is also affected by other factors such as the horseshoe design (Kane *et al.*, 1996; Peterson *et al.*, 2008).

Ratzlaff *et al.* (2005) identified an inverse relationship between track rebound rate and negative acceleration peaks of all hooves and concluded that any factors reducing deceleration of the hooves will increase stride efficiency by allowing smoother transition from braking to propulsion and therefore may be important in determining the safety of a racing surface.

## Chapter 1 Literature review

In late stance and during breakover, the horizontal load on the surface is completely reversed to provide a propulsive force. Both braking and propulsion phases determine the properties required for the track surface in terms of shear strength; it has to reduce the magnitude of the abrupt deceleration of the hoof during braking and not fail in shear during propulsion (Biewener, 2003; Clayton, 2004; Peterson *et al.*, 2008; Reiser *et al.*, 2000) and any shear failure during propulsion may have an impact on horse performance (Biewener, 2003; Peterson *et al.*, 2008; Thomason and Peterson, 2008). However, if a surface inhibits slip or decreases the rate of energy dissipation there may be an increased risk of injury, indeed, a shorter slip distance has been associated with higher vertical and horizontal loading rates and the energy that is not dissipated by the ground surface needs to be dissipated by the horse limb (Gustas *et al.*, 2001; Parsons *et al.*, 2011).

The magnitude of vertical forces applied to the hoof and limb during stance have been linked to extreme angles of fetlock hyperextension (McGuigan and Wilson, 2003; Symons *et al.*, 2016). Those extreme angles increase the load transferred to the suspensory apparatus, and they are related to musculoskeletal injuries around the fetlock joint, which is the region most affected by musculoskeletal injuries (Le Jeune *et al.*, 2003; Santschi, 2008; Singer *et al.*, 2013; Symons *et al.*, 2016).

Generally, racetrack mechanical properties affect both the performance of the racehorse and the safety of a race. For example, loading rates have been observed to be higher on harder surfaces, so the surface needs to be soft enough to absorb the impact force (Chateau *et al.*, 2010; Gustas *et al.*, 2006b; Mahaffey *et al.*, 2013); on the other hand, stride lengths have been reported to be longer on harder surfaces, suggesting a greater efficiency, so the surface needs to be hard enough so as not to affect the performance of the horse (Mahaffey *et al.*, 2013). To optimize the racetrack surface, both aspects have to be accounted for, in this example, the hardness of the track needs to be determined not to affect the horse performance while reducing the injury risk factor. However, little is said about how to quantify these properties, and the balance of performance and safety properties is even more complicated by the interdependence between some properties.

To conclude, it is important to study racetrack surfaces to determine the cause of musculoskeletal injuries. For this reason, devices have been developed and the surface properties have been compared against injury rates. However, the relationships between surface properties, risk of injuries and performance are very complicated and/or unknown and do not currently allow specification of the ideal track properties. In order to clarify these relationships, it is necessary to understand how soft tissues are affected by changes in the track properties. To try to answer this question, a model needs to be used.

## IV. Equine modelling

The installation of new racetrack surfaces is expensive and the experimental data collection required to test these can be difficult to obtain, time consuming and necessitates the use of animals in research. Computational models may make it easier to survey a wide range of racetrack surface mechanical properties to gain insight into their effects on racehorse limb motions and musculoskeletal tissue loads that are difficult to measure *in vivo* (Symons *et al.*, 2016). Several studies have been published describing initial models of the equine forelimb (Swanstrom *et al.*, 2005; Symons *et al.*, 2016).

Mathematical modelling is a useful tool for evaluating muscle and joint loading during movement (Harrison *et al.*, 2010). This approach has been used extensively to determine musculoskeletal function in human movement (Pandy and Zajac, 1991; Pandy, 2001; Pandy and Andriacchi, 2010; Shelburne *et al.*, 2004; Shelburne *et al.*, 2006; Van Soest *et al.*, 1993; Zajac, 1993). However, relatively few studies have used it to study equine movement and those are described in the following sections.

### IV.A. The spring model

The spring model is the model most developed for equine simulations. The idea of the spring model first came from the observation that a kangaroo's hop is powered by spring-like tendons that allow it to literally bounce along the ground (Alexander and Vernon, 1975). The spring-mass representation has since been generalized to all animals as it has been noticed that, while moving, they prefer a particular stride frequency and speed for each gait (Heglund and Taylor, 1988; Pennycuik, 1975). Gait is not the only parameter determining the preferred stride frequency; others also affect it, such as body stiffness (Blickhan, 1989). This preferred frequency appears to maximize the utilization of strain energy (Blickhan, 1989; Harrison *et al.*, 2010). It is now clear that the role of elastic mechanisms in movement extends well beyond obviously springy gaits such as hopping, influencing the mechanics, energetics and control of a wide range of activities (Roberts and Azizi, 2011). The role of tendons as elastic structures that store and return elastic energy makes them integral to the spring-mass model (Blickhan, 1989; Cavagna *et al.*, 1977; Ker, 1981; McGuigan and Wilson, 2003; McMahon, 1985; McMahon and Cheng, 1990; Thorpe *et al.*, 2012).

Generally, animals use a bouncing gait during rapid terrestrial locomotion as it allows the animal to minimize energy expenditure (Blickhan, 1989; Cavagna *et al.*, 1977; Harrison *et al.*, 2010; Heglund *et al.*, 1982). Empirical and theoretical approaches have demonstrated that the use of elastic mechanisms also occurs during walking, and some studies suggest that elastic mechanisms are an essential part of both walking and running gaits (Roberts and Azizi, 2011). By these mechanisms, some animals can store elastic strain energy from ground reaction forces in elastic tissues, and some studies

have estimated that up to 70% of the kinetic energy delivered during landing could be stored, which can then be used for take-off (Alexander and Vernon, 1975; Blickhan, 1989; Dickinson *et al.*, 2000; Harrison *et al.*, 2010; Roberts and Azizi, 2011). The benefit of a springy gait is that most of the work is done by tendons, which is metabolically cheaper than muscle work. The utilization of tendon elasticity is, however, not completely free as they work in series with muscles and can only act as useful springs when muscles generate force (Roberts and Azizi, 2011). This can be explained thanks to two effects. The “Fenn effect” states that active muscles use more energy when performing positive or negative work than when only generating force (Fenn, 1924). Energy stored in tendons thus reduces the rate of energy consumption of each active muscle fibre by allowing muscles to generate force without doing work, or doing less work (Roberts and Azizi, 2011). The second effect is the influence of tendon mechanisms on the recruited muscle volume. Due to the force-velocity properties of muscles, force can be produced with fewer active muscle fibres if the muscle operates at low or zero shortening velocity (Gabaldon *et al.*, 2008; Roberts *et al.*, 1997). Moreover, this elastic behaviour of the leg can stabilise movement, having the ability to recover from a perturbation with limited, or no change in control strategies (Blickhan *et al.*, 2007; Ghigliazza *et al.*, 2005). Familiar tendon springs, connective tissue elements that hold muscles together, and the molecular constituents of muscles themselves all provide spring-like actions that may significantly influence muscle and locomotor function (Roberts and Azizi, 2011).

For tendon springs to operate effectively, their mechanical properties must be matched to their function. One of the key parameters for elastic mechanisms is tendon stiffness, which is tuned by remodelling to optimize the operation of the muscle-tendon-load system (Roberts and Azizi, 2011). For instance, tendon stiffness increases in response to long-term exercise (Arampatzis *et al.*, 2007; Buchanan and Marsh, 2001). However, there is a lack of consensus on whether such exposure to exercise leads to changes in tendon dimensions, material properties, both or none (Buchanan and Marsh, 2001; Kasashima *et al.*, 2002; Moffat *et al.*, 2008; Seynnes *et al.*, 2009). These studies did demonstrate that tendon properties are more plastic than previously thought (Roberts and Azizi, 2011).

Therefore, the animal’s musculoskeletal system can be considered mechanically as an actively-driven, non-linear, multicomponent spring-mass model. Using this concept, Blickhan (1989) chose to model it with a point mass bouncing passively on a massless spring without viscous losses. The advantages of this model are its simplicity and its transparency with respect to the influence of physical and morphological conditions. This model describes the interdependency of the parameters characterizing running and hopping (Blickhan, 1989; Farley *et al.*, 1993; McMahon and Cheng, 1990; Roberts and

Azizi, 2011). Blickhan (1989) found this model was successful in predicting and describing general features of animal locomotion.

The spring-mass model has been shown to be able to discriminate different gaits and explain some leg responses. For example, human walking and running can be identified by the vertical position of the centre of mass at mid-stance (when the hip of the stance leg passes over the ankle). During walking, the body's centre of mass is at its highest position at mid-stance, whereas it is at its lowest point at mid-stance during running due to the shock-absorbing flexion mechanisms of the knee and hip (Cavagna *et al.*, 1976; McMahon and Cheng, 1990). If the limb is modelled as an inverted pendulum, at walk, work is done to raise the centre of mass in the first half of stance. This raising of the centre of mass results in storage of potential energy, and this is returned as kinetic energy during the second half of the step as the centre of mass falls forward. When running, changes of forward kinetic and gravitational potential energy are in phase and therefore cannot exchange with one another to smooth out fluctuations of total mechanical energy over a step (Cavagna *et al.*, 1976; McMahon and Cheng, 1990). However, that energy can be stored in tendons at mid-stance as elastic energy. These general features of walking and running have been recognised in the gait of birds and quadrupedal mammals, as well as humans (Cavagna *et al.*, 1976; Cavagna *et al.*, 1977). McMahon and Cheng (1990) found good agreement between the experimental records and the calculation of vertical accelerations versus vertical displacement and concluded it supports the validity of the model, even if some differences were observed between experiment and model. The differences observed were: an early rise in vertical force in the experimental records for the man running, followed by a fall, before a rise to a second peak at mid-step; and, take-off occurs when the mass is somewhat higher than it was on landing in the experimental records for the man and the kangaroo.

Another example of the utility of this model relates to the responses to ground perturbations, such as sudden change in surface stiffness, which have been demonstrated to be due, at least in part, to the spring-like behaviour of the leg in human runners. An unexpected change in surface stiffness led to changes in leg stiffness that were faster than typical reflex responses and preceded changes in electromyograph activity. This response was attributed to passive mechanical reactions of the spring-like limb (Moritz and Farley, 2004; Roberts and Azizi, 2011). However, the mechanism of these actions is not very clear. The elastic action of the tendons as well as the action of muscles, but also actions of other elastic elements in series with the muscles, might be involved (Roberts and Azizi, 2011; van der Krogt *et al.*, 2009). The idea that some elastic responses of the support limb are actually explained by active muscle function is supported by studies on guinea fowl and humans (Daley and Biewener, 2006; Ferris *et al.*, 1998; Roberts and Azizi, 2011). Muscles undergoing a stretch-shorten cycle could produce

some of the spring-like function of the leg and might provide some of the rapid mechanical feedback observed experimentally (Ferris *et al.*, 1998; Roberts and Azizi, 2011).

In the specific case of equine locomotion, storage and utilization of elastic strain energy is thought to be particularly significant (Harrison *et al.*, 2010). This property comes in particular from the hyperextension of the fetlock joint, which causes the long digital flexor tendons to stretch and results in the storage and release of elastic strain energy (Biewener, 1998; Harrison *et al.*, 2010).

Due to its anatomical properties, the forelimb can be modelled as two compression springs in series, one for the proximal limb from the scapula to the elbow and one for the distal leg from the elbow to the hoof (McGuigan and Wilson, 2003; Wilson *et al.*, 2001). The distal limb is acting as a passive spring, by the action of the hyperextension of the fetlock joint (Bobbert *et al.*, 2007; Harrison *et al.*, 2010; McGuigan and Wilson, 2003; Witte *et al.*, 2004). The main joints acting on changing the length of the distal limb (127 mm at gallop) are the metacarpophalangeal and distal interphalangeal joints. The extension of the metacarpophalangeal joint is controlled by three main structures; the superficial and deep digital flexors and the suspensory ligament (Dyce *et al.*, 2010). During locomotion, these structures are subject to high strains and forces (Biewener, 1998; Dimery *et al.*, 1986; Meershoek *et al.*, 2001; Stephens *et al.*, 1989) and the suspensory ligament and flexor tendons are the location where 50% of racehorse injuries occur (Williams *et al.*, 2001). The role of the digital flexor muscles are to tension their tendons, and it has been observed that these muscles are able to change their length during gait by only a few millimetres due to their pennation (McGuigan and Wilson, 2003; Wilson *et al.*, 2001). The limb force and metacarpophalangeal joint angle are linked by a linear relationship. McGuigan and Wilson (2003) determined this relationship and used it to predict the vertical ground reaction force during a 12 m.s<sup>-1</sup> gallop on a treadmill.

The proximal limb is more active and its vertical length can change by around 12 mm (McGuigan and Wilson, 2003), caused by the flexion of the shoulder and of the elbow. The extension of the shoulder is controlled by the biceps and supraspinatus and the extension of the elbow by the triceps and the digital flexors (Dyce *et al.*, 2010). The other muscles appear to act as stabilizers or co-contract with the agonists. The possible role of the proximal limb is to tune the properties of the whole limb to adapt its compliance to the ground surface hardness or to complement the distal spring (McGuigan and Wilson, 2003).

To conclude, the spring models allow us to understand the general behaviour of the limb. However, it is worth noting that even if animals' movements are very similar to a spring-mass model, they are not just elastic bouncing with some deviations. One of the limitations is the inability to account for the

differences between take-off and landing; the legs are stiffer during landing than during take-off (Blickhan, 1989). Furthermore, these descriptions do not describe the mechanisms of response of the limb to a change of ground surface. Therefore, another method is needed to model the limb and observe the changes in the mechanical behaviour of discrete joints and tissues, and observe the different roles of each muscle and ligament.

### IV.B. Musculoskeletal model

#### IV.B.1. The different approaches

Musculoskeletal models include segment, joint, muscle-tendon, and ligament information (Swanstrom *et al.*, 2005). There are two different categories of simulation, the forward dynamics approach and the inverse dynamics approach.

The forward dynamic simulation is the calculation of the movement/displacement from forces (Schellenberg *et al.*, 2015). The input data for this approach are a proximal-driving force, a distal ground reaction force model, muscle activations, and initial positions and velocities (Swanstrom *et al.*, 2005). The main difficulty is to find a physiologically feasible set of controls for muscle activity (Schellenberg *et al.*, 2015). OpenSim (National Center for Simulation in Rehabilitation Research, CA) is a software package using this approach (Alamdari and Krovi, 2017; Rajagopal *et al.*, 2016).

The inverse dynamic simulation is the calculation of segment forces and moments from motion capture data. Optimisation functions can be added to this approach to distribute the net intersegmental forces between the different muscles. The advantages of inverse dynamics compared to forward dynamics are that the inverse dynamics simulation is quicker and is relatively computationally inexpensive. The problem with this approach is that the movement is considered as quasi-static to compute the muscle forces when the movement studied is not (Schellenberg *et al.*, 2015). AnyBody Modeling System™ (AnyBody Technology A/S, Denmark) is a software using this approach (Alamdari and Krovi, 2017).

Schellenberg *et al.* (2015) proposed alternative methods combining both inverse and forward approaches or combining electromyography data and joint kinematic data.

#### IV.B.2. Reasons

The reasons for musculoskeletal modelling are to calculate quantities that can otherwise only be measured by invasive means, like muscle tensions and joint contact forces, from components that can be measured by non-invasive means, such as segment kinematics, ground reaction forces and muscle activities using respectively motion capture, force plates and electromyography (Moissenet *et al.*,

2017; Rajagopal *et al.*, 2016). Musculoskeletal models can also be used to understand how muscles coordinate and contribute to body weight support and propulsion, and how muscle coordination impacts joint contact forces (Rajagopal *et al.*, 2016).

The above advantages and usefulness of musculoskeletal models are the reason why they have been developed most frequently for humans and have been used in different fields such as orthopaedic surgery, neurology, sport and ergonomics (Delp *et al.*, 1994; Higginson *et al.*, 2006; Manal and Buchanan, 2005; McLean *et al.*, 2003; Pandy *et al.*, 1990; Paul *et al.*, 2005; Piazza and Delp, 2001; Piazza *et al.*, 2003; Rasmussen *et al.*, 2012; Reinbolt *et al.*, 2009; Steele *et al.*, 2012; To *et al.*, 2005; Van der Krogt *et al.*, 2013; Wu *et al.*, 2009).

In the specific case of equine musculoskeletal models, they have been developed for use in research on the locomotor system (Lawson *et al.*, 2007; McGuigan and Wilson, 2003; Swanstrom *et al.*, 2005), to evaluate or aid diagnosis of clinical problems, and evaluate different interventions (Buchner *et al.*, 1996; Buchner *et al.*, 2003). Equine musculoskeletal models have also been used for teaching or demonstration (Tomlinson *et al.*, 2003).

One of the major interests of equine musculoskeletal models is the possibility to study the loads in muscles, tendons and ligaments, which is important to understand the origin of musculoskeletal injuries (Lawson *et al.*, 2007). A number of studies have measured tendon strain *in vivo* by implanting strain gauge transducers directly in the tendons of live subjects (Butcher *et al.*, 2009; Jansen *et al.*, 1993a; Jansen *et al.*, 1993b; Lochner *et al.*, 1980), but invasive experiments are limited for ethical and practical reasons (Harrison *et al.*, 2010). In particular, attaching strain gauges to the tendons is likely to affect the gait pattern of the animal (Jansen *et al.*, 1998) and the data have not been recorded for all important tendons simultaneously across a wide range of gait speeds (Harrison *et al.*, 2010). Moreover, local measurements of tendon strain may not always accurately reflect the total change in length of the tendon (Harrison *et al.*, 2010). Harrison *et al.* (2010) concluded that musculoskeletal modelling could be more powerful than invasive experiments, if the models can be appropriately validated.

Another use of equine musculoskeletal models is to predict racehorse limb biomechanics on race surfaces prior to installation (Symons *et al.*, 2014b) and to survey the effects of a wide range of race surface mechanical properties (Symons *et al.*, 2016). Indeed, it may be difficult to carry out studies on different racetrack surfaces as their installations are expensive and it is then not feasible to install them just for experiments. Moreover, experimental data collection on live racehorses is difficult, time-consuming and necessitates the use of animals in research (Symons *et al.*, 2016).

#### IV.B.3. Equine musculoskeletal models

Few musculoskeletal models of the equine limb have been proposed and are often limited to the distal limb. Furthermore, many of the models available have only used highly simplified descriptions for their tendon paths (Lawson *et al.*, 2007).

Brown *et al.* (2003b) developed a model comprising eight segments. In this model, the authors did not model the proximal sesamoid bones but they did separate the metacarpus and the distal row of the carpal bones. Based on this model, Harrison *et al.* (2010) created their own model. The forelimb was modelled with eight segments (humerus, radius and ulna, proximal row of carpal bones, distal row of carpal bones and the metacarpus, proximal sesamoid bones, proximal phalanx, middle phalanx, distal phalanx). The soft tissue structure was composed of nine muscle-tendon units (extensor carpi radialis, common digital extensor, lateral digital extensor, ulnaris lateralis, flexor carpi ulnaris, flexor carpi radialis, superficial digital flexor, deep digital flexor, lacertus fibrosus) and six ligamentous structures (interosseous muscle or suspensory ligament, accessory ligament of superficial digital flexor, accessory ligament of deep digital flexor, medial and lateral oblique sesamoidean ligaments, straight sesamoidean ligament, with extensor branches also considered as extensions of interosseous muscle). Symons *et al.* (2016) used the same muscles and added the extensor carpi obliquus. The behaviour of the ligaments and tendons (force-length curves) in Harrison's (2010) model were obtained by fitting polynomial functions to describe experimental data. To create subject-specific models, they scaled the body morphometry and the lengths and paths of the muscle-tendon units to kinematic and morphometric measurements obtained for each animal. They scaled the segmental inertial properties to each animal's weight using regression equations reported by Buchner *et al.* (1997).

The model used by Lawson *et al.* (2007) was a subject-specific, link-segment model written in Matlab™ (Mathworks Inc., MA), taking its input from motion capture, and producing tendon strain calculations and a 3D animation. In their model, they represented the third metacarpal bone, the first, second and third phalanges and the sesamoid bones. The sesamoid bones were modelled to allow a more accurate description of the tendon paths, but their positions were not recorded. Within the model, the palmar sesamoidean ligament was modelled as a rigid body uniting the proximal sesamoid bones into a single, solid structure. The model also included virtual ligaments to tie the proximal and distal sesamoid bones to the proximal and distal phalanges, respectively. The movement of the proximal sesamoid bones was modelled using both their attachment to the proximal phalanx by an isometric ligament and a constraint of remaining in optimal contact with the articular surface of the third metacarpal. The same principles were used to model the movement of the distal sesamoid bones. As the model was limited to the height of the carpus, the proximal origin of the deep digital flexor muscle was not

included but was replaced by a virtual origin at the level of the proximal limit of the model, and following the orientation of the accessory ligament. The insertion of the deep digital flexor tendon was taken as the centroid of its large attachment site on the distal phalanx. To represent the path of the deep digital flexor tendon, they added some wrapping surfaces to constrain the tendons to not penetrating bones. They used the same process for the superficial digital flexor tendon. The suspensory ligament origin was modelled as a point taken at the centre of the broad attachment to the proximal metacarpus and its attachment to the distal row of carpal bones was ignored. A virtual insertion at the midpoint of the insertions of its medial and lateral divisions on the corresponding sesamoid bones was also included.

A major limitation of musculoskeletal models is the accuracy of the model inputs. Carbone *et al.* (2015) stated that the reliability of force predictions is affected by the accuracy, in particular, of the musculoskeletal geometry, which is represented by muscle moment arms and is one of the most sensitive parameters (Hoy *et al.*, 1990; Out *et al.*, 1996). Its estimation depends on the identification of the muscle-tendon lines-of-action (Pal *et al.*, 2007; Rohrle *et al.*, 1984). Moreover, errors in the estimated position of muscle attachment sites have been shown to affect muscle force predictions (Carbone *et al.*, 2012).

Lawson *et al.* (2007) used their model to study the consequences of modifying the superficial and deep digital flexor tendon paths on their strains. They found the computed movement of the proximal sesamoid bones to be in agreement with the one recorded *in vitro*. However, this study was mainly a sensitivity analysis to determine the accuracy needed for insertion and origin sites in musculoskeletal modelling.

Brown *et al.* (2003b) found their model provided good representation of the muscle paths and calculated the moment arm and force generated by each muscle. However, they did not have the opportunity to compare the computed moment arms and forces to real measurements. They reported some differences with data from the literature, in particular at the carpal and metacarpophalangeal joints. Harrison *et al.* (2010) computed the force developed in tendons, muscles and ligaments as well as contact forces in joints. The joint angles, ground reaction forces and net joint torques they computed were in general agreement with results reported in the literature.

Symons *et al.* (2016) combined forward and inverse dynamics in their model. The fetlock and hoof kinematic profiles simulated by this model had similar shapes and comparable peak magnitudes compared to experimental data. The deviations they observed occurred mainly at the end of the

stance phase and after key events such as fetlock hyperextension. They also found the fetlock hyperextension to occur earlier in simulations than in measured data.

### IV.B.4. Modelling challenges

The main challenge in musculoskeletal modelling is to build subject-specific models without intensive and time-consuming manual interventions. To represent different subjects without entirely reconfiguring the model template, it is necessary to scale a generic model. One method is to apply simple linear scaling laws to generic models, which are based on one or more cadaver specimens (Arnold *et al.*, 2010; Delp *et al.*, 1990; Horsman *et al.*, 2007). The problem with this method is that the variability in musculoskeletal geometry between individuals is not taken into account (Duda *et al.*, 1996; White *et al.*, 1989). Several studies have focused on creating subject-specific models based on imaging or functional measurements but their clinical application on a large scale has not been demonstrated (Blemker *et al.*, 2007; Carbone *et al.*, 2015; Hainisch *et al.*, 2012; Hausselle *et al.*, 2014; Scheys *et al.*, 2011). Another scaling method is to use the medical images of the individual subject and incorporate them in the generic model (Carbone *et al.*, 2013; Pellikaan *et al.*, 2014).

A challenge specific to equine limb musculoskeletal modelling is to represent the stay apparatus. Indeed, the interactions between the digital flexor muscles and their accessory ligaments have not been studied when a detailed mathematical model of these interactions are necessary to determine accurately the forces generated by the muscles, tendons and ligaments and for a thorough analysis of the work done by each of these structures (Harrison *et al.*, 2010).

To conclude, spring models are good approximations for kinematic and energy studies, with the properties of the spring linked to the morphometry of the animal. The problem with this type of model is its inability to describe the roles of the different elements of the leg (muscles, ligaments, etc.) and their interactions. Therefore, the spring model cannot be used for understanding musculoskeletal injury mechanisms. Musculoskeletal models are more adapted for this purpose. The equine models developed so far have largely been limited to the distal limb. The objective of this study is to develop a preliminary 3D musculoskeletal model of the whole equine forelimb to study the effects of the perturbations on the limb response and to assess whether the response occurs acutely in the perturbed stance phase or in the next stance phase. Moreover, the model developed will include the proximal limb, and then it will take into account the interactions between the two parts of the limb.

## V. Conclusion

The Thoroughbred industry is the most economically important part of the New Zealand equine industry (Rogers *et al.*, 2017). Unfortunately, within the industry there is significant wastage with

musculoskeletal injury accounting for the majority of the losses of horses and training days (Perkins *et al.*, 2004b).

Thoroughbred racehorses are most often affected by musculoskeletal injuries of the forelimb, which are the main cause of involuntary retirement, death and rest periods for rehabilitation (Bolwell *et al.*, 2017b; Parkin, 2008; Perkins *et al.*, 2004b). These musculoskeletal injuries have economic costs through medical or surgical care, time lost from racing as well as public perception (Perkins *et al.*, 2004b).

A number of studies have focused on identifying risk factors and on how to reduce the risk of musculoskeletal injuries. Track surfaces have been recognized as one of the main modifiable risk factors (Peterson *et al.*, 2008; Robin *et al.*, 2009; Setterbo *et al.*, 2011). For this reason, racetrack surface is one of the major areas of research (Parkin, 2008). Despite the number of studies on this topic, the relationships between racetrack surface type, properties and the risk of injuries are very complex and remain unclear. In some situations, changing racetrack surface properties could then decrease the risk of one type of musculoskeletal injury but increase another type (Parkin, 2008).

For this reason, it is necessary to understand how tendons and ligaments transmitting force in the limb respond to different surface properties. It should then be possible to determine the properties reducing the risk of a specific musculoskeletal injury while checking they are not increasing the risk of musculoskeletal injury in another element of the limb. The best way to answer these questions is to use a musculoskeletal model. Indeed, they have been developed to illustrate and understand how animals interact with the environment (Alexander, 2003) but allow also to study the loads in muscles, tendons and ligaments, which is important to understand the origin of musculoskeletal injuries (Lawson *et al.*, 2007). To date, the equine musculoskeletal models developed have focused mostly on the distal limb. Therefore, as stated in the Introduction, the objectives of this study were to:

- To develop a preliminary 3D musculoskeletal model of the whole equine forelimb based on data published in the literature and derived from anatomical measurements (Part 1)
- To determine the effects of the perturbations by the ground surface on the limb response with the musculoskeletal model developed and to assess whether the response occurs acutely in the perturbed stance phase or in the next stance phase (Part 2)

This project has been approved by Massey University Animal Ethics Committee (MUAEC Protocol 17/20).

## VI. References

- Alamdari, A. and Krovi, V. N. (2017) 'Chapter 2, A review of computational musculoskeletal analysis of human lower extremities', In Ueda, J. and Kurita, Y. (eds.) *Human Modelling for Bio-inspired Robotics: Mechanical Engineering in Assistive Technologies*: Academic Press, pp. 37-73.
- Alexander, R. M. and Vernon, A. (1975) 'The mechanics of hopping by kangaroos (Macropodidae)', *Journal of Zoology*, 177(2), pp. 265-303.
- Alexander, R. M. (2003) 'Modelling approaches in biomechanics', *Philosophical Transactions: Biological Sciences*, 358(1437), pp. 1429-1435.
- Arampatzis, A., Karamanidis, K., Morey-Klapsing, G., De Monte, G. and Stafiliadis, S. (2007) 'Mechanical properties of the triceps surae tendon and aponeurosis in relation to intensity of sport activity', *Journal of Biomechanics*, 40(9), pp. 1946-1952.
- Arnold, E. M., Ward, S. R., Lieber, R. L. and Delp, S. L. (2010) 'A model of the lower limb for analysis of human movement', *Annals of Biomedical Engineering*, 38(2), pp. 269-279.
- Arthur, R. M. (2010) 'Comparison of racing fatality rates on dirt, synthetic, and turf at four California racetracks', *Proceedings of 56th Annual Convention of the American Association of Equine Practitioners*, 56, pp. 405-408.
- Back, W., Schamhardt, H. C., Savelberg, H. H. C. M., Van den Bogert, A. J., Bruin, G., Hartman, W. and Barneveld, A. (1995) 'How the horse moves: 1. Significance of graphical representations of equine forelimb kinematics', *Equine Veterinary Journal*, 27(1), pp. 31-38.
- Barrey, E. (1990) 'Investigation of the vertical hoof force distribution in the equine forelimb with an instrumented horseboot', *Equine Veterinary Journal*, 22(S9), pp. 35-38.
- Barrey, E., Landjerit, B. and Wolter, R. 'Shock and vibration during the hoof impact on different track surfaces'. *Equine Exercise Physiology. International Conference on Equine Exercise Physiology*, 97-106.
- Biewener, A. A. (1998) 'Muscle-tendon stresses and elastic energy storage during locomotion in the horse', *Comparative Biochemistry and Physiology Part B: Biochemistry and Molecular Biology*, 120(1), pp. 73-87.
- Biewener, A. A. (2003) *Animal Locomotion. Oxford animal biology series* Oxford Oxford University Press, p. 48-50.
- Bjorck, G. (1958) 'Studies on the draught forces of horses: development of a method using strain gauges for measuring forces between hoof and ground', *Acta agriculturae Scandinavica* 8, Supplement 4.
- Blemker, S. S., Asakawa, D. S., Gold, G. E. and Delp, S. L. (2007) 'Image-based musculoskeletal modeling: Applications, advances, and future opportunities', *Journal of Magnetic Resonance Imaging*, 25(2), pp. 441-451.
- Blickhan, R. (1989) 'The spring-mass model for running and hopping', *Journal of Biomechanics*, 22(11-12), pp. 1217-1227.
- Blickhan, R., Seyfarth, A., Geyer, H., Grimmer, S., Wagner, H. and Gunther, M. (2007) 'Intelligence by mechanics', *Philosophical transactions. Series A, Mathematical, physical, and engineering sciences*, 365(1850), pp. 199-220.
- Bobbert, M. F., Gomez Alvarez, C. B., van Weeren, P. R., Roepstorff, L. and Weishaupt, M. A. (2007) 'Validation of vertical ground reaction forces on individual limbs calculated from kinematics of horse locomotion', *Journal of Experimental Biology*, 210(11), pp. 1885-1896.
- Bolwell, C. F., Rogers, C. W., Gee, E. K. and Rosanowski, S. M. (2016) 'Descriptive statistics and the pattern of horse racing in New Zealand. 1. Thoroughbred racing', *Animal Production Science*, 56(1), pp. 77-81.
- Bolwell, C. F., Rogers, C. W., Gee, E. K. and Rosanowski, S. M. (2017a) 'Commercial equine production in New Zealand. 3. The racing and sport industries', *Animal Production Science*.
- Bolwell, C. F., Rogers, C. W., Gee, E. K. and McIlwraith, C. W. (2017b) 'Epidemiology of musculoskeletal injury during racing on New Zealand racetracks 2005-2011', *Animals*, 7(8), pp. 62.

- Brown, N. A. T., Pandy, M. G., Kawcak, C. E. and McIlwraith, C. W. (2003b) 'Force- and moment-generating capacities of muscles in the distal forelimb of the horse', *Journal of Anatomy*, 203(1), pp. 101-113.
- Buchanan, C. I. and Marsh, R. L. (2001) 'Effects of long-term exercise on the biomechanical properties of the Achilles tendon of guinea fowl', *Journal of Applied Physiology*, 90(1), pp. 164-171.
- Buchner, H. H. F., Savelberg, H. H. C. M., Schamhardt, H. C. and Barneveld, A. (1996) 'Limb movement adaptations in horses with experimentally induced fore- or hindlimb lameness', *Equine Veterinary Journal*, 28(1), pp. 63-70.
- Buchner, H. H. F., Savelberg, H. H. C. M., Schamhardt, H. C. and Barneveld, A. (1997) 'Inertial properties of Dutch warmblood horses', *Journal of Biomechanics*, 30(6), pp. 653-658.
- Buchner, H. H. F., Obermuller, S. and Scheidl, M. (2003) 'Load distribution in equine lameness: a centre of mass analysis at the walk and the trot', *Pferdeheilkunde*, 19(5), pp. 491-499.
- Butcher, M. T., Hermanson, J. W., Ducharme, N. G., Mitchell, L. M., Soderholm, L. V. and Bertram, J. E. A. (2009) 'Contractile behavior of the forelimb digital flexors during steady-state locomotion in horses (*Equus caballus*): An initial test of muscle architectural hypotheses about in vivo function', *Comparative Biochemistry and Physiology Part A: Molecular & Integrative Physiology*, 152(1), pp. 100-114.
- Carbone, V., Van der Krogt, M. M., Koopman, H. F. J. M. and Verdonshot, N. (2012) 'Sensitivity of subject-specific models to errors in musculo-skeletal geometry', *Journal of Biomechanics*, 45(14), pp. 2476-2480.
- Carbone, V., Van der Krogt, M. M., Vigneron, L., Schepers, J., Kolk, S., Koopman, B. and Verdonshot, N. 'A streamlined modeling workflow to obtain subject-specific musculoskeletal models of lower extremity based on MRI scan and dynamometry'. *XXIV Congress of the International Society of Biomechanics*.
- Carbone, V., Fluit, R., Pellikaan, P., Krogt, M. M. v. d., Janssen, D., Damsgaard, M., Vigneron, L., Feilkas, T., Koopman, H. F. J. M. and Verdonshot, N. (2015) 'TLEM 2.0 – A comprehensive musculoskeletal geometry dataset for subject-specific modeling of lower extremity', *Journal of Biomechanics*, 48(5), pp. 734-741.
- Cavagna, G. A., Thys, H. and Zamboni, A. (1976) 'The sources of external work in level walking and running', *The Journal of Physiology*, 262(3), pp. 639-657.
- Cavagna, G. A., Heglund, N. C. and Taylor, C. R. (1977) 'Mechanical work in terrestrial locomotion: two basic mechanisms for minimizing energy expenditure', *American Journal of Physiology*, 233(5), pp. 243-261.
- Chateau, H., Robin, D., Simonelli, T., Pacquet, L., Pourcelot, P., Falala, S., Denoix, J.-M. and Crevier-Denoix, N. (2009a) 'Design and validation of a dynamometric horseshoe for the measurement of three-dimensional ground reaction force on a moving horse', *Journal of Biomechanics*, 42(3), pp. 336-340.
- Chateau, H., Robin, D., Falala, S., Pourcelot, P., Valette, J. P., Ravary, B., Denoix, J.-M. and Crevier-Denoix, N. (2009b) 'Effects of a synthetic all-weather waxed track versus a crushed sand track on 3D acceleration of the front hoof in three horses trotting at high speed', *Equine Veterinary Journal*, 41(3), pp. 247-251.
- Chateau, H., Holden, L., Robin, D., Falala, S., Pourcelot, P., Estoup, P., Denoix, J.-M. and Crevier-Denoix, N. (2010) 'Biomechanical analysis of hoof landing and stride parameters in harness trotter horses running on different tracks of a sand beach (from wet to dry) and on an asphalt road', *Equine Veterinary Journal* 42(S38), pp. 488-495.
- Cheney, J. A., Shen, C. K. and Wheat, J. D. (1973) 'Relationship of racetrack surface to lameness in the Thoroughbred racehorse', *American Journal of Veterinary Research*, 34(10), pp. 1285-1289.
- Clanton, C., Kobluk, C., Robinson, R. A. and Gordon, B. (1991) 'Monitoring surface conditions of a Thoroughbred racetrack', *Journal of the American Veterinary Medical Association*, 198(4), pp. 613-620.

- Clayton, H. M. (2004) *The Dynamic Horse : A Biomechanical Guide To Equine Movement And Performance*. Mason, MI: Sport Horse Publications.
- Clegg, P. D. (2011) 'Musculoskeletal disease and injury, now and in the future. Part 1: Fractures and fatalities', *Equine Veterinary Journal*, 43(6), pp. 643-649.
- Crevier-Denoix, N., Pourcelot, P., Ravary, B., Robin, D., Falala, S., Uzel, S., Grison, A.-C., Valette, J.-P., Denoix, J.-M. and Chateau, H. (2009) 'Influence of track surface on the equine superficial digital flexor tendon loading in two horses at high speed trot', *Equine Veterinary Journal*, 41(3), pp. 257-261.
- Crevier-Denoix, N., Pourcelot, P., Holden-Douilly, L., Camus, M., Falala, S., Ravary-Plumioën, B., Vergari, C., Desquilbet, L. and Chateau, H. (2013b) 'Discrimination of two equine racing surfaces based on forelimb dynamic and hoof kinematic variables at the canter', *The Veterinary Journal* 198(S1), pp. 124-129.
- Daley, M. A. and Biewener, A. A. (2006) 'Running over rough terrain reveals limb control for intrinsic stability', *Proceedings of the National Academy of Sciences of the United States of America*, 103(42), pp. 15681-15686.
- Delp, S. L., Loan, J. P., Hoy, M. G., Zajac, F. E., Topp, E. L. and Rosen, J. M. (1990) 'An interactive graphics-based model of the lower extremity to study orthopaedic surgical procedures', *IEEE Transactions on Biomedical Engineering*, 37(8), pp. 757-767.
- Delp, S. L., Komattu, A. V. and Wixson, R. L. (1994) 'Superior displacement of the hip in total joint replacement: Effects of prosthetic neck length, neck-stem angle, and anteversion angle on the moment-generating capacity of the muscles', *Journal of Orthopaedic Research*, 12(6), pp. 860-870.
- Dickinson, M. H., Farley, C. T., Full, R. J., Koehl, M. A. R., Kram, R. and Lehman, S. (2000) 'How animals move: an integrative view', *Science*, 288(5463), pp. 100-106.
- Dimery, N. J., Alexander, R. M. and Ker, R. F. (1986) 'Elastic extension of leg tendons in the locomotion of horses (*Equus caballus*)', *Journal of Zoology*, 210(3), pp. 415-425.
- Drevemo, S. and Hjerten, G. 'Evaluation of a shock absorbing woodchip layer on a harness race-track'. *Equine Exercise Physiology. International Conference on Equine Exercise Physiology*, 107-102.
- Drevemo, S., Hjerten, G. and Johnston, C. (1994) 'Drop hammer tests of Scandinavian harness racetracks', *Equine Veterinary Journal*, 26(S17), pp. 35-38.
- Duda, G. N., Brand, D., Freitag, S., Lierse, W. and Schneider, E. (1996) 'Variability of femoral muscle attachments', *Journal of Biomechanics*, 29(9), pp. 1185-1190.
- Dyce, K. M., Sack, W. O. and Wensing, C. J. G. (2010) *Textbook of Veterinary Anatomy, 4th Edition*. W. B. Saunders.
- Dyrhe-Poulsen, P., Smedegaard, H. H., Roed, J. and Korsgaard, E. (1994) 'Equine hoof function investigated by pressure transducers inside the hoof and accelerometers mounted on the first phalanx', *Equine Veterinary Journal*, 26(5), pp. 362-366.
- Farley, C. T., Glasheen, J. and McMahon, T. A. (1993) 'Running springs: speed and animal size', *The journal of Experimental Biology*, 185(1), pp. 71-86.
- Fenn, W. O. (1924) 'The relation between the work performed and the energy liberated in muscular contraction', *The Journal of Physiology*, 58(6), pp. 373-395.
- Ferris, D. P., Louie, M. and Farley, C. T. (1998) 'Running in the real world: adjusting leg stiffness for different surfaces', *Proceedings of the Royal Society B: Biological Sciences*, 265(1400), pp. 989-994.
- Frederick, F. H. and Henderson, J. M. (1970) 'Impact force measurement using preloaded transducers', *American Journal of Veterinary Research*, 31(12), pp. 2279-2283.
- Gabalton, A. M., Nelson, F. E. and Roberts, T. J. (2008) 'Relative shortening velocity in locomotor muscles: turkey ankle extensors operate at low  $V/V_{max}$ ', *American Journal of Physiology. Regulatory, integrative and comparative physiology*, 294(1), pp. R200-R210.
- Gee, E. K., Rogers, C. W. and Bolwell, C. F. (2017) 'Commercial equine production in New Zealand. 1. Reproduction and breeding', *Animal Production Science*.

- Ghigliazza, R. M., Altendorfer, R., Holmes, P. and Koditschek, D. (2005) 'A simply stabilized running model', *SIAM Review*, 47(3), pp. 519-549.
- Gustas, P., Johnston, C., Roepstorff, L. and Drevemo, S. (2001) 'In vivo transmission of impact shock waves in the distal forelimb of the horse', *Equine Veterinary Journal*, 33(S33), pp. 11-15.
- Gustas, P., Johnston, C., Roepstorff, L., Drevemo, S. and Lanshammar, H. (2004) 'Relationships between fore- and hindlimb ground reaction force and hoof deceleration patterns in trotting horses', *Equine Veterinary Journal*, 36(8), pp. 737-742.
- Gustas, P., Johnston, C. and Drevemo, S. (2006b) 'Ground reaction force and hoof deceleration patterns on two different surfaces at the trot', *Equine and Comparative Exercise Physiology*, 3(4), pp. 209-216.
- Hainisch, R., Gfoehler, M., Zubayer-UI-Karim, M. and Pandy, M. G. (2012) 'Method for determining musculotendon parameters in subject-specific musculoskeletal models of children developed from MRI data', *Multibody System Dynamics*, 28(1-2), pp. 143-146.
- Harrison, S. M., Whitton, R. C., Kawcak, C. E., Stover, S. M. and Pandy, M. G. (2010) 'Relationship between muscle forces, joint loading and utilization of elastic strain energy in equine locomotion', *The Journal of Experimental Biology*, 213(Pt23), pp. 3998-4009.
- Hausselle, J., Assi, A., El Helou, A., Jolivet, E., Pillet, H., Dion, E., Bonneau, D. and Skalli, W. (2014) 'Subject-specific musculoskeletal model of the lower limb in a lying and standing position', *Computer Methods in Biomechanics and Biomedical Engineering*, 17(5), pp. 480-487.
- Heglund, N. C., Cavagna, G. A. and Taylor, C. R. (1982) 'Energetics and mechanics of terrestrial locomotion. III. Energy changes of the center of mass as a function of speed and body size in birds and mammals', *Journal of Experimental Biology*, 97(1), pp. 41-56.
- Heglund, N. C. and Taylor, C. R. (1988) 'Speed, stride frequency and energy cost per stride: how do they change with size and gait?', *Journal of Experimental Biology*, 138(1), pp. 301-318.
- Herzog, W. and Leonard, T. R. (1991) 'Validation of optimization models that estimate the forces exerted by synergistic muscles', *Journal of Biomechanics*, 24(S1), pp. 31-39.
- Higginson, J. S., Zajac, F. E., Neptune, R. R., Kautz, S. A. and Delp, S. L. (2006) 'Muscle contributions to support during gait in an individual with post-stroke hemiparesis', *Journal of Biomechanics*, 39(10), pp. 1769-1777.
- Hill, T., Carmichael, D., Maylie, G. and Krook, L. (1986) 'Track condition and racing injuries in Thoroughbred horses', *The Cornell veterinarian*, 76(4), pp. 361-379.
- Hill, W. T. (2003) 'Survey of injuries in Thoroughbreds at the New York Racing Association tracks', *Clinical Techniques in Equine Practice*, 2(4), pp. 323-328.
- Hitchens, P. L., Morrice-West, A. V., Stevenson, M. A. and Whitton, R. C. (2019) 'Meta-analysis of risk factors for racehorse catastrophic musculoskeletal injury in flat racing', *The Veterinary Journal*, 245, pp. 29-40.
- Hjerten, G. and Drevemo, S. (1994) 'Semi-quantitative analysis of hoofstrike in the horse', *Journal of Biomechanics*, 27(8), pp. 997-1004.
- Horsman, M. D. K., Koopman, H. F. J. M., Helm, F. C. T. v. d., Prose, L. P. and Veeger, H. E. J. (2007) 'Morphological muscle and joint parameters for musculoskeletal modelling of the lower extremity', *Clinical Biomechanics*, 22(2), pp. 239-247.
- Hoy, M. G., Zajac, F. E. and Gordon, M. E. (1990) 'A musculoskeletal model of the human lower extremity: The effect of muscle, tendon, and moment arm on the moment-angle relationship of musculotendon actuators at the hip, knee, and ankle', *Journal of Biomechanics*, 23(2), pp. 157-169.
- Jansen, M. O., Van den Bogert, A. J., Riemersma, D. J. and Schamhardt, H. C. (1993a) 'In vivo tendon forces in the forelimb of ponies at the walk, validated by ground reaction force measurements', *Acta Anatomica*, 146(2-3), pp. 162-167.
- Jansen, M. O., van Buiten, A., Van den Bogert, A. J. and Schamhardt, H. C. (1993b) 'Strain of the musculus interosseus medius and its rami extensorii in the horse, deduced from in vivo kinematics', *Acta Anatomica*, 147(2), pp. 118-124.

- Jansen, M. O., Schamhardt, H. C., van den Bogert, A. J. and Hartman, W. (1998) 'Mechanical properties of the tendinous equine interosseus muscle are affected by in vivo transducer implantation', *Journal of Biomechanics*, 31(5), pp. 485-490.
- Johnston, C., Roepstorff, L., Drevemo, S. and Roneus, N. (1995) 'Kinematics of the distal forelimb during the stance phase in the fast trotting Standardbred', *Equine Veterinary Journal*, 27(S18), pp. 170-174.
- Johnston, C. and Back, W. (2006) 'Hoof ground interaction: when biomechanical stimuli challenge the tissues of the distal limb', *Equine Veterinary Journal*, 38(7), pp. 634-641.
- Kai, M., Takahashi, T., Aoki, O. and Oki, H. (1999) 'Influence of rough track surfaces on components of vertical forces in cantering Thoroughbred horses', *Equine Veterinary Journal*, 31(S30), pp. 214-217.
- Kai, M., Aoki, O., Hiraga, A., Oki, H. and Tokuriki, M. (2000) 'Use of an instrument sandwiched between the hoof and shoe to measure vertical ground reaction forces and three-dimensional acceleration at the walk, trot, and canter in horses', *American Journal of Veterinary Research*, 61(8), pp. 979-985.
- Kane, A. J., Stover, S. M., Gardner, I. A., Case, J. T., Johnson, B. J., Read, D. H. and Ardans, A. (1996) 'Horseshoe characteristics as possible risk factors for fatal musculoskeletal injury of Thoroughbred racehorses', *American Journal of Veterinary Research*, 57(8), pp. 1147-1152.
- Kasashima, Y., Smith, R. K. W., Birch, H. L., Takahashi, T., Kusano, H. and Goodship, A. E. (2002) 'Exercise-induced tendon hypertrophy: cross-sectional area changes during growth are influenced by exercise', *Equine Veterinary Journal*, 34(S34), pp. 264-268.
- Ker, R. F. (1981) 'Dynamic tensile properties of the plantaris tendon of sheep (*Ovis aries*)', *Journal of Experimental Biology*, 93(1), pp. 283-302.
- Lahm, A., Uhl, M., Haberstroh, J. and Mrosek, E. (2004) 'Articular cartilage degeneration after acute subchondral bone damage. An experimental study in dogs with histopathological grading', *Acta Orthopaedica Scandinavica*, 75(6), pp. 762-767.
- Lahm, A., Uhl, M., Edlich, M., Erggelet, C., Haberstroh, J. and Kreuz, P. C. (2005) 'An experimental canine model for subchondral lesions of the knee joint', *The Knee*, 12(1), pp. 51-55.
- Lanovaz, J. L., Clayton, H. M. and Watson, L. G. (1998) 'In vitro attenuation of impact shock in equine digits', *Equine Veterinary Journal*, 30(S26), pp. 96-102.
- Larkin, M. (2011) 'Racetrack surfaces just one factor in horse racing fatalities', *Journal of the American Veterinary Medical Association*, 238(5), pp. 550-551.
- Lawson, S. E. M., Chateau, H., Pourcelot, P., Denoix, J.-M. and Crevier-Denoix, N. (2007) 'Sensitivity of an equine distal limb model to perturbations in tendon paths, origins and insertions', *Journal of Biomechanics*, 40(11), pp. 2510-2516.
- Le Jeune, S. S., MacDonald, M. H., Stover, S. M., Taylor, K. T. and Gerdes, M. (2003) 'Biomechanical investigation of the association between suspensory ligament injury and lateral condylar fracture in Thoroughbred racehorses', *Veterinary Surgery*, 32(6), pp. 585-597.
- Lochner, F. K., Milne, D. W., Mills, E. J. and Groom, J. J. (1980) 'In vivo and in vitro measurement of tendon strain in the horse', *American Journal of Veterinary Research*, 41(12), pp. 1929-1937.
- Mahaffey, C. A., Peterson, M. L. and Roepstorff, L. (2013) 'The effects of varying cushion depth on dynamic loading in shallow sand thoroughbred horse dirt racetracks', *Biosystem Engineering*, 114(2), pp. 178-186.
- Manal, K. and Buchanan, T. S. (2005) 'Use of an EMG-driven biomechanical model to study virtual injuries', *Medicine and Science in Sports and Exercise*, 37(11), pp. 1917-1923.
- McGuigan, M. P. and Wilson, A. M. (2003) 'The effect of gait and digital flexor muscle activation on limb compliance in the forelimb of the horses *Equus caballus*', *The journal of Experimental Biology*, 206(Pt8), pp. 1325-1336.
- McLean, S. G., Su, A. and Van den Bogert, A. J. (2003) 'Development and validation of a 3-D model to predict knee joint loading during dynamic movement', *Journal of Biomechanical Engineering*, 125(6), pp. 864-874.

- McMahon, T. A. (1985) 'The role of compliance in mammalian running gaits', *Journal of Experimental Biology*, 115(1), pp. 263-282.
- McMahon, T. A. and Cheng, G. C. (1990) 'The mechanics of running: how does stiffness couple with speed?', *Journal of biomechanics*, 23(S1), pp. 65-78.
- Meershoek, L. S., Schamhardt, H. C., Roepstorff, L. and Johnston, C. (2001) 'Forelimb tendon loading during jumping landings and the influence of fence height', *Equine Veterinary Journal*, 33(S33), pp. 6-10.
- Merkens, H. W., Schamhardt, H. C., Van Osch, G. J. and Hartman, W. (1993) 'Ground reaction force patterns of Dutch Warmbloods at the canter', *American Journal of Veterinary Research*, 54(5), pp. 670-674.
- Merkens, H. W. and Schamhardt, H. C. (1994) 'Relationships between ground reaction force patterns and kinematics in the walking and trotting horse', *Equine Veterinary Journal*, 26(S17), pp. 67-70.
- Moffat, P. A., Firth, E. C., Rogers, C. W., Smith, R. K. W., Barneveld, A., Goodship, A. E., Kawcak, C. E., McIlwraith, C. W. and Van Weeren, P. R. (2008) 'The influence of exercise during growth on ultrasonographic parameters of the superficial digital flexor tendon of young Thoroughbred horses', *Equine Veterinary Journal*, 40(2), pp. 136-140.
- Mohammed, H. O., Hill, T. and Lowe, J. (1991) 'Risk factors associated with injuries in Thoroughbred horses', *Equine Veterinary Journal*, 23(6), pp. 445-448.
- Mohammed, H. O., Hill, T. and Lowe, J. (1992) 'The risk of severity of limb injuries in racing Thoroughbred horses', *The Cornell veterinarian*, 82(3), pp. 331-341.
- Moissenet, F., Modenese, L. and Dumas, R. (2017) 'Alterations of musculoskeletal models for a more accurate estimation of lower limb joint contact forces during normal gait: A systematic review', *Journal of Biomechanics*, 63, pp. 8-20.
- Moritz, C. T. and Farley, C. T. (2004) 'Passive dynamics change leg mechanics for an unexpected surface during human hopping', *Journal of Applied Physiology*, 97(4), pp. 1313-1322.
- Oikawa, M., Inada, S., Fujisawa, A., Yamakawa, H. and Asano, M. (2000) 'The use of a racetrack hardness measurement system', *Equine Practice*, 22(4), pp. 22-29.
- Oosterlinck, M., Pille, F., Huppes, T., Gasthuys, F. and Back, W. (2010a) 'Comparison of pressure plate and force plate gaits kinetics in sound Warmblood at walk and trot', *The Veterinary Journal*, 186(3), pp. 347-351.
- Oosterlinck, M., Pille, F., Back, W., Dewulf, J. and Gasthuys, F. (2010b) 'Use of a stand-alone pressure plate for the objective evaluation of forelimb symmetry in sound ponies at walk and trot', *The Veterinary Journal*, 183(3), pp. 305-309.
- Out, L., Vrijkotte, T. G., van Soest, A. J. and Bobbert, M. F. (1996) 'Influence of the parameters of a human triceps surae muscle model on the isometric torque-angle relationship', *Journal of Biomechanical Engineering*, 118(1), pp. 17-25.
- Pal, S., Langenderfer, J. E., Q., S. J., Laz, P. J., Petrella, A. J. and Rullkoetter, P. J. (2007) 'Probabilistic modeling of knee muscle moment arms: effects of methods, origin-insertion, and kinematic variability', *Annals of Biomedical Engineering*, 35(9), pp. 1632-1642.
- Palmer, J. L., Bertone, A. L., Malemud, C. J. and Mansour, J. (1996) 'Biochemical and biomechanical alterations in equine articular cartilage following an experimentally-induced synovitis', *Osteoarthritis and Cartilage*, 4(2), pp. 127-137.
- Pandy, M. G., Zajac, F. E., Sim, E. and Levine, W. S. (1990) 'An optimal control model for maximum-height human jumping', *Journal of Biomechanics*, 23(12), pp. 1185-1198.
- Pandy, M. G. and Zajac, F. E. (1991) 'Optimal muscular coordination strategies for jumping', *Journal of Biomechanics*, 24(1), pp. 1-10.
- Pandy, M. G. (2001) 'Computer modeling and simulation of human movement', *Annual Review of Biomedical Engineering*, 3, pp. 245-273.
- Pandy, M. G. and Andriacchi, T. P. (2010) 'Muscle and joint function in human locomotion', *Annual Review of Biomedical Engineering*, 12, pp. 401-433.

- Parkin, T., Clegg, P. D., French, N. P., Proudman, C. J., Riggs, C. M., Singer, E. R., Webbon, P. M. and Morgan, K. L. (2004a) 'Race- and course-level risk factors for fatal distal limb fracture in racing Thoroughbreds', *Equine Veterinary Journal*, 36(6), pp. 521-526.
- Parkin, T., French, N. P., Riggs, C. M., Morgan, K. L., Clegg, P. D., Proudman, C. J., Singer, E. R. and Webbon, P. M. (2004b) 'Risk of fatal distal limb fractures among Thoroughbreds involved in the five types of racing in the United Kingdom', *Veterinary Record*, 154(16), pp. 493-497.
- Parkin, T. (2008) 'Epidemiology of racetrack injuries in racehorses', *Veterinary Clinics of North America: Equine Practice*, 24(1), pp. 1-19.
- Parsons, K. J., Spence, A. J., Morgan, R., Thompson, J. A. and Wilson, A. M. (2011) 'High speed field kinematics of foot contact in elite galloping horses in training', *Equine Veterinary Journal*, 43(2), pp. 216-222.
- Paul, C., Belloti, M., Jezernik, S. and Curt, A. (2005) 'Development of a human neuro-musculo-skeletal model for investigation of spinal cord injury', *Biological Cybernetics*, 93(3), pp. 153-170.
- Pellikaan, P., Van der Krogt, M. M., Carbone, V., Fluit, R., Vigneron, L., Van Deun, J., Verdonshot, N. and Koopman, H. F. J. M. (2014) 'Evaluation of a morphing based method to estimate muscle attachment sites of the lower extremity', *Journal of Biomechanics*, 47(5), pp. 1144-1150.
- Pennycuik, C. J. (1975) 'On the running of the gnu (*Connochaetes taurinus*) and other animals', *Journal of Experimental Biology*, 63(3), pp. 775-799.
- Perkins, N. R., Reid, S. W. and Morris, R. S. (2004a) 'Effect of training location and time period on racehorse performance in New Zealand. 1. Descriptive analysis', *New Zealand Veterinary Journal*, 52(5), pp. 236-242.
- Perkins, N. R., Reid, S. W. and Morris, R. S. (2004b) 'Profiling the New Zealand Thoroughbred racing industry. 2. Conditions interfering with training and racing', *New Zealand Veterinary Journal*, 53(1), pp. 69-76.
- Peterson, M. L., McIlwraith, C. W. and Reiser, R. F. (2008) 'Development of a system for the in-situ characterisation of Thoroughbred horse racing track surfaces', *Biosystem Engineering*, 101(2), pp. 260-269.
- Peterson, M. L. and McIlwraith, C. W. (2008) 'Effect of track maintenance on mechanical properties of a dirt racetrack: A preliminary study', *Equine Veterinary Journal* 40(6), pp. 602-605.
- Peterson, M. L., Reiser, R. F., Kuo, P.-H., Radford, D. W. and McIlwraith, C. W. (2010) 'Effect of temperature on race times on a synthetic surface', *Equine Veterinary Journal*, 42(4), pp. 351-357.
- Piazza, S. J. and Delp, S. L. (2001) 'Three-dimensional dynamic simulation of total knee replacement motion during a step-up task', *Journal of Biomechanical Engineering*, 123(6), pp. 599-606.
- Piazza, S. J., Adamson, R. L., Moran, M. F., Sanders, J. O. and Sharkey, N. A. (2003) 'Effects of tensioning errors in split transfers of tibialis anterior and posterior tendons', *The Journal of bone and joint surgery*, 85(5), pp. 858-865.
- Pratt, G. W. and O'Connor, J. T. (1976) 'Force plate studies of equine biomechanics', *American Journal of Veterinary Research*, 37(11), pp. 1251-1255.
- Pratt, G. W. 'Racing surfaces: A survey of mechanical behavior'. *Proceedings of the annual convention of the American Association of Equine Practitioners. Annual convention of the American Association of Equine Practitioners*, 321-331.
- Pratt, G. W. (1985) 'Racetrack surface biomechanics', *Equine Veterinary Data*, 6(13), pp. 193-202.
- Pratt, G. W. (1997) 'Model for injury to the foreleg of the Thoroughbred racehorse', *Equine Veterinary Journal*, 29(S23), pp. 30-32.
- Radin, E. L., Parker, H. G., Pugh, J. W., Steinberg, R. S., Paul, I. L. and Rose, R. M. (1973) 'Response of joints to impact loading - III. Relationship between trabecular microfractures and cartilage degeneration', *Journal of Biomechanics*, 6(1), pp. 51-54.
- Radin, E. L., Yang, K. H., Riegger, C., Kish, V. L. and O'Connor, J. J. (1991) 'Relationship between lower limb dynamics and knee joint pain', *Journal of Orthopaedic Research*, 9(3), pp. 398-405.

- Radin, E. L. (1999) 'Subchondral bone changes and cartilage damage', *Equine Veterinary Journal*, 31(2), pp. 94-95.
- Rajagopal, A., Dembia, C. L., DeMers, M. S., Delp, D. D., Hicks, J. L. and Delp, S. L. (2016) 'Full body musculoskeletal model for muscle-driven simulation of human gait', *IEEE Transactions on Biomedical Engineering*, 63(10), pp. 2068-2079.
- Ramzan, P. H. L. and Palmer, L. (2011) 'Musculoskeletal injuries in Thoroughbred racehorses: A study of three large training yards in Newmarket, UK (2005-2007)', *The Veterinary Journal*, 187(3), pp. 325-329.
- Rasmussen, J., Holmberg, L. J., Sorensen, K., Kwan, M., Andersen, M. S. and de Zee, M. (2012) 'Performance optimization by musculoskeletal simulation', *Movement and Sports Sciences - Science et Motricite*, 75(1), pp. 73-83.
- Ratzlaff, M. H., Grant, B. D., Frame, J. M. and Hyde, M. L. 'Locomotor forces of galloping horses'. *Equine Exercise Physiology. International Conference on Equine Exercise Physiology*, 574-586.
- Ratzlaff, M. H., Hyde, M. L., Grant, B. D., Balch, O. K. and Wilson, P. D. (1990) 'Measurement of vertical forces and temporal components of the strides of horses using instrumented shoes', *Journal of Equine Veterinary Science*, 10(1), pp. 23-35.
- Ratzlaff, M. H., Wilson, P. D., Hyde, M. L., Balch, O. K. and Grant, B. D. (1993) 'Relationships between locomotor forces, hoof position and joint motion during the support phase of the stride of galloping horses', *Acta Anatomica*, 146(2-3), pp. 200-204.
- Ratzlaff, M. H., Hyde, M. L., Hutton, D. V., Rathgeber, R. A. and Balch, O. K. (1997) 'Interrelationships between moisture content of the track, dynamic properties of the track and the locomotor forces exerted by galloping horses', *Journal of Equine Veterinary Science*, 17(1), pp. 35-42.
- Ratzlaff, M. H., Wilson, P. D., Hutton, D. V. and Slinker, B. K. (2005) 'Relationships between hoof-acceleration patterns of galloping horses and dynamic properties of the track', *American Journal of Veterinary Research*, 66(4), pp. 589-595.
- Reinbolt, J. A., Fox, M. D., Schwartz, M. H. and Delp, S. L. (2009) 'Predicting outcomes of rectus femoris transfer surgery', *Gait Posture*, 30(1), pp. 100-105.
- Reiser, R. F., Peterson, M. L., McIlwraith, C. W. and Woodward, B. (2000) 'Simulated effects of racetrack material properties on the vertical loading of the equine forelimb', *Sports Engineering*, 3(1), pp. 1-11.
- Rezendes, A. (2007) 'Thoroughbred racetracks installing synthetic surfaces', *Journal of the American Veterinary Medical Association*, 230(7), pp. 985.
- Roberts, T. J., Marsh, R. L., Weyand, P. G. and Taylor, C. R. (1997) 'Muscular force in running turkeys: the economy of minimizing work', *Science*, 275(5303), pp. 1113-1115.
- Roberts, T. J. and Azizi, E. (2011) 'Flexible mechanisms: the diverse roles of biological springs in vertebrate movement', *Journal of Experimental Biology*, 212(3), pp. 353-361.
- Robin, D., Chateau, H., Pacquet, L., Falala, S., Valette, J.-P., Pourcelot, P., Ravary, B., Denoix, J.-M. and Crevier-Denoix, N. (2009) 'Use of a 3D dynamometric horseshoe to assess the effects of an all-weather waxed track and a crushed sand track at high speed trot: Preliminary study', *Equine Veterinary Journal*, 41(3), pp. 253-256.
- Roepstorff, L. and Drevemo, S. (1993) 'Concept of a force-measuring horseshoe', *Acta Anatomica* 146(2-3), pp. 114-119.
- Roepstorff, L., Johnston, C. and Drevemo, S. (1994) 'The influences of different treadmill constructions on ground reaction forces as determined by the use of a force-measuring horseshoe', *Equine Veterinary Journal*, 26(S17), pp. 71-74.
- Rogers, C. W., Gee, E. K. and Bolwell, C. F. (2014) 'Reproductive production constraints within the New Zealand racing industry', *Journal of Equine Veterinary Science*, 34(1), pp. 164.
- Rogers, C. W., Gee, E. K. and Bolwell, C. F. (2017) 'Chapter 8 Horse Production', In Stafford, K. (ed.) *Livestock Production in New Zealand*: Massey University Press.
- Rohrle, H., Scholten, R., Sigolotto, C., Sollbach, W. and Kellner, H. (1984) 'Joint forces in the human pelvis-leg skeleton during walking', *Journal of Biomechanics*, 17(6), pp. 409-424.

- Roland, E. S., Hull, M. L. and Stover, S. M. (2005) 'Design and demonstration of a dynamometric horseshoe for measuring ground reaction loads of horses during racing conditions', *Journal of Biomechanics*, 38(10), pp. 2102-2112.
- Rollot, Y., Lecuyer, E., Chateau, H. and Crevier-Denoix, N. (2004) 'Development of a 3D model of the equine distal forelimb and of a GRF shoe for noninvasive determination of in vivo tendon and ligament loads and strains', *Equine Veterinary Journal*, 36(8), pp. 677-682.
- Rosanowski, S. M., Chang, Y. M., Stirk, A. J. and Verheyen, K. L. P. (2016) 'Descriptive epidemiology of veterinary events in flat racing Thoroughbreds in Great Britain (2000 to 2013)', *Equine Veterinary Journal*, 49(3), pp. 275-281.
- Santschi, E. M. (2008) 'Articular Fetlock Injuries in Exercising Horses', *Veterinary Clinics of North America: Equine Practice*, 24(1), pp. 117-132.
- Schamhardt, H. C., Van den Bogert, A. J. and Hartman, W. (1993) 'Measurement techniques in animal locomotion analysis', *Acta Anatomica*, 146(2-3), pp. 123-129.
- Schellenberg, F., Oberhofer, K., Taylor, W. R. and Lorenzetti, S. (2015) 'Review of modelling techniques for in vivo muscle force estimation in the lower extremities during strength training', *Computational and Mathematical Methods in Medicine*, 2015.
- Scheys, L., Desloovere, K., Suetens, P. and Jonkers, I. (2011) 'Level of subject-specific detail in musculoskeletal models affects hip moment arm length calculation during gait in pediatric subjects with increased femoral anteversion', *Journal of Biomechanics*, 44(7), pp. 1346-1353.
- Seireg, A. and Arvikar, R. J. (1973) 'A mathematical model for evaluation of forces in lower extremities of the musculo-skeletal system', *Journal of Biomechanics*, 6(3), pp. 323-326.
- Serink, M. T., Nachemson, A. and Hansson, G. (1977) 'The effect of impact loading on rabbit knee joints', *Acta Orthopaedica Scandinavica*, 48(3), pp. 250-262.
- Setterbo, J. J., Garcia, T. C., Campbell, I. P., Reese, J. L., Morgan, J. M., Kim, S. Y., Hubbard, M. and Stover, S. M. (2009) 'Hoof accelerations and ground reaction forces of Thoroughbred racehorses measured on dirt, synthetic, and turf track surfaces', *American Journal of Veterinary Research*, 70(10), pp. 1220-1229.
- Setterbo, J. J., Yamaguchi, A., Hubbard, M., Upadhyaya, S. K. and Stover, S. M. (2011) 'Effects of equine racetrack surface type, depth, boundary area, and harrowing on dynamic surface properties measured using a track-testing device in a laboratory setting', *Sports Engineering*, 14(2-4), pp. 119-137.
- Setterbo, J. J., Fyhrie, P. B., Hubbard, M., Upadhyaya, S. K. and Stover, S. M. (2013) 'Dynamic properties of a dirt and a synthetic equine racetrack surface measured by a track-testing device', *Equine Veterinary Journal*, 45(1), pp. 25-30.
- Seynnes, O. R., Erskine, R. M., Maganaris, C. N., Longo, S., Simoneau, E. M., Grosset, J. F. and Narici, M. V. (2009) 'Training-induced changes in structural and mechanical properties of the patellar tendon are related to muscle hypertrophy but not to strength gains', *Journal of Applied Physiology*, 107(2), pp. 523-530.
- Shelburne, K. B., Pandey, M. G., Anderson, F. C. and Torry, M. R. (2004) 'Pattern of anterior cruciate ligament force in normal walking', *Journal of Biomechanics*, 37(6), pp. 797-805.
- Shelburne, K. B., Torry, M. R. and Pandey, M. G. (2006) 'Contributions of muscles, ligaments, and the ground-reaction force to tibiofemoral joint loading during normal gait', *Journal of Orthopaedic Research*, 24(10), pp. 1983-1990.
- Singer, E. R., Garcia, T. C. and Stover, S. M. (2013) 'How do metacarpophalangeal joint extension, collateromotion and axial rotation influence dorsal surface strains of the equine proximal phalanx at different loads in vitro?', *Journal of Biomechanics*, 46(4), pp. 738-744.
- Steele, K. M., Van der Krogt, M. M., Schwartz, M. H. and Delp, S. L. (2012) 'How much muscle strength is required to walk in a crouch gait?', *Journal of Biomechanics*, 45(15), pp. 2564-2569.
- Stephens, P. R., Nunamaker, D. M. and Butterweck, D. M. (1989) 'Application of a Hall-effect transducer for measurement of tendon strains in horses', *American Journal of Veterinary Research*, 50(7), pp. 1089-1095.

- Stover, S. M. (2003) 'The epidemiology of Thoroughbred racehorse injuries', *Clinical Techniques in Equine Practice*, 2(4), pp. 312-322.
- Sun, T. C., Riggs, C. M., Cogger, N., Wright, J. and Al-Alawneh, J. I. (2019) 'Non-catastrophic and catastrophic fractures in racing Thoroughbreds at the Hong Kong Jockey Club', *Equine Veterinary Journal*, 51(1), pp. 77-82.
- Swanstrom, M. D., Zarucco, L., Hubbard, M., Stover, S. M. and Hawkins, D. A. (2005) 'Musculoskeletal modeling and dynamic simulation of the Thoroughbred equine forelimb during stance phase of the gallop', *Journal of Biomechanical Engineering*, 127(2), pp. 318-328.
- Symons, J. E., Garcia, T. C. and Stover, S. M. (2014a) 'Distal hindlimb kinematics of galloping Thoroughbred racehorses on dirt and synthetic racetrack surfaces', *Equine Veterinary Journal*, 46(2), pp. 227-232.
- Symons, J. E., Fyhrie, D. P., Hawkins, D. A., Upadhyaya, S. K. and Stover, S. M. (2014b) 'Race surface model development in a musculoskeletal modelling environment', *Procedia Engineering*, 72, pp. 913-918.
- Symons, J. E., Hawkins, D. A., Fyhrie, D. P., Upadhyaya, S. K. and Stover, S. M. (2016) 'Modelling the interaction between racehorse limb and race surface', *Procedia Engineering*, 147, pp. 175-180.
- Thomason, J. J. and Peterson, M. L. (2008) 'Biomechanical and mechanical investigations of the hoof-track interface in racing horses', *Veterinary Clinics of North America: Equine Practice*, 24(1), pp. 53-77.
- Thorpe, C. T., Udeze, C. P., Birch, H. L., Clegg, P. D. and Screen, H. R. C. (2012) 'Specialization of tendon mechanical properties results from interfascicular differences', *Journal of the Royal Society Interface*, 9(76), pp. 3108-3117.
- To, C. S., Kirsch, R. F., Kobetic, R. and Triolo, R. J. (2005) 'Simulation of a functional neuromuscular stimulation powered mechanical gait orthosis with coordinated joint locking', *IEEE Transactions on Neural System and Rehabilitation Engineering*, 13(2), pp. 227-235.
- Tomlinson, J. E., Redding, W. R., Berry, C. and Smallwood, J. E. (2003) 'Computed tomographic anatomy of the equine tarsus', *Veterinary Radiology & Ultrasound*, 44(2), pp. 174-178.
- Tranquille, C. A., Walker, V. A., Hernlund, E., Egenvall, A., Roepstorff, L., Peterson, M. L. and Murray, R. C. (2015) 'Effect of superficial harrowing on surface properties of sand with rubber and waxed-sand with fibre riding arena surfaces: a preliminary study', *The Veterinary Journal*, 203(1), pp. 59-64.
- van der Krogt, M. M., de Graaf, W. W., Farley, C. T., Moritz, C. T., Richard Casius, L. J. and Bobbert, M. F. (2009) 'Robust passive dynamics of the musculoskeletal system compensate for unexpected surface changes during human hopping', *Journal of Applied Physiology*, 107(3), pp. 801-808.
- Van der Krogt, M. M., Seth, A., Steele, K. M., Bar-On, L., Desloovere, K., Harlaar, J. and Delp, S. L. (2013) 'A model of muscle spasticity in opensim', *Gait Posture*, 38(S1), pp. S16.
- Van Soest, A. J., Schwab, A. L., Bobbert, M. F. and van Ingen Schenau, G. J. (1993) 'The influence of the biarticularity of the gastrocnemius muscle on vertical-jumping achievement', *Journal of Biomechanics*, 26(1), pp. 1-8.
- White, S. C., Yack, H. J. and Winter, D. A. (1989) 'A three-dimensional musculoskeletal model for gait analysis. Anatomical variability estimates', *Journal of Biomechanics*, 22(8-9), pp. 885-893.
- Willemsen, M. A., Jacobs, M. W. H. and Schamhardt, H. C. (1999) 'In vitro transmission and attenuation of impact vibrations in the distal forelimb', *Equine Veterinary Journal*, 31(S30), pp. 245-248.
- Williams, R. B., Harkins, L. S., Hammond, C. J. and Wood, J. L. N. (2001) 'Racehorse injuries, clinical problems and fatalities recorded on British racecourses from flat racing and National Hunt racing during 1996, 1997 and 1998', *Equine Veterinary Journal*, 33(5), pp. 478-486.
- Wilson, A. M., McGuigan, M. P., Su, A. and Borgert, A. J. v. d. (2001) 'Horses damp the spring in their step', *Nature* 414, pp. 895-899.
- Witte, T. H., Knill, K. and Wilson, A. M. (2004) 'Determination of peak vertical ground reaction force from duty factor in the horse (*Equus caballus*)', *Journal of Experimental Biology*, 207(Pt21), pp. 3639-3648.

## Predicting horse limb responses to surface variations

- Wu, J. Z., Chiou, S. S. and Pan, C. S. (2009) 'Analysis of musculoskeletal loadings in lower limbs during stilts walking in occupational activity', *Annals of Biomedical Engineering*, 37(6), pp. 1177-1189.
- Zajac, F. E. (1993) 'Muscle coordination of movement: A perspective', *Journal of Biomechanics*, 26(S1), pp. 109-124.
- Zebarth, B. J. and Sheard, R. W. (1985) 'Impact and shear resistance of turf grass racing surfaces for Thoroughbreds', *American Journal of Veterinary Research*, 46(4), pp. 778-784.

PART 1  
CREATING THE MUSCULOSKELETAL  
MODEL

# Chapter 2

## Collecting Ligament and tendon properties

### I. Introduction

Developing a musculoskeletal model requires knowledge of the morphology and material properties for the different tissues. The aim of this part was to gather all the anatomical data required to create a musculoskeletal model of the equine forelimb with the AnyBody Modeling System™ (AnyBody Technology A/S, Denmark; hereafter called AnyBody). Some of the tissue measurements utilised have been reported in the literature. The 3D representations of the bones and the 3D geometries of the joints were generated from computed tomography (CT) of a Thoroughbred forelimb.

### II. Segment properties

Two properties are required to model a segment: its mass and its principal moments of inertia. The 3D image of the segment is not necessary but it helps to define the joint geometry and ligament and tendon path.

A right forelimb was obtained from a 6-year old Thoroughbred mare euthanized for a non-orthopaedic reason. After removing all soft tissues, excluding joint capsules, the limb was positioned with the joints in the anatomical standing position. The horse limb was too long to be CT-scanned in a single attempt, and so it was scanned in two separate passes. The proximal limb was scanned to the level of the distal metacarpus, and then the distal limb was scanned up to the carpus, such that the metacarpus was included in both scans. Four pins (ordinary sewing pins) were inserted into the metacarpus, in different planes, to be able later to have a reference frame to align the two CT scans in the same global reference frame, which is important to assure the joint geometry. Small (6mm) spherical markers were placed on the pins. The limb was scanned using a Philip spiral CT scanner (Phillips Brilliance 16-slice helical scanner, Phillips Healthcare, The Netherlands). The CT scans were acquired by Massey University Radiology Department Imaging with voxel size 0.8 mm x 0.8 mm x 0.8 mm, a 1 mm slice thickness and a 0.5 mm overlay.

The CT scan was then processed using YaDiV (Welfenlab, Leibniz Universität Hannover, Germany). YaDiV (“Yet Another Dicom Viewer”) is a program to visualize and segment data in DICOM format,

such as the files created by CT scanner. A 3D image was created for each single bone, and the centre of mass and principal moments of inertia were computed using Solidworks®.

### III. Muscle-tendon properties

#### III.A. Muscle-tendon properties required for modelling

AnyBody allows the use of three different muscle models: the simple model, the 2-element Hill model and the 3-element Hill model. The simple model represents only the contractile element of the muscle. The 2-element Hill model represents a contractile element for the muscle fibres and a serial elastic element for the tendon. In this model, the force-length and the force-velocity relationships of the contractile element as well as the force-length relationship of the serial element are linear. The 3-element Hill model includes a contractile element for the active muscle fibres, a non-linear serial elastic element for the tendon and a non-linear parallel elastic element for the passive part of the muscle fibres.

All the muscle models require the origin and insertion sites of the muscles. A muscle with more than one origin and one insertion sites therefore have to be modelled as several muscles. The other properties required to model the muscle-tendon units depend on the model chosen. The properties required for the 2- and 3-element Hill models are the nominal strength, which is also called the maximal isometric muscle force; the nominal tendon length and the maximum contraction velocity or the percentage of fast twitch fibres. Some properties can be added in the muscle-tendon unit definition but are not mandatory, such as the optimal muscle fibre length or the volume of the muscle fibres. All the properties that are required and that can be added for each muscle model are listed in Table 1.

## Predicting horse limb responses to surface variations

Table 1 Muscle properties that are required or that can be added for each muscle model

Model	Properties required	Properties that can be added
Simple model	- F0: nominal strength	- Lf0: optimal muscle fibre length - Vol0: volume of the muscle fibres
2-element Hill model	- F0 - Lt0: nominal tendon length - V0: maximum contraction velocity	- Lf0 - Vol0 - Lfbar: nominal fibre length - Epsilon0: optimal tendon strain - Epsilonbar: nominal tendon strain
3-element Hill model	- F0 - Lt0 - Fcfast: percentage of fast twitch fibres	- Lf0 - Vol0 - Lfbar - Epsilon0 - Epsilonbar - Gamma0: optimal pennation angle - Jt: shape constant for the tendon element force relationships - Jpe: shape constant for the parallel elastic element force relationships - K1: normalized contraction velocity - K2: contribution to normalized maximum velocity for fast fibres - PEFactor: relative stiffness parameter for the parallel elastic element - Gammabar: nominal pennation angle

### III.B. Muscle-tendon data

The muscle-tendon units that were included in the AnyBody model are the lateral digital extensor (LDE), common digital extensor (CDE), extensor carpi radialis (ECR), extensor carpi obliquus (ECO), ulnaris lateralis (UL), flexor carpi radialis (FCR), flexor carpi ulnaris (FCU), deep digital flexor (DDF) and superficial digital flexor (SDF). In the proximal part of the limb, the muscles modelled are the biceps and triceps.

The origin and insertion sites were identified from anatomical drawings from the lab (reported in the Appendix) and from key anatomy textbooks Dyce *et al.* (2010) and Budras *et al.* (1994). They were then reported on the 3D picture of the corresponding segment using Solidworks®, which generated the local coordinates of these sites.

The nominal strength of the distal muscles were reported by Brown *et al.* (2003b). They first found the muscle volume and muscle fibre length by dissecting seven forelimbs from five Thoroughbred horses. Then, they computed the physiological cross-sectional area by dividing the muscle volume by

the muscle fibre length, and they finally obtained the nominal strength by multiplying the physiological cross-sectional area by the maximum muscle stress (taken as 300 kPa). The nominal strength for the biceps and triceps were reported by Watson and Wilson (2007). They first measured the muscle weight and muscle fibre length from seven biceps and twelve triceps from 20 fresh riding horse cadavers of unknown breed (the muscles of one type were from different horses). Then, they computed the physiological cross-sectional area by dividing the muscle mass by its density (taken as  $1.1 \text{ g.cm}^{-3}$ ), and again by the fibre length. They obtained the nominal strength as Brown *et al.* (2003b), by multiplying the physiological cross-sectional area by the maximum muscle stress (taken as 300 kPa).

The optimal muscle fibre lengths and the optimal pennation angles are two properties required for modelling. However, the data that are generally reported are the fibre length and pennation angle in the rest position. As an approximation, the properties measured at rest were considered as the optimal values. The muscle fibre length and pennation angles for the distal muscles have been reported by Brown *et al.* (2003b). These data were also determined by dissection in the laboratory, and the complete list of measurements is presented in the Appendix. One Thoroughbred forelimb was dissected and the muscle fibre lengths and pennation angle were measured with a ruler and a protractor. The data from both sources were in good agreement for most of the muscles. Indeed, the muscle fibre length was reported to be 0.0422m and 0.037m for LDE, 0.076m and 0.078m for ECR, 0.0174m and 0.015m for UL, 0.0897m and 0.075m for FCR, 0.0183m and 0.02m for FCU, and 0.0075m and 0.008m for SDF by Brown *et al.* (2003b) and in the laboratory respectively. The pennation angles were reported to be 17.5° and 17° for LDE, 34.3° and 30° for UL, 6.7° and 7° for FCR, 31.6° and 32° for FCU, 21.6° and 23° for DDF, and 41.6° and 40° for SDF by Brown *et al.* (2003b) and in the laboratory respectively. For CDE, the data from the laboratory separated the properties between the lower and upper parts of the muscle, and the muscle fibre length and the pennation angle were respectively measured to be 0.085m and 15° on the lower part and 0.11m and 10° on the upper part while Brown *et al.* (2003b) just reported these values to be 0.0814m and 13.3° without distinction between the upper and lower parts. Larger differences were observed in the muscle fibre length of DDF and pennation angle of ECR. For DDF, the optimal muscle fibre length was reported to be 0.0202m by Brown *et al.* (2003b) and 0.072m at the laboratory. The pennation angle of ECR was reported to be 16° by Brown *et al.* (2003b) and 30° by the data from the laboratory. In addition, the data for ECO was only available at the laboratory, the muscle fibre was measured to be 0.019m and the pennation angle to be 23°. The measurements used in the model were those from Brown *et al.* (2003b) because they were collected from seven Thoroughbred specimen whereas the dataset from the laboratory was generated from a single dissection. The fibre length for the biceps and triceps were reported by

Watson and Wilson (2007), and they estimated the pennation angle of the biceps and triceps to be 45°.

The volume of distal muscle was also measured and reported by Brown *et al.* (2003a) using the same horse dissection material (seven forelimbs from five Thoroughbred horses). The volume of the biceps and triceps can be deduced from the data reported by Watson and Wilson (2007), by dividing the muscle mass by the density (taken as 1.1 g.cm<sup>-3</sup>). The maximum contraction velocity was estimated to be 10 fibre lengths per second for all muscles except for SDF and DDF, for which it was estimated to be respectively 1.6 and 3.2 fibre lengths per second (Swanstrom *et al.*, 2005). The percentage of fast twitch fibres was computed from the percentage of slow twitch muscle fibres reported by Brown *et al.* (2003b). The percentage of fast twitch fibres for the biceps and triceps were estimated to be 50%. The last property, the ratio of tendon length to muscle-tendon length was not required to model the muscle-tendon unit but was required to scale the model. This ratio can be computed from the laboratory dissection dataset or from the data reported by Zarucco *et al.* (2006). Both sets of data were measured from the dissection of a unique Thoroughbred forelimb. The results from both sources were in reasonable agreement, the ratio was computed to be 0.60 and 0.65 for LDE, 0.35 and 0.41 for ECR, 0.41 and 0.40 for ECO, 0.32 and 0.34 for FCR, 0.04 and 0.06 for FCU, 0.57 and 0.53 for the humeral head of DDF, 0.71 and 0.73 for the radial head of DDF and 0.54 and 0.52 for SDF from the data reported by Zarucco *et al.* (2006) and from the laboratory, respectively. For CDE, the ratio was computed to be 0.68 with Zarucco's (2006) data and 0.69 for its radial head and 0.66 for its humeral head with the data from the laboratory. Larger differences were observed for UL and for the ulnar head of the DDF. They were respectively computed to be 0.23 and 0.74 from Zarucco's (2006) data and 0.38 and 0.64 from the laboratory dissection data. For this data, an average of both were used except for CDE, for which the laboratory dissection data were used because they differentiate the radial and humeral heads. The tendon and muscle-tendon lengths were not found in the literature. The muscle data that were used in the AnyBody model are reported in Table 2.

## Chapter 2 Collecting Tendon and Ligament Properties

Table 2 Muscle data used for the AnyBody Thoroughbred forelimb model, obtained from published literature (1-5) and from laboratory dissection data (6)

Muscles	Nominal strength FO (N)	Optimal muscle fibre length Lf0 (m)	Volume of the muscle fibres Vol0 (cm <sup>3</sup> )	Maximum contraction velocity V0 (m.s <sup>-1</sup> )	Optimal pennation angle γ0 (°)	Percentage of fast twitch fibres Fcfast (%)	Ratio of tendon length to muscle length TL/ML
Lateral Digital Extensor	401.6 <sup>(1)</sup>	0.0422 <sup>(1)</sup>	53.4 <sup>(2)</sup>	0.422 <sup>(3)</sup>	17.5 <sup>(1)</sup>	50 <sup>(1)</sup>	0.63 <sup>(4)</sup>
Common Digital Extensor	1,044.4 <sup>(1)</sup>	0.0814 <sup>(1)</sup>	295.3 <sup>(2)</sup>	0.814 <sup>(3)</sup>	13.3 <sup>(1)</sup>	50 <sup>(1)</sup>	0.69 <sup>(6)</sup> radial 0.66 <sup>(6)</sup> humeral
Extensor Carpi Radialis	2,891.7 <sup>(1)</sup>	0.076 <sup>(1)</sup>	754.4 <sup>(2)</sup>	0.76 <sup>(3)</sup>	16.0 <sup>(1)</sup>	79 <sup>(1)</sup>	0.38 <sup>(4)</sup>
Extensor Carpi Obiquus		0.019 <sup>(5)</sup>		0.19 <sup>(3)</sup>	23 <sup>(5)</sup>		0.41 <sup>(4)</sup>
Ulnaris Lateralis	5,731.1 <sup>(1)</sup>	0.0174 <sup>(1)</sup>	337.1 <sup>(2)</sup>	0.174 <sup>(3)</sup>	34.3 <sup>(1)</sup>	50 <sup>(1)</sup>	0.30 <sup>(4)</sup>
Flexor Carpi Radialis	535.5 <sup>(1)</sup>	0.0897 <sup>(1)</sup>	166.4 <sup>(2)</sup>	0.897 <sup>(3)</sup>	6.7 <sup>(1)</sup>	64 <sup>(1)</sup>	0.33 <sup>(4)</sup>
Flexor Carpi Ulnaris	3,982.5 <sup>(1)</sup>	0.0183 <sup>(1)</sup>	245.1 <sup>(2)</sup>	0.183 <sup>(3)</sup>	31.6 <sup>(1)</sup>	60 <sup>(1)</sup>	0.05 <sup>(4)</sup>
Deep Digital Flexor	9,504.3 <sup>(1)</sup>	0.0202 <sup>(1)</sup>	524.5 humeral 89.4 ulnar 41.6 radial <sup>(2)</sup>	0.065 <sup>(3)</sup>	21.6 <sup>(1)</sup>	61 <sup>(1)</sup>	0.55 <sup>(4)</sup> humeral 0.69 <sup>(4)</sup> ulnar 0.72 <sup>(4)</sup> radial
Superficial Digital Flexor	9,096.6 <sup>(1)</sup>	0.0075 <sup>(1)</sup>	227.4 <sup>(2)</sup>	0.012 <sup>(3)</sup>	41.6 <sup>(1)</sup>	43 <sup>(1)</sup>	0.53 <sup>(4)</sup>
Biceps	Lateral head	10,503.4 <sup>(5)</sup>	0.0063 <sup>(5)</sup>	217.7 <sup>(5)</sup>	0.063 <sup>(3)</sup>	45 <sup>(5)</sup>	50
	Medial head	4,213.4 <sup>(5)</sup>	0.0286 <sup>(5)</sup>	385.7 <sup>(5)</sup>	0.286 <sup>(3)</sup>	45 <sup>(5)</sup>	50
Triceps	Long head	5,067.9 <sup>(5)</sup>	0.2219 <sup>(5)</sup>	3,690.2 <sup>(5)</sup>	2.219 <sup>(3)</sup>	45 <sup>(5)</sup>	50
	Lateral head	1,031.3 <sup>(5)</sup>	0.2059 <sup>(5)</sup>	707.0 <sup>(5)</sup>	2.059 <sup>(3)</sup>	45 <sup>(5)</sup>	50
	Medial head	383.4 <sup>(5)</sup>	0.1322 <sup>(5)</sup>	145.4 <sup>(5)</sup>	1.322 <sup>(3)</sup>	45 <sup>(5)</sup>	50

<sup>(1)</sup> Brown *et al.* (2003b), <sup>(2)</sup> Brown *et al.* (2003a), <sup>(3)</sup> Computed: V0 estimated to be 10 fiber lengths per second for all muscles but for SDF and DDF, for which it is estimated to be respectively 1.6 and 3.2 fiber lengths per second (Swanstrom *et al.*, 2005), <sup>(4)</sup> Mean of Zarucco's (2006) data and data from the laboratory, <sup>(5)</sup> Watson and Wilson (2007), <sup>(6)</sup> Computed from data collected in the laboratory

## IV. Ligament properties

The properties required to model the ligaments in AnyBody are their attachment sites, their slack length and their strain-force values. A ligament with more than one origin and one insertion sites has

to be modelled as several ligaments. All the ligament data were found in the literature (Agut *et al.*, 2009; Brown *et al.*, 2003b; Budras *et al.*, 1994; Dyce *et al.*, 2010; Jansen and Savelberg, 1994; Legg *et al.*, 2019). The origin and insertion sites were identified on anatomical drawings from the laboratory dissection and from Dyce *et al.* (2010) and Budras *et al.* (1994). They were then reported on the 3D picture of the corresponding segment using Solidworks®, which gave the local coordinates of these sites.

The slack length has only been found for the suspensory ligament and was reported by Brown *et al.* (2003b). As the slack length reported would have been specific to the limb studied by Brown *et al.* (2003b), it was not useful to try to incorporate that length into this model, and so slack length was determined from the bony geometry of the limb segments and joints in the same way as all the other ligaments. The strain and associated force were found in different sources. Those for the sesamoidean ligaments and all the collateral ligaments were computed from the data collected on Thoroughbred forelimb dissection by Legg *et al.* (2019), and these data are presented in the Appendix. For the suspensory ligaments and the accessory ligament of DDF, the strain ( $\epsilon_1$ ) and corresponding stress ( $\sigma_1$ ) were reported by Jansen and Savelberg (1994), from the dissection of 12 specimen from eight horses and ponies whose breeds were not reported. The force ( $F_1$ ) associated to  $\epsilon_1$  was then computed as  $F_1 = \sigma_1 \times S$ ; with  $S$  the cross-section area of the ligament reported by Agut *et al.* (2009). No force-strain data were found for the accessory ligament of SDF and so were taken as the same as for the accessory ligament of DDF. For the same reason, the data for the coffin collateral ligaments were taken to be the same as for the collateral ligaments of the proximal interphalangeal joint.

No data were found for the lacertus fibrosus. For this reason, the force-strain relationship used was the force-strain relationship of the straight sesamoidean ligament and was modified when modelling to provide enough forces when strained to balance the forces within the limb. The ligament data that were used in the AnyBody model are reported in Table 3.

Table 3 Ligament data used for modelling which was obtained from published literature

Ligaments		Strain value for which the corresponding force is available $\epsilon_1$	Force associated to the strain $\epsilon_1$ F1 (N)
Suspensory ligaments		0.116 <sup>b</sup>	6,300 <sup>c</sup>
Accessory ligament of DDF		0.124 <sup>b</sup>	6020 <sup>c</sup>
Accessory ligament of SDF		0.124 <sup>b</sup>	6020 <sup>c</sup>
Sesamoidean ligaments	Straight	0.21 <sup>a</sup>	716.5 <sup>a</sup>
	Medial Oblique	0.42 <sup>a</sup>	597.8 <sup>a</sup>
	Lateral Oblique	0.33 <sup>a</sup>	388.5 <sup>a</sup>
	Medial collateral	0.68 <sup>a</sup>	234.6 <sup>a</sup>
	Lateral collateral	0.42 <sup>a</sup>	181.1 <sup>a</sup>
Elbow collateral ligaments	Lateral	0.47 <sup>a</sup>	523.9 <sup>a</sup>
	Caudal Medial	0.51 <sup>a</sup>	590.7 <sup>a</sup>
	Cranial Medial	0.21 <sup>a</sup>	794.0 <sup>a</sup>
Carpal collateral ligaments	Lateral	0.26 <sup>a</sup>	633.9 <sup>a</sup>
	Medial	0.28 <sup>a</sup>	649.1 <sup>a</sup>
Fetlock collateral ligaments	Lateral	0.42 <sup>a</sup>	740.5 <sup>a</sup>
	Medial	0.43 <sup>a</sup>	1084.1 <sup>a</sup>
Coffin collateral ligaments	Lateral	0.34 <sup>a</sup>	552.6 <sup>a</sup>
	Medial	0.42 <sup>a</sup>	605.2 <sup>a</sup>

<sup>a</sup> Legg *et al.* (2019); <sup>b</sup> Jansen and Savelberg (1994); <sup>c</sup> Computed as  $F = \sigma \times S$ ,  $\sigma$  the stress from Jansen and Savelberg (1994), S the cross-section area from Agut *et al.* (2009); The data for the coffin collateral ligaments and for the accessory ligament of SDF were taken as the same as for the proximal interphalangeal joint and for the accessory ligament of DDF, respectively.

## V. Conclusion and discussion

The data required to develop the musculoskeletal model were sourced from the published literature and/or were available from material measured in the laboratory dissection. The slack length of the ligaments, except for the suspensory ligament, could not be found in the literature. However, even if they had been, they could not have been used because they would be specific to the horse from which the data were collected and not specific to the horse from which the bone geometries were collected. The slack length of the ligaments were thus directly estimated in the musculoskeletal model (Chapter 3) by measuring the ligament lengths with the segments positioned as in the standing horse.

The data were taken from the literature pertaining specifically to Thoroughbreds. However, such data were not always available. That is specifically the case for the data reported by Jansen and Savelberg (1994). In addition, to compute the force-strain values for the suspensory ligaments and accessory

## Predicting horse limb responses to surface variations

ligament of DDF, data were taken from different studies and therefore different equine specimens, which reduces the homogeneity of the data. Even if all the data were obtained from Thoroughbred limb dissection, they would not be specific to the Thoroughbred limb used here to model the 3D geometries of the bones and joints. So, the overall dataset presented in this chapter, and used in the model, should be considered generic to this preliminary model of the Thoroughbred forelimb.

## VI. References

- Agut, A., Martinez, M. L., Sanchez-Valverde, M. A., Soler, M. and Rodriguez, M. J. (2009) 'Ultrasonographic characteristics (cross-sectional area and relative echogenicity) of the digital flexor tendons and ligaments of the metacarpal region in Purebred Spanish horses', *The Veterinary Journal*, 180(3), pp. 377-383.
- Brown, N. A., Kawcak, C. E., McIlwraith, C. W. and Pandy, M. G. (2003a) 'Architectural properties of distal forelimb muscles in horses, *Equus caballus*', *Journal of Morphology*, 258(1), pp. 106-114.
- Brown, N. A. T., Pandy, M. G., Kawcak, C. E. and McIlwraith, C. W. (2003b) 'Force- and moment-generating capacities of muscles in the distal forelimb of the horse', *Journal of Anatomy*, 203(1), pp. 101-113.
- Budras, K.-D., Sack, W. O. and Rock, S. (1994) *Anatomy of the horse: An illustrated text, 2nd edition*. Naples Florida: Mosby-Wolfe.
- Dyce, K. M., Sack, W. O. and Wensing, C. J. G. (2010) *Textbook of Veterinary Anatomy, 4th Edition*. W. B. Saunders.
- Jansen, M. O. and Savelberg, H. H. C. M. (1994) 'Stress and strain of equine tendons of the forelimb at failure', *Equine Veterinary Journal*, 26(S17), pp. 57-60.
- Legg, K. A., Colborne, G. R., Gee, E. K. and Rogers, C. W. (2019) 'Elastic properties of collateral and sesamoid ligaments in the forelimbs of equine cadavers', *American Journal of Veterinary Research*, 80(10), pp. 923-930.
- Swanstrom, M. D., Zarucco, L., Hubbard, M., Stover, S. M. and Hawkins, D. A. (2005) 'Musculoskeletal modeling and dynamic simulation of the Thoroughbred equine forelimb during stance phase of the gallop', *Journal of Biomechanical Engineering*, 127(2), pp. 318-328.
- Watson, J. C. and Wilson, A. M. (2007) 'Muscle architecture of biceps brachii, triceps brachii and supraspinatus in the horse', *Journal of Anatomy*, 210(1), pp. 32-40.
- Zarucco, L., Wisner, E. R., Swanstrom, M. D. and Stover, S. M. (2006) 'Image fusion of computed tomographic and magnetic resonance images for the development of a three-dimensional musculoskeletal model of the equine forelimb', *Veterinary Radiology & Ultrasound*, 47(6), pp. 553-562.

# Chapter 3

## Development of the musculoskeletal model

### I. Introduction

Musculoskeletal models permit studying and understanding of the muscle coordination within the horse limb and the interaction of the components of the limb with various ground surfaces without requiring the use of invasive methods (for example, to measure stress or tension within the ligaments and muscles) or installing different ground surfaces (Moissenet *et al.*, 2017; Rajagopal *et al.*, 2016; Symons *et al.*, 2014b; Symons *et al.*, 2016).

Musculoskeletal models include segment, joint, muscle-tendon, and ligament information (Swanstrom *et al.*, 2005). There are two different categories of simulation: the forward dynamics approach and the inverse dynamics approach. The software used to create the musculoskeletal model is the AnyBody Modeling System™ (hereafter called AnyBody), which is based in the inverse dynamics approach (Alamdari and Krovi, 2017).

This chapter reports the different steps that were followed to create the musculoskeletal from the data gathered in the previous chapter (Chapter 2) to the final version of the preliminary model after a few improvements required to run the model with kinematic data.

### II. Materials and methods

#### II.A. Limb components

At present in the literature, only a few musculoskeletal models of the equine limb have been proposed and these have often been limited to the distal limb. The models published in the literature have been described in detail in Chapter 1 and a summary of the models and the anatomical components included in comparison to the AnyBody model used within this thesis are summarized in Table 4.

### Chapter 3 Development of the musculoskeletal model

Table 4 Summary of the models published in the literature, the model used in this study and the key differences between these models

Model	Brown <i>et al.</i> (2003b)	Swanstrom <i>et al.</i> (2005) and Symons <i>et al.</i> (2016)	Lawson <i>et al.</i> (2007)	Harrison <i>et al.</i> (2010)	Model developed in this study
Software	SIMM (Software for Interactive Musculoskeletal Modeling, MusculoGraphics, Inc., Chicago, IL)	SIMM (Software for Interactive Musculoskeletal Modeling, MusculoGraphics, Inc., Chicago, IL)	Matlab™ (Mathworks Inc., MA)	OpenSim (National Center for Simulation in Rehabilitation Research, CA)	AnyBody Modeling System™ (AnyBody Technology A/S, Denmark)
Segments					
Scapula	Not included	Not included	Not included	Not included	Included
Humerus	Included	Not included as segment but distal third represented	Not included	Included	Included
Radius, ulna	Included	Included	Not included	Included	Included
Proximal row of carpal bones	Included in one segment	Included	Not included	Included in one segment	Included in one segment
Accessory carpal bone		Included	Not included		
Distal row of carpal bones	Included	Included in one segment	Not included	Included in one segment	
Metacarpus	Included		Included		
Proximal sesamoid bones	Included in one segment	Included	Included	Included	
Proximal phalanx		Included	Included	Included	Included in one segment
Middle phalanx	Included	Included	Included	Included	
Distal phalanx	Included	Included	Included	Included in one segment	Included in one segment
Navicular bone	Not included	Included	Included		
Hoof	Not included	Included	Not included	Not included	Not included
Shoe	Not included	Included	Not included	Not included	Not included

## Predicting horse limb responses to surface variations

Muscles					
Abductor Pollicis Longus	Included	Not included	Not included	Not included	Not included
Lacertus Fibrosus	Not included	Not included	Not included	Included	Included as ligament
Extensor Carpi Obliquus	Not included	Included	Not included	Not included	Included
Extensor Carpi Radialis	Included	Included	Not included	Included	Included
Lateral Digital Extensor	Included	Included	Not included	Included	Included
Common Digital Extensor	Included	Included	Not included	Included	Included
Ulnaris Lateralis	Included	Included	Not included	Included	Included
Flexor Carpi Ulnaris	Included	Included	Not included	Included	Included
Flexor Carpi Radialis	Included	Included	Not included	Included	Included
Superficial Digital Flexor	Included	Included	Tendon included	Included	Included
Deep Digital Flexor	Included	Included	Tendon included	Included	Included

### II.B. The Anybody Modeling System™

The AnyBody musculoskeletal modelling software provides two types of simulation: kinematics and inverse dynamics. The kinematics programme only calculates the position of the different limb segments based on the input gait data. This data can be obtained via either marker positions or by angular position of the joints. The inverse dynamics programme uses data from the kinematics programme and computes the forces within the ligaments and muscle-tendon units (the muscle-tendons are considered as one structure). The loads are shared between the different muscles by optimisation. A number of different optimization functions are available within AnyBody, including linear, quadratic, polynomial, minmax and composite.

Linear optimization uses an objective function of the type  $G = \sum_i A_i$ , where  $A_i$  is the activity of the muscle  $i$ . With this optimisation, a minimal number of muscles are recruited to balance the system. This strategy is not physiological, but it does provide the ability to determine the important muscles in a given posture and external load. The results derived using this approach can be used in scenarios such as modelling different options for tendon transfer surgery.

The quadratic optimization uses an objective function of the type  $G = \sum_i (A_i)^2$ . Contrary to the linear optimization, this function would distribute the load between several muscles. In practise, this optimisation is one of the most frequently used because it agrees well with experimental measurements.

The polynomial optimization uses an objective function of the type  $G = \sum_i (A_i)^p$ , with  $p$  as an integer between 3 and 5. Generally, when the value of  $p$  increases, the load is increasingly shared between the different muscles. However, it can underestimate activation and deactivation time, and they can be reported to function at a rate within the model that is faster than what is biologically plausible.

The min/max (which is for minimizing the maximum muscle activity) optimisation is based on the polynomial optimisation with  $p$  tending to infinity, and which shares the load between muscles so that the activity (ratio of muscle force to maximal muscle force) is as small as possible for all the muscles. This method is useful to determine the perceived effort, or how the effort to provide is felt by a person or an animal. For example, if two muscles (with different maximal force) have to provide the same force, the effort to provide that force with the weaker muscle (the one that has the smallest maximal force) will be felt greater than the effort to provide the same force with the stronger muscle. This would be translated by the min/max optimization with a higher maximal muscle activity with the weaker muscle than with the stronger muscle. However, it suffers from the same limitations as the polynomial optimisation, as the prediction can generate data describing the muscles activated and deactivated faster than what is biologically possible.

Finally, the composite optimisation is a combination of the linear and quadratic optimization. It combines the load sharing to enable the organism to use its full strength when approaching its limit and the minimisation of the number of muscles recruited under small loads.

Based on these explanations of the different optimization functions, the quadratic and polynomial optimization functions have been tested within the model development procedure. The quadratic optimization function was not able to share the load between the muscles and find a solution. The polynomial optimization function had been tested with the different value of  $p$ . However, with  $p=4$  and  $p=5$ , the muscles were activated and deactivated very quickly at any time of the stride, and it was not possible to determine when a muscle was working or not in the stride cycle. For these reasons, the optimization function used in the musculoskeletal model was the polynomial optimization function with  $p=3$ .

### III. Development of the model

#### III.A. Segments and initial positions

A segment was created for each single bone, using the 3D images from the CT and their mechanical properties described in the literature or obtained from dissections within the lab (Chapter 2). From the processed CT scan images, a local reference frame was oriented on each bone. The origin was on

the centre of mass of the bone, the x-axis was defined as the transverse axis, the z-axis as the long axis of the bone, and the orthogonal y-axis completed the reference frame. An example is provided in Figure 2 for the Scapula segment with its local reference frame. In addition, a general reference frame was created using the pins added in the metacarpus during the CT data capture process. The initial position of each bone was determined by the position of its centre of mass in the general reference frame, which gave the initial translation of the bone ( $r_0$ ), and by the rotation between the (local) reference frame on the bone and the global reference frame, which gave the initial rotation of the bone.

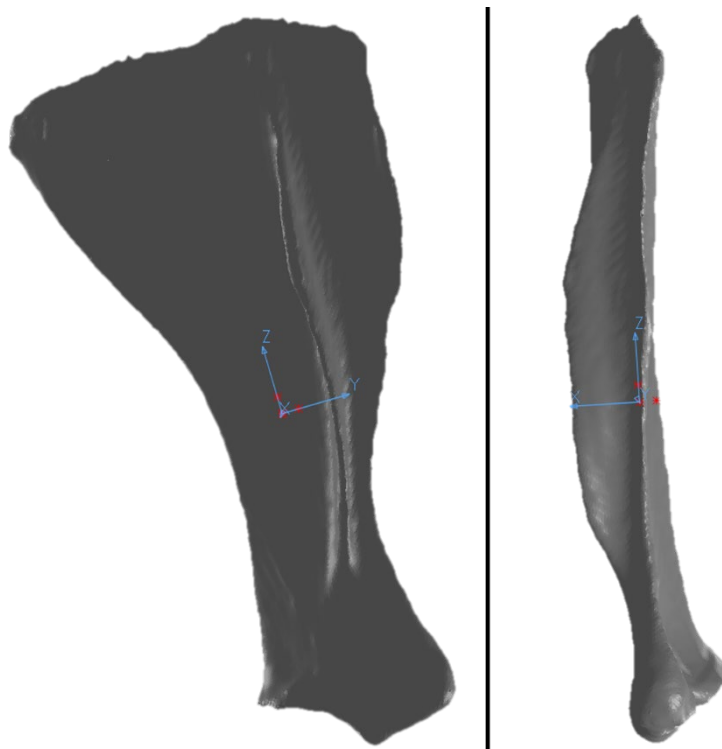


*Figure 2 CT derived image of the Scapula segment with its local reference frame on the estimated centre of mass. Lateral view on the left, cranial view on the right.*

The local coordinates of the points representing the muscle and ligament origin and insertion sites on the segmental bony surfaces were described in Chapter 2. These coordinates were used to create the points on the segment in AnyBody. The muscle-tendon units were then created using the simplest model, which requires only the maximum isometric force ( $F_0$ ). The ligaments were added in the musculoskeletal model.

### III.B. Joints, markers and kinematics

To run the kinematic programme within AnyBody, it was necessary to define the joints and markers tracked during the kinematic data collection. The methodology for the collection of the kinematic data has been described in detail in chapter 4.

It was necessary to identify two new sets of points from the kinematic data. The first set of points was to define the joint of interest (Shoulder, Elbow, Carpal, Fetlock and Coffin joints) and the second was to generate a link between the model and the kinematic data collected. The points, “joint markers”, were created on the medial and lateral sides of the centre of rotation of the joints. The middle of the sets of lateral and medial joint markers were computed using their 3D coordinates and defined as “joint points” to define the joints. An example of the definition of these points is provided in Figure 3 for the antebrachio-carpal joint point and carpal markers.

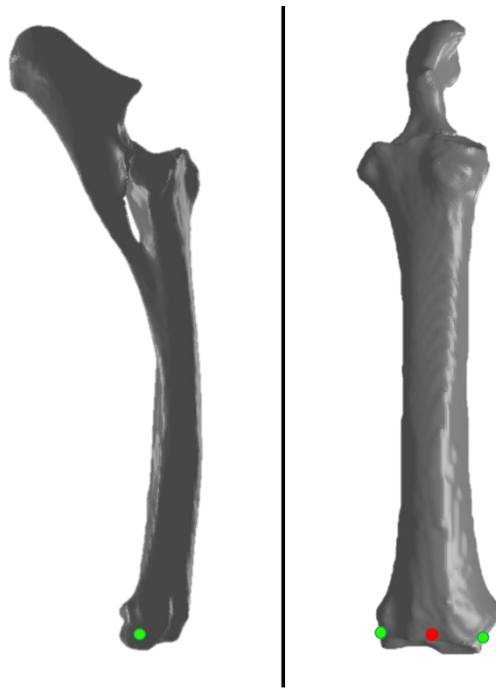


*Figure 3 Position of markers (green points) and antebrachio-carpal joint point (red point) on the antebrachium segment. Lateral (on the left) and cranial (on the right) views of the radius-ulna 3D image. All three points are superimposed on the lateral view*

The AnyKinEqSimpleDriver function provided the subroutine to constrain the measured translations and/or rotations between the joint points defined earlier in this model, to the given distance and angle values derived from the CT-scan images and the translational and rotational velocities (zero in this case). All the joints, with the exception of the carpus, were initially defined with three degrees-of-freedom (corresponding to the three rotations in the anatomical planes). The joints between the

carpal bones and the carpometacarpal joint were totally constrained, such that the movement at the carpus included only the antebrachiocarpal joint (called carpal joint).

A function was added to the model to read the kinematic data file (AnyInputC3D). To relate the model created to the data imported, it was necessary to define connections. The first dataset required was the Initialization file (defined in chapter 4). First, the AnyKinDriverMarker function was used to position the segments by attributing the measured position of the corresponding joint markers to each of the joint markers defined earlier in the model. Since this made the degrees-of-freedom per joint greater than the number of constraints, the joints were then completely constrained (as the carpal bones earlier), blocking all translations and rotations between the segments.

Once the segment endpoints were located in the kinematic reference frame by means of the joint markers, the local coordinates of the segmental markers identifying each of the segments were computed (i.e. the coordinates of these markers were obtained in the reference frame of the corresponding segment). This method required that the model was divided into two parts or stages, called Initialization and DynamicTrial.

During the Initialization process, the segments were positioned by the joint markers and the local coordinates of the segmental markers were computed and recorded in files. During the DynamicTrial, the files created previously were read to create the segmental markers on the corresponding segment. It is important to note that both parts are “independent”; it is not necessary to always run both parts, but it is required to run at least once the Initialization part to obtain the data subsequently used in the DynamicTrial part. For example, if two gait files correspond to a same initialization file, it is necessary to run the Initialization with the Initialization file first, but it is not required to run it again between the two gait files.

### III.C. Scaling functions

It was possible to run the kinematics programme without scaling the model. However, the joint angles computed were not realistic when compared to the published literature and varied substantially between horses, indicating a problem of scaling. Within the model it is possible to scale the individual bone segments using the joint markers (the markers placed on the lateral and medial side of the centre of rotation of the joints when collecting the Initialization file, as explained in Chapter 4). The first scaling function coded was scaling each individual bone in the three dimensions by the factor  $\frac{\text{Bone length measured on live horse}}{\text{Length of the model bone}}$ . As illustrated in Figure 4, this scaling function can be problematic when one of the bones is bigger and the other one smaller (the bone of the live horse compared to

the CT scanned bones). Indeed, if the scaling values are different between bones then these can change the joint surfaces variably. This can lead to unrealistic joint geometries.

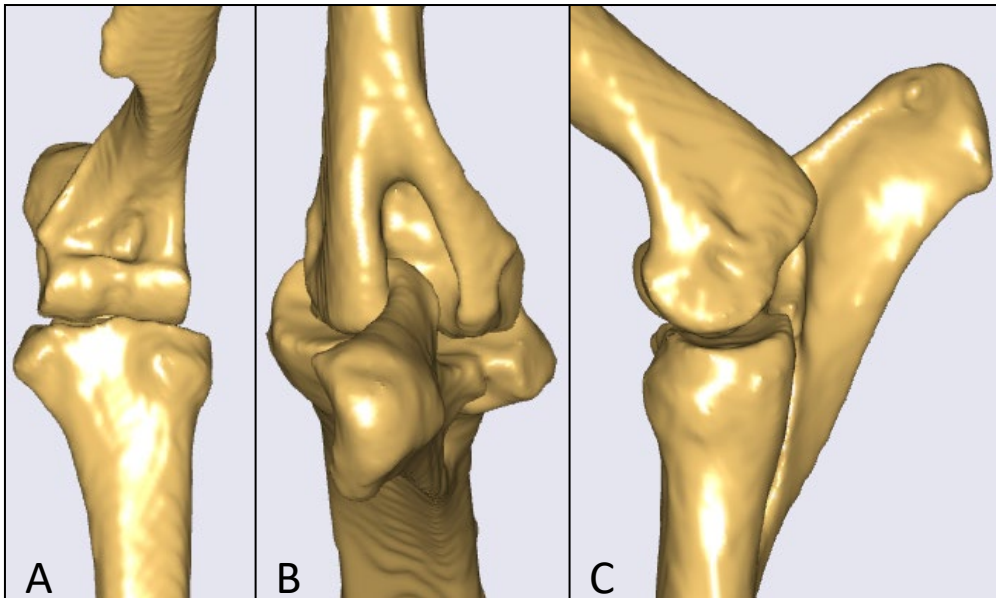


Figure 4 Dorsal (A), ventro-caudal (B) and medial (C) views of the elbow with the brachium and antebrachium scaled with the first scaling function.

The second option was to scale by the length of the bone, but leave the cross-sectional area unscaled. As illustrated in Figure 5, this method resulted in obvious gross distortion of the shape/ geometry of some bones outside the normal variation in geometry expected from the literature or from the dissection material. The result of this incorrect geometry was alteration in the inertial properties of the segment and incorrect anatomical locations for origin and insertion sites of the muscles and ligaments.

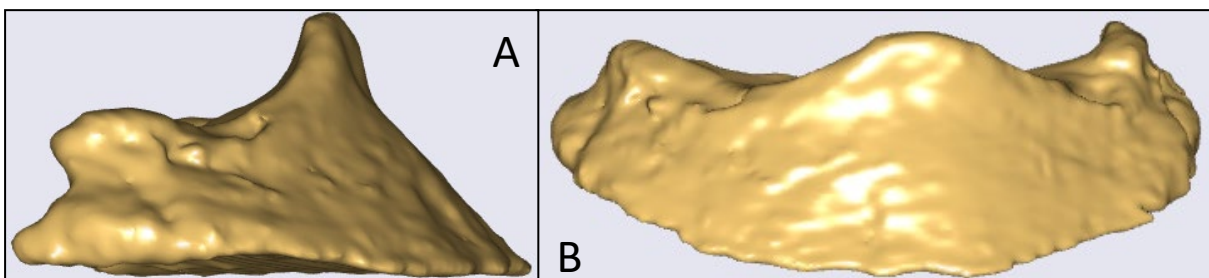


Figure 5 Lateral (A) and dorso-caudal (B) views of the distal phalanx scaled by the second scaling function

The last solution applied was to scale the bones along the vertical axis by the factor described above and to scale the cross sectional area by the general factor  $\frac{\text{Total length of the live horse limb}}{\text{Total length of the CT-scanned limb}}$  (illustrated in Figure 6).

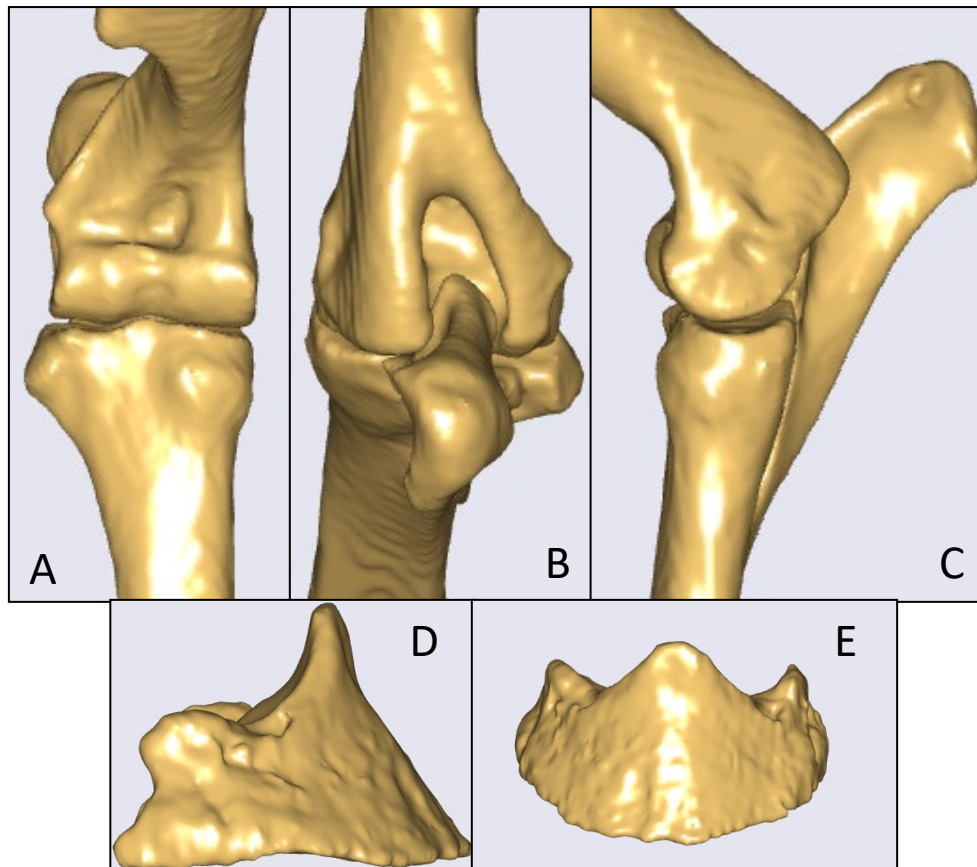
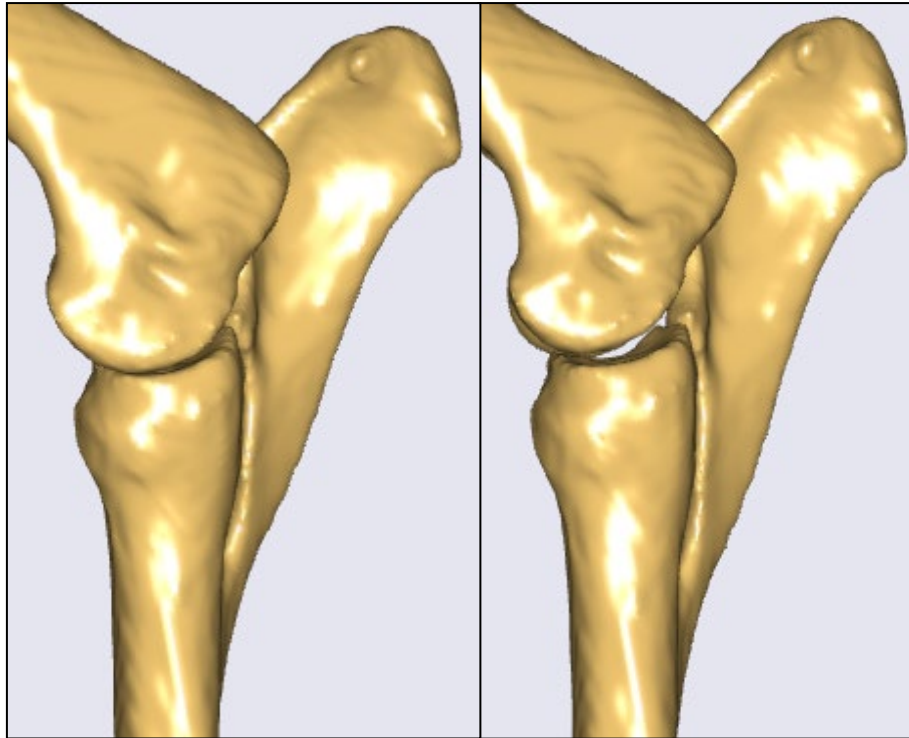


Figure 6 Dorsal (A), ventro-caudal (B) and medial (C) views of the elbow and lateral (D) and dorso-caudal (E) views of the distal phalanx with all segments scaled by the third scaling function

Moreover, scaling the bones also required scaling the slack length of the ligaments, so a function was written to measure the length of the ligaments in the standing position, which was then considered as the slack length. These steps (scaling the bones and slack length of ligaments) were made before those described earlier in the paragraphs III.A and III.B, which resulted in a first loop called “Scaling”.

Subsequent testing revealed another problem with the scaling function when running the model, that the joint geometries were modified and again resulted in definitions that were outside biological plausibility. This was due to the positions of the joint points being scaled with the segment in which they are defined, rather than across the joint. Thus, if the two segments composing a joint do not have the same vertical scaling factor, the joint geometry is subsequently modified (Figure 7).



*Figure 7 Problem of joint geometry due to scaling. Medial views of the elbow of the CT-scanned bones (on the left) and of the scaled segments (on the right)*

To appropriately scale the joint space, points were added on the bony surface at each joint contact surface for each bone. The displacement vector was defined as the vector between the bony joint contact surface points of the joint, and its coordinates for the CT-scanned limb were saved. These vectors were then scaled by the general factor in the horizontal transverse and horizontal cranio-caudal directions and by the average of the scaling factors of the two bones composing the joint in the vertical direction. The joint point representing the centre of rotation (for example, on the proximal humerus for the shoulder joint) was kept and the one on the other bone was suppressed to achieve agreement in scaling. This process was repeated throughout the limb to achieve appropriate scaling around the joints.

During the scaling phase, the coordinates of the centre of rotation of each joint were computed in the reference frame of the segment in which it was not defined (for example on the scapula for the shoulder joint). The rotations between the segments were saved in files as they are necessary to constrain the rotations of the joints. The final scaling function with all the features described is illustrated in Figure 8 for the elbow joint.



*Figure 8 Medial view of the elbow with the segments and joint geometries scaled by the final scaling function*

Using this latest scaling function, the joint angles during locomotion were computed again. As a result of this scaling, the amplitude of movement of the joint angles were within biological plausibility and were observed to have greater consistency between horses with the AnyBody model.

#### III.D. Changing the segment definitions

A remaining problem of the scaling function was the scaling of the smallest bones, especially the carpal bones. Indeed, due to the shape of the bones within the carpus, it is difficult to define the z-axis (long axis of the bone) which is primarily used for scaling. With consideration of the structure of the carpus and the articulation across the carpal bones the simple constraining of the carpus to a simple single articulation provided an elegant solution to this scaling problem. Constraining the antebrachiocondylar joint to a simple hinge joint also reflected the way the joint markers were defining the carpus within the kinematic study. Therefore, the carpus was included in the same segment as the metacarpus, reducing the number of segments in the model to six:

- 1- Scapula
- 2- Brachium
- 3- Antebrachium
- 4- All 7 carpal bones, metacarpus and both proximal sesamoid bones as a segment
- 5- Pastern with proximal and middle phalanges combined as a segment
- 6- Distal phalanx and distal sesamoid bone as a segment.

These new segment definitions had also the advantage of having their inertial properties previously reported by Buchner *et al.* (1997), which was more accurate than evaluating them with SolidWorks®.

### III.E. Kinetic study

The next step in development of the complete model was the computation of the forces within the muscles. To check the ability of the model to calculate the kinetic variables, 6 virtual muscles were created for each joint to provide the forces required for flexion/extension, abduction/adduction and external/internal rotation movements; and 12 virtual muscles were created to provide the forces required for positioning the scapula (3 translations and 3 rotations). These virtual muscles were only defined by a movement (translation along an axis or rotation about an axis), a direction of action and a maximal isometric force. It was then possible to run the inverse dynamics function in the model. By recording the force within the tendons and muscles, it appeared that the “real” muscles were not used (no forces were computed within them). This could have been related to the use of the optimisation function within AnyBody to optimise the load sharing between the muscles. Indeed, if the maximal forces of the virtual muscles are much greater than those of the “real” muscles, the model will preferentially use the virtual muscles. The maximal forces of the “real” muscles were increased and the maximal forces of the virtual muscles were decreased as much as possible. However, the virtual muscles were still doing most of the work.

In order to understand the contribution of the virtual muscles in the model, the abduction/adduction and axial rotation movements were computed and were revealed to be quite important. The model was then limited to flexion/extension, and the muscle models used were changed to a 2-element Hill model. Using the 2-element Hill model resulted in the real muscles providing forces. However, the real muscles were still unable to provide the forces necessary and it was, thus, still not possible to remove the virtual muscles.

The last muscle model tested was the 3-element model. It was tested for all muscles because it uses the pennation angle, which is an important variable to determine the role of a muscle in terms of its ability to shorten during concentric activation. With this muscle model, the activation and deactivation of the muscles with a pennation angle greater than 20° were observed to be closer to those reported by Harrison *et al.* (2012), and these muscles were observed to provide greater forces than previously. However, the muscles with a pennation angle less than 20° provided smaller forces than with the previous muscle model. It was then decided to keep a 3-element Hill model for the muscles whose pennation angle was greater than 20° and return to a 2-element Hill model for the others. It was possible to remove all the virtual muscles for the elbow, carpal and fetlock joints and to reduce the peak isometric force of the virtual muscles for the coffin. As most of the muscles acting on the shoulder and between the trunk and the scapula were not included in this model, it would not be possible to remove the virtual muscles acting on them.

## Predicting horse limb responses to surface variations

A new function had to be created to measure and save the muscle-tendon unit during scaling, and to compute the tendon length at peak isometric force during Initialization and DynamicTrial. The calculation of the tendon length at peak isometric force was based on the muscle-tendon length saved during the scaling part and two parameters, the proportion of tendon length (relative to the muscle-tendon length) and the deformation at peak isometric force. To change the state of the ligaments from unstrained to a little strained in the standing position of the horse, a factor was introduced to slightly reduce their slack lengths.

The final step of modelling was to create a ground reaction force. Two main methods were identified. The first is to model a force plate and create a function that would compute a force based on data collected. The second method is to create a prediction function. Force data were not able to be collected during the gait study and thus the second method (prediction) was the one that was selected for this model. The prediction function was created using the tools provided in the AnyBody Managed Model Repository. The force is computed using the mass of the limb and the friction forces between the segment and the ground. The prediction function requires “ground contact” points to compute a force; the force will be predicted depending on some parameters relative to these points, such as their velocities and heights. For this, some points (Figure 9) were added on the distal phalanx. The parameters that defined when to compute a force have been modified and those chosen (a limit velocity of  $15\text{m}\cdot\text{s}^{-1}$  and a limit vertical distance of 10 cm) provided a force during the whole stance phase but a force was also generated during the lowest part of the swing phase. A function has then been included to compute and save the height and velocity of the hoof contact points. After analysing them, the parameters chosen were  $14\text{m}\cdot\text{s}^{-1}$  for the limit velocity and 5cm for the limit vertical distance.

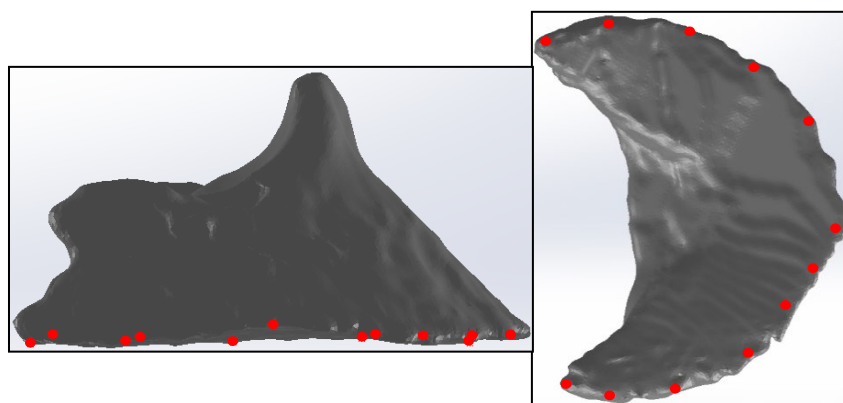


*Figure 9 Lateral (on the left) and cranial (on the right) of the distal phalanx with the contact points (red points)*

### III.F. Final version

Hereafter, “input” will refer to the data relative to a horse used for collecting gait data. For example, the segment lengths of the live horse are inputs but not the CT-scanned bones, which are part of the model.

The final version of the musculoskeletal model of the Thoroughbred forelimb is representing in Figure 10. To summarise, the final model is composed of three parts: Scaling, Initialization, DynamicTrial.

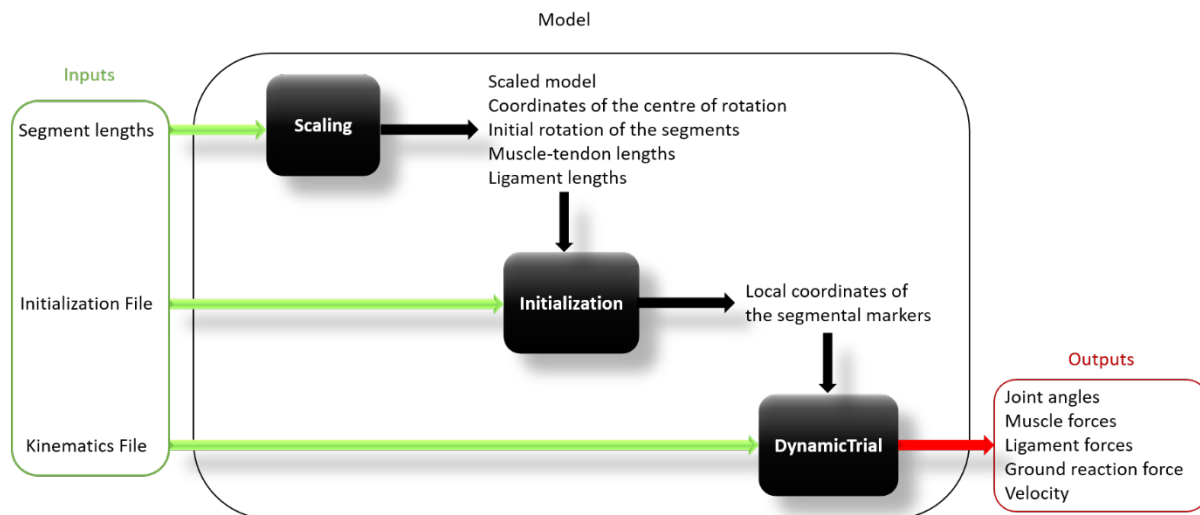


Figure 10 Diagram of the model

The Scaling part can only be run with the kinematic programme. It positions the segments by the distances and rotations of the nodes on the joint bony surfaces and scales the segments and joint geometries. It then computes the local coordinates on the segment that does not contain the centre of rotation of the joints (on the scapula for the shoulder, on the antebrachium for the elbow, on the carpo-metacarpal segment for the carpal joint, on the pastern for the fetlock and on the hoof for the coffin). It also computes the flexion, abduction and axial rotation of the joints, and the lengths of the muscle-tendon units and ligaments, so all the data for the scaled model are saved.

The Initialization part can likewise only be run with the kinematic program. It positions the segments by using the marker locations from the Initialization file while constraining all the joint translations to be null and all the joint abduction and rotation, as well as the flexion of the shoulder and coffin, with the data computed in the Scaling part. The only movement allowed in this part is thus the flexion/extension of the elbow, carpal and fetlock joints. It then computes the local coordinates of the segmental markers.

The DynamicTrial part can be run with either the kinematics or the inverse dynamics. However, to compute the forces within the muscles, it is necessary to run the inverse dynamics. Only the flexion and extension of the limb joint is allowed, the translations of the joint are constrained to be null and the joint axial rotations and abductions are constrained to be those saved in the scaling part. For each step, the model positions the segments by using the segmental markers and respecting the joint constraints. For the whole motion, it computes the individual joint angles, muscle forces, ligament and tendon strains, the predicted ground reaction force, and the velocity of the horse.

All parts of the model do not need to be run every time. The Scaling part only has to be run only when the data are from another horse and the Initialization part when the initialization file is changed. The DynamicTrial is run for every gait file.

## IV. Conclusion & Discussion

There are a number of limitations in the preliminary model, which are detailed below.

The segments have been defined based on those for which it is possible to collect kinematic data. However, it means the proximal sesamoid bones could not be modelled as a separate segment and had to be included in another segment. The insertion and origin sites of the tendons and ligaments that are localized on the proximal sesamoid bones were modelled in the pastern segment and the metacarpal segment, respectively. The strain in these tendons and ligaments depend on the angle between the proximal sesamoid bones and the metacarpus or the pastern, but in the musculoskeletal model, they depended on the angle between the metacarpus and the pastern. It is then expected that the strain in these tendons and ligaments would be overestimated.

The points used to define the joints, to define the lateral and medial sides of the centre of rotation of the joints or to define the attachment sites of the soft tissues, as well as the reference frame of each segment were defined manually using SolidWorks®. That could introduce some errors in the path definition of the tendons and ligaments and so modify their actions on the joints they are crossing. Indeed, the reliability of force predictions depends on the accuracy of the musculoskeletal geometry, represented by muscle moment arms and estimated by the identification of the muscle-tendon lines-of-action, in terms of attachment sites and via points (Carbone *et al.*, 2012; Carbone *et al.*, 2015; Hoy *et al.*, 1990; Out *et al.*, 1996; Pal *et al.*, 2007; Rohrle *et al.*, 1984).

The musculoskeletal model developed in this chapter was based on the bone geometries of one Thoroughbred. To be used with the data collected from live horses, the model has to be scaled. The scaling functions that were implemented scaled the model linearly. It can be supposed that it would

be a good approximation to scale the model for horses of the same breed and of reasonably similar size. However, if this method were to be employed to model a horse with drastically different mass or dimensions than the Thoroughbred from which the model was constructed (for instance, a draught horse or a pony), it is likely that the model would behave unrealistically. A future study should evaluate whether the outputs from such a scaled model behaved linearly or allometrically.

A predicted ground reaction force from the mass of the limb segments was not sufficient to model the true effects of the limb plus superincumbent trunk at the hoof-ground interface and so this calculated force was not realistic during the stance phase. Ground reaction forces are required to model the moments of force around the limb joints, for determination of mechanical power during gait, but not to determine strain in ligaments from the segmental orientations. Therefore, only kinematic data from the motion of the limb segments were used to model the length changes in the tendons and ligaments caused by the segmental rotations about the joints. In addition, the scapulo-thoracic "joint" was not considered in the development of the model due to the artefact caused by real motion of the scapula under the skin markers and the presence of the saddle, which would have made this impossible to correct. Biceps and triceps were included in the model from their origins on the scapula. Other (extrinsic) muscles acting across the shoulder joint have their origins on the thorax. These muscles were not included in the model, which would have led to overestimation of the forces in triceps and biceps, and that overestimate would have then been transmitted to the other muscles and ligaments through joint momentum. This is why the strains in the soft tissues, computed directly from their lengths using the segmental kinematic data, have been studied and not the stresses.

Notwithstanding the limitations of this preliminary model of the forelimb, it was tested in the next Chapter with kinematic data from horses at trot and canter. The results computed with these data will then be compared to joint excursions reported in the literature to assess whether the outputs from the model approximate established data in the literature.

## V. References

- Alamdari, A. and Krovi, V. N. (2017) 'Chapter 2, A review of computational musculoskeletal analysis of human lower extremities', In Ueda, J. and Kurita, Y. (eds.) *Human Modelling for Bio-inspired Robotics: Mechanical Engineering in Assistive Technologies*: Academic Press, pp. 37-73.
- Brown, N. A. T., Pandy, M. G., Kawcak, C. E. and McIlwraith, C. W. (2003b) 'Force- and moment-generating capacities of muscles in the distal forelimb of the horse', *Journal of Anatomy*, 203(1), pp. 101-113.
- Buchner, H. H. F., Savelberg, H. H. C. M., Schamhardt, H. C. and Barneveld, A. (1997) 'Inertial properties of Dutch warmblood horses', *Journal of Biomechanics*, 30(6), pp. 653-658.
- Carbone, V., Van der Krogt, M. M., Koopman, H. F. J. M. and Verdonshot, N. (2012) 'Sensitivity of subject-specific models to errors in musculo-skeletal geometry', *Journal of Biomechanics*, 45(14), pp. 2476-2480.
- Carbone, V., Fluit, R., Pellikaan, P., Krogt, M. M. v. d., Janssen, D., Damsgaard, M., Vigneron, L., Feilkas, T., Koopman, H. F. J. M. and Verdonshot, N. (2015) 'TLEM 2.0 – A comprehensive musculoskeletal geometry dataset for subject-specific modeling of lower extremity', *Journal of Biomechanics*, 48(5), pp. 734-741.
- Harrison, S. M., Whitton, R. C., Kawcak, C. E., Stover, S. M. and Pandy, M. G. (2010) 'Relationship between muscle forces, joint loading and utilization of elastic strain energy in equine locomotion', *The journal of Experimental Biology*, 213(Pt23), pp. 3998-4009.
- Harrison, S. M., Whitton, R. C., King, M., Haussler, K. K., Kawcak, C. E., Stover, S. M. and Pandy, M. G. (2012) 'Forelimb muscle activity during equine locomotion', *The journal of Experimental Biology*, 215(17), pp. 2980-2991.
- Hoy, M. G., Zajac, F. E. and Gordon, M. E. (1990) 'A musculoskeletal model of the human lower extremity: The effect of muscle, tendon, and moment arm on the moment-angle relationship of musculotendon actuators at the hip, knee, and ankle', *Journal of Biomechanics*, 23(2), pp. 157-169.
- Lawson, S. E. M., Chateau, H., Pourcelot, P., Denoix, J.-M. and Crevier-Denoix, N. (2007) 'Sensitivity of an equine distal limb model to perturbations in tendon paths, origins and insertions', *Journal of Biomechanics*, 40(11), pp. 2510-2516.
- Moissenet, F., Modenese, L. and Dumas, R. (2017) 'Alterations of musculoskeletal models for a more accurate estimation of lower limb joint contact forces during normal gait: A systematic review', *Journal of Biomechanics*, 63, pp. 8-20.
- Out, L., Vrijkotte, T. G., van Soest, A. J. and Bobbert, M. F. (1996) 'Influence of the parameters of a human triceps surae muscle model on the isometric torque-angle relationship', *Journal of Biomechanical Engineering*, 118(1), pp. 17-25.
- Pal, S., Langenderfer, J. E., Q., S. J., Laz, P. J., Petrella, A. J. and Rullkoetter, P. J. (2007) 'Probabilistic modeling of knee muscle moment arms: effects of methods, origin-insertion, and kinematic variability', *Annals of Biomedical Engineering*, 35(9), pp. 1632-1642.
- Rajagopal, A., Dembia, C. L., DeMers, M. S., Delp, D. D., Hicks, J. L. and Delp, S. L. (2016) 'Full body musculoskeletal model for muscle-driven simulation of human gait', *IEEE Transactions on Biomedical Engineering*, 63(10), pp. 2068-2079.
- Rohrle, H., Scholten, R., Sigolotto, C., Sollbach, W. and Kellner, H. (1984) 'Joint forces in the human pelvis-leg skeleton during walking', *Journal of Biomechanics*, 17(6), pp. 409-424.
- Swanstrom, M. D., Zarucco, L., Hubbard, M., Stover, S. M. and Hawkins, D. A. (2005) 'Musculoskeletal modeling and dynamic simulation of the Thoroughbred equine forelimb during stance phase of the gallop', *Journal of Biomechanical Engineering*, 127(2), pp. 318-328.
- Symons, J. E., Fyhrie, D. P., Hawkins, D. A., Upadhyaya, S. K. and Stover, S. M. (2014b) 'Race surface model development in a musculoskeletal modelling environment', *Procedia Engineering*, 72, pp. 913-918.

### Chapter 3 Development of the musculoskeletal model

Symons, J. E., Hawkins, D. A., Fyhrie, D. P., Upadhyaya, S. K. and Stover, S. M. (2016) 'Modelling the interaction between racehorse limb and race surface', *Procedia Engineering*, 147, pp. 175-180.

# Chapter 4

## Testing the preliminary model with gait data

### I. Introduction

The aim of this part of the thesis was to test the performance of the preliminary AnyBody (AnyBody Modeling System™, AnyBody Technology A/S, Denmark) model in describing the sagittal plane excursions of the forelimb joints during trot and canter, and to compare the outputs from the model against other studies reported in the literature. The musculoskeletal model developed earlier (in Chapter 3) was driven with kinematic data recorded from gait trials with four Thoroughbred horses.

### II. Method & Material

#### II.A. Experimental setup

Gait data were collected from four Thoroughbreds on three consecutive days in an indoor riding arena (60m x 30m) at a commercial equestrian centre. The surface of the indoor school consisted of a sand mixture, approximately 6 cm deep on top of crushed limestone. A runway was set up along the length of the arena, to capture at least one complete stride at trot and at canter. To facilitate the correct passage of the horse through the calibrated measurement area, poles were laid on the sand to create an entrance to the runway (Figure 11). The right and left boundaries of the runway were sketched in the sand to enable positioning and aiming of cameras for recording limb movements during at least one complete stride. A cubic volume of space was mapped out to include the first landing of the right forelimb through to the next landing of the same limb, plus additional length at each end to account for variation in landing position from trial to trial. The height of this cubic volume of space was approximately 2m, to capture markers on the horse's limb from the hoof to the scapula.

To collect motion data from markers on the limb, a six-camera Qualisys system was used (Qualisys AB, Gothenborg, Sweden). The six cameras were positioned on one side of the runway, and oriented so that:

- All the cameras had the central part of the runway in their field of view.
- All the forelimb markers during at least a whole stride (at trot and canter) were in the field of view of at least three cameras

## Chapter 4 Testing the preliminary model with gait data

The complete set-up is illustrated in Figure 11. The whole cubic volume of interest was then calibrated with the use of a reference frame and a calibration wand using Qualisys Track Manager. The reference frame was a static L-shaped frame placed level on the surface with four markers that identified the sagittal and transverse axes of the runway and set the global coordinates of the calibrated space. Two markers situated exactly 600 mm apart on a T-shaped wand were used to calibrate the entire cubic volume by moving the wand in multiple (3D) orientations in the field of view of all cameras and encompassing the entire 3D volume of the runway.

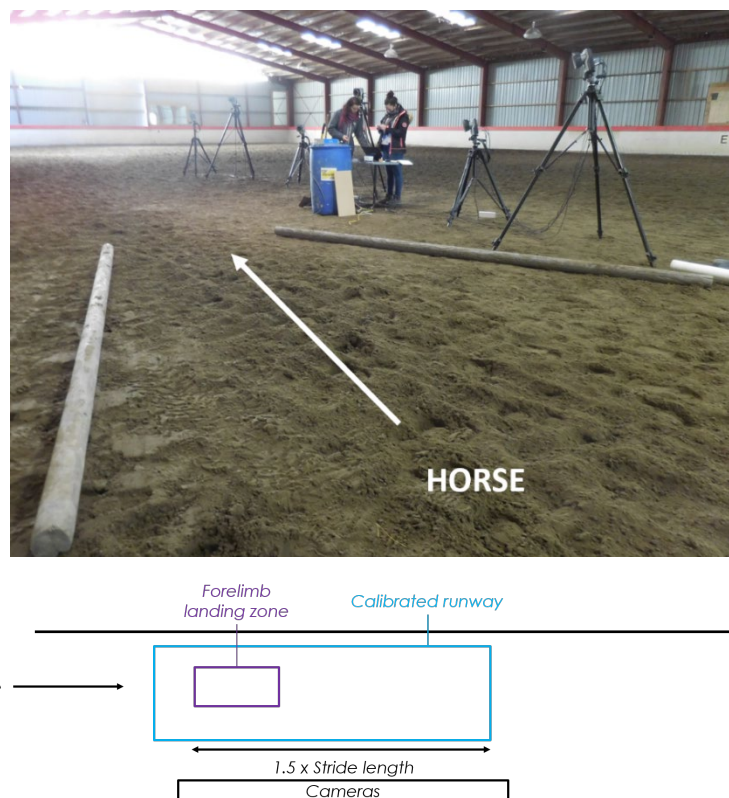


Figure 11 Picture of the camera set-up used to collect gait data (on top) and diagram of the camera set-up (on bottom). The horse forelimb was aimed to land in the “forelimb landing zone” represented on the diagram, which match the zone just after the poles on the ground.

### II.B. Markers

Two types of files were necessary, as outlined in Figure 10 in Chapter 3. The first was called “Initialization file” and the second “gait file”.

Eighteen passive spherical reflective markers (called “segmental markers”) were taped to the skin of the forelimb with a group of three per limb segment (scapula, brachium, antebrachium, carpus/metacarpus, pastern and hoof). Eight additional passive spherical markers (called “joint

markers”) were taped on the centre of rotation of each joint: one on the lateral side of the shoulder, elbow, carpus, fetlock and coffin and one on the medial side of the carpus, fetlock and coffin. The marker set is illustrated in Figure 12. The horse was then brought into the calibrated volume to record the full marker set for 2 seconds while standing still (unridden). The data file obtained was the Initialization file. It was later used to locate the segmental markers in the model at the correct positions relative to the joint markers.



*Figure 12 Picture of a horse equipped with the whole set of markers used to collect the Initialization data*

Once these data were collected, the eight joint markers were removed, leaving only the segmental markers. The horse was then ridden in front of the cameras for multiple trials at trot and canter and the data saved. The trials were repeated until at least five good files were obtained for each gait. A gait data file was identified as “good” if the right forelimb landed squarely in the landing zone (Figure 11) and the entire stride was captured in the calibrated runway space. The runway was raked between trials to ensure the ground surface was not compacted by the previous passage.

The kinematic data collected were then processed with Qualisys Track Manager and converted to c3d format.

### III. Results

Kinematic data files were considered “good” and kept for processing in the model if all the marker trajectories were recorded from the beginning of a stance phase to the end of the following swing

phase. Horse velocity was computed as the average velocity of the three Scapula segment markers over the whole stride.

### III.A. Kinematic files

#### III.A.1. Trot files

The number of good files at trot were greater than expected. Between seven and nineteen files were kept for each horse. For all the 53 files from the four horses, horse velocity varied between  $2.11 \text{ m}\cdot\text{s}^{-1}$  and  $3.72 \text{ m}\cdot\text{s}^{-1}$  with an average of  $2.79 \pm 0.39 \text{ m}\cdot\text{s}^{-1}$ ; stance phase duration varied between 0.280 s and 0.470 s with an average of  $0.364 \pm 0.045 \text{ s}$ ; and the swing phase duration varied between 0.305 s and 0.435 s with an average of  $0.394 \pm 0.034 \text{ s}$ .

The detailed trot file characteristics per horse are presented in Table 5. From this Table, it is particularly noticeable that the stance phase was shorter than the swing phase for three horses but was longer for Horse 2. This difference is probably due to velocity, which was observed to be slower for that same horse compared to the others.

*Table 5 Trot data files, details per horse: number of files, velocity, stance phase duration and swing phase duration (average  $\pm$  standard deviation).*

Horse	Number of files	Velocity ( $\text{m}\cdot\text{s}^{-1}$ )	Stance phase duration (s)	Swing phase duration (s)
Horse1	15	$2.99 \pm 0.32$	$0.323 \pm 0.028$	$0.416 \pm 0.010$
Horse2	19	$2.36 \pm 0.12$	$0.410 \pm 0.030$	$0.359 \pm 0.027$
Horse3	12	$3.04 \pm 0.10$	$0.342 \pm 0.009$	$0.420 \pm 0.012$
Horse4	7	$3.08 \pm 0.32$	$0.365 \pm 0.037$	$0.398 \pm 0.032$
<b>Total</b>	<b>53</b>	<b><math>2.79 \pm 0.39</math></b>	<b><math>0.364 \pm 0.045</math></b>	<b><math>0.394 \pm 0.034</math></b>

#### III.A.2. Right lead canter files

Between three and nine files were kept for each horse for the right lead canter. The data were collected from the right forelimb, which means that the data collected here were those of the leading forelimb. For all the 23 files from the four horses, horse velocity varied between  $3.55 \text{ m}\cdot\text{s}^{-1}$  and  $4.54 \text{ m}\cdot\text{s}^{-1}$  with an average of  $4.09 \pm 0.27 \text{ m}\cdot\text{s}^{-1}$ ; stance phase duration varied between 0.215 s and 0.285 s with an average of  $0.245 \pm 0.019 \text{ s}$ ; and the swing phase duration varied between 0.310 s and 0.390 s with an average of  $0.355 \pm 0.023 \text{ s}$ .

The detailed right lead canter file characteristics per horse are presented in Table 6.

## Predicting horse limb responses to surface variations

Table 6 Right lead canter data files, details per horse: number of files, velocity, stance phase duration and swing phase duration (average  $\pm$  standard deviation).

Horse	Number of files	Velocity (m.s <sup>-1</sup> )	Stance phase duration (s)	Swing phase duration (s)
Horse1	6	4.12 $\pm$ 0.26	0.230 $\pm$ 0.012	0.372 $\pm$ 0.012
Horse2	9	4.02 $\pm$ 0.30	0.253 $\pm$ 0.014	0.336 $\pm$ 0.017
Horse3	5	4.17 $\pm$ 0.14	0.236 $\pm$ 0.009	0.373 $\pm$ 0.012
Horse4	3	4.11 $\pm$ 0.42	0.263 $\pm$ 0.029	0.347 $\pm$ 0.021
<b>Total</b>	<b>23</b>	<b>4.09 <math>\pm</math> 0.27</b>	<b>0.245 <math>\pm</math> 0.019</b>	<b>0.355 <math>\pm</math> 0.023</b>

### III.A.3. Left lead canter files

Between two and eight files were kept for each horse for the left lead canter. The data were collected from the right forelimb, which means that the data collected here were those of the trailing forelimb. For all the 21 files from the four horses, horse velocity varied between 3.94 m.s<sup>-1</sup> and 5.62 m.s<sup>-1</sup> with an average of 4.44  $\pm$  0.33 m.s<sup>-1</sup>; stance phase duration varied between 0.215 s and 0.265 s with an average of 0.243  $\pm$  0.014 s; and the swing phase duration varied between 0.320 s and 0.410 s with an average of 0.361  $\pm$  0.024 s.

The detailed left lead canter file characteristics are presented in Table 7.

Table 7 Left lead canter data files, details per horse: number of files, velocity, stance phase duration and swing phase duration (average  $\pm$  standard deviation).

Horse	Number of files	Velocity (m.s <sup>-1</sup> )	Stance phase duration (s)	Swing phase duration (s)
Horse1	3	4.11 $\pm$ 0.15	0.242 $\pm$ 0.019	0.370 $\pm$ 0.013
Horse2	8	4.52 $\pm$ 0.14	0.245 $\pm$ 0.011	0.336 $\pm$ 0.013
Horse3	8	4.31 $\pm$ 0.07	0.248 $\pm$ 0.010	0.380 $\pm$ 0.014
Horse4	2	5.08 $\pm$ 0.77	0.218 $\pm$ 0.004	0.370 $\pm$ 0.000
<b>Total</b>	<b>21</b>	<b>4.44 <math>\pm</math> 0.33</b>	<b>0.243 <math>\pm</math> 0.014</b>	<b>0.361 <math>\pm</math> 0.024</b>

### III.B. Sagittal plane joint movements

Joint angles were computed for all gait files collected. To enable consistent definition of the stance-swing transition time across the four horses, the joint excursions were time-normalized in stance and swing phases separately, so that -1 corresponds to the beginning of the stance phase, 0 to the end of

the stance phase and beginning of the swing phase and 1 to the end of the swing phase. The joint angles were defined so that  $0^\circ$  corresponds to the segments being aligned, a positive angle to a flexed position and a negative angle to an extended position.

### III.B.1. Coffin joint excursion

Figure 13 illustrates the joint angle definition for the coffin joint, in a position near the maximal measured extension on the left, near the maximal measured flexion on the right and in an intermediate position in the middle.

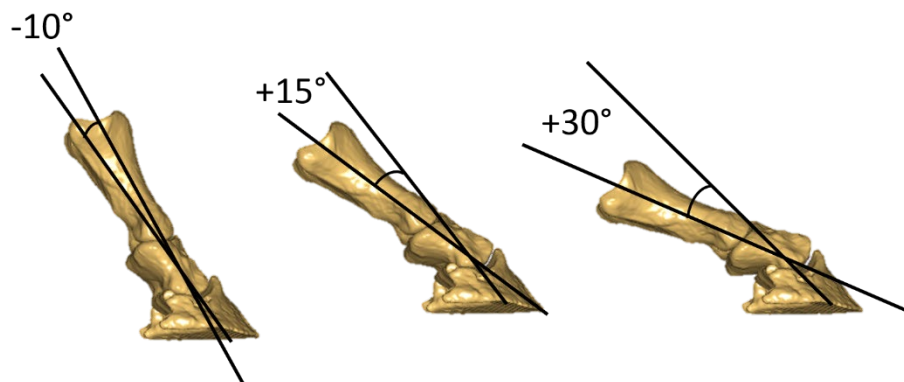


Figure 13 Example of coffin angles. Joint angle is defined as the angle between the long axis of the metacarpus segment and the long axis of the pastern segment, as indicated. The positive sign corresponds to a flexed position and the negative sign to an extended position.

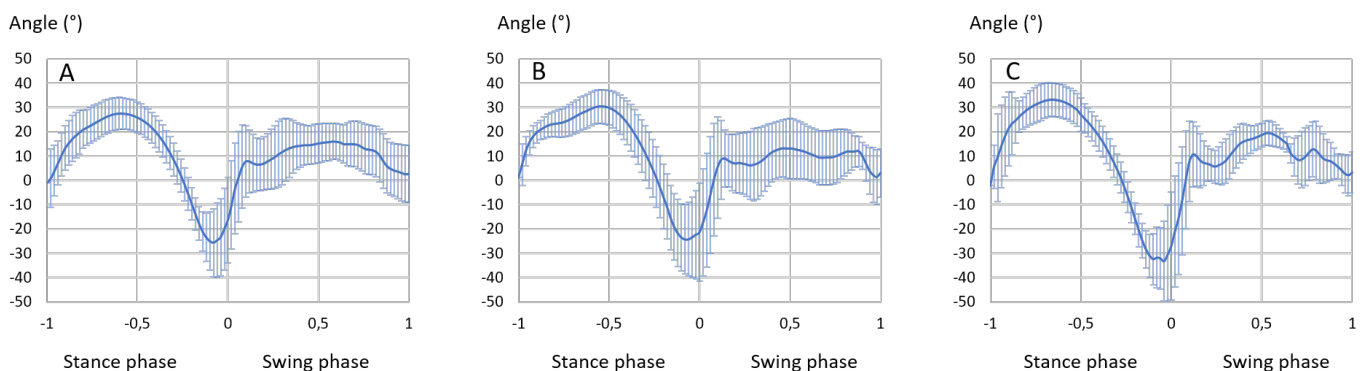


Figure 14 Right forelimb coffin joint excursions at trot (A), right lead canter (B) and left lead canter (C). The graphs present the average and standard deviation computed from all the gait data files ( $n=53$  files for trot,  $n=23$  for right lead canter and  $n=21$  files for left lead canter). The data were time-normalized from -1 to 0 as stance phase and from 0 to 1 as swing phase.

The coffin joint excursion computed by the model for all three gaits are presented in Figure 14. Flexion and extension peaks and their time of occurrence during the stance phase and the maximal extension and flexion values during the swing phase were compared to data reported in the literature. The coffin joint excursions have been reported in the literature for trot gait only and are reported in Table 8. The coffin flexion and extension peaks at right or left lead canter have not been reported in the literature.

## Predicting horse limb responses to surface variations

Table 8 Right forelimb coffin flexion and extension peaks at trot. Amplitude and time of occurrence reported in the literature and computed in the model (average  $\pm$  standard deviation). The data were time-normalized from -1 to 0 as stance phase and from 0 to 1 as swing phase.

	Data from	Back (2001)	This study
During the stance phase	The coffin joint is first flexing up to	25.8°	28.4 $\pm$ 6.4°
	at time	-0.62	-0.60 $\pm$ 0.05
	It is then extending up to	-24.8°	-27.6 $\pm$ 15°
	at time	-0.08	-0.11 $\pm$ 0.14
During the swing phase	The coffin joint moves in swing between extension of	2.3°	6.6 $\pm$ 19.0°
	and flexion of	17.3°	22.3 $\pm$ 9.0°

In the model, at right lead canter, the coffin joint first flexes up to  $30.8 \pm 6.9^\circ$  (average  $\pm$  standard deviation) at time  $-0.55 \pm 0.08$ , and it then extends to  $-29.7 \pm 18.0^\circ$  at time  $-0.09 \pm 0.06$  before oscillating in the swing phase between  $1.5 \pm 10.0^\circ$  and  $20.3 \pm 9.7^\circ$ .

In the model, at left lead canter, the coffin joint first flexes to  $35.5 \pm 11.6^\circ$  at time  $-0.68 \pm 0.08$ , it then extends to  $-40.0 \pm 17.0^\circ$  at time  $-0.09 \pm 0.05$  before oscillating in the swing phase between  $2.2 \pm 8.4^\circ$  and  $23.6 \pm 6.8^\circ$ .

### III.B.2. Fetlock joint excursion

Figure 15 illustrates the joint angle definition for the fetlock joint, in a position near the maximal measured extension on the left, near the maximal measured flexion on the right and in an intermediate position in the middle.

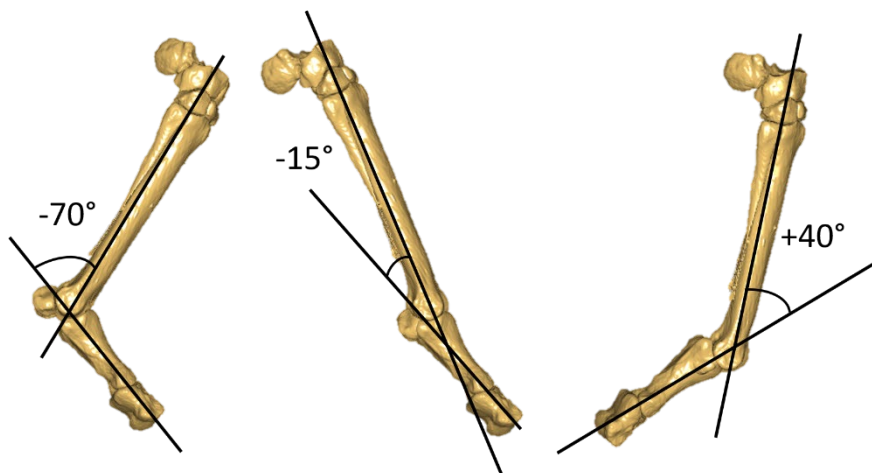


Figure 15 Example of fetlock angles. Joint angle is defined as the angle between the long axis of the metacarpus segment and the long axis of the pastern segment, as indicated. The positive sign corresponds to a flexed position and the negative sign to an extended position.

## Chapter 4 Testing the preliminary model with gait data

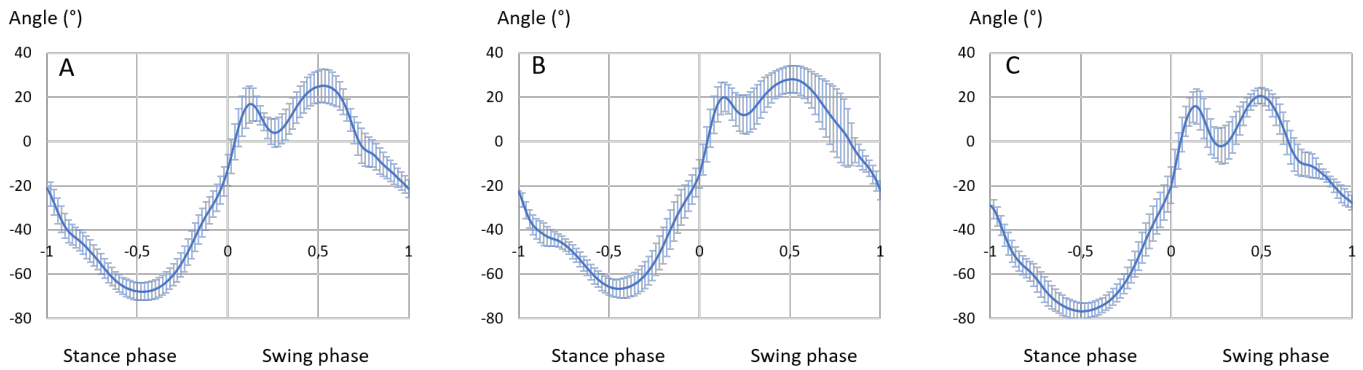


Figure 16 Right forelimb fetlock joint excursions at trot (A), right lead canter (B) and left lead canter (C). The graphs present the average and standard deviation computed from all the gait data files ( $n=53$  files for trot,  $n=23$  for right lead canter and  $n=21$  files for left lead canter). The data were time-normalized from -1 to 0 as stance phase and from 0 to 1 as swing phase.

The fetlock joint excursions computed by the model for all three gaits are represented in Figure 16. To compare the data computed by the model to the data reported in the literature, flexion and extension peaks and their time of occurrence during both the stance and the swing phases were compared. The data for the fetlock joint excursion are reported in Table 9 for trot, in Table 10 for right lead canter and in Table 11 for left lead canter.

Table 9 Right forelimb fetlock flexion and extension peaks at trot. Amplitude and time of occurrence reported in the literature and computed in the model (average  $\pm$  standard deviation). The data were time-normalized from -1 to 0 as stance phase and from 0 to 1 as swing phase.

	Data from	Clayton <i>et al.</i> (2011)	Back (2001)	This study
During the stance phase	The fetlock joint extends to	-61.5°	-65.1°	-67.9 $\pm$ 4.0°
	at time	-0.52	-0.46	-0.48 $\pm$ 0.04
During the swing phase	It then flexes to	8.5°	7.2°	18.9 $\pm$ 2.5°
	at time	0.17	0.11	0.13 $\pm$ 0.04
	before extending to	-1.5°	-9.4°	2.8 $\pm$ 6.0°
	at time	0.31	0.27	0.27 $\pm$ 0.03
	It finally flexes to	13.5°	14.2°	26.4 $\pm$ 7.0°
	at time	0.53	0.56	0.52 $\pm$ 0.05

## Predicting horse limb responses to surface variations

Table 10 Right forelimb fetlock flexion and extension peaks at right lead canter. Amplitude and time of occurrence reported in the literature and computed in the model (average  $\pm$  standard deviation). The data were time-normalized from -1 to 0 as stance phase and from 0 to 1 as swing phase.

	Data from	Back (2001)	Crevier-Denoix <i>et al.</i> (2013a)		This study
			On turf	On synthetic	
During the stance phase	The fetlock joint extends to	-58°	-75°		-66.8 $\pm$ 4.4°
	at time	-0.44	-0.48	-0.45	-0.44 $\pm$ 0.04
During the swing phase	It then flexes to	18°	21°	19°	21.5 $\pm$ 7.0°
	at time	0.12	0.1	0.12	0.16 $\pm$ 0.07
	before extending to	12°	13°		12.5 $\pm$ 9.5°
	at time	0.22	0.18	0.19	0.26 $\pm$ 0.02
	It finally flexes to	23°	42°		29.7 $\pm$ 6.8°
	at time	0.45	0.44	0.46	0.51 $\pm$ 0.08

Table 11 Right forelimb fetlock flexion and extension peaks at left lead canter. Amplitude and time of occurrence reported in the literature and computed in the model (average  $\pm$  standard deviation). The data were time-normalized from -1 to 0 as stance phase and from 0 to 1 as swing phase.

	Data from	Back (2001)	Crevier-Denoix <i>et al.</i> (2013a)		This study
			On turf	On synthetic	
During the stance phase	The fetlock joint extends to	-62°	-79°	-75°	-76.8 $\pm$ 3.6°
	at time	-0.4	-0.48	-0.45	-0.50 $\pm$ 0.03
During the swing phase	It then flexes to	18°	19°	17°	17.0 $\pm$ 7.9°
	at time	0.1	0.07	0.11	0.13 $\pm$ 0.02
	before extending to	-1°	5°	3°	-2.7 $\pm$ 8.5°
	at time	0.23	0.19	0.21	0.27 $\pm$ 0.03
	It finally flexes to	15°	23°		21.3 $\pm$ 3.9°
	at time	0.43	0.47	0.49	0.50 $\pm$ 0.02

III.B.3. Carpal joint excursion

Figure 17 illustrates the joint angle definition for the carpal joint, in a position near the maximal measured extension on the left, near the maximal measured flexion on the right and in an intermediate position in the middle.

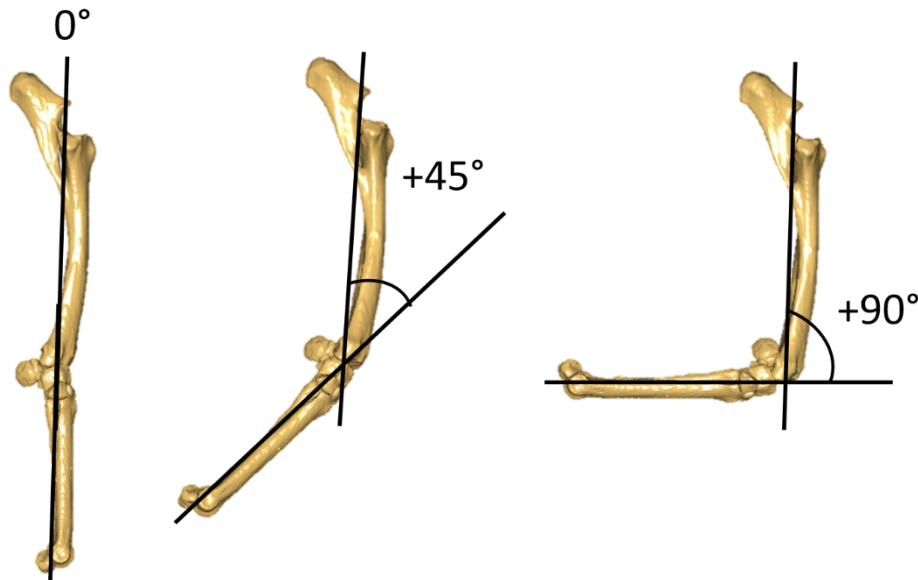


Figure 17 Example of carpal angles. Joint angle is defined as the angle between the long axis of the antebrachium segment and the long axis of the metacarpus segment, as indicated. The positive sign corresponds to a flexed position.

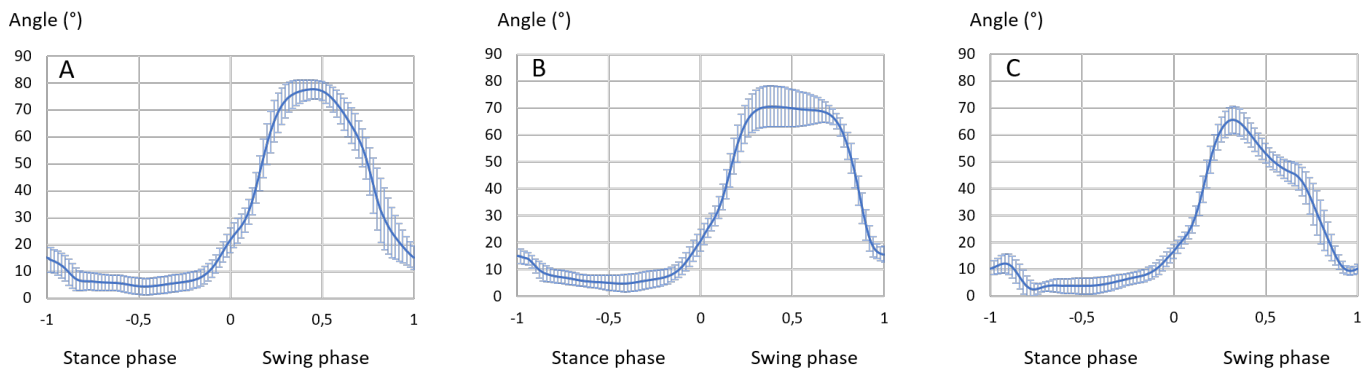


Figure 18 Right forelimb carpal joint excursions at trot (A), right lead canter (B) and left lead canter (C). The graphs present the average and standard deviation computed from all the gait data files ( $n=53$  files for trot,  $n=23$  for right lead canter and  $n=21$  files for left lead canter). The data were time-normalized from -1 to 0 as stance phase and from 0 to 1 as swing phase.

The carpal joint excursions computed by the model for all three gaits are represented in Figure 18. To compare the data computed by the model to the data reported in the literature, the carpal joint angle at impact (beginning of the stance phase), the maximal hyperextension angle and its time of occurrence during the stance phase and the flexion peak and its time of occurrence during the swing phase were compared. The data for the carpal joint excursion are reported in Table 12 for trot, in Table 13 for right lead canter and in Table 14 for left lead canter.

## Predicting horse limb responses to surface variations

Table 12 Right forelimb carpal flexion and extension peaks at trot. Amplitude and time of occurrence reported in the literature and computed in the model (average  $\pm$  standard deviation). The data were time-normalized from -1 to 0 as stance phase and from 0 to 1 as swing phase.

	Data from	Clayton <i>et al.</i> (2011)	Back (2001)	This study
During the stance phase	The carpal joint at impact is	5°	7.2°	15.0 $\pm$ 4.6°
	and it then extends to	-5°	-1°	4.0 $\pm$ 2.9°
	at time	-0.5	-0.81	-0.57 $\pm$ 0.17
During the swing phase	It flexes to	75°	88.5°	79.2 $\pm$ 3.4°
	at time	0.38	0.37	0.44 $\pm$ 0.08

Table 13 Right forelimb carpal flexion and extension peaks at right lead canter. Amplitude and time of occurrence reported in the literature and computed in the model (average  $\pm$  standard deviation). The data were time-normalized from -1 to 0 as stance phase and from 0 to 1 as swing phase.

	Data from	Back (2001)	Crevier-Denoix <i>et al.</i> (2013a)		This study
			On turf	On synthetic	
During the stance phase	The carpal joint at impact is	5°	2°		15.3 $\pm$ 2.6°
	and it then extends to	-1°	-8°		4.5 $\pm$ 3.1°
	at time	-0.66	-0.7	-0.65	-0.46 $\pm$ 0.13
During the swing phase	It flexes to	78°	92°	94°	72.2 $\pm$ 6.6°
	at time	0.31	0.3	0.32	0.52 $\pm$ 0.16

## Chapter 4 Testing the preliminary model with gait data

Table 14 Right forelimb carpal flexion and extension peaks at left lead canter. Amplitude and time of occurrence reported in the literature and computed in the model (average  $\pm$  standard deviation). The data were time-normalized from -1 to 0 as stance phase and from 0 to 1 as swing phase.

	Data from	Back (2001)	Crevier-Denoix <i>et al.</i> (2013a)		This study
			On turf	On synthetic	
During the stance phase	The carpal joint at impact is	5°	2°		10.1 $\pm$ 2.5°
	and it then extends to	-4°	-6°	-5°	1.3 $\pm$ 2.5°
	at time	-0.73	-0.78		-0.74 $\pm$ 0.08
During the swing phase	It flexes to	82°	82°		65.5 $\pm$ 5.0°
	at time	0.27	0.27	0.3	0.32 $\pm$ 0.02

### III.B.4. Elbow joint excursion

Figure 19 illustrates the joint angle definition for the elbow joint, in a position near the maximal measured extension on the left, near the maximal measured flexion on the right and in an intermediate position in the middle.

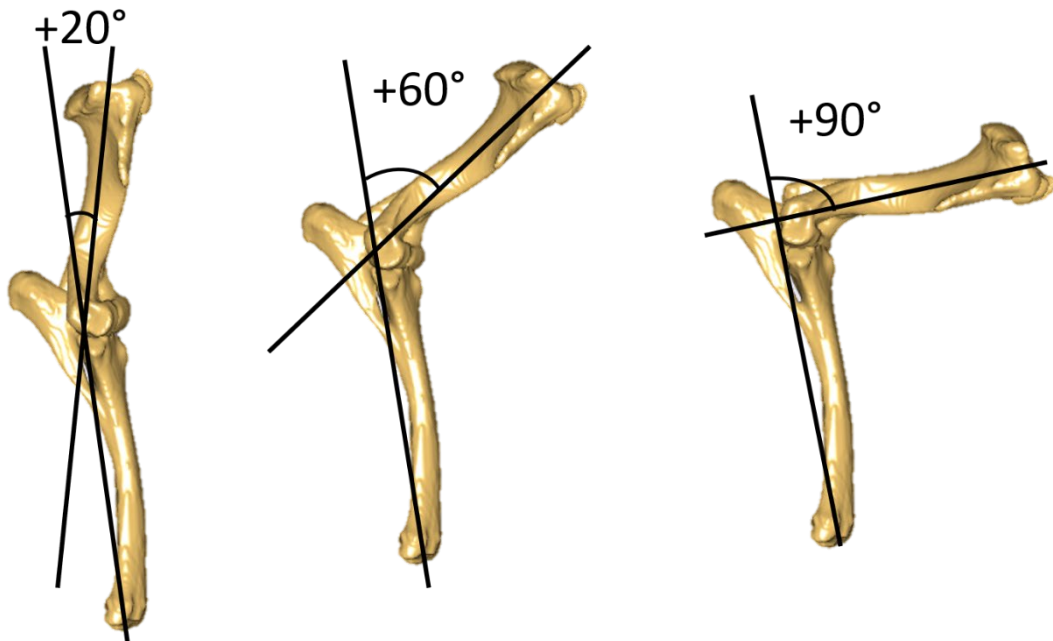


Figure 19 Example of elbow joint angles. Joint angle is defined as the angle between the long axis of the brachium segment and the long axis of the antebrachium segment, as indicated. The positive sign corresponds to a flexed position.

## Predicting horse limb responses to surface variations

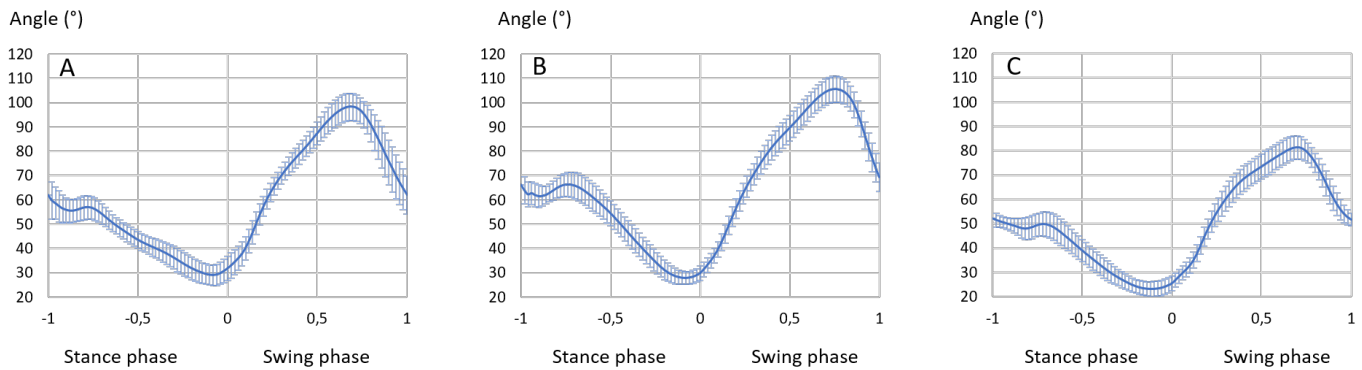


Figure 20 Right forelimb elbow joint excursions at trot (A), right lead canter (B) and left lead canter (C). The graphs present the average and standard deviation computed from all the gait data files ( $n=53$  files for trot,  $n=23$  for right lead canter and  $n=21$  files for left lead canter). The data were time-normalized from -1 to 0 as stance phase and from 0 to 1 as swing phase.

The elbow joint excursions computed by the model for all three gaits are represented in Figure 20. To compare the data computed by the model to the data reported in the literature, the flexion and extension peaks and their time of occurrence were compared. The data for the elbow joint excursion are reported in Table 15 for trot, in Table 16 for right lead canter and in Table 17 for left lead canter.

Table 15 Right forelimb elbow flexion and extension peaks at trot. Amplitude and time of occurrence reported in the literature and computed in the model (average  $\pm$  standard deviation). The data were time-normalized from -1 to 0 as stance phase and from 0 to 1 as swing phase.

	Data from	Clayton <i>et al.</i> (2011)	Back (2001)	This study
During the stance phase	The elbow joint begins to extend before slightly flexing to	Non available	57°	56.7 $\pm$ 5.2°
	at time		-0.69	-0.78 $\pm$ 0.02
	and extends to	35°	35.5°	28.5 $\pm$ 4.1°
	at time	-0.1	-0.07	-0.08 $\pm$ 0.03
During the swing phase	The elbow joint flexes to	95°	94.4°	98.5 $\pm$ 5.4°
	at time	0.66	0.4	0.69 $\pm$ 0.04

## Chapter 4 Testing the preliminary model with gait data

*Table 16 Right forelimb elbow flexion and extension peaks at right lead canter. Amplitude and time of occurrence reported in the literature and computed in the model (average  $\pm$  standard deviation). The data were time-normalized from -1 to 0 as stance phase and from 0 to 1 as swing phase.*

	Data from	Back (2001)	Crevier-Denoix <i>et al.</i> (2013a)		This study
			On turf	On synthetic	
During the stance phase	The elbow joint begins to extend before slightly flexing to	50°	41°	38°	66.7 $\pm$ 5.2°
	at time	-0.56	-0.55		-0.74 $\pm$ 0.03
	and extends to	26°	15°		27.3 $\pm$ 2.6°
	at time	-0.06	-0.05	0.01	-0.08 $\pm$ 0.04
During the swing phase	The elbow joint flexes to	91°	92°		106.0 $\pm$ 5.2°
	at time	0.6	0.59	0.62	0.75 $\pm$ 0.03

*Table 17 Right forelimb elbow flexion and extension peaks at left lead canter. Amplitude and time of occurrence reported in the literature and computed in the model (average  $\pm$  standard deviation). The data were time-normalized from -1 to 0 as stance phase and from 0 to 1 as swing phase.*

	Data from	Back (2001)	Crevier-Denoix <i>et al.</i> (2013a)		This study
			On turf	On synthetic	
During the stance phase	The elbow joint begins to extend before slightly flexing to	43°	32°	33°	50.3 $\pm$ 5.1°
	at time	-0.6	-0.53	-0.5	-0.74 $\pm$ 0.04
	and extends to	23°	14°	15°	23.0 $\pm$ 3.1°
	at time	-0.1	-0.03	0.01	-0.12 $\pm$ 0.04
During the swing phase	The elbow joint flexes to	82°	82°		81.8 $\pm$ 4.4°
	at time	0.62	0.57	0.62	0.70 $\pm$ 0.03

### III.B.5. Shoulder joint excursion

Figure 21 illustrates the joint angle definition for the shoulder joint within its amplitude, in a position near the maximal measured extension on the left, near the maximal measured flexion on the right and in an intermediate position in the middle.

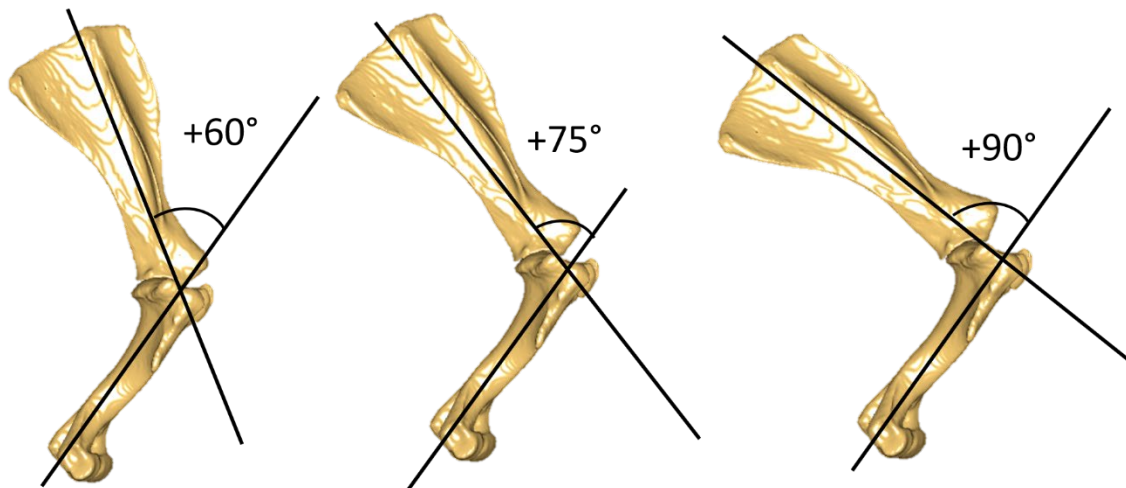


Figure 21 Example of shoulder joint angles. Joint angle is defined as the angle between the long axis of the scapula segment and the long axis of the brachium segment, as indicated. The positive sign corresponds to a flexed position.

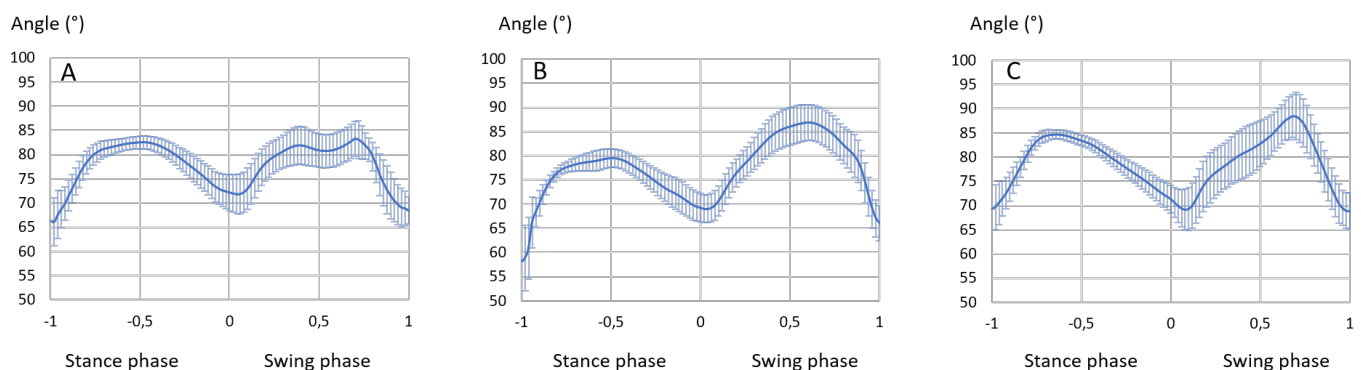


Figure 22 Right forelimb shoulder joint excursions at trot (A), right lead canter (B) and left lead canter (C). The graphs present the average and standard deviation computed from all the gait data files ( $n=53$  files for trot,  $n=23$  for right lead canter and  $n=21$  files for left lead canter). The data were time-normalized from -1 to 0 as stance phase and from 0 to 1 as swing phase.

The shoulder joint excursion computed by the model for all three gaits are represented in Figure 22. This excursion is very different to the one reported by Back (2001) at trot. No data for the shoulder joint excursion at canter was reported in the literature. At trot, the only value compared was the maximal flexion of the shoulder during the stance phase. The model computed a maximal flexion of  $82.8 \pm 1.3^\circ$  occurring at time  $-0.52 \pm 0.1$  whereas Back (2001) reported a maximal flexion of  $89^\circ$  occurring at  $-0.64$ . In the following chapters, the shoulder joint excursion will be studied by the flexion peak during the stance phase, the extension peak at the stance-swing phase transition and the maximal flexion during the swing phase.

At trot, the shoulder joint flexed to  $82.8 \pm 1.3^\circ$  at time  $-0.52 \pm 0.10$ , and it then extended to  $71.6 \pm 3.9^\circ$  at  $0.02 \pm 0.05$ . Finally, it flexed to  $84.0 \pm 3.4^\circ$  at time  $0.73 \pm 0.06$ .

At right lead canter, the shoulder joint flexed to  $80.0 \pm 1.8^\circ$  at time  $-0.52 \pm 0.09$ , and it then extended to  $68.6 \pm 2.9^\circ$  at time  $0.02 \pm 0.04$ . Finally, it flexed to  $87.1 \pm 3.7^\circ$  at time  $0.59 \pm 0.05$ .

At left lead canter, the shoulder joint flexed to  $84.9 \pm 1.0^\circ$  at time  $-0.65 \pm 0.05$ , and it then extended to  $68.6 \pm 4.4^\circ$  at time  $0.08 \pm 0.04$ . Finally, it flexed to  $88.8 \pm 4.8^\circ$  at time  $0.69 \pm 0.03$ .

### III.C. Tendon and ligament strains

The risk of injuries of the tendons and ligaments are likely related to the maximal strain they reach. For this reason, the data compared were the maximal strains computed by the musculoskeletal model to the maximal strains reported in the literature.

The maximal strain in the suspensory ligaments computed by the model was observed during the stance phase and was  $0.222 \pm 0.010$  at trot,  $0.220 \pm 0.011$  at right lead canter and  $0.244 \pm 0.008$  at left lead canter. It was reported to be between 0.04 and 0.08 at trot, canter and gallop in the literature (Dimery *et al.*, 1986; Harrison *et al.*, 2010; Jansen *et al.*, 1993b; Swanstrom *et al.*, 2005).

The maximal strain in the extensor branches computed by the model was  $0.196 \pm 0.015$  at trot,  $0.197 \pm 0.016$  at right lead canter and  $0.214 \pm 0.012$  at left lead canter. The only value found in the literature was the strain at impact and was reported to be 0.01 by Jansen *et al.* (1993b).

The maximal strain in the tendon of the SDF computed by the model was  $0.050 \pm 0.004$  at trot,  $0.059 \pm 0.004$  at right lead canter and  $0.057 \pm 0.007$  at left lead canter. Swanstrom *et al.* (2005) and Harrison *et al.* (2010) reported the maximal strain to be 0.05 at gallop and 0.04 at trot, respectively. The values reported by Dimery *et al.* (1986) were higher, 0.09 at gallop and 0.07 at trot.

The maximal strain in the accessory ligament of the SDF computed by the model was  $0.118 \pm 0.004$  at trot,  $0.117 \pm 0.004$  at right lead canter and  $0.125 \pm 0.003$  at left lead canter. Swanstrom *et al.* (2005) reported it to be 0.08 at gallop.

The strain in the tendons of the DDF were computed by head. The maximal strain computed in the humeral head of the DDF was  $0.049 \pm 0.005$  at trot,  $0.057 \pm 0.005$  at right lead canter and  $0.058 \pm 0.011$  at left lead canter. The maximal strain in the ulnar head was  $0.063 \pm 0.004$  at trot,  $0.060 \pm 0.004$  at right lead canter and  $0.062 \pm 0.007$  at left lead canter. Finally, the maximal strain in the radial head was  $0.112 \pm 0.009$  at trot,  $0.106 \pm 0.008$  at right lead canter, and  $0.110 \pm 0.013$  at left lead canter. Swanstrom *et al.* (2005) and Harrison *et al.* (2010) reported the maximal strain to be 0.025 at gallop

and 0.015 at trot, respectively. The values reported by Dimery *et al.* (1986) were higher, 0.04 at gallop and 0.03 at trot.

The maximal strain in the accessory ligament of the DDF computed by the model was  $0.163 \pm 0.008$  at trot,  $0.164 \pm 0.009$  at right lead canter and  $0.187 \pm 0.019$  at left lead canter. Swanstrom *et al.* (2005) and Harrison *et al.* (2010) reported the maximal strain to be 0.08 at gallop and 0.06 at trot, respectively.

The oblique sesamoidean ligament was modelled as two ligaments. Its strain was computed as the average of the strains computed in the two ligaments modelling it. The maximal strain computed by the model in the oblique sesamoidean ligament was  $0.774 \pm 0.048$  at trot,  $0.763 \pm 0.052$  at right lead canter and  $0.860 \pm 0.048$  at left lead canter.

As for the oblique sesamoidean ligament, the straight sesamoidean ligament was modelled as two ligaments, and its strain was considered as the average of the strains computed in the two modelled ligaments. The maximal strain computed by the model in the straight sesamoidean ligament was  $0.321 \pm 0.026$  at trot,  $0.316 \pm 0.028$  at right lead canter and  $0.366 \pm 0.027$  at left lead canter.

The maximal strain computed in the lacertus fibrosus was  $0.108 \pm 0.005$  at trot,  $0.105 \pm 0.005$  at right lead canter and  $0.112 \pm 0.004$  at left lead canter. Contrary to the other soft tissues, which reached their maximal strain during the stance phase, the lacertus fibrosus reaches its maximal strain at the stance-swing phase transition and was measured at the end of the stance phase for some files and at the beginning of the swing phase for others.

## IV. Conclusion & Discussion

Reports in the literature indicate that stance times (as a percentage of stride time) depend on the velocity of the horse, but there will also be minor effects if the horse is ridden, as opposed to being led in hand, or run on a treadmill. In general, the stance phase approximates 39-40% of the stride duration for trot at  $3.7 - 4.8 \text{ m}\cdot\text{s}^{-1}$  (Cano *et al.*, 2001) and the stance duration recorded in this study was 48% of the stride duration for a slower trot ( $2.4 - 3.1 \text{ m}\cdot\text{s}^{-1}$ ). Likewise, stance phase approximates 35% of the stride duration for the leading forelimb at a  $7.0 \text{ m}\cdot\text{s}^{-1}$  right lead canter and 34% of the stride duration for the trailing forelimb at a  $7.0 \text{ m}\cdot\text{s}^{-1}$  right lead canter (Back, 2001). In this study, stance durations were 41% and 40% of the stride duration for a  $4.1 \text{ m}\cdot\text{s}^{-1}$  right lead canter and a  $4.4 \text{ m}\cdot\text{s}^{-1}$  left lead canter, respectively. Stance phase duration shortens when horse velocity increases. For example, for the right forelimb at right lead canter, stance phase is 37% at  $5 \text{ m}\cdot\text{s}^{-1}$  and 31% at  $8.5 \text{ m}\cdot\text{s}^{-1}$  (Robilliard *et al.*, 2007) and the stance durations computed in this study agree with those reports.

While processing the gait files, it was noted that the hoof markers sometimes disappeared during break-over (at the end of the stance phase). This was especially true at the canter speed and is the main reason why fewer files were kept for canter trials. In contrast, more files were kept for trot, probably due to the slower and more controlled break-over at the stance-swing transition which tended to result in fewer lost marker trajectories, or shorter gaps that were possible to fill manually by interpolation. It was clear that a better marker system was required to enable consistent marker data from the hoof. Subsequently, a frame was developed that attached to the lateral hoof wall and placed the markers further above the sand surface in such a position that the markers would not rotate out of the view of the cameras when the distal limb was flexed into early swing (see Method, Chapter 5).

Notwithstanding differences in trotting and cantering speeds, the joint excursions computed by the model are in reasonable agreement with the literature. Few studies have reported the coffin joint excursion, and the coffin joint excursions computed in this study were compared to data reported by Back (2001). The fetlock joint excursions computed by the model were in agreement with the literature except during the swing phase at trot, when the fetlock joint was observed to be more flexed compared to the data from the literature. The carpal joint was observed to be more flexed during the stance phase compared to the data from the literature and its flexion peak during the swing phase was smaller at both right and left lead canters. The elbow joint excursion computed by the model was in good agreement with the data from the literature. Finally, the shoulder joint excursion is not often reported, and the data computed by the model was discrepant against that reported by about  $6^\circ$  in its flexion peak at midstance.

Differences between the data computed by the musculoskeletal model and data reported in the literature may have different origins. First, the studies were performed in different places, which means the horses used for the different studies may have had different training, histories and be accustomed to different ground surfaces. In addition, data reported in the literature came from horses of different breeds. Back (2001) used Dutch Warmbloods, Clayton *et al.* (2011) and Crevier-Denoix *et al.* (2013a) did not report the breed of the horses they used (but it may have been variable), and data were collected from Thoroughbreds of variable size in this study. Variations in joint excursions at canter may also be expected depending on whether the leading forelimb is right or left due to handedness or a preferred limb. Velocity will have contributed to variation between the model-derived and published values used for comparison. Trotting speeds varied across the different studies: velocity in Back's (2001) treadmill study was fixed at  $4\text{m}\cdot\text{s}^{-1}$ , it was  $3 \pm 0.15\text{m}\cdot\text{s}^{-1}$  in Clayton *et al.*'s (2011) study and  $2.8 \pm 0.4\text{m}\cdot\text{s}^{-1}$  in this study. For right lead canter, velocity in Back's (2001)

treadmill study was fixed at  $7\text{m}\cdot\text{s}^{-1}$ , it was  $8.5 \pm 0.6 \text{ m}\cdot\text{s}^{-1}$  on turf and  $8.4 \pm 0.4 \text{ m}\cdot\text{s}^{-1}$  on synthetic in Crevier-Denoix *et al.*'s (2013a) study and  $4.1 \pm 0.3 \text{ m}\cdot\text{s}^{-1}$  in this study. For left lead canter, velocity in Back's (2001) treadmill study was fixed at  $7\text{m}\cdot\text{s}^{-1}$ , it was  $8.4 \pm 0.6 \text{ m}\cdot\text{s}^{-1}$  on turf and  $8.3 \pm 0.4 \text{ m}\cdot\text{s}^{-1}$  on synthetic in Crevier-Denoix *et al.*'s (2013a) study and  $4.4 \pm 0.3 \text{ m}\cdot\text{s}^{-1}$  in this study. Velocity affects ground reaction forces in stance, with larger forces observed at higher speeds within the same gait. Velocity also affects joint excursions in the swing phase due to inertia of the segments and the shorter swing times at faster speeds with their concomitantly greater angular accelerations. The effect of ground surface and more importantly the use of a treadmill with a fixed velocity range needs to be considered with any comparison of published data. Back (2001) used a treadmill and the horses were unriden. In Clayton *et al.*'s (2011) study, the horses were led at hand unriden. In Crevier-Denoix *et al.*'s (2013a) study, the horses were ridden on turf and synthetic tracks and in this study the horses were ridden on a sand surface by their regular riders. Finally, the methods used to collect the data were different. Back (2001) used photodiode skin markers, Clayton *et al.* (2011) used skin and bone pin triad markers, Crevier-Denoix *et al.* (2013a) used reflective skin markers, a set of markers screwed on the lateral hoof wall and a dynamometric horseshoe, and in this study skin markers were used. The marker placements for calibration of the segmental marker sets against the locations of the joints at the segmental endpoints identify the centres of rotation of the limb joints, and variable identification of these centres between studies are another likely source of variability in the output data.

The shoulder excursion computed by the musculoskeletal model (skin displacement not corrected) was different to that reported by Back (2001) (skin displacement corrected) and so is probably, at least partly, a consequence of skin movement. Back *et al.* (1995) studied the effect of skin movement on the shoulder joint excursion. Their results showed the shape of the joint excursion curve was different before and after correcting for skin displacement and the amplitudes changed up to  $5^\circ$ . Van Weeren *et al.* (1990) reported the skin could move up to 4 cm over the distal scapula. Considering this displacement and that the scapula measures around 40 cm (based on the scapula in this study), it means the scapula angle could be turned by  $10^\circ$  around the transverse axis compared to the position measured with markers on the skin. The model is over-constrained, with 11 degrees-of-freedom (six degrees-of-freedom for positioning the scapula, and five one-degree-of-freedom joints) and 36 constraints (three markers by segment). The over-constrained state of the model means the position of each segment is computed using the location of its own markers but also those of the markers of the proximal and distal segments. That would explain why the joint excursions computed by the AnyBody model for elbow, carpal, fetlock and coffin joints are mostly in agreement with data reported in the literature. However, larger skin displacement is observed over the scapula and combined with

the fact that the scapula is not connected to a more proximal segment, means the position of the scapula is not as reliable, which likely led to an unrealistic shoulder excursion.

Strains in the tendons and ligaments were computed by the model to be much higher than reported in the literature. For the suspensory ligament, this was around five times higher in the model. The maximal strain of the tendon and accessory ligament of the SDF computed were close to that reported for gallop (Swanstrom *et al.*, 2005). Finally, the maximal strains observed in the tendons and in the accessory ligament of the DDF were about twice as large as the values reported by Swanstrom *et al.* (2005) for gallop but were similar to those reported by Dimery *et al.* (1986) for gallop. Like for the joint excursions, the differences observed in the strain of the soft tissues may be at least partly due to the methods. Harrison *et al.* (2010) computed the strains using a musculoskeletal model and gait data collected from three Quarter Horses equipped of three markers on hoof, pastern, metacarpus, radius and humerus. In their study, horses were led by hand at a trotting velocity of  $1.4 \pm 0.1 \text{m}\cdot\text{s}^{-1}$ . Swanstrom *et al.* (2005) computed the strains in a model using kinematic data from a horse galloping at  $18 \text{m}\cdot\text{s}^{-1}$ . Dimery *et al.* (1986) computed the strains *in vitro* at joint angles determined from sagittal recordings of a horse trotting and galloping, but the velocity data were not reported. In addition, the strains in the soft tissues with an actual origin or insertion site on the proximal sesamoid bones are likely to be overestimated as, in the AnyBody model, they were attached to the other segment. For example, the insertion site of the suspensory ligaments and the origin sites of the oblique and straight sesamoid ligaments are located on the proximal sesamoid bones, but they were attached to the pastern segment and to the metacarpus segment in this model, respectively. That resulted in greater strain amplitude calculated for these tissues.

To conclude, the data computed by the musculoskeletal model developed in this chapter are in reasonable agreement with the data reported in the literature. The discrepancies observed in joint excursions and maximal strain of soft tissues between the studies likely originated from between-study differences like velocity, marker placement, breed of the horse and type of locomotion (treadmill vs. overground, ridden vs. led in hand). Accepting that the model computes joint and segment kinematics reliably, it was proposed to advance to the next phase of study, which was to study the discrete effects of perturbations to the limb by hard and soft surfaces.

## V. References

- Back, W., Schamhardt, H. C., Savelberg, H. H. C. M., Van den Bogert, A. J., Bruin, G., Hartman, W. and Barneveld, A. (1995) 'How the horse moves: 1. Significance of graphical representations of equine forelimb kinematics', *Equine Veterinary Journal*, 27(1), pp. 31-38.
- Back, W. (2001) 'Chapter 5, Intra-limb coordination: the forelimb and the hind limb', In Back, W. and Clayton, H.M. (eds.) *Equine Locomotion*. London: W. B. Saunders.
- Cano, M. R., Vivo, J., Miro, F., Morales, J. L. and Galisteo, A. M. (2001) 'Kinematic characteristics of Andalusian, Arabian and Anglo-Arabian horses: a comparative study', *Research in Veterinary Science*, 71(2), pp. 147-153.
- Clayton, H. M., Sha, D. H. and Mullineaux, D. R. (2011) 'Three-dimensional torques and power of horse forelimb joints at trot', *arXiv e-prints*.
- Crevier-Denoix, N., Falala, S., Holden-Douilly, L., Camus, M., Martino, J., Ravary-Plumioën, B., Vergari, C., Desquilbet, L., Denoix, J.-M., Chateau, H. and Pourcelot, P. (2013a) 'Comparative kinematic analysis of the leading and trailing forelimbs of horses cantering on a turf and a synthetic surface', *Equine Veterinary Journal*, 45(S45), pp. 54-61.
- Dimery, N. J., Alexander, R. M. and Ker, R. F. (1986) 'Elastic extension of leg tendons in the locomotion of horses (*Equus caballus*)', *Journal of Zoology*, 210(3), pp. 415-425.
- Harrison, S. M., Whitton, R. C., Kawcak, C. E., Stover, S. M. and Pandy, M. G. (2010) 'Relationship between muscle forces, joint loading and utilization of elastic strain energy in equine locomotion', *The journal of Experimental Biology*, 213(Pt23), pp. 3998-4009.
- Jansen, M. O., van Buiten, A., Van den Bogert, A. J. and Schamhardt, H. C. (1993b) 'Strain of the musculus interosseus medius and its rami extensorii in the horse, deduced from in vivo kinematics', *Acta Anatomica*, 147(2), pp. 118-124.
- Robilliard, J. J., Pfau, T. and Wilson, A. M. (2007) 'Gait characterisation and classification in horses', *The journal of Experimental Biology*, 210(2), pp. 187-197.
- Swanstrom, M. D., Zarucco, L., Hubbard, M., Stover, S. M. and Hawkins, D. A. (2005) 'Musculoskeletal modeling and dynamic simulation of the Thoroughbred equine forelimb during stance phase of the gallop', *Journal of Biomechanical Engineering*, 127(2), pp. 318-328.
- Van Weeren, P. R., Van den Bogert, A. J. and Barneveld, A. (1990) 'Quantification of skin displacement in the proximal parts of the walking horse', *Equine Veterinary Journal*, 22(S9), pp. 110-118.

PART 2  
STUDY OF THE HORSE LIMB RESPONSE  
TO GROUND HARDNESS PERTURBATION

# Chapter 5

## Gait data collection with perturbations

### I. Introduction

Racetrack surface consistency has been reported to be one of the most important risk factors for racehorse musculoskeletal injuries (MSI). Minimising musculoskeletal injuries is important as MSI accounts for the retirement of 26% of all Thoroughbreds that begin racing training and therefore represents unnecessary welfare cost and economic cost to the industry (Perkins *et al.*, 2004b; Setterbo *et al.*, 2011). In order to understand what occurs within the horse limb, the aim in this chapter was to collect gait data with perturbations to the ground surface to input in the musculoskeletal model developed in the previous chapter (Chapter 4).

### II. Material & Method

#### II.A. Experimental set-up

The method used to collect the first series of gait data (Chapter 3) was subsequently improved before collecting the gait data with perturbations. One issue observed during the initial data collection was the tendency of the hoof markers to disappear after breakover of the hoof as they rotated out of the view of the cameras. Due to their proximity to the sand surface, they also tended to pick up sand, which obscured the reflective surface of the marker. For this reason, different camera set-ups and marker sets were tested before continuing with the setup reported below.

To avoid having to multiply the number of trials and for comparison of each stance phase between perturbation conditions, both the stance phase when the hoof hit the ground in the perturbation area and the following stance phase needed to be collected in the same trial. Data were collected in an indoor riding arena (60m x 30m) at a commercial equestrian centre. The surface of the indoor arena consisted of sand, approximately 6 cm deep. In the middle of the length of the arena, a “perturbation pit” (18 cm x 120 cm x 120 cm) was excavated. The kinematic measurement volume of interest was then defined from the perturbation pit to the following stance phase with a height corresponding to the highest point on the scapula of the horse. As in the previous study (Chapter 4) approach poles were placed on the ground to guide the horse and rider into the calibrated runway.

A 6-camera Qualisys system was used to collect the data. The cameras were positioned on one side of the runway and aimed so that any point in the measurement volume of interest was in the field of view of at least three cameras.

To calibrate the camera system, a reference frame and a calibration wand from a Qualisys carbon fibre calibration kit were used (as outlined in Chapter 4). The residuals of the calibration data were checked to be less than 0.5 mm for each camera; if this was not the case, the space was calibrated again.

## II.B. Perturbation pit

To create the perturbation, the hole dug was filled with wood stringers, sand and foam as described and illustrated in Figure 23.

- Baseline: Wood stringers (12 cm x 12 cm x 120 cm) were placed side by side in the perturbation pit and the rest of the depth was achieved by covering the wood stringers with 6 cm of sand such that the surface was flush with the rest of the runway.
- Hard perturbation: The wood stringers were removed, and 5 cm of sand was added to the pit. The wood stringers were then positioned side by side in the pit, and covered with approximately 1 cm of sand.
- Soft perturbation: The wood stringers were placed in the pit, and covered with a 5 cm foam slab. This was then covered with approximately 1cm of sand such that the surface was again flush with the rest of the runway.

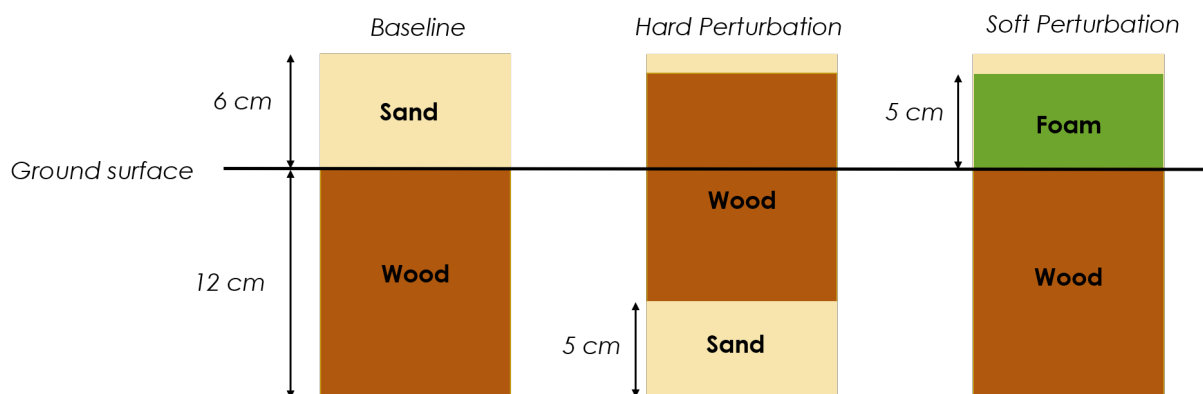


Figure 23 Diagram illustrating the filling of the perturbation pit to create the perturbation. The hole is filled with 12cm of wood and covered with 6cm of sand for the baseline (on the left); with 5cm of sand in the bottom and 12cm of wood and covered with 1cm of sand for the hard perturbation (in the middle); and with 12cm of wood covered with 5cm of foam and 1cm of sand for the soft perturbation (on the right).

Four spherical retroreflective markers (1cm diameter) were placed as reference markers on the four corners of the perturbation pit to identify the pit in the kinematic data.

## II.C. Horses

Data were collected from five privately owned Thoroughbred horses used in equestrian sport. The horses ranged in body mass from 450kg to 600kg. The horses were ridden by their usual riders, and

## Predicting horse limb responses to surface variations

data collected on five different days. Each horse was observed at trot and deemed to be sound prior to the start of each data collection day.

Three spherical retroreflective markers (1cm diameter) were taped on the craniolateral aspect of each of the segments (Scapula; Brachium; Antebrachium; Carpus and Metacarpus; Pastern) of the right forelimb. To solve the problem of hoof markers disappearing from the field of view of the cameras, a light T-shaped metal frame was fastened to the lateral side of the hoof. Three markers were applied to it, such that they were raised off the sand surface by approximately 10 cm. This way, when the hoof rotated into swing at the end of stance, the markers remained visible to the laterally-placed cameras.

Following application of the markers, the horse was walked to habituate to the markers. The horse was then brought in front of the cameras and the joint markers were placed on the centres of rotation of the joints. Shoulder and elbow joints just had one lateral marker, while carpal, fetlock and coffin joints had both medial and lateral markers. Once the horse was positioned in the calibrated measurement volume with all joint and segmental markers visible to the cameras, the marker position data were registered by the cameras. This file was called the "Initialization file". The marker setup is illustrated in Figure 24.



*Figure 24 Horse forelimb equipped with the segmental and joint markers to collect the Initialization file. Cranio-lateral view (on the left) and lateral view (in the middle) of the whole forelimb and cranio-lateral view of the distal forelimb (from carpus to hoof) on the right*

The joint markers were then removed, leaving only the marker triads identifying the individual limb segments. The horses were ridden in a straight line along the runway, with at least five strides in a straight line in the approach to the calibrated space, and five strides after leaving the calibrated space to ensure consistent strides in the calibrated space. Kinematic data were collected at a sampling rate of 200Hz for seven seconds. The data collection was triggered manually as the horse was entering the runway, approximately two strides out. The horses were ridden in front of the cameras as many times as necessary to collect data with the right forelimb landing cleanly in the middle of the perturbation pit a minimum of five times, and the four markers on the corners of the perturbation pit allowed assessment of hoof placement in each trial. Horses were ridden at trot first, and then at right lead canter, so that the limb recorded was the leading forelimb.

To reduce the time taken to change the perturbation pit between conditions, each horse began with the hard perturbation, followed by the baseline and finished with the soft perturbation. Over each perturbation condition, the trotting data were collected first and the canter data next. The ground surface over the perturbation and the rest of the runway was raked to ensure consistency between trials and also to ensure the perturbation pit was not distinguishable from the disturbed surface.

#### II.D. Qualisys software

Gait data were collected and processed with an infrared 6-camera Qualisys system. A snapshot of the markers for a file is shown in Figure 25, below.

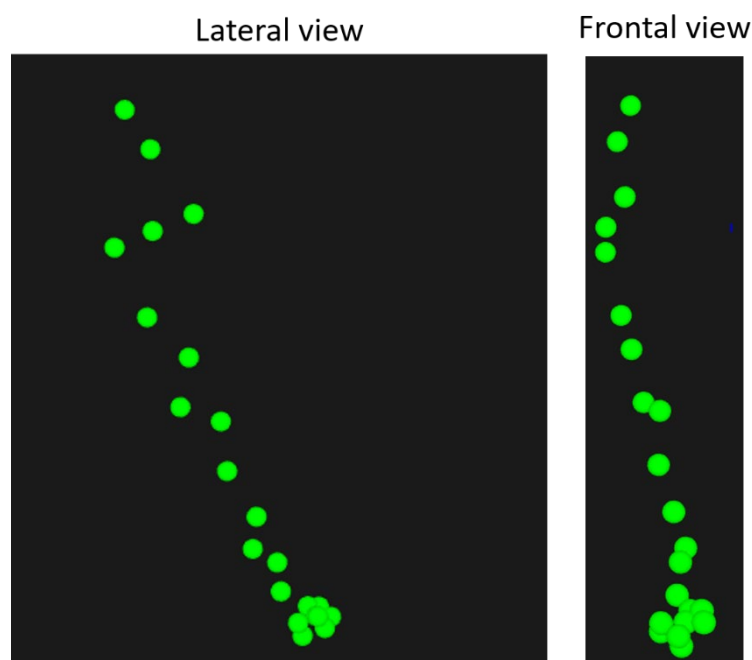


Figure 25 Snapshot of the marker positions on the whole forelimb at the beginning of the stance phase for a trial at trot with Qualisys Track Manager software

## Predicting horse limb responses to surface variations

Where there were gaps in the data caused by a marker disappearing for less than ten frames, the Qualisys software automatically interpolated across the gap to fill it, using a polynomial spline function. Any gaps greater than 10 frames were filled in post-processing with operator assistance, again using a spline function but with the option of smoothing the filled trajectory by adjusting the start and end points of the gap (Figure 26). This was easy to do in the stance phase, and through the middle of the swing phase where the marker trajectory was consistent, but where a marker was rapidly accelerating or decelerating, as occurs at the beginning and end of the stance or swing phase, the operator needed to decide whether the solved trajectory was reasonable. This was checked by viewing the marker position in relation to adjacent tracked markers through the trajectory.

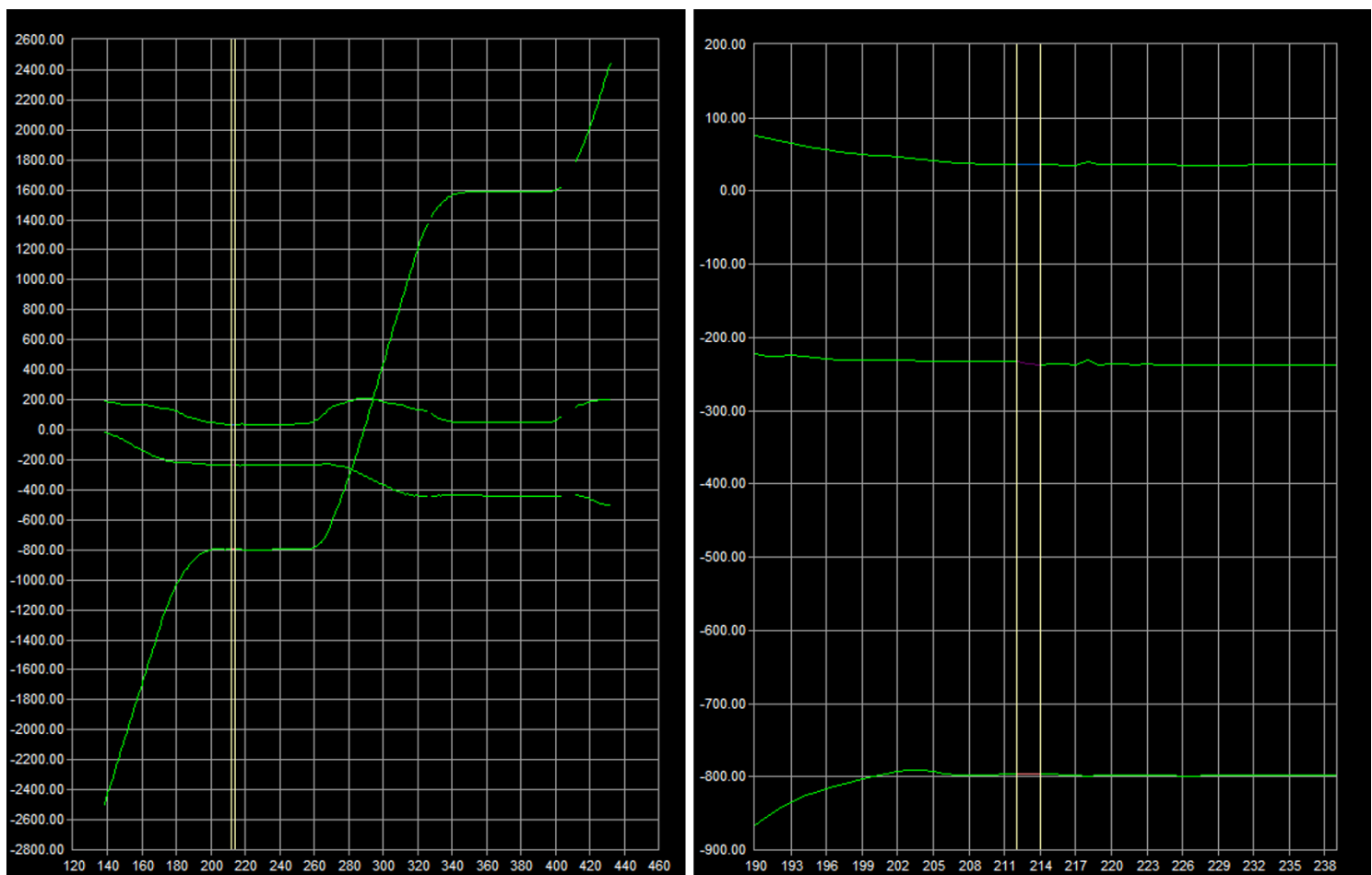


Figure 26 Example of trajectory with gaps to fill (on the left) and zoom on one gap being filled (on the right) using the Qualisys interface

If a marker's gap-filled trajectory could not be accepted, the gap was left open or the trial was abandoned. Finally, when all the trajectories were generated, the file was converted to c3d format for use in AnyBody.

### III. Results

In this section, only the basic stride characteristics will be reported. Joint angular data and soft tissue strains will be reported in Chapter 6. Gait data files were considered “good” and kept to be used in the model if:

- The right forelimb hoof landed near the middle of the perturbation pit (checked through the marker positions on the hoof and on the perturbation pit corners).
- All the marker trajectories were registered from at least the beginning of the perturbed stance phase to the end of the second stance phase.

Horse velocity was computed as the average velocity of the three Scapula segment markers over the whole stride (from the beginning of the perturbed stance phase to the end of the swing phase).

#### III.A. Trot files

Except for Horse 5 at trot in the baseline condition, for which ten good files were obtained, the number of good files per condition and per horse were between four and seven. From all files for all horses under all perturbation conditions, velocity varied between  $2.85 \text{ m}\cdot\text{s}^{-1}$  and  $3.81 \text{ m}\cdot\text{s}^{-1}$  with a weighted average of  $3.25 \pm 0.19 \text{ m}\cdot\text{s}^{-1}$ ; the perturbed (first) stance phase duration varied between  $0.232 \text{ s}$  and  $0.388 \text{ s}$  with an average of  $0.330 \pm 0.030 \text{ s}$ ; the swing phase duration varied between  $0.308 \text{ s}$  and  $0.452 \text{ s}$  with an average of  $0.393 \pm 0.031 \text{ s}$ ; and the second stance phase duration varied between  $0.228 \text{ s}$  and  $0.384 \text{ s}$  with an average of  $0.335 \pm 0.030 \text{ s}$ .

The range of velocity is larger over the hard and soft perturbation conditions (respectively  $0.96 \text{ m}\cdot\text{s}^{-1}$  and  $0.81 \text{ m}\cdot\text{s}^{-1}$ ) than over the baseline condition ( $0.46 \text{ m}\cdot\text{s}^{-1}$ ). This difference could lead to confounding of the effect of velocity on the limb response with the effect of the soft and hard perturbation on the limb response.

The detailed data per horse and per condition, along with weighted averages per horse, are reported in Table 18. It can be observed that the swing phase is longer than the perturbed stance phase for all the perturbation conditions, except for Horse 4 over the hard perturbation condition. This difference may be due to the horse velocity. Indeed, it was observed to be the slowest for this horse over that condition and the only one to be below  $3 \text{ m}\cdot\text{s}^{-1}$  ( $2.98 \pm 0.09 \text{ m}\cdot\text{s}^{-1}$ ). The second stance phase was observed to be as long as the perturbed stance phase, except for Horses 3 and 5 over the hard perturbation condition.

## Predicting horse limb responses to surface variations

Table 18 Trot data files, details per horse: number of files, velocity, 1<sup>st</sup> and 2<sup>nd</sup> stance phase durations and swing phase duration (average  $\pm$  standard deviation) for each perturbation condition

		Horse 1	Horse 2	Horse 3	Horse 4	Horse 5	Weighted average
Baseline data	Number of files	5	5	5	7	10	32
	Velocity (m.s <sup>-1</sup> )	3.28 $\pm$ 0.04	3.20 $\pm$ 0.05	3.25 $\pm$ 0.06	3.17 $\pm$ 0.08	3.17 $\pm$ 0.14	3.20 $\pm$ 0.10
	1 <sup>st</sup> Stance phase duration (s)	0.322 $\pm$ 0.015	0.333 $\pm$ 0.009	0.352 $\pm$ 0.010	0.349 $\pm$ 0.011	0.317 $\pm$ 0.048	0.333 $\pm$ 0.031
	Swing phase duration (s)	0.414 $\pm$ 0.021	0.408 $\pm$ 0.012	0.372 $\pm$ 0.007	0.400 $\pm$ 0.021	0.409 $\pm$ 0.050	0.402 $\pm$ 0.033
	2 <sup>nd</sup> Stance phase duration (s)	0.312 $\pm$ 0.017	0.323 $\pm$ 0.013	0.347 $\pm$ 0.013	0.358 $\pm$ 0.015	0.319 $\pm$ 0.053	0.331 $\pm$ 0.035
Hard perturbation data	Number of files	5	7	7	4	4	27
	Velocity (m.s <sup>-1</sup> )	3.37 $\pm$ 0.08	3.03 $\pm$ 0.12	3.27 $\pm$ 0.05	2.98 $\pm$ 0.09	3.72 $\pm$ 0.08	3.25 $\pm$ 0.26
	1 <sup>st</sup> Stance phase duration (s)	0.321 $\pm$ 0.019	0.359 $\pm$ 0.017	0.321 $\pm$ 0.010	0.361 $\pm$ 0.020	0.276 $\pm$ 0.014	0.330 $\pm$ 0.033
	Swing phase duration (s)	0.388 $\pm$ 0.012	0.412 $\pm$ 0.008	0.358 $\pm$ 0.013	0.365 $\pm$ 0.021	0.401 $\pm$ 0.011	0.385 $\pm$ 0.025
	2 <sup>nd</sup> Stance phase duration (s)	0.310 $\pm$ 0.018	0.362 $\pm$ 0.009	0.346 $\pm$ 0.011	0.363 $\pm$ 0.010	0.321 $\pm$ 0.033	0.342 $\pm$ 0.026
Soft perturbation data	Number of files	4	6	5	5	4	24
	Velocity (m.s <sup>-1</sup> )	3.29 $\pm$ 0.06	3.20 $\pm$ 0.12	3.32 $\pm$ 0.06	3.20 $\pm$ 0.17	3.58 $\pm$ 0.16	3.30 $\pm$ 0.18
	1 <sup>st</sup> Stance phase duration (s)	0.318 $\pm$ 0.011	0.321 $\pm$ 0.005	0.344 $\pm$ 0.017	0.353 $\pm$ 0.021	0.289 $\pm$ 0.012	0.327 $\pm$ 0.025
	Swing phase duration (s)	0.382 $\pm$ 0.015	0.418 $\pm$ 0.019	0.358 $\pm$ 0.014	0.371 $\pm$ 0.029	0.421 $\pm$ 0.017	0.390 $\pm$ 0.032
	2 <sup>nd</sup> Stance phase duration (s)	0.324 $\pm$ 0.021	0.331 $\pm$ 0.008	0.354 $\pm$ 0.007	0.354 $\pm$ 0.019	0.284 $\pm$ 0.009	0.331 $\pm$ 0.028

When comparing the stance and swing phase durations between perturbation conditions, differences can be observed between the baseline and hard perturbation conditions. However, these differences do not seem to be related to velocity differences. For example, while velocity is faster for Horses 1 and 5 over the hard perturbation condition (respectively 3.37  $\pm$  0.08 m.s<sup>-1</sup> and 3.72  $\pm$  0.08 m.s<sup>-1</sup>) than over the baseline condition (respectively 3.28  $\pm$  0.04 m.s<sup>-1</sup> and 3.17  $\pm$  0.14 m.s<sup>-1</sup>), the perturbed stance phase duration is similar for both conditions for Horse 1 (0.322  $\pm$  0.015 s and 0.321  $\pm$  0.019 s) but is

shorter over the hard perturbation condition ( $0.276 \pm 0.014$  s) than over the baseline condition ( $0.317 \pm 0.048$  s) for Horse 5. While velocity is slower for Horses 2 and 4 over the hard perturbation condition (respectively  $3.03 \pm 0.12$  m.s<sup>-1</sup> and  $2.98 \pm 0.09$  m.s<sup>-1</sup>) than over the baseline condition (respectively  $3.20 \pm 0.05$  m.s<sup>-1</sup> and  $3.17 \pm 0.08$  m.s<sup>-1</sup>), the perturbed stance phase duration is similar for both conditions for Horse 4 ( $0.349 \pm 0.011$  s and  $0.361 \pm 0.020$  s) but is longer over the hard perturbation condition ( $0.359 \pm 0.017$  s) than over the baseline condition ( $0.333 \pm 0.009$  s) for Horse 2. Both the perturbed stance phase and second stance phase durations are similar between the baseline and the soft perturbation conditions except for Horse 5, for which they were observed to be shorter over the soft perturbation condition than over the baseline condition. However, that could be due to the velocity being faster over the soft perturbation condition ( $3.58 \pm 0.16$  m.s<sup>-1</sup>) than over the baseline condition ( $3.17 \pm 0.14$  m.s<sup>-1</sup>) for that horse.

### III.B. Canter files

The number of good files per condition and per horse were between two and seven. From all files for all horses under all perturbation conditions, the velocity varied between  $4.17$  m.s<sup>-1</sup> and  $6.12$  m.s<sup>-1</sup> with a weighted average of  $4.93 \pm 0.34$  m.s<sup>-1</sup>; the perturbed (first) stance phase varied between  $0.171$  s and  $0.321$  s with an average of  $0.227 \pm 0.020$  s; the swing phase duration varied between  $0.289$  s and  $0.380$  s with an average of  $0.346 \pm 0.024$  s; the second stance phase duration varied between  $0.191$  s and  $0.308$  s with an average of  $0.230 \pm 0.018$  s.

The detailed data per horse and per condition, along with weighted averages per horse, are reported in Table 19. It can be observed that for all horses over all conditions, the perturbed stance phase was shorter than the swing phase and there were only very small differences between durations of the first and second stance phase. In addition, it can be observed that the perturbed and stance phase durations and the swing phase duration are similar between perturbation conditions for all horses, except both stance phase durations that were longer over the soft perturbation condition ( $0.280 \pm 0.059$  s and  $0.276 \pm 0.047$  s) than over the baseline condition ( $0.241 \pm 0.007$  s and  $0.244 \pm 0.007$  s, respectively) for Horse 2 and the second stance phase was shorter over the soft perturbation condition ( $0.225 \pm 0.006$  s) than over the baseline condition ( $0.246 \pm 0.009$  s) for Horse 4.

## Predicting horse limb responses to surface variations

Table 19 Right lead canter data files, details per horse: number of files, velocity, 1<sup>st</sup> and 2<sup>nd</sup> stance phase durations and swing phase duration (average  $\pm$  standard deviation) for each perturbation condition

		Horse 1	Horse 2	Horse 3	Horse 4	Horse 5	Weighted average
Baseline data	Number of files	5	6	4	6	3	24
	Velocity (m.s <sup>-1</sup> )	4.78 $\pm$ 0.11	4.52 $\pm$ 0.20	5.12 $\pm$ 0.18	4.72 $\pm$ 0.19	5.50 $\pm$ 0.04	4.85 $\pm$ 0.35
	1 <sup>st</sup> Stance phase duration (s)	0.226 $\pm$ 0.004	0.241 $\pm$ 0.007	0.232 $\pm$ 0.004	0.242 $\pm$ 0.006	0.203 $\pm$ 0.006	0.232 $\pm$ 0.014
	Swing phase duration (s)	0.362 $\pm$ 0.011	0.369 $\pm$ 0.008	0.308 $\pm$ 0.008	0.339 $\pm$ 0.004	0.367 $\pm$ 0.002	0.349 $\pm$ 0.023
	2 <sup>nd</sup> Stance phase duration (s)	0.226 $\pm$ 0.006	0.244 $\pm$ 0.007	0.233 $\pm$ 0.003	0.246 $\pm$ 0.009	0.204 $\pm$ 0.002	0.234 $\pm$ 0.015
Hard perturbation data	Number of files	6	4	6	5	7	28
	Velocity (m.s <sup>-1</sup> )	4.87 $\pm$ 0.25	4.55 $\pm$ 0.17	4.96 $\pm$ 0.11	4.74 $\pm$ 0.30	5.48 $\pm$ 0.30	4.97 $\pm$ 0.40
	1 <sup>st</sup> Stance phase duration (s)	0.222 $\pm$ 0.005	0.225 $\pm$ 0.011	0.230 $\pm$ 0.005	0.242 $\pm$ 0.011	0.195 $\pm$ 0.012	0.221 $\pm$ 0.019
	Swing phase duration (s)	0.350 $\pm$ 0.004	0.360 $\pm$ 0.012	0.297 $\pm$ 0.010	0.332 $\pm$ 0.007	0.362 $\pm$ 0.008	0.340 $\pm$ 0.026
	2 <sup>nd</sup> Stance phase duration (s)	0.228 $\pm$ 0.007	0.244 $\pm$ 0.014	0.239 $\pm$ 0.005	0.237 $\pm$ 0.008	0.209 $\pm$ 0.014	0.230 $\pm$ 0.016
Soft perturbation data	Number of files	7	2	6	3	6	24
	Velocity (m.s <sup>-1</sup> )	4.83 $\pm$ 0.15	4.48 $\pm$ 0.10	5.13 $\pm$ 0.06	4.96 $\pm$ 0.37	5.13 $\pm$ 0.16	4.97 $\pm$ 0.25
	1 <sup>st</sup> Stance phase duration (s)	0.230 $\pm$ 0.009	0.280 $\pm$ 0.059	0.228 $\pm$ 0.007	0.236 $\pm$ 0.018	0.206 $\pm$ 0.006	0.228 $\pm$ 0.024
	Swing phase duration (s)	0.353 $\pm$ 0.006	0.372 $\pm$ 0.000	0.321 $\pm$ 0.008	0.344 $\pm$ 0.004	0.368 $\pm$ 0.008	0.349 $\pm$ 0.020
	2 <sup>nd</sup> Stance phase duration (s)	0.229 $\pm$ 0.006	0.276 $\pm$ 0.047	0.230 $\pm$ 0.005	0.225 $\pm$ 0.006	0.206 $\pm$ 0.011	0.227 $\pm$ 0.022

## IV. Discussion & Conclusion

Kinematic data files were collected on the baseline surface, and on the hard and soft perturbing surfaces. The number of files collected varied for each horse, ranging from four to ten for the trotting trials and from two to seven for the right lead canter trials. The quality of the canter data on the soft surface was reduced in two horses, with disappearing markers causing gaps in the data stream that

led to the trial being rejected in post-processing. The markers typically affected were those on the pastern and hoof, and the gaps in the data typically occurred in the stance-swing and swing-stance transitions, where the velocity of the marker changed abruptly. In the landing phase on the soft surface at canter, a shower of sand could reduce the visibility of the marker momentarily, and this was enough to obscure it from one or more cameras. As the angular velocity of the joints is largest during these transition phases, the gaps in the data could not be reliably filled by interpolation, as the spline algorithm would move the marker position along a trajectory that was artificially smooth and resulted in unrealistic calculated joint excursions in the distal joints. As these distal joints were important for calculation of strain in the elements of the suspensory apparatus, the unrealistic joint excursions could not be accepted in those cases.

Nonetheless, the number of files collected and processed for each horse at each gait and under each perturbation condition were more consistent than those collected and processed during the first kinematic data collection. The set of markers used in this study was deemed more reliable to collect consistent data and where small gaps had to be filled by manual interference in post-processing, the resulting data stream was assessed to be unaffected by evaluation of relative marker position against adjacent markers.

Horse velocity was only controlled by the riders, who were instructed to ride with consistent velocity across trials. The aim was consistent velocity across trials within a horse, but some variability was observed, although this variability was largest between horses. The variable size and mass of the horse would have accounted for some of this variation, with Horse 5 (the largest horse) tending to be the fastest at canter. Velocity is associated with increased ground reaction forces and concomitantly with increased joint angular excursions (Behnke, 2018; Hobbs and Clayton, 2019; McLaughlin *et al.*, 1996). For that reason, the statistical treatment of the joint angular and soft tissue strain data in the following chapter includes trial velocity as a factor.

As was observed for the first series of gait data collected (Chapter 4), the stance phase durations were more affected by the change of velocity than the swing phase duration. Indeed, by comparing the data collected at trot and at canter, both stance phase durations were reduced by around 30% at canter compared to trot, whereas the swing phase duration was reduced only by around 10%.

In conclusion, across the three perturbation conditions, the average trotting velocity varied by 0.10  $\text{m}\cdot\text{s}^{-1}$  and the average canter velocity varied by 0.12  $\text{m}\cdot\text{s}^{-1}$  and these differences were smaller than the standard deviations per horse. Across the horses per condition, Horse 5 had the largest difference in velocity at trot (0.55  $\text{m}\cdot\text{s}^{-1}$ ) and at canter (0.37  $\text{m}\cdot\text{s}^{-1}$ ) but the others averaged only 0.13  $\text{m}\cdot\text{s}^{-1}$  at both

## Predicting horse limb responses to surface variations

trot and canter, and these differences varied in their direction, reflected in the small differences in the weighted averages across the three conditions. By including horse and velocity as factors in subsequent analyses of joint angular excursions and soft tissues strains, any small velocity effect will be accounted for in the statistical assessment of the effects of each surface on these dependent variables.

## V. References

- Behnke, R. (2018) 'Numerical time-domain modelling of hoof-ground interaction during the stance phase', *Equine Veterinary Journal*, 50(4), pp. 519-524.
- Hobbs, S. J. and Clayton, H. M. (2019) 'Collisional mechanics of the diagonal gaits of horses over a range of speeds', *Peer Journal*, Sep 17;7:e7689.
- McLaughlin, R. M., Gaughan, E. M., Roush, J. K. and Skaggs, C. L. (1996) 'Effects of subject velocity on ground reaction force measurements and stance times in clinically normal horses at the walk and trot', *American Journal of Veterinary Research*, 57(1), pp. 7-11.
- Perkins, N. R., Reid, S. W. and Morris, R. S. (2004b) 'Profiling the New Zealand Thoroughbred racing industry. 2. Conditions interfering with training and racing', *New Zealand Veterinary Journal*, 53(1), pp. 69-76.
- Setterbo, J. J., Yamaguchi, A., Hubbard, M., Upadhyaya, S. K. and Stover, S. M. (2011) 'Effects of equine racetrack surface type, depth, boundary area, and harrowing on dynamic surface properties measured using a track-testing device in a laboratory setting', *Sports Engineering*, 14(2-4), pp. 119-137.

# Chapter 6

## Limb response to perturbations

### I. Introduction

Of all the Thoroughbreds that enter race training, two thirds will be retired prematurely, half of them involuntarily. In 78% of these cases, the cause is musculoskeletal injury (Perkins *et al.*, 2004b). This means that 26% of all Thoroughbred racehorses are retired because of musculoskeletal injuries. Musculoskeletal injuries were reported to be the main cause of involuntarily retirement, death and rest periods for rehabilitation (Bolwell *et al.*, 2017b; Parkin, 2008; Perkins *et al.*, 2004b). Most musculoskeletal injuries affect the distal forelimb, and the tissues most affected are the superficial digital flexor tendon, the suspensory ligament, the deep digital flexor tendon and its check ligament and the sesamoidean ligaments (Hill, 2003; Rosanowski *et al.*, 2016).

Racetrack surface properties have been recognized as one of the main modifiable risk factors for musculoskeletal injury (Peterson *et al.*, 2008; Robin *et al.*, 2009; Setterbo *et al.*, 2011). For this reason, racetrack surface is a major area of research (Parkin, 2008). Among all the racetrack surface properties, hardness and consistency were reported as the most important properties implicated in racehorse musculoskeletal injuries. However, inconsistency of the track has only been the focus of epidemiologic studies.

The aim in this chapter was to determine the effects of perturbations by the ground surface on the horse limb response with the musculoskeletal model developed in Chapter 3 and to assess whether the response occurs acutely in the perturbed stance phase or in the next stance phase. To date, no data have been found about such a study in the literature.

### II. Material & Methods

The kinematic files collected in the previous chapter (Chapter 5) were used in the musculoskeletal model developed in Chapter 3. The musculoskeletal model included five one-degree-of-freedom joints, 11 muscles and 17 ligaments.

The data computed by the musculoskeletal model were time-normalised, such that -1 corresponds to the beginning of the perturbed stance phase, 0 to the end of the perturbed stance phase and beginning of the swing phase, 1 to the end of the swing phase and beginning of the second stance phase and 2 to the end of the second stance phase. This allowed average curves to be generated from

the data across the five horses, notwithstanding small variations in percentage stance and swing times.

The effects of the perturbation condition on the joint excursions were studied through their effects on the joint flexion and extension peaks (the discrete and repeatable peak angles reached by the joints and their time of occurrence). For the ligaments and tendons, the values studied were their maximal strains during both the perturbed stance phase and the second stance phase.

The effect of the perturbation condition was tested first at trot and then at canter, using a statistical model coded with R (CRAN, <https://cran.r-project.org/>, version 3.6.0). The statistical model was an ANOVA (analysis of variance). The independent variables included in the ANOVA were the perturbation condition and the horse velocity. 'Horse' was included as a random variable to account for variation in joint motion between horses. The perturbation condition was a discrete variable, with the level one being the baseline condition. Thus, the values associated with the baseline condition were used as reference to calculate the effects of the soft and hard perturbation conditions. Thus, the statistical formula used in R was: *lme(tested~Speed + Condition, random = ~1|Horse, data = Data)*, with 'tested' the tested value, 'Condition' the perturbation condition, 'Speed' the horse velocity, 'Horse' as the identifier associated to each horse and 'Data' as the database in which all the data were gathered.

### III. Results

#### III.A. Statistical results of the joint excursions

##### III.A.1. Coffin joint: sagittal angle

###### III.A.1.a. At trot

The average and standard error of the mean (SEM) for the coffin joint excursions at trot over the perturbation conditions are represented in Figure 27, with the points (angle value A and normalised time t) that have been tested in the statistical model and reported in the following table.

## Predicting horse limb responses to surface variations

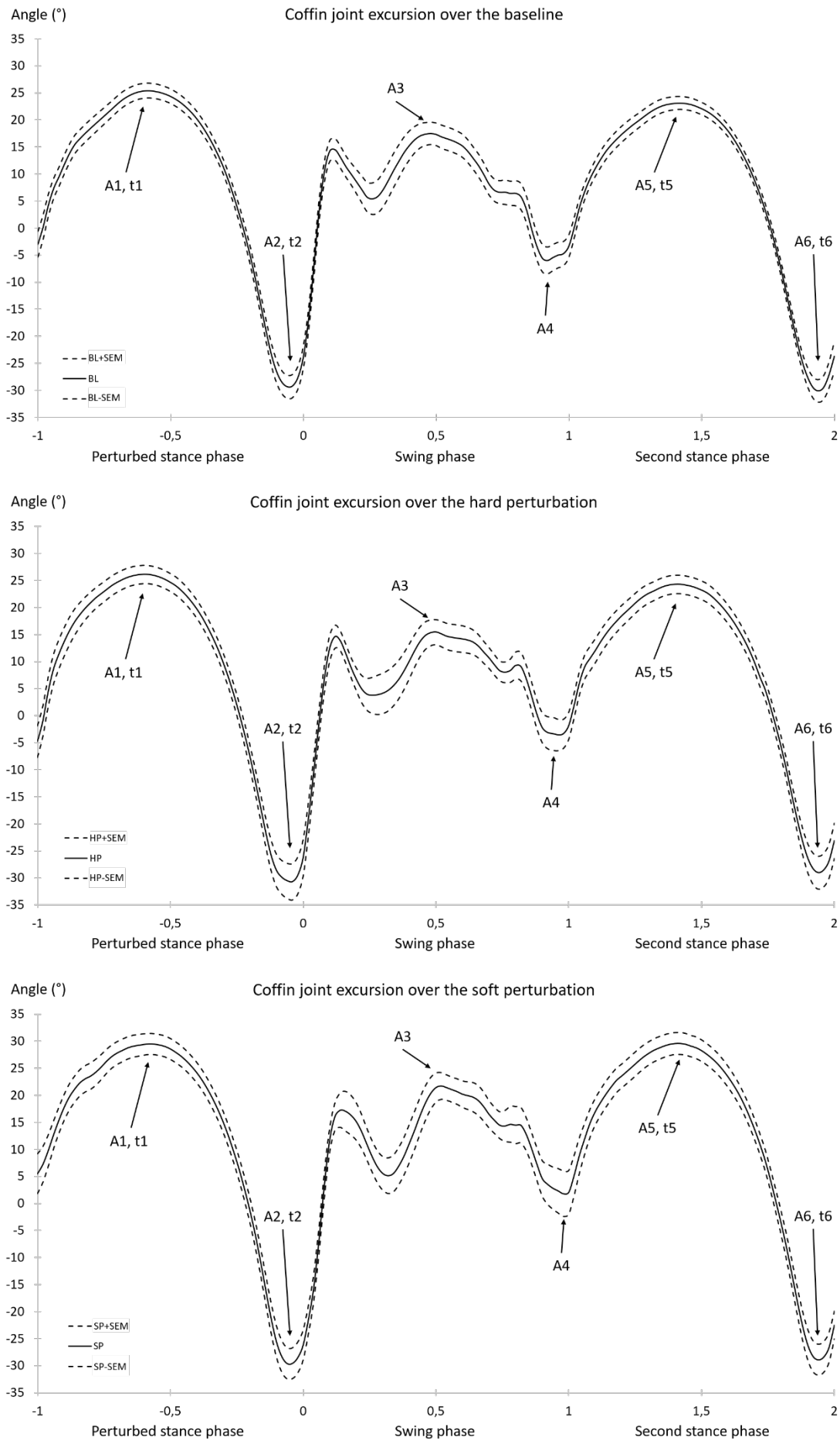


Figure 27 Coffin joint excursion at trot over the baseline (BL, on top), over the hard perturbation (HP, in the middle) and over the soft perturbation (SP, on bottom). The curves represent the averages (plain lines) and the standard error of mean (dotted lines) of the coffin joint excursion at trot computed for all the files ( $n=32$  files for BL;  $n=27$  files for HP and  $n=24$  files for SP). Time was normalized from -1 to 0 as the perturbed stance phase, from 0 to 1 as the swing phase and from 1 to 2 as the second stance phase.

Table 20 reports the weighted averages of the coffin joint peak flexion and extension values and their time of occurrence at trot over the different perturbation conditions, accounting for horse and velocity differences such that the differences between averages account for the effects of the perturbation condition. It is worth noting that the coffin excursion was more variable across horses during the swing phase and so the weighted statistical averages reported in Table 20 do not match the arithmetic averages illustrated in Figure 27.

*Table 20 Coffin joint excursion at trot: peak values and their time of occurrence over the baseline, the hard and the soft perturbation conditions (average  $\pm$  SEM).*

Condition	Baseline	Hard Perturbation	Soft Perturbation
Velocity (m.s <sup>-1</sup> )	3.20 $\pm$ 0.02	3.25 $\pm$ 0.05	** 3.30 $\pm$ 0.04
A1 (°)	25.4 $\pm$ 1.4	25.6 $\pm$ 1.7	** 27.7 $\pm$ 2.0
t1	-0.60 $\pm$ 0.01	-0.60 $\pm$ 0.01	-0.59 $\pm$ 0.01
A2 (°)	-31.0 $\pm$ 2.1	-31.6 $\pm$ 3.3	-31.8 $\pm$ 2.7
t2	-0.05 $\pm$ 0.00	-0.06 $\pm$ 0.01	-0.05 $\pm$ 0.00
A3 (°)	22.7 $\pm$ 1.7	** 19.3 $\pm$ 1.9	** 26.4 $\pm$ 2.6
A4 (°)	-10.1 $\pm$ 1.9	-9.8 $\pm$ 2.9	* -8.4 $\pm$ 3.1
A5 (°)	23.5 $\pm$ 1.2	23.7 $\pm$ 1.7	** 28.1 $\pm$ 2.1
t5	1.40 $\pm$ 0.01	1.40 $\pm$ 0.01	1.42 $\pm$ 0.01
A6 (°)	-32.4 $\pm$ 2.2	** -29.1 $\pm$ 3.1	-31.0 $\pm$ 2.7
t6	1.94 $\pm$ 0.01	1.93 $\pm$ 0.01	1.95 $\pm$ 0.01

*Significant differences from the baseline due to the effect of the perturbation condition are noted \*\* if p-value < 0.01 and \* if p-value < 0.05*

*In the first column, the values A and t correspond respectively to the angular position and the time of occurrence of the extension and flexion peaks identified in Figure 27. A3 and A4 are respectively the maximal flexion and extension during the swing phase*

At trot, the hard perturbation affected the coffin joint excursion by decreasing the maximal flexion angle during the swing phase (A3) by 3.4° and by decreasing extension at the end of second stance phase (A6) by 3.3°.

At trot, the soft perturbation affected the coffin joint excursion by increasing flexion peak during the perturbed stance phase (A1) by 2.3°, by increasing the maximal flexion angle during the swing phase (A3) by 3.7°, by decreasing the maximal extension during the swing phase (A4) by 1.7° and by increasing the flexion peak during the second stance phase (A5) by 4.6°.

## Predicting horse limb responses to surface variations

### III.A.1.b. *At right lead canter*

The average and SEM for the coffin joint excursion at right lead canter over the perturbation conditions are represented in Figure 28, with the points (angle value A and normalised time t) that have been tested in the statistical model and reported in the following table.

## Chapter 6 Limb response to perturbations

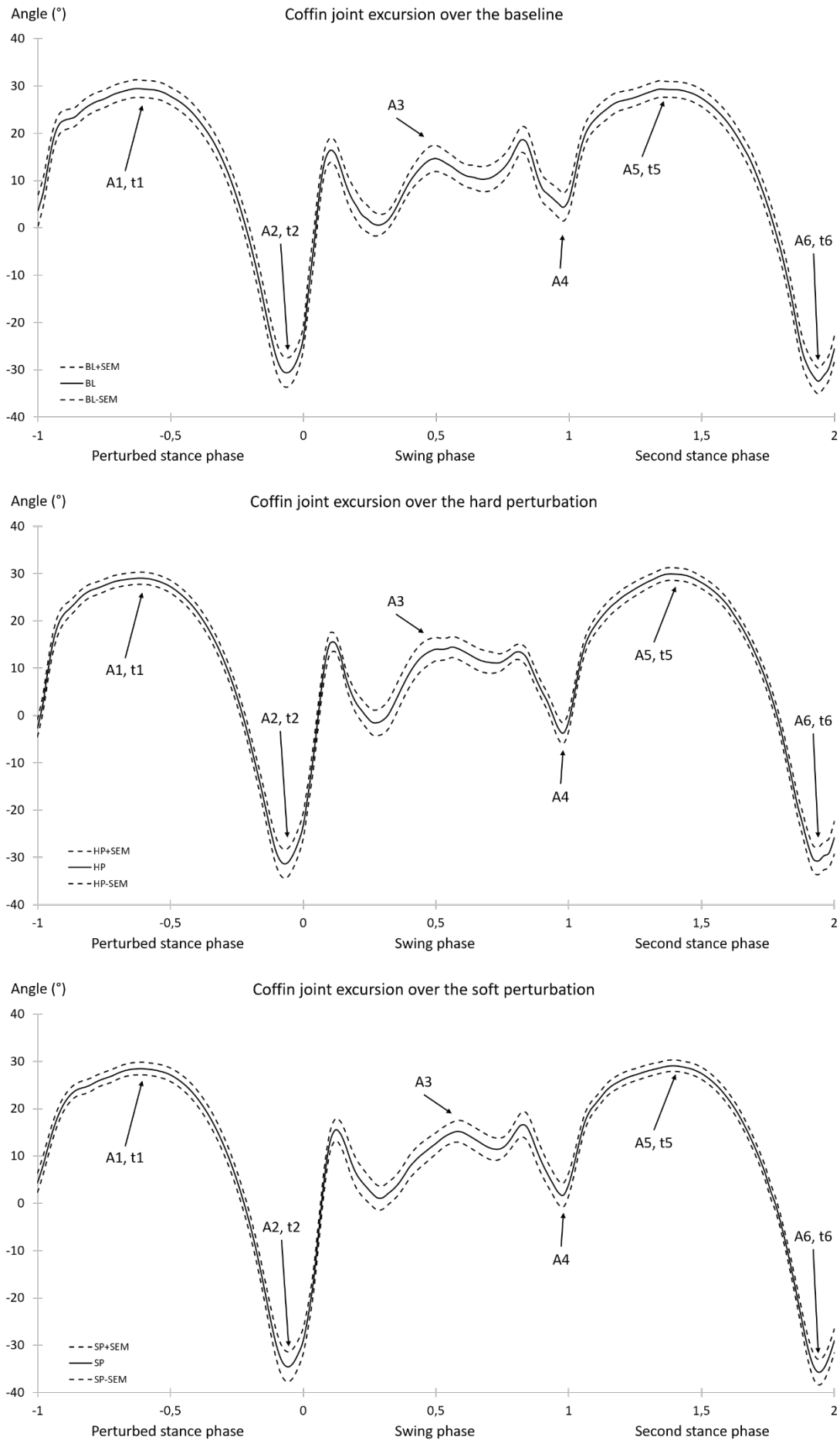


Figure 28 Coffin joint excursion at right lead canter over the baseline (BL, on top), over the hard perturbation (HP, in the middle) and over the soft perturbation (SP, on bottom). The curves represent the averages (plain lines) and the standard error of mean (dotted lines) of the coffin joint excursion at canter computed for all the files ( $n=24$  files for BL;  $n=28$  files for HP and  $n=24$  files for SP). Time was normalized from -1 to 0 as the perturbed stance phase, from 0 to 1 as the swing phase and from 1 to 2 as the second stance phase.

## Predicting horse limb responses to surface variations

Table 21 reports the weighted averages of the coffin joint peak flexion and extension values and their time of occurrence at right lead canter over the different perturbation conditions, accounting for horse and velocity differences such that the differences between averages account for the effects of the perturbation condition. As for trot, the coffin excursion was more variable across horses during the swing phase and so the weighted statistical averages reported in Table 21 do not match the arithmetic averages illustrated in Figure 28.

*Table 21 Coffin joint excursion at right lead canter: peak values and their time of occurrence over the baseline, the hard and the soft perturbation conditions (average  $\pm$  SEM).*

Condition	Baseline	Hard Perturbation	Soft Perturbation
Velocity (m.s <sup>-1</sup> )	4.85 $\pm$ 0.07	4.97 $\pm$ 0.07	4.97 $\pm$ 0.05
A1 (°)	29.5 $\pm$ 1.8	30.2 $\pm$ 1.3	* 31.3 $\pm$ 1.3
t1	-0.64 $\pm$ 0.02	-0.65 $\pm$ 0.02	-0.62 $\pm$ 0.01
A2 (°)	-31.8 $\pm$ 3.0	-31.7 $\pm$ 3.0	-31.7 $\pm$ 3.1
t2	-0.07 $\pm$ 0.00	-0.07 $\pm$ 0.01	-0.06 $\pm$ 0.00
A3 (°)	24.6 $\pm$ 2.5	23.7 $\pm$ 1.9	26.9 $\pm$ 1.8
A4 (°)	-6.4 $\pm$ 1.7	-8.2 $\pm$ 1.7	-4.9 $\pm$ 1.3
A5 (°)	29.0 $\pm$ 1.7	30.9 $\pm$ 1.4	* 31.4 $\pm$ 1.3
t5	1.36 $\pm$ 0.02	1.38 $\pm$ 0.01	1.39 $\pm$ 0.01
A6 (°)	-31.7 $\pm$ 3.2	-28.6 $\pm$ 3.5	-30.3 $\pm$ 3.1
t6	1.92 $\pm$ 0.01	1.88 $\pm$ 0.04	1.90 $\pm$ 0.04

*Significant differences from the baseline due to the effect of the perturbation condition are noted \*\* if p-value < 0.01 and \* if p-value < 0.05*

*In the first column, the values A and t correspond respectively to the angular position and the time of occurrence of the extension and flexion peaks identified in Figure 28. A3 and A4 are respectively the maximal flexion and extension during the swing phase*

At right lead canter, the hard perturbation did not have any significant effect on the coffin joint excursion.

At right lead canter, the soft perturbation condition affected the coffin joint excursion by increasing the flexion peak during the perturbed stance phase (A1) by 1.8° and the flexion peak during the second stance phase (A5) by 2.4°.

III.A.2. Fetlock joint: sagittal angle

III.A.2.a. *At trot*

The average and SEM for the fetlock joint excursion at trot over the perturbation conditions are represented in Figure 29, with the points (angle value A and normalised time t) that have been tested in the statistical model and reported in the following table.

## Predicting horse limb responses to surface variations

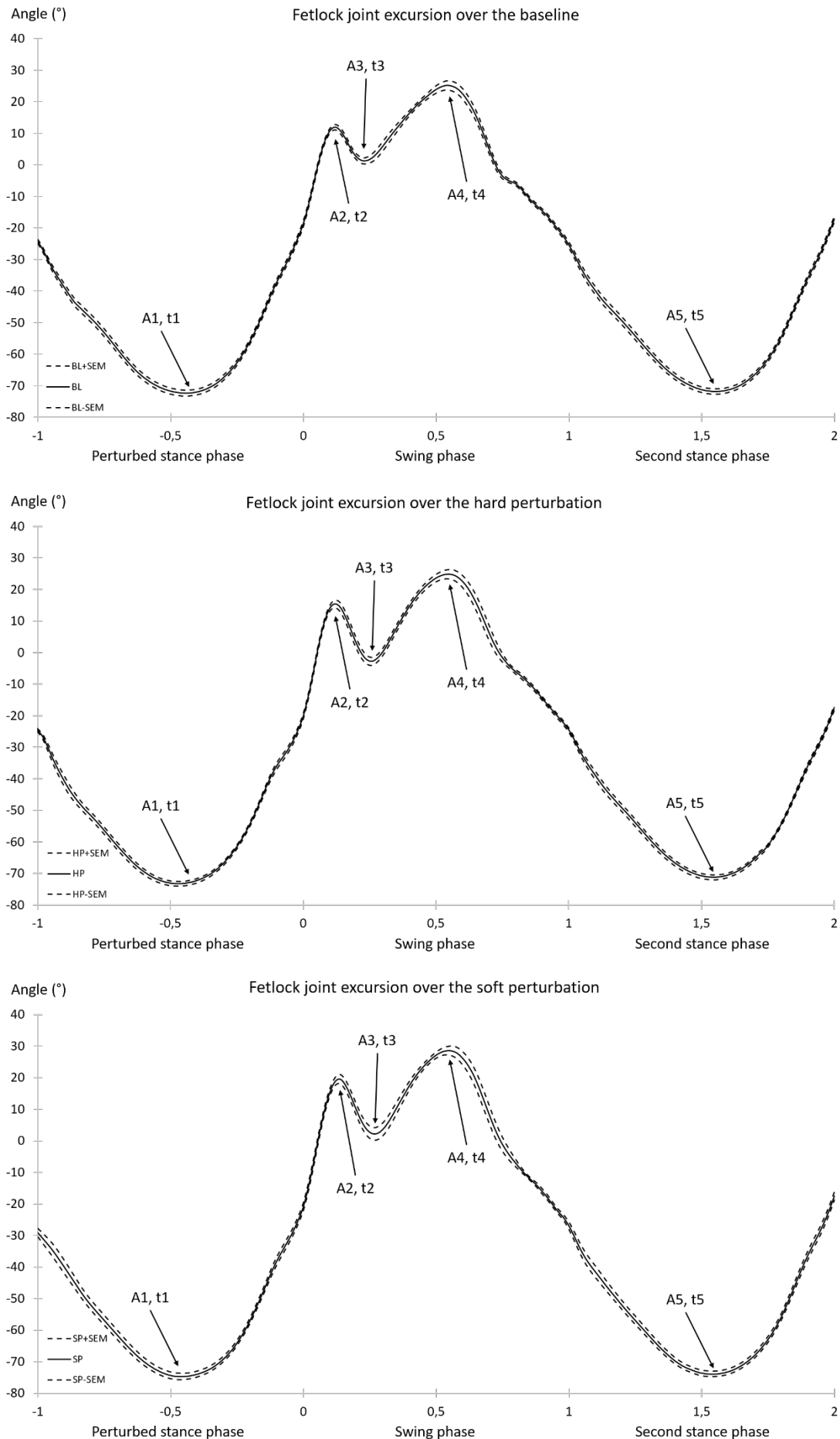


Figure 29 Fetlock joint excursion at trot over the baseline (BL, on top), over the hard perturbation (HP, in the middle) and over the soft perturbation (SP, on bottom). The curves represent the averages (plain lines) and the standard error of mean (dotted lines) of the fetlock joint excursion at trot computed for all the files ( $n=32$  files for BL;  $n=27$  files for HP and  $n=24$  files for SP). Time was normalized from -1 to 0 as the perturbed stance phase, from 0 to 1 as the swing phase and from 1 to 2 as the second stance phase.

Table 22 reports the weighted averages of the fetlock joint peak flexion and extension values and their time of occurrence at trot over the different perturbation conditions, accounting for horse and velocity differences such that the differences between averages account for the effects of the perturbation condition.

Table 22 Fetlock joint excursion at trot: peak values and their time of occurrence over the baseline, the hard and the soft perturbation conditions (average  $\pm$  SEM).

Condition	Baseline	Hard Perturbation	Soft Perturbation
Velocity (m.s <sup>-1</sup> )	3.20 $\pm$ 0.02	3.25 $\pm$ 0.05	** 3.30 $\pm$ 0.04
A1 (°)	-73.0 $\pm$ 0.9	-72.6 $\pm$ 0.8	-73.7 $\pm$ 1.0
t1	-0.44 $\pm$ 0.00	-0.47 $\pm$ 0.00	-0.46 $\pm$ 0.01
A2 (°)	14.5 $\pm$ 0.7	** 16.9 $\pm$ 1.2	** 20.8 $\pm$ 1.4
t2	0.18 $\pm$ 0.02	0.13 $\pm$ 0.00	0.16 $\pm$ 0.00
A3 (°)	2.4 $\pm$ 1.7	** -1.6 $\pm$ 1.2	3.8 $\pm$ 1.9
t3	0.28 $\pm$ 0.01	0.26 $\pm$ 0.01	0.27 $\pm$ 0.01
A4 (°)	27.1 $\pm$ 1.5	27.0 $\pm$ 1.7	** 31.1 $\pm$ 1.5
t4	0.52 $\pm$ 0.01	0.52 $\pm$ 0.01	0.53 $\pm$ 0.01
A5 (°)	-72.6 $\pm$ 0.9	** -70.5 $\pm$ 0.8	-72.8 $\pm$ 0.9
t5	1.55 $\pm$ 0.00	1.55 $\pm$ 0.01	1.54 $\pm$ 0.01

Significant differences from the baseline due to the effect of the perturbation condition are noted \*\* if  $p$ -value < 0.01 and \* if  $p$ -value < 0.05

In the first column, the values A and t correspond respectively to the angular position and the time of occurrence of the consecutive flexion and extension peaks identified in Figure 29

At trot, the hard perturbation condition affected the fetlock joint excursion by increasing the first flexion peak during the swing phase (A2) by 2.4°, by increasing the following extension peak (A3) by 4.0° and by decreasing the hyperextension during the second stance phase (A5) by 2.1°.

At trot, the soft perturbation condition affected the fetlock joint excursion by increasing the first flexion peak during the swing phase (A2) by 6.3°, and the second flexion peak during the swing phase (A4) by 4.0°.

#### III.A.2.b. At right lead canter

The average and SEM for the fetlock joint excursion at right lead canter over the perturbation conditions are represented in Figure 30, with the points (angle value A and normalised time t) that have been tested in the statistical model and reported in the following table.

## Predicting horse limb responses to surface variations

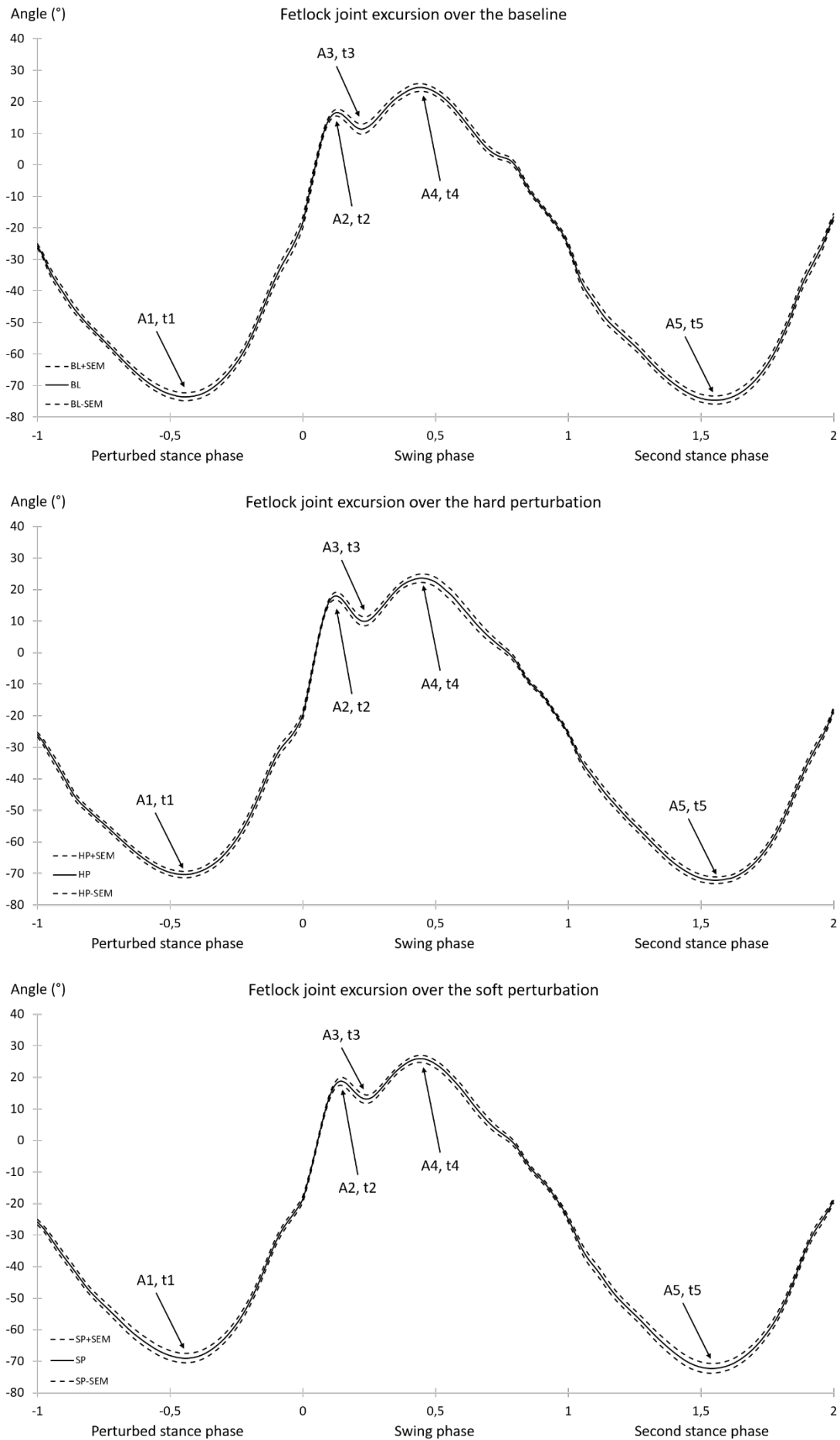


Figure 30 Fetlock joint excursion at right lead canter over the baseline (BL, on top), over the hard perturbation (HP, in the middle) and over the soft perturbation (SP, on bottom). The curves represent the averages (plain lines) and the standard error of mean (dotted lines) of the fetlock joint excursion at canter computed for all the files ( $n=24$  files for BL;  $n=28$  files for HP and  $n=24$  files for SP). Time was normalized from -1 to 0 as the perturbed stance phase, from 0 to 1 as the swing phase and from 1 to 2 as the second stance phase.

Table 23 reports the weighted averages of the fetlock joint peak flexion and extension values and their time of occurrence at right lead canter over the different perturbation conditions, accounting for horse and velocity differences such that the differences between averages account for the effects of the perturbation condition.

Table 23 Fetlock joint excursion at canter: peak values and their time of occurrence over the baseline, the hard and the soft perturbation conditions (average  $\pm$  SEM).

Condition	Baseline	Hard Perturbation	Soft Perturbation
Velocity (m.s <sup>-1</sup> )	4.85 $\pm$ 0.07	4.97 $\pm$ 0.07	4.97 $\pm$ 0.05
A1 (°)	-72.4 $\pm$ 1.2	** -71.0 $\pm$ 1.0	** -70.8 $\pm$ 1.5
t1	-0.44 $\pm$ 0.01	-0.45 $\pm$ 0.01	-0.44 $\pm$ 0.01
A2 (°)	18.8 $\pm$ 0.9	* 20.3 $\pm$ 1.0	** 20.8 $\pm$ 1.1
t2	0.23 $\pm$ 0.02	0.19 $\pm$ 0.02	0.20 $\pm$ 0.02
A3 (°)	13.7 $\pm$ 1.9	** 11.3 $\pm$ 1.5	14.2 $\pm$ 1.4
t3	0.31 $\pm$ 0.02	0.29 $\pm$ 0.02	0.28 $\pm$ 0.01
A4 (°)	23.8 $\pm$ 1.4	23.9 $\pm$ 1.5	* 25.3 $\pm$ 1.2
t4	0.45 $\pm$ 0.01	0.47 $\pm$ 0.01	0.46 $\pm$ 0.01
A5 (°)	-73.6 $\pm$ 1.2	-72.7 $\pm$ 1.1	-73.7 $\pm$ 1.5
t5	1.55 $\pm$ 0.01	1.56 $\pm$ 0.01	1.55 $\pm$ 0.01

Significant differences from the baseline due to the effect of the perturbation condition are noted \*\* if p-value < 0.01 and \* if p-value < 0.05

In the first column, the values A and t correspond respectively to the angular position and the time of occurrence of the consecutive flexion and extension peaks identified in Figure 30

At right lead canter, the hard perturbation condition affected the fetlock joint excursion by decreasing hyperextension during the perturbed stance phase (A1) by 1.4°, by increasing the flexion peak during the swing phase (A2) by 1.5° and by increasing the following extension peak (A3) by 2.4°.

At right lead canter, the soft perturbation condition affected the fetlock joint excursion by decreasing hyperextension during the perturbed stance phase (A1) by 1.6°, and by increasing the first and second flexion peaks during the swing phase (A2 and A4) by 2.0° and 1.5°, respectively.

### III.A.3. Carpal joint: sagittal angle

#### III.A.3.a. At trot

The average and SEM for the carpal joint excursion at trot over the perturbation conditions are represented in Figure 31, with the points (angle value A and normalised time t) that have been tested in the statistical model and reported in the following table.

## Predicting horse limb responses to surface variations

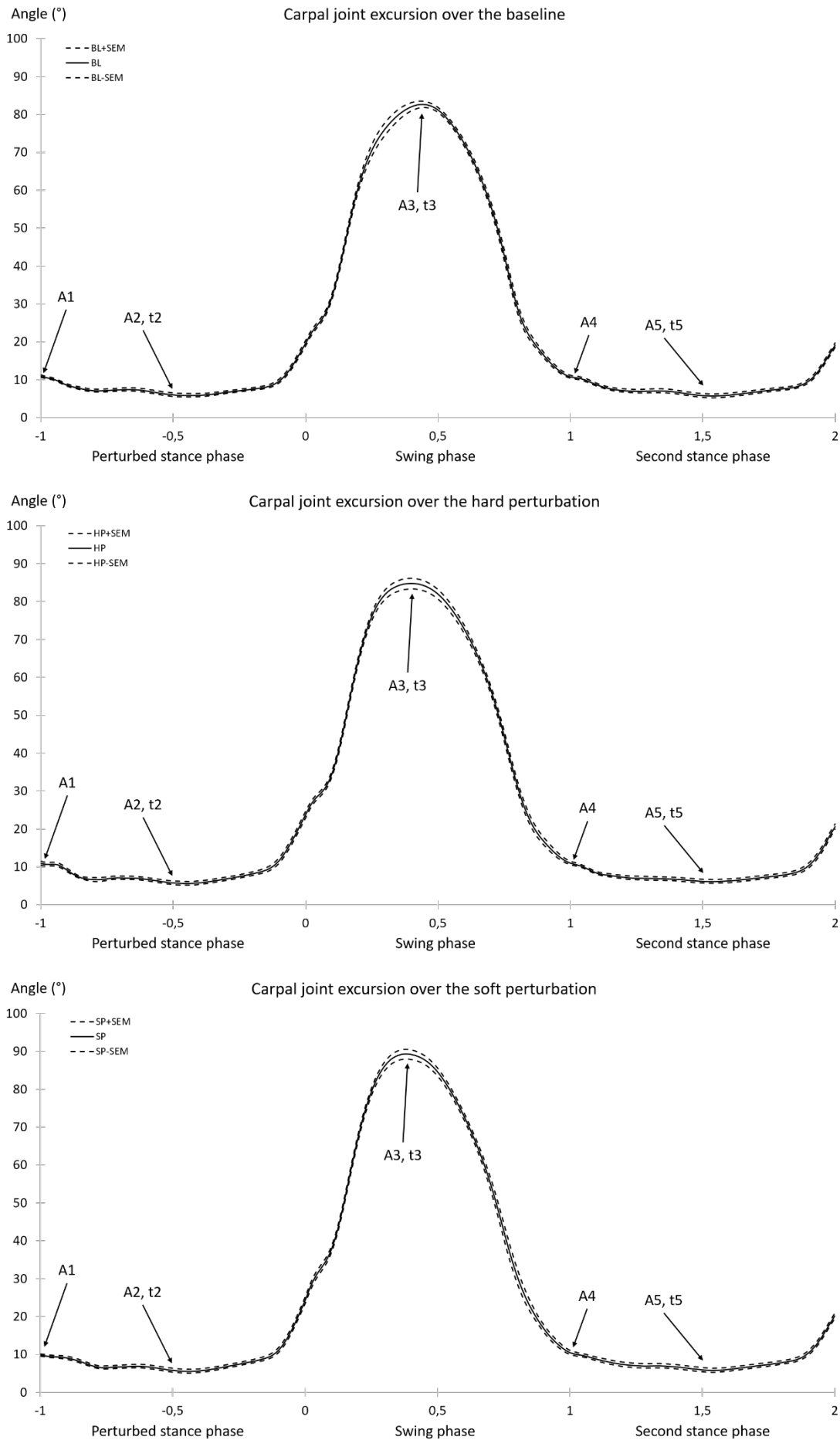


Figure 31 Carpal joint excursion at trot over the baseline (BL, on top), over the hard perturbation (HP, in the middle) and over the soft perturbation (SP, on bottom). The curves represent the averages (plain lines) and the standard error of mean (dotted lines) of the carpal joint excursion at trot computed for all the files ( $n=32$  files for BL;  $n=27$  files for HP and  $n=24$  files for SP). Time was normalized from -1 to 0 as the perturbed stance phase, from 0 to 1 as the swing phase and from 1 to 2 as the second stance phase.

Table 24 reports the averages of the carpal joint flexion and extension values and their time of occurrence at trot over the different perturbation conditions, accounting for horse and velocity differences such that the differences between averages account for the effects of the perturbation condition.

Table 24 Carpal joint excursion at trot: peak values and their time of occurrence over the baseline, the hard and the soft perturbation conditions (average  $\pm$  SEM).

Condition	Baseline	Hard Perturbation	Soft Perturbation
Velocity (m.s <sup>-1</sup> )	3.20 $\pm$ 0.02	3.25 $\pm$ 0.05	** 3.30 $\pm$ 0.04
A1 (°)	10.7 $\pm$ 0.3	10.9 $\pm$ 0.5	10.1 $\pm$ 0.3
A2 (°)	5.6 $\pm$ 0.4	** 4.9 $\pm$ 0.5	5.4 $\pm$ 0.5
t2	-0.46 $\pm$ 0.02	** -0.63 $\pm$ 0.04	-0.50 $\pm$ 0.03
A3 (°)	84.8 $\pm$ 0.9	86.1 $\pm$ 1.3	** 89.6 $\pm$ 1.3
t3	0.42 $\pm$ 0.01	0.41 $\pm$ 0.01	0.39 $\pm$ 0.01
A4 (°)	10.7 $\pm$ 0.4	10.9 $\pm$ 0.5	10.5 $\pm$ 0.6
A5 (°)	5.5 $\pm$ 0.5	5.6 $\pm$ 0.5	5.6 $\pm$ 0.5
t5	1.50 $\pm$ 0.03	1.46 $\pm$ 0.03	1.50 $\pm$ 0.03

Significant differences from the baseline due to the effect of the perturbation condition are noted \*\* if  $p$ -value < 0.01 and \* if  $p$ -value < 0.05

In the first column, the values A and t correspond respectively to the angular position and the time of occurrence of the consecutive flexion and extension peaks identified in Figure 31. A1 and A4 are the carpal joint angle at hoof impact beginning the perturbed stance phase and the second stance phase, respectively.

At trot, the hard perturbation condition affected the carpal joint excursion by increasing hyperextension during the perturbed stance phase (A2) by 0.7°, and by making that peak earlier (t2) by 0.17. The relative time change (0.17) corresponds to a real time change of about 0.056 s (the perturbed stance lasted 0.330  $\pm$  0.003 s, average  $\pm$  SEM).

At trot, the soft perturbation condition affected the carpal joint excursion by increasing the flexion peak during the swing phase (A3) by 4.8°.

### III.A.3.b. At right lead canter

The average and SEM for the carpal joint excursion at right lead canter over the perturbation conditions are represented in Figure 32, with the points (angle value A and normalised time t) that have been tested in the statistical model and reported in the following table.

## Predicting horse limb responses to surface variations

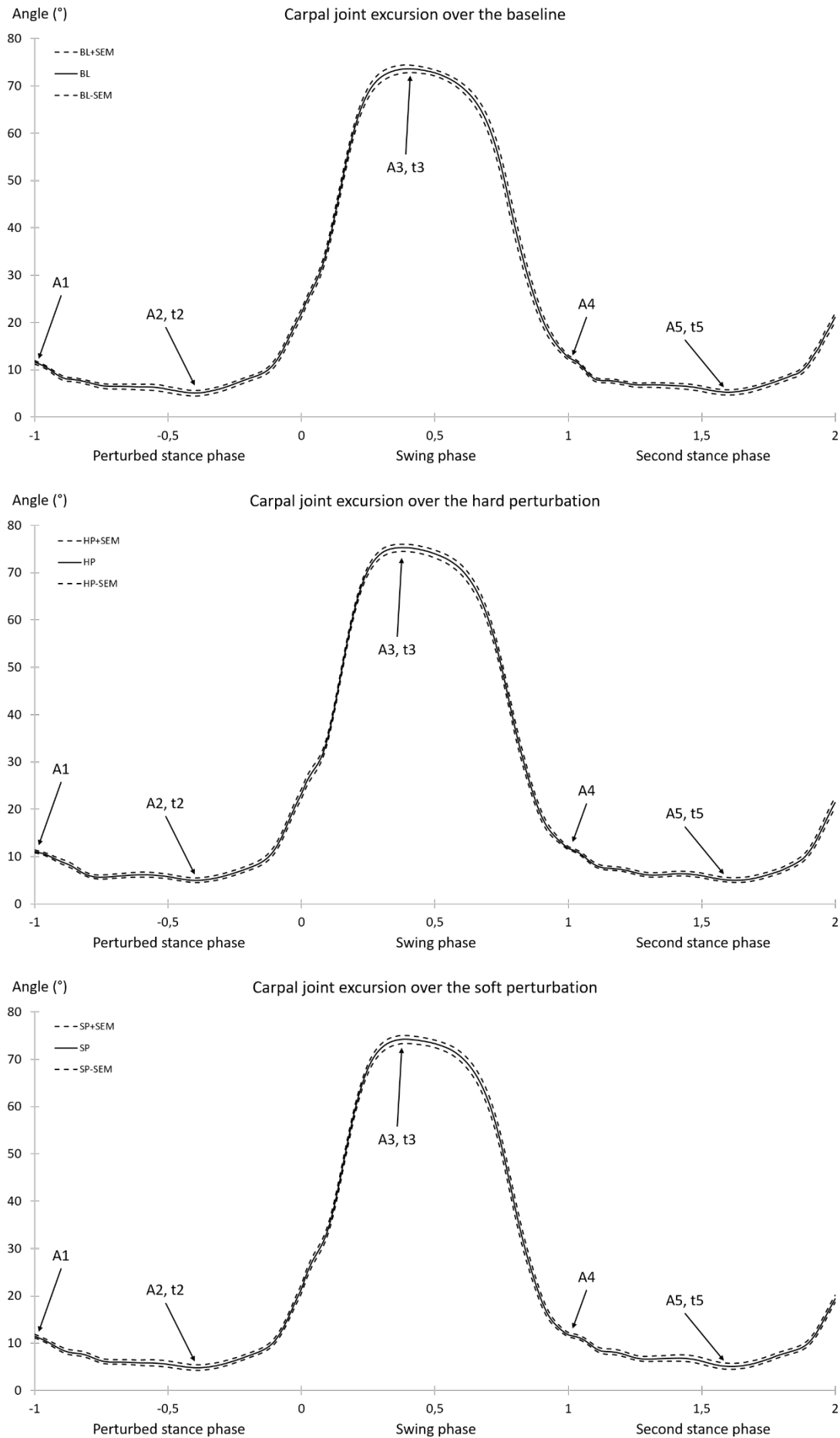


Figure 32 Carpal joint excursion at right lead canter over the baseline (BL, on top), over the hard perturbation (HP, in the middle) and over the soft perturbation (SP, on bottom). The curves represent the averages (plain lines) and the standard error of mean (dotted lines) of the carpal joint excursion at canter computed for all the files (n=24 files for BL; n=28 files for HP and n=24 files for SP). Time was normalized from -1 to 0 as the perturbed stance phase, from 0 to 1 as the swing phase and from 1 to 2 as the second stance phase.

Table 25 reports the weighted averages of the carpal joint flexion and extension values and their time of occurrence at right lead canter over the different perturbation conditions, accounting for horse and velocity differences such that the differences between averages account for the effects of the perturbation condition.

Table 25 Carpal joint excursion at canter: peak values and their time of occurrence over the baseline, the hard and the soft perturbation conditions (average  $\pm$  SEM).

Condition	Baseline	Hard Perturbation	Soft Perturbation
Velocity (m.s <sup>-1</sup> )	4.85 $\pm$ 0.07	4.97 $\pm$ 0.07	4.97 $\pm$ 0.05
A1 (°)	11.7 $\pm$ 0.4	11.3 $\pm$ 0.3	11.9 $\pm$ 0.4
A2 (°)	5.0 $\pm$ 0.6	4.9 $\pm$ 0.4	5.0 $\pm$ 0.5
t2	-0.48 $\pm$ 0.04	-0.54 $\pm$ 0.03	-0.53 $\pm$ 0.04
A3 (°)	73.9 $\pm$ 0.6	** 77.1 $\pm$ 0.7	** 76.5 $\pm$ 0.7
t3	0.42 $\pm$ 0.02	0.39 $\pm$ 0.02	0.41 $\pm$ 0.02
A4 (°)	12.7 $\pm$ 0.5	* 11.9 $\pm$ 0.3	12.2 $\pm$ 0.4
A5 (°)	4.9 $\pm$ 0.5	4.6 $\pm$ 0.4	5.3 $\pm$ 0.6
t5	1.50 $\pm$ 0.04	1.53 $\pm$ 0.03	1.50 $\pm$ 0.04

Significant differences from the baseline due to the effect of the perturbation condition are noted \*\* if  $p$ -value < 0.01 and \* if  $p$ -value < 0.05

In the first column, the values A and t correspond respectively to the angular position and the time of occurrence of the consecutive flexion and extension peaks identified in Figure 32. A1 and A4 are the carpal joint angle at hoof impact beginning the perturbed stance phase and the second stance phase, respectively.

At right lead canter, the hard perturbation condition affected the carpal joint excursion by increasing the flexion peak during the swing phase (A3) by 3.2° and by decreasing the joint angle at impact of the second stance phase (A4) by 0.8°.

At right lead canter, the soft perturbation condition affected the carpal joint excursion by increasing the flexion peak during the swing phase (A3) by 2.6°.

### III.A.4. Elbow joint: sagittal angle

#### III.A.4.a. At trot

The average and SEM for the elbow joint excursion at trot over the perturbation conditions are represented in Figure 33, with the points (angle value A and normalised time t) that have been tested in the statistical model and reported in the following table.

## Predicting horse limb responses to surface variations

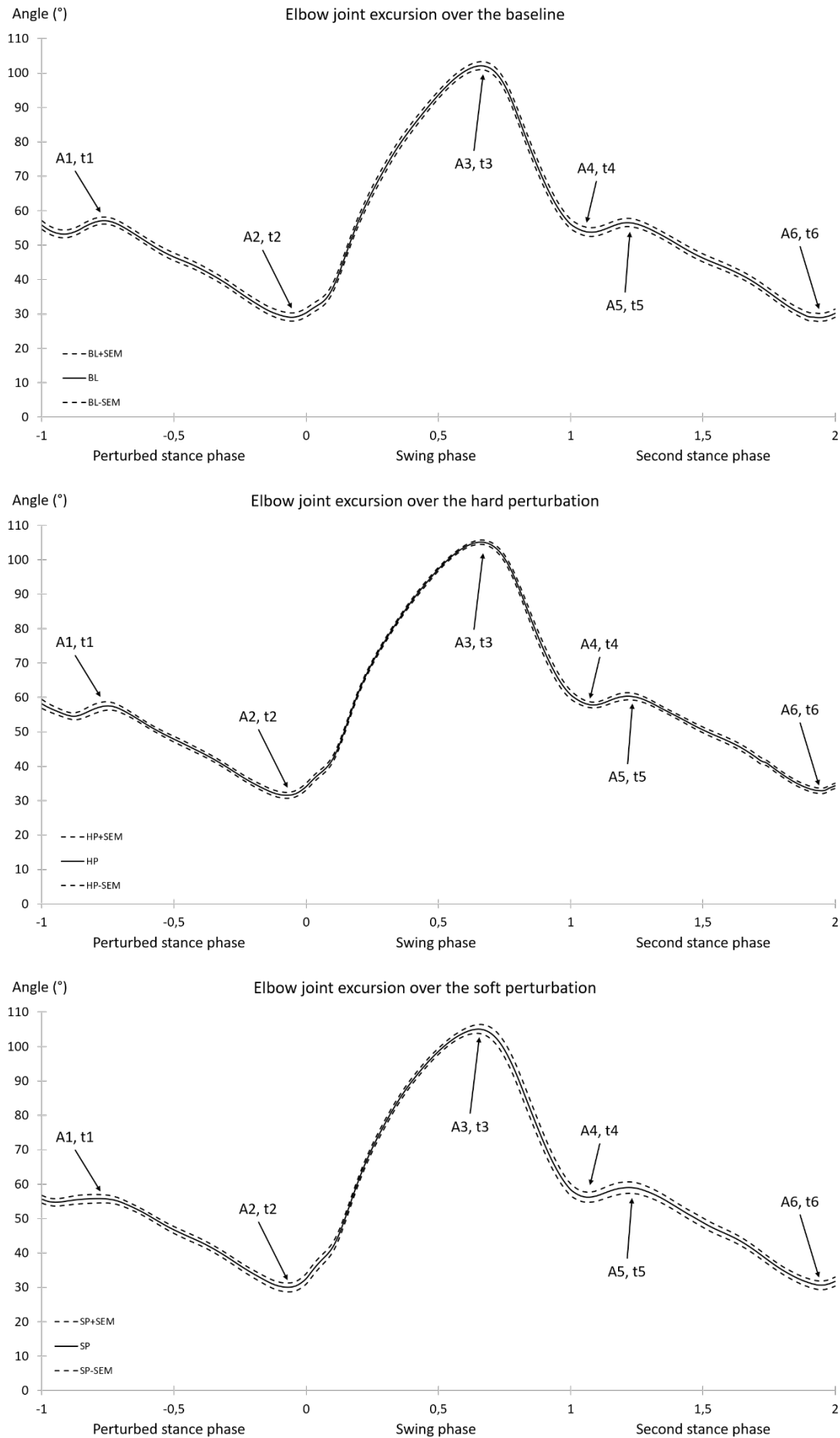


Figure 33 Elbow joint excursion at trot over the baseline (BL, on top), over the hard perturbation (HP, in the middle) and over the soft perturbation (SP, on bottom). The curves represent the averages (plain lines) and the standard error of mean (dotted lines) of the elbow joint excursion at trot computed for all the files ( $n=32$  files for BL;  $n=27$  files for HP and  $n=24$  files for SP). Time was normalized from -1 to 0 as the perturbed stance phase, from 0 to 1 as the swing phase and from 1 to 2 as the second stance phase.

Table 26 reports the averages of the elbow joint peak flexion and extension values and their time of occurrence of the elbow joint excursion at trot over the different perturbation conditions, accounting for horse and velocity differences such that the differences between averages account for the effects of the perturbation condition.

Table 26 Elbow joint excursion at trot: peak values and their time of occurrence over the baseline, the hard and the soft perturbation conditions (average  $\pm$  SEM).

Condition	Baseline	Hard Perturbation	Soft Perturbation
Velocity (m.s <sup>-1</sup> )	3.20 $\pm$ 0.02	3.25 $\pm$ 0.05	** 3.30 $\pm$ 0.04
A1 (°)	58.2 $\pm$ 1.0	57.4 $\pm$ 1.2	** 55.8 $\pm$ 1.2
t1	-0.77 $\pm$ 0.00	-0.75 $\pm$ 0.01	-0.77 $\pm$ 0.01
A2 (°)	30.1 $\pm$ 1.2	30.1 $\pm$ 0.9	** 28.6 $\pm$ 1.3
t2	-0.05 $\pm$ 0.01	-0.07 $\pm$ 0.01	-0.07 $\pm$ 0.01
A3 (°)	103.4 $\pm$ 1.2	* 104.8 $\pm$ 0.7	104.6 $\pm$ 1.2
t3	0.66 $\pm$ 0.00	0.66 $\pm$ 0.01	0.66 $\pm$ 0.01
A4 (°)	54.8 $\pm$ 1.2	* 56.2 $\pm$ 0.9	54.4 $\pm$ 1.5
t4	1.09 $\pm$ 0.01	1.08 $\pm$ 0.01	1.08 $\pm$ 0.01
A5 (°)	57.8 $\pm$ 1.2	59.7 $\pm$ 1.0	58.7 $\pm$ 1.7
t5	1.21 $\pm$ 0.00	1.21 $\pm$ 0.01	1.23 $\pm$ 0.01
A6 (°)	29.8 $\pm$ 1.2	** 31.1 $\pm$ 0.8	29.1 $\pm$ 1.2
t6	1.94 $\pm$ 0.01	1.94 $\pm$ 0.01	1.95 $\pm$ 0.01

Significant differences from the baseline due to the effect of the perturbation condition are noted \*\* if  $p$ -value < 0.01 and \* if  $p$ -value < 0.05

In the first column, the values A and t correspond respectively to the angular position and the time of occurrence of the consecutive flexion and extension peaks identified in Figure 33.

At trot, the hard perturbation condition affected the elbow joint excursion by increasing flexion during the swing phase (A3) by 1.4°, by decreasing extension at the swing-stance phase transition (A4) by 1.4° and by decreasing extension at the end of the second stance phase (A6) by 1.3°.

At trot, the soft perturbation condition affected the elbow joint excursion by decreasing flexion at the beginning of the perturbed stance phase (A1) by 2.4°, and by increasing extension at the end of the perturbed stance phase (A2) by 1.5°.

#### III.A.4.b. At right lead canter

The average and SEM for the elbow joint excursion at right lead canter over the perturbation conditions are represented in Figure 34, with the points (angle value A and normalised time t) that have been tested in the statistical model and reported in the following table.

## Predicting horse limb responses to surface variations

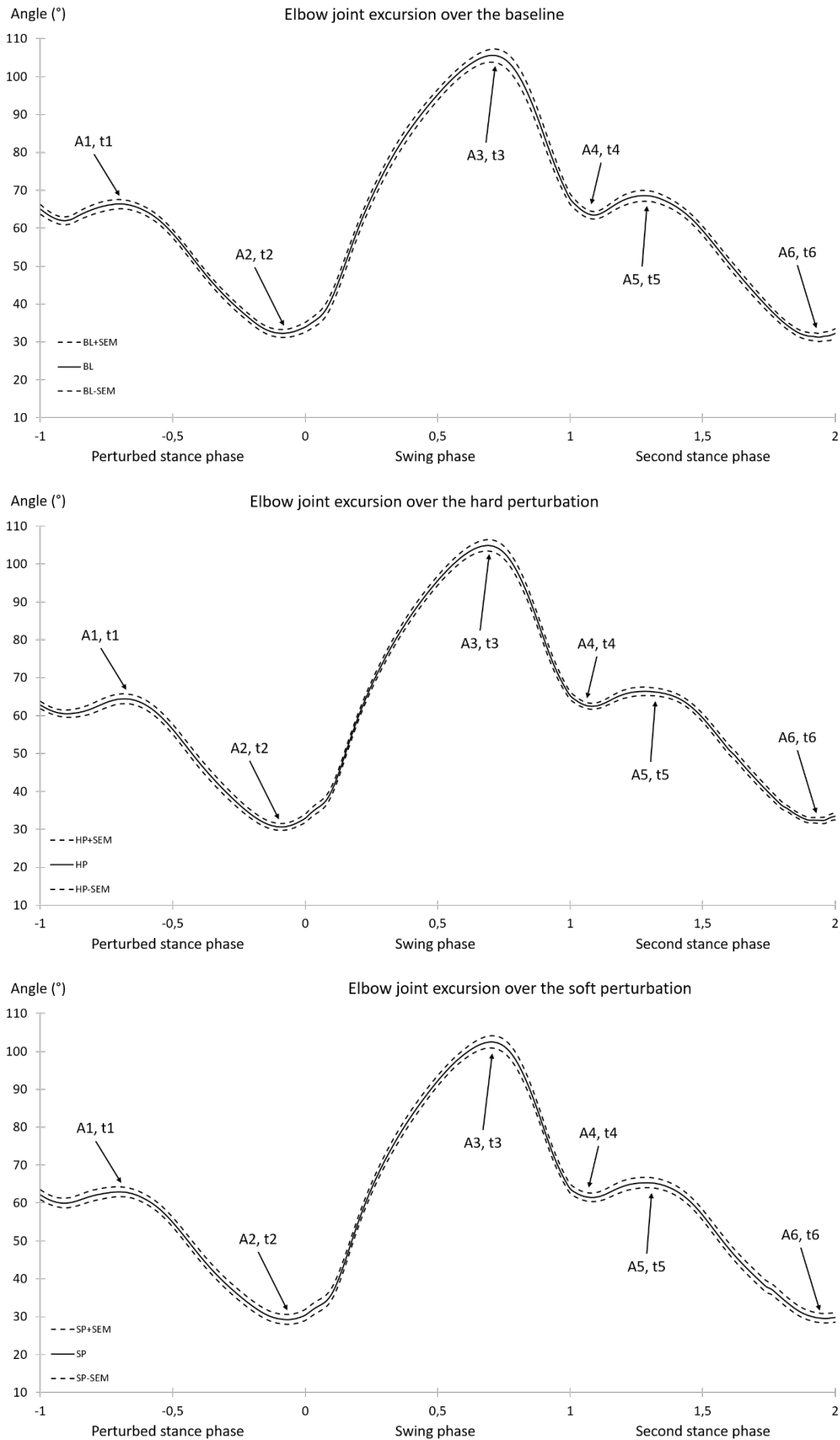


Figure 34 Elbow joint excursion at right lead canter over the baseline (BL, on top), over the hard perturbation (HP, in the middle) and over the soft perturbation (SP, on bottom). The curves represent the averages (plain lines) and the standard error of mean (dotted lines) of the elbow joint excursion at canter computed for all the files (n=24 files for BL; n=28 files for HP and n=24 files for SP). Time was normalized from -1 to 0 as the perturbed stance phase, from 0 to 1 as the swing phase and from 1 to 2 as the second stance phase.

Table 27 reports the averages of the elbow joint peak flexion and extension values and their time of occurrence at right lead canter over the different perturbation conditions, accounting for horse and velocity differences such that the differences between averages account for the effects of the perturbation condition.

*Table 27 Elbow joint excursion at canter: peak values and their time of occurrence over the baseline, the hard and the soft perturbation conditions (average  $\pm$  SEM).*

Condition	Baseline	Hard Perturbation	Soft Perturbation
Velocity (m.s <sup>-1</sup> )	4.85 $\pm$ 0.07	4.97 $\pm$ 0.07	4.97 $\pm$ 0.05
A1 (°)	65.6 $\pm$ 1.2	66.1 $\pm$ 1.3	65.6 $\pm$ 1.3
t1	-0.70 $\pm$ 0.01	-0.69 $\pm$ 0.01	-0.72 $\pm$ 0.01
A2 (°)	30.6 $\pm$ 1.1	31.1 $\pm$ 0.84	30.1 $\pm$ 1.2
t2	-0.07 $\pm$ 0.01	-0.09 $\pm$ 0.01	-0.07 $\pm$ 0.01
A3 (°)	104.5 $\pm$ 1.7	* 106.1 $\pm$ 1.5	105.1 $\pm$ 1.6
t3	0.71 $\pm$ 0.01	0.69 $\pm$ 0.01	0.71 $\pm$ 0.01
A4 (°)	62.3 $\pm$ 1.0	62.7 $\pm$ 0.7	62.0 $\pm$ 1.1
t4	1.08 $\pm$ 0.00	1.08 $\pm$ 0.01	1.08 $\pm$ 0.01
A5 (°)	67.7 $\pm$ 1.4	67.8 $\pm$ 1.1	67.4 $\pm$ 1.3
t5	1.29 $\pm$ 0.01	1.28 $\pm$ 0.01	1.28 $\pm$ 0.01
A6 (°)	30.4 $\pm$ 1.0	** 32.7 $\pm$ 0.8	30.3 $\pm$ 1.1
t6	1.92 $\pm$ 0.01	1.91 $\pm$ 0.02	1.93 $\pm$ 0.01

*Significant differences from the baseline due to the effect of the perturbation condition are noted \*\* if p-value < 0.01 and \* if p-value < 0.05*

*In the first column, the values A and t correspond respectively to the angular position and the time of occurrence of the consecutive flexion and extension peaks identified in Figure 34.*

At right lead canter, the hard perturbation condition affected the elbow joint excursion by increasing flexion during the swing phase (A3) by 1.6° and by decreasing extension during the second stance phase (A6) by 2.3°.

At right lead canter, the soft perturbation condition did not have any significant effect on the elbow joint excursion.

### III.A.5. Shoulder joint: sagittal angle

#### III.A.5.a. At trot

The average and SEM for the shoulder joint excursion at trot over the perturbation conditions are represented in Figure 35, with the points (angle value A and normalised time t) that have been tested in the statistical model and reported in the following table.

## Predicting horse limb responses to surface variations

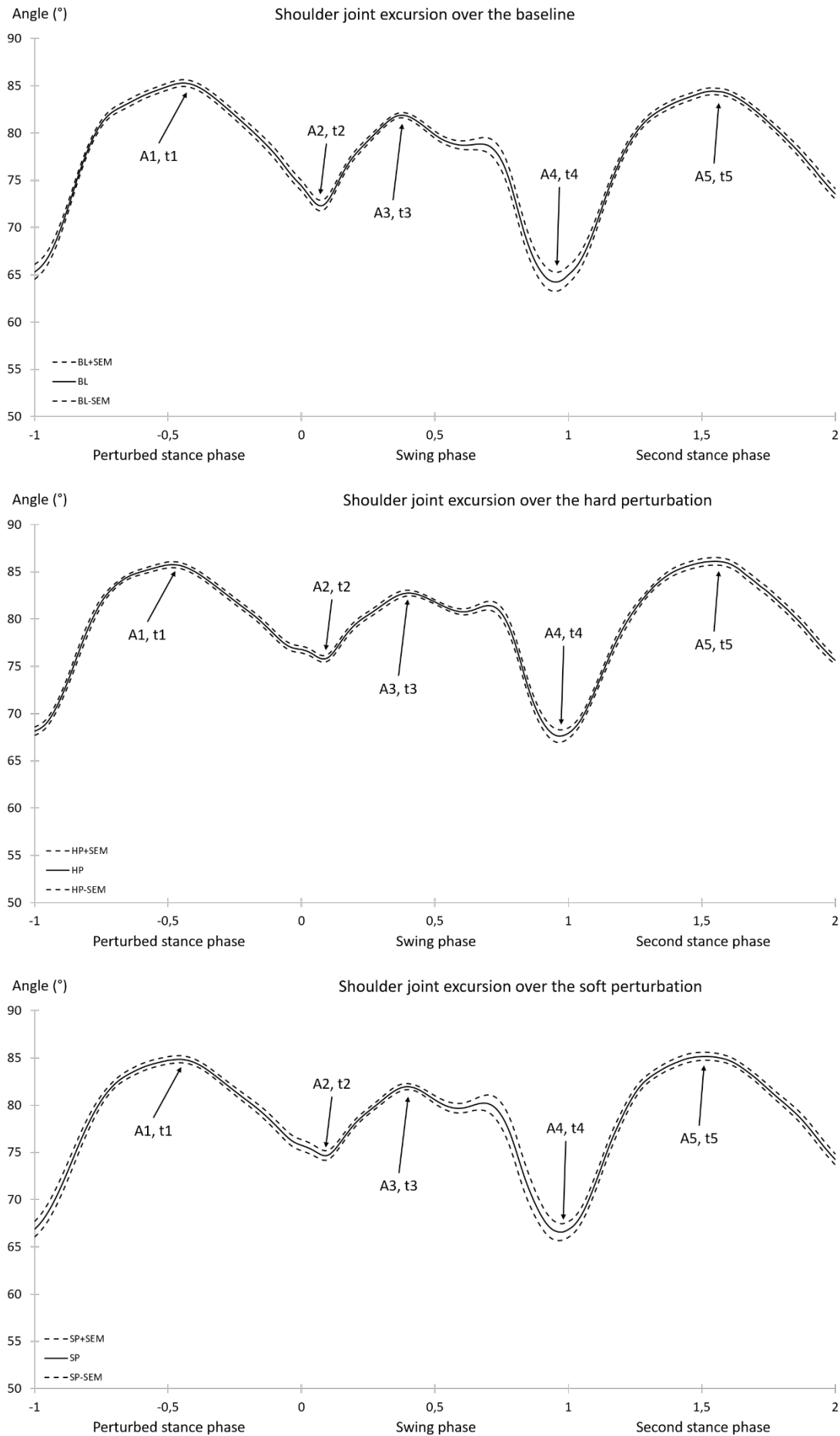


Figure 35 Shoulder joint excursion at trot over the baseline (BL, on top), over the hard perturbation (HP, in the middle) and over the soft perturbation (SP, on bottom). The curves represent the averages (plain lines) and the standard error of mean (dotted lines) of the shoulder joint excursion at trot computed for all the files ( $n=32$  files for BL;  $n=27$  files for HP and  $n=24$  files for SP). Time was normalized from -1 to 0 as the perturbed stance phase, from 0 to 1 as the swing phase and from 1 to 2 as the second stance phase.

Table 28 reports the weighted averages of the shoulder joint peak flexion and extension values and their time of occurrence at trot over the different perturbation conditions, accounting for horse and velocity differences such that the differences between averages account for the effects of the perturbation condition.

*Table 28 Shoulder joint excursion at trot: peak values and their time of occurrence over the baseline, the hard and the soft perturbation conditions (average  $\pm$  SEM).*

Condition	Baseline	Hard Perturbation	Soft Perturbation
Velocity (m.s <sup>-1</sup> )	3.20 $\pm$ 0.02	3.25 $\pm$ 0.05	** 3.30 $\pm$ 0.04
A1 (°)	85.8 $\pm$ 0.4	85.6 $\pm$ 0.3	** 84.8 $\pm$ 0.4
t1	-0.44 $\pm$ 0.00	** -0.50 $\pm$ 0.01	-0.47 $\pm$ 0.01
A2 (°)	72.8 $\pm$ 0.5	** 74.9 $\pm$ 0.3	** 73.9 $\pm$ 0.5
t2	0.07 $\pm$ 0.00	0.07 $\pm$ 0.01	0.08 $\pm$ 0.01
A3 (°)	82.4 $\pm$ 0.3	82.8 $\pm$ 0.3	82.0 $\pm$ 0.3
t3	0.38 $\pm$ 0.02	**0.42 $\pm$ 0.03	**0.42 $\pm$ 0.04
A4 (°)	65.0 $\pm$ 1.0	** 66.2 $\pm$ 0.7	64.8 $\pm$ 1.0
t4	0.96 $\pm$ 0.01	0.98 $\pm$ 0.01	0.98 $\pm$ 0.01
A5 (°)	85.0 $\pm$ 0.4	** 85.9 $\pm$ 0.4	85.1 $\pm$ 0.4
t5	1.54 $\pm$ 0.01	1.54 $\pm$ 0.01	1.51 $\pm$ 0.02

*Significant differences from the baseline due to the effect of the perturbation condition are noted \*\* if p-value < 0.01 and \* if p-value < 0.05*

*In the first column, the values A and t correspond respectively to the angular position and the time of occurrence of the consecutive flexion and extension peaks identified in Figure 35.*

At trot, the hard perturbation condition affected the shoulder joint excursion by making the flexion peak during the perturbed stance phase earlier (t1) by 0.06, by decreasing extension at the stance-swing phase transition (A2) by 2.1°, by delaying the maximal flexion angle during the swing phase (t3) by 0.04, by decreasing extension at the swing-stance phase transition (A4) by 1.2° and by increasing flexion during the second stance phase (A5) by 0.9°. The changes in relative time (0.06 and 0.04) correspond to changes in real time of 0.020 s (for 0.06, the perturbed stance phase lasted 0.330  $\pm$  0.003 s, average  $\pm$  SEM) and 0.013 s (for 0.04, the swing phase lasted 0.393  $\pm$  0.003 s, average  $\pm$  SEM).

At trot, the soft perturbation condition affected the shoulder joint excursion by decreasing flexion during the perturbed stance phase (A1) by 1.0°, by decreasing extension at the stance-swing phase transition (A2) by 1.1° and by delaying the maximal flexion angle during the swing phase (t3) by 0.04. That corresponds to a change of 0.013 s in real time (the swing phase lasted 0.393  $\pm$  0.003 s, average  $\pm$  SEM).

III.A.5.b. *At right lead canter*

The average and SEM for the shoulder joint excursion at right lead canter over the perturbation conditions are represented in Figure 36, with the points (angle value A and normalised time t) that have been tested in the statistical model and reported in the following table.

## Chapter 6 Limb response to perturbations

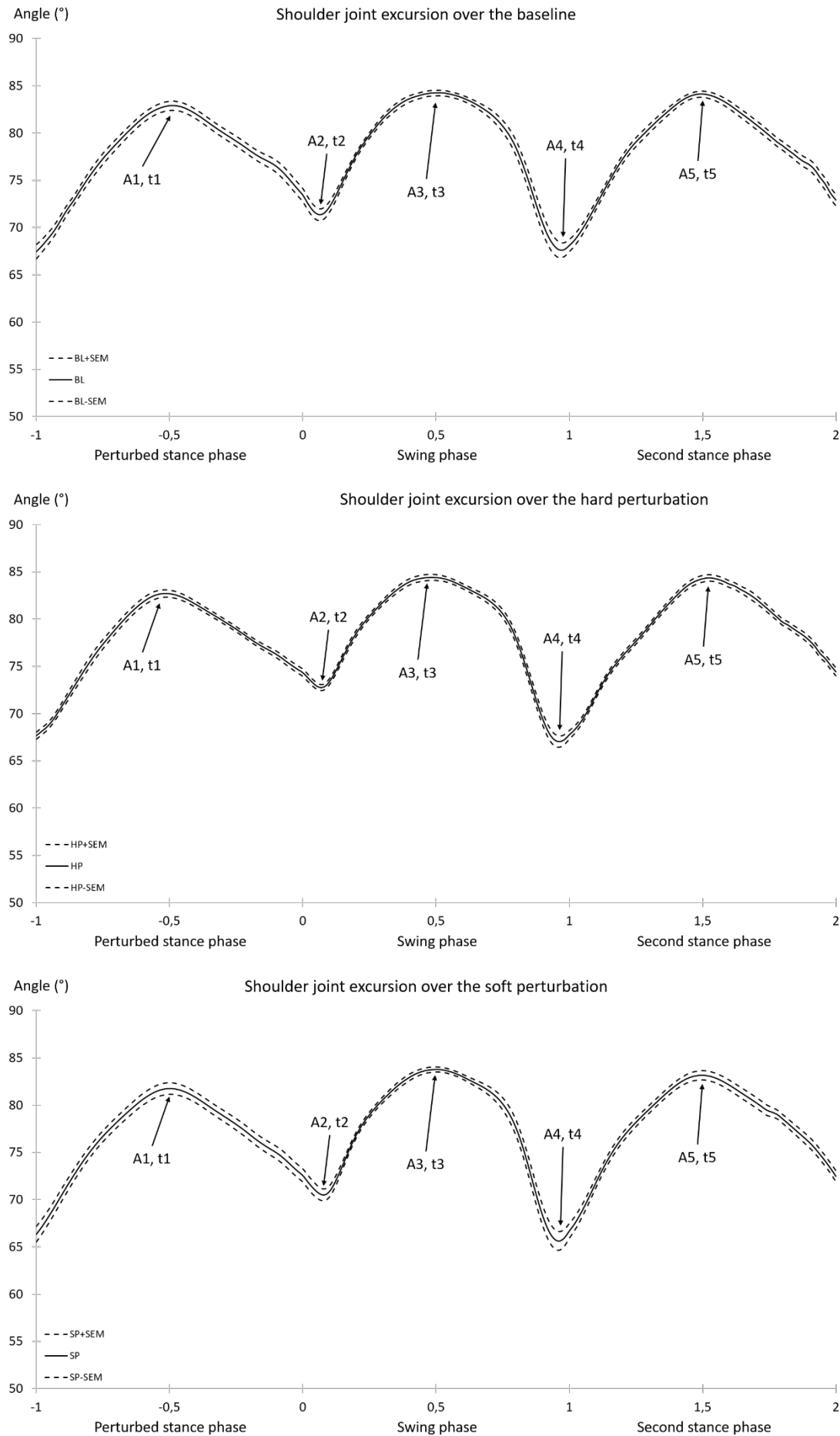


Figure 36 Shoulder joint excursion at right lead canter over the baseline (BL, on top), over the hard perturbation (HP, in the middle) and over the soft perturbation (SP, on bottom). The curves represent the averages (plain lines) and the standard error of mean (dotted lines) of the shoulder joint excursion at canter computed for all the files ( $n=24$  files for BL;  $n=28$  files for HP and  $n=24$  files for SP). Time was normalized from -1 to 0 as the perturbed stance phase, from 0 to 1 as the swing phase and from 1 to 2 as the second stance phase.

## Predicting horse limb responses to surface variations

Table 29 reports the weighted averages of the shoulder joint peak flexion and extension values and their time of occurrence at right lead canter over the different perturbation conditions, accounting for horse and velocity differences such that the differences between averages account for the effects of the perturbation condition.

*Table 29 Shoulder joint excursion at canter: peak values and their time of occurrence over the baseline, the hard and the soft perturbation conditions (average  $\pm$  SEM).*

Condition	Baseline	Hard Perturbation	Soft Perturbation
Velocity (m.s <sup>-1</sup> )	4.85 $\pm$ 0.07	4.97 $\pm$ 0.07	4.97 $\pm$ 0.05
A1 (°)	82.8 $\pm$ 0.5	83.2 $\pm$ 0.4	82.1 $\pm$ 0.6
t1	-0.49 $\pm$ 0.01	-0.51 $\pm$ 0.01	-0.50 $\pm$ 0.01
A2 (°)	70.8 $\pm$ 0.6	** 72.8 $\pm$ 0.3	70.8 $\pm$ 0.6
t2	0.06 $\pm$ 0.00	0.07 $\pm$ 0.00	0.08 $\pm$ 0.00
A3 (°)	84.4 $\pm$ 0.3	* 84.9 $\pm$ 0.3	84.6 $\pm$ 0.2
t3	0.53 $\pm$ 0.02	0.51 $\pm$ 0.01	0.51 $\pm$ 0.02
A4 (°)	66.3 $\pm$ 0.8	67.0 $\pm$ 0.6	66.0 $\pm$ 1.0
t4	0.97 $\pm$ 0.01	0.97 $\pm$ 0.01	0.97 $\pm$ 0.01
A5 (°)	84.0 $\pm$ 0.3	84.8 $\pm$ 0.4	83.4 $\pm$ 0.5
t5	1.50 $\pm$ 0.01	1.52 $\pm$ 0.01	1.50 $\pm$ 0.01

*Significant differences from the baseline due to the effect of the perturbation condition are noted \*\* if p-value < 0.01 and \* if p-value < 0.05*

*In the first column, the values A and t correspond respectively to the angular position and the time of occurrence of the consecutive flexion and extension peaks identified in Figure 36.*

At right lead canter, the hard perturbation condition affected the shoulder joint excursion by decreasing extension at the stance-swing phase transition (A2) by 2.0° and by increasing flexion during the swing phase (A3) by 0.5°.

At right lead canter, the soft perturbation condition did not have any significant effect on the shoulder joint excursion.

### III.B. Statistical results of the ligament and tendon strains

To study the effect of the perturbation condition, the maximal strain during the perturbed stance phase and during the second stance phase were tested in the statistical model. As for joint excursions, variability due to horse and velocity were accounted for in the model by including these variables as independent factors.

The maximal strain of the ligaments and tendons were computed as the difference between the maximal length they reached and their slack length divided by the slack length ( $\frac{L_{max}-L_0}{L_0}$ , with  $L_{max}$  the maximal length reached and  $L_0$  the slack length) and so are presented without units.

## III.B.1. Ligament and tendon strains during stance at trot

Table 30 reports the averages of the maximal strains of the studied ligaments and tendons during the perturbed stance phase and the second stance phase over the different perturbation conditions at trot.

Table 30 Maximal strains computed within the tendons and ligaments at trot during the perturbed stance phase and the following stance phase over the perturbation conditions (average  $\pm$  SEM).

		Maximal strain during the first stance phase			Maximal strain during the second stance phase		
		Baseline	Hard Perturbation	Soft Perturbation	Baseline	Hard Perturbation	Soft Perturbation
Velocity (m.s <sup>-1</sup> )		3.20 $\pm$ 0.02	3.25 $\pm$ 0.05	3.30 $\pm$ 0.04	3.20 $\pm$ 0.02	3.25 $\pm$ 0.05	3.30 $\pm$ 0.04
Suspensory Ligament		0.233 $\pm$ 0.002	0.233 $\pm$ 0.002	0.235 $\pm$ 0.002	0.233 $\pm$ 0.002	** 0.228 $\pm$ 0.002	0.233 $\pm$ 0.002
Extensor Branches		0.204 $\pm$ 0.004	0.203 $\pm$ 0.003	** 0.208 $\pm$ 0.004	0.201 $\pm$ 0.003	* 0.197 $\pm$ 0.003	** 0.207 $\pm$ 0.004
Superficial Digital Flexor	Tendon	0.054 $\pm$ 0.000	0.054 $\pm$ 0.000	0.054 $\pm$ 0.000	0.054 $\pm$ 0.000	0.054 $\pm$ 0.000	** 0.056 $\pm$ 0.001
	Accessory Ligament	0.121 $\pm$ 0.001	0.121 $\pm$ 0.000	0.122 $\pm$ 0.001	0.121 $\pm$ 0.001	** 0.119 $\pm$ 0.000	0.121 $\pm$ 0.001
Deep digital Flexor	Humeral Tendon	0.053 $\pm$ 0.001	0.051 $\pm$ 0.001	0.052 $\pm$ 0.001	0.053 $\pm$ 0.001	0.053 $\pm$ 0.001	0.054 $\pm$ 0.001
	Ulnar Tendon	0.068 $\pm$ 0.000	0.068 $\pm$ 0.000	** 0.071 $\pm$ 0.000	0.068 $\pm$ 0.000	0.067 $\pm$ 0.000	** 0.071 $\pm$ 0.001
	Radial Tendon	0.120 $\pm$ 0.001	0.119 $\pm$ 0.001	** 0.124 $\pm$ 0.001	0.120 $\pm$ 0.001	0.119 $\pm$ 0.001	** 0.125 $\pm$ 0.001
	Accessory Ligament	0.170 $\pm$ 0.001	* 0.169 $\pm$ 0.001	* 0.169 $\pm$ 0.002	0.170 $\pm$ 0.001	* 0.167 $\pm$ 0.001	0.169 $\pm$ 0.001
Oblique Sesamoidean Ligament		0.826 $\pm$ 0.014	0.821 $\pm$ 0.011	0.831 $\pm$ 0.014	0.820 $\pm$ 0.013	** 0.798 $\pm$ 0.010	0.822 $\pm$ 0.012
Straight Sesamoidean Ligament		0.349 $\pm$ 0.008	0.346 $\pm$ 0.006	0.352 $\pm$ 0.008	0.346 $\pm$ 0.007	** 0.334 $\pm$ 0.005	0.347 $\pm$ 0.007
Lacertus Fibrosus		0.110 $\pm$ 0.001	** 0.113 $\pm$ 0.001	** 0.114 $\pm$ 0.001	---	---	---

Significant differences from the baseline due to the effect of the perturbation condition are noted \*\* if  $p$ -value < 0.01 and \* if  $p$ -value < 0.05

Note that the maximal strain of the lacertus occurred at the stance-swing phase transition, occurring sometimes at the end of the stance phase and other times at the beginning of the swing phase. Therefore, it was sometimes not possible to compute the maximal strain relative to the second stance phase and so those values have not been reported.

At trot, the hard perturbation condition significantly decreased the maximal strain in the accessory ligament of the deep digital flexor (ALDDF) and increased the strain in the lacertus fibrosus during the first stance phase. During the second stance phase, the hard perturbation significantly decreased the maximal strain in the suspensory ligament, the extensor branches, the accessory ligament of the superficial digital flexor (ALSDF), the ALDDF, and in the oblique and straight sesamoidean ligaments.

At trot, during the perturbed stance phase, the soft perturbation condition increased the maximal strains in the extensor branches, the ulnar and radial heads of the DDF, and in the lacertus fibrosus. It also decreased the maximal strain in the ALDDF. During the second stance phase, the soft perturbation condition increased the maximal strain within the extensor branches, the tendon of SDF and the ulnar and radial heads of DDF.

### III.B.2. Ligament and tendon strains during stance at canter

Table 31 reports the averages of the maximal strains during the perturbed stance phase and the second stance phase over the different perturbation conditions at right lead canter.

## Chapter 6 Limb response to perturbations

*Table 31 Maximal strains computed within the tendons and ligaments at canter during the perturbed stance phase and the following stance phase over the perturbation conditions (average  $\pm$  SEM). Horse and velocity differences were accounted for and the effect of velocity were removed in the averages presented here*

		Maximal strain during the first stance phase			Maximal strain during the second stance phase		
Condition		Baseline	Hard Perturbation	Soft Perturbation	Baseline	Hard Perturbation	Soft Perturbation
Velocity (m.s <sup>-1</sup> )		4.85 $\pm$ 0.07	4.97 $\pm$ 0.07	4.97 $\pm$ 0.05	4.85 $\pm$ 0.07	4.97 $\pm$ 0.07	4.97 $\pm$ 0.05
Suspensory Ligament		0.232 $\pm$ 0.002	** 0.229 $\pm$ 0.002	** 0.228 $\pm$ 0.003	0.234 $\pm$ 0.002	0.233 $\pm$ 0.002	0.234 $\pm$ 0.003
Extensor Branches		0.206 $\pm$ 0.004	0.205 $\pm$ 0.003	0.206 $\pm$ 0.005	0.208 $\pm$ 0.004	0.208 $\pm$ 0.003	* 0.211 $\pm$ 0.005
Superficial Digital Flexor	Tendon	0.064 $\pm$ 0.001	0.063 $\pm$ 0.001	0.064 $\pm$ 0.001	0.065 $\pm$ 0.001	0.065 $\pm$ 0.001	0.066 $\pm$ 0.001
	Accessory Ligament	0.121 $\pm$ 0.001	* 0.120 $\pm$ 0.001	* 0.119 $\pm$ 0.001	0.121 $\pm$ 0.001	0.121 $\pm$ 0.001	0.121 $\pm$ 0.001
Deep digital Flexor	Humeral Tendon	0.062 $\pm$ 0.001	0.061 $\pm$ 0.001	0.062 $\pm$ 0.001	0.064 $\pm$ 0.001	0.063 $\pm$ 0.001	0.064 $\pm$ 0.001
	Ulnar Tendon	0.062 $\pm$ 0.001	0.062 $\pm$ 0.001	0.062 $\pm$ 0.001	0.062 $\pm$ 0.001	0.063 $\pm$ 0.001	0.063 $\pm$ 0.001
	Radial Tendon	0.108 $\pm$ 0.001	0.109 $\pm$ 0.001	0.109 $\pm$ 0.001	0.109 $\pm$ 0.001	0.110 $\pm$ 0.001	0.111 $\pm$ 0.001
	Accessory Ligament	0.168 $\pm$ 0.001	** 0.166 $\pm$ 0.002	** 0.165 $\pm$ 0.002	0.168 $\pm$ 0.002	0.167 $\pm$ 0.002	0.167 $\pm$ 0.002
Oblique Sesamoidean Ligament		0.820 $\pm$ 0.016	** 0.806 $\pm$ 0.014	** 0.805 $\pm$ 0.020	0.831 $\pm$ 0.016	0.821 $\pm$ 0.014	0.833 $\pm$ 0.020
Straight Sesamoidean Ligament		0.346 $\pm$ 0.009	** 0.338 $\pm$ 0.008	** 0.338 $\pm$ 0.011	0.352 $\pm$ 0.009	0.346 $\pm$ 0.008	0.353 $\pm$ 0.011
Lacertus Fibrosus		0.109 $\pm$ 0.001	0.110 $\pm$ 0.001	0.110 $\pm$ 0.001			

*Significant differences from the baseline due to the effect of the perturbation condition are noted \*\* if p-value < 0.01 and \* if p-value < 0.05*

As it was for trot, the maximal strain in the lacertus fibrosus occurred at the stance-swing phase transition, occurring sometimes at the end of the stance phase and other times at the beginning of the swing phase. Therefore, it was sometimes not possible to compute the maximal strain during that period (at the end of the second stance phase) and so those values have not been reported.

At right lead canter, during the perturbed stance phase, the hard perturbation significantly decreased the maximal strains in the suspensory ligament, the ALSDF, the ALDDF, and the oblique and straight sesamoidean ligaments. During the second stance phase, the hard perturbation did not have any significant effect on the maximal strains of the studied tendons and ligaments.

At right lead canter, during the perturbed stance phase, the soft perturbation significantly decreased the maximal strains in the suspensory ligament, the ALSDF, the ALDDF, and the oblique and straight sesamoidean ligaments. During the second stance phase, the soft perturbation significantly increased the maximal strain in the extensor branches.

#### IV. Summary of joint excursions and soft tissue strains

The limb responses to the hard and soft perturbations are summarised below. The discrete effects in mid-stance and mid-swing are noted, but, with the exception of the shoulder joint excursion and strain in lacertus fibrosus, peaks occurring at the stance-swing (St-swing) and swing-stance phase transition are not.

*Table 32 Main effects of the hard perturbation on the joint excursions and tendon and ligament strains at trot*

	<b>Perturbed stance phase</b>	<b>Mid-swing phase</b>	<b>Second stance phase</b>
Coffin	<i>No effect</i>	<b>Less flexed</b>	<i>No effect</i>
Fetlock	<i>No effect</i>	<i>No effect</i>	<b>Less hyperextended</b>
Carpus	<b>More hyperextended</b>	<i>No effect</i>	<i>No effect</i>
Elbow	<i>No effect</i>	<b>More flexed</b>	<i>No effect</i>
Shoulder	<b>More flexed (St-swing)</b>	<i>No effect</i>	<b>More flexed</b>
Suspensory Ligament	<i>No effect</i>	---	<b>Less strained</b>
Extensor branches	<i>No effect</i>	---	<b>Less strained</b>
Tendon of SDF	<i>No effect</i>	---	<i>No effect</i>
Accessory ligament of SDF	<i>No effect</i>	---	<b>Less strained</b>
Tendon of DDF	<i>No effect</i>	---	<i>No effect</i>
Accessory ligament of DDF	<b>Less strained</b>	---	<b>Less strained</b>
Oblique sesamoidean ligament	<i>No effect</i>	---	<b>Less strained</b>
Straight sesamoidean ligament	<i>No effect</i>	---	<b>Less strained</b>
Lacertus fibrosus	<b>More strained</b>	---	---

## Chapter 6 Limb response to perturbations

Table 33 Main effects of the hard perturbation on the joint excursions and tendon and ligament strains at canter

	<b>Perturbed stance phase</b>	<b>Mid-swing phase</b>	<b>Second stance phase</b>
Coffin	<i>No effect</i>	<i>No effect</i>	<i>No effect</i>
Fetlock	<b>Less hyperextended</b>	<i>No effect</i>	<i>No effect</i>
Carpus	<i>No effect</i>	<b>More flexed</b>	<i>No effect</i>
Elbow	<i>No effect</i>	<b>More flexed</b>	<i>No effect</i>
Shoulder	<b>More flexed (St-Swing)</b>	<b>More flexed</b>	<i>No effect</i>
Suspensory Ligament	<b>Less strained</b>	---	<i>No effect</i>
Extensor branches	<i>No effect</i>	---	<i>No effect</i>
Tendon of SDF	<i>No effect</i>	---	<i>No effect</i>
Accessory ligament of SDF	<b>Less strained</b>	---	<i>No effect</i>
Tendon of DDF	<i>No effect</i>	---	<i>No effect</i>
Accessory ligament of DDF	<b>Less strained</b>	---	<i>No effect</i>
Oblique sesamoidean ligament	<b>Less strained</b>	---	<i>No effect</i>
Straight sesamoidean ligament	<b>Less strained</b>	---	<i>No effect</i>
Lacertus fibrosus	<b>More strained</b>	---	---

Table 34 Main effects of the soft perturbation on the joint excursions and tendon and ligament strains at trot

	<b>Perturbed stance phase</b>	<b>Mid-swing phase</b>	<b>Second stance phase</b>
Coffin	<b>More flexed</b>	<b>More flexed</b>	<b>More flexed</b>
Fetlock	<i>No effect</i>	<b>More flexed</b>	<i>No effect</i>
Carpus	<i>No effect</i>	<b>More flexed</b>	<i>No effect</i>
Elbow	<b>More extended</b>	<i>No effect</i>	<i>No effect</i>
Shoulder	<b>More flexed (St-Swing)</b>	<i>No effect</i>	<i>No effect</i>
Suspensory Ligament	<i>No effect</i>	---	<i>No effect</i>
Extensor branches	<b>More strained</b>	---	<b>More strained</b>
Tendon of SDF	<i>No effect</i>	---	<b>More strained</b>
Accessory ligament of SDF	<i>No effect</i>	---	<i>No effect</i>
Tendon of DDF	<b>More strained</b>	---	<b>More strained</b>
Accessory ligament of DDF	<b>Less strained</b>	---	<i>No effect</i>
Oblique sesamoidean ligament	<i>No effect</i>	---	<i>No effect</i>
Straight sesamoidean ligament	<i>No effect</i>	---	<i>No effect</i>
Lacertus fibrosus	<b>More strained</b>	---	---

## Predicting horse limb responses to surface variations

Table 35 Main effects of the soft perturbation on the joint excursions and tendon and ligament strains at canter

	<b>Perturbed stance phase</b>	<b>Mid-swing phase</b>	<b>Second stance phase</b>
Coffin	<b>More flexed</b>	<i>No effect</i>	<b>More flexed</b>
Fetlock	<b>Less hyperextended</b>	<b>More flexed</b>	<i>No effect</i>
Carpus	<i>No effect</i>	<b>More flexed</b>	<i>No effect</i>
Elbow	<i>No effect</i>	<i>No effect</i>	<i>No effect</i>
Shoulder	<i>No effect</i>	<i>No effect</i>	<i>No effect</i>
Suspensory Ligament	<i>No effect</i>	---	<i>No effect</i>
Extensor branches	<i>No effect</i>	---	<b>More strained</b>
Tendon of SDF	<b>Less strained</b>	---	<i>No effect</i>
Accessory ligament of SDF	<b>Less strained</b>	---	<i>No effect</i>
Tendon of DDF	<i>No effect</i>	---	<b>More strained</b>
Accessory ligament of DDF	<b>Less strained</b>	---	<i>No effect</i>
Oblique sesamoidean ligament	<b>Less strained</b>	---	<i>No effect</i>
Straight sesamoidean ligament	<b>Less strained</b>	---	<i>No effect</i>
Lacertus fibrosus	<i>No effect</i>	---	---

Overall, at both trot and canter, the hard perturbation resulted in a more compliant proximal limb spring in the perturbed stance phase, as evidenced by increased shoulder flexion and although this was associated with increased strain in Lacertus fibrosus, it was also associated with decreased strain or no effect in the other ligaments and tendons in both stance phases. The elbow and carpal joints were more flexed in the intervening swing phase. Less fetlock hyperextension in either stance phase was likewise associated with reduced strain in the distal ligaments. In contrast, the soft perturbation resulted in more coffin joint flexion in both stance phases, and this was associated with reduced strain in ALDDF but more strain in the tendons of DDF and in the extensor branches of the suspensory ligament. The increased shoulder flexion observed at trot was again associated with increased strain in lacertus fibrosus.

## V. Conclusion

In a multisegment, multiarticular limb, the total limb support moment must be sufficient to support the superincumbent body during stance. As observed in Chapter 4, there is a consistent template of joint motions per joint, albeit with some variability between trials in a horse and with some greater variability between horses. From stride to stride, a horse may vary the excursion of one joint and compensate for that change by varying the excursion of another joint and, in doing so, will maintain

the overall limb support moment. The ability to vary individual joint contributions to the total limb support moment might make the effects of a minor ground surface perturbation difficult to interpret. However, as seen in Figures 27 through 36, there were some discrete compensations in response to the perturbations. These compensations were not always maintained between trot and canter, and it is possible that the larger forces and shorter stance duration experienced at canter precluded the necessity or potential for the limb to adjust its stiffness in response to the perturbations in this study.

In theory, locomotion on softer ground reduces the requirement of the limb joints to behave as shock absorbers, as the soft ground is absorptive. The tuneable “limb spring” (McGuigan and Wilson, 2003) can stiffen in response to a softer surface, and become more compliant through joint flexion on a harder surface as the limb absorbs the concussive impacts. Previous investigators (McGuigan and Wilson, 2003; Wilson *et al.*, 2001) have proposed a model of the limb as consisting of a proximal spring (shoulder and elbow) and a distal spring (carpus, fetlock and coffin).

### V.A. Response to perturbations at trot

In response to the hard perturbation, during the perturbed stance phase, the hyperextension of the carpal joint was increased and occurred earlier and the shoulder flexion peak occurred earlier. These joint effects were associated with decreased strain in the accessory ligament of the deep digital flexor and to increased strain in the lacertus fibrosus. During the swing phase, the amplitude of the coffin joint oscillations was reduced but the amplitude of movements in the other distal joints (fetlock and carpal) were increased, suggesting increased swing energy caused by the observed increased elbow flexion and concomitant passive flexion by the carpus and fetlock. Indeed, the first fetlock flexion peak during the swing phase and the following fetlock extension peak were increased, and the carpal flexion peak was increased. The main amplitude effect in shoulder joint excursion was observed at the stance-swing phase transition where the decreased extension of the shoulder was associated with increased strain in lacertus fibrosus. The immediate effects of the hard perturbation were minimal at trot, but the effects were manifested in the second stance phase. The shoulder and elbow joints were more flexed at the swing-stance phase transition and the shoulder joint was more flexed at mid-stance (of the second stance phase). At the end of the second stance phase, fetlock hyperextension was reduced and the coffin joint was less extended, and this was associated with reduced strain in all the distal ligaments. The increased compliance observed in the elbow and shoulder joints under the influence of the hard perturbation was most likely responsible for all of the aforementioned effects.

In response to the soft perturbation, during the perturbed stance phase, the coffin joint flexion peak was increased and this may have been due to the tendency of the toe of the hoof to rotate into the surface with the reduced stiffness of the surface. The effect would have been to reduce the strain in

the ALDDF and to increase strain in the extensor branches of the suspensory ligament due to their attachment to the digital extensor tendon, and both of these effects were observed. Increased elbow extension in the perturbed stance phase and decreased shoulder extension at the stance-swing phase transition were again associated with increased strain in *lacertus fibrosus*. The stiffening of the proximal limb, along with increased activation and tension of the digital flexors, would lead to storage of strain energy distally and may have been responsible for the observed increases in flexion of the coffin, fetlock and carpal joints in mid-swing. During the second stance phase, only the coffin joint flexion peak was increased and this was associated with increased strain in the extensor branches, in the tendon of the SDF and in the ulnar and radial tendons of the DDF.

The changes observed in the shoulder and elbow excursions during the perturbed stance phase were most likely due to muscular action. Within the scope of the current model, it is not possible to determine if this was a reflex or a voluntary reaction. In humans, spinal reflexes can counter limb perturbations in as little as 20-40 ms, and these are followed by longer latency responses of 50-105 ms (Pruszynski *et al.*, 2008). Perturbation studies typically use perturbing displacements or forces that are well outside the variability normally inherent in a movement, and which exceed the thresholds of muscle afferent feedback. The acceleration pattern of the hoof is more deterministic on a harder surface, whereas it is more random on softer surfaces (Burn, 2006). In any case, the duration of the perturbed stance phase at trot would have been sufficient for the proximal musculature to achieve a compensatory reflex effect. The timing of the observed swing phase effects was, on the other hand, well-within the capacity of voluntary responses but as previously discussed, the changes in joint excursions during the swing phase could also be the consequences of the muscular stiffness changes during the perturbed stance phase.

### V.B. Response to perturbations at right lead canter

In response to the hard perturbation, during the perturbed stance phase, fetlock hyperextension was decreased which led to concomitant decreased strains in the suspensory ligaments, ALDDF and ALSDF and in the oblique and straight sesamoidean ligaments. During the swing phase, elbow and carpal flexion peaks were increased, and so the distal transfer of swing energy led to increases in the passive, inertial motion of the fetlock joint. Shoulder extension at the stance-swing phase transition was decreased resulting in an increase in strain in *lacertus fibrosus*, and the resultant storage of strain energy in that ligament meant the following flexion peak in swing was slightly increased. Finally, during the second stance phase, with the exception of a small increase in elbow extension at the end of stance, there were no effects on joint motions compared to baseline, and no effects on ligament and tendon strains.

In response to the soft perturbation, during the perturbed stance phase, the coffin flexion peak was increased and the fetlock extension peak was decreased. That resulted in decreased strain in the suspensory ligaments, ALDDF and ALSDF and in the oblique and straight sesamoidean ligaments. There were no compensations by the proximal joints. During the swing phase, the carpal and fetlock flexion peaks were increased. Finally, during the second stance phase, only the coffin flexion peak was increased, which led to increased strain in the extensor branches.

Overall, at canter, there were comparatively fewer compensations on the perturbed surfaces compared to trot, and it is possible that the rate of loading of the joints and suspensory structures early in the perturbed stance phase precludes even a reflex response being effective in that period. Or, it is also possible that the loading of the limbs at canter is dominated by the ground reaction forces and any muscular response from the proximal muscles would only be sufficient to maintain the baseline joint motions. The distal suspensory apparatus was less strained in both hard and soft perturbed stance phases but the DDF showed no effect. This could be an artefact of the forces not being predicted, and correcting the force prediction functions might reveal that tension generated in the DDF and SDF was responsible for holding up the fetlock and decreasing tension in the accessory ligaments. However, current theory suggests that the digital flexors become more compliant under conditions of hard ground (Wilson *et al.*, 2001) and so these results are equivocal. Nevertheless, it can be speculated that a surface change either way triggers a reflex at canter that causes stiffening of the suspensory muscles, which would in turn reduce the fetlock extension. The energy stored in the suspensory apparatus during the perturbed stance phase would be increased and released in the following swing phase resulting in increased amplitude of joint movements, and these were observed under both perturbation conditions.

## VI. Discussion

The consequences of the ground hardness perturbation conditions on the ligaments and tendons were studied through their strains computed from the joint angular positions. Because the forces were not studied, it was not known how a small variation in maximal strains would convert in force variations, and how the danger of injury would be affected. This is why even the smallest variations in maximal strains were reported.

In the majority of cases, where the ligaments were more strained, this occurred in the soft perturbation trials at trot. There were two possible factors contributing to this: the discrete effect of the surface, and the velocity of the horse. The preceding Tables reveal that the velocity was, on average,  $0.1\text{m}\cdot\text{s}^{-1}$  faster over the soft perturbing surface, compared to the baseline. Although

statistically significant, this is a very small difference, and most gait studies accept variation in velocity of 10% around a mean before rejecting data. Also, trial 'velocity' was included in the statistical analysis of the model output, and as such, the value for strain was assessed accounting for the effect of velocity. Further, although not significantly greater, the mean velocity during the hard perturbation trial was likewise  $0.05 \text{ m}\cdot\text{s}^{-1}$  faster than baseline, but in most cases the computed distal ligament strains were smaller. At canter, velocity was not significantly faster in either perturbation condition, compared to baseline, although it was marginally greater in both in real terms. At canter, the main effect of the perturbation was a reduction in computed distal ligament strains.

'Horse' was also included in the statistical model, assuming variable joint excursions and ligament and tendon strains by each horse but assuming a same reaction by each horse to the perturbations. However, the reaction to perturbation might depend on the relative fitness of the horse and its principal use and activity (jumping, pleasure riding...). The selection criteria only included belonging to the Thoroughbred breed and being clinically sound in the period before and during data collection. The interaction between factors of the statistical model was not considered due to the small subject pool, the number of trials per horse and the restricted velocity range per horse. The musculoskeletal model was scaled to match the dimensions of each horse's limb, and there may have been artefacts around the scaling of mass to segment lengths.

Limitations to interpretation of the model outputs will be discussed in the final chapter, but as already discussed, the forces predicted through the muscle model here were derived from the ground reaction force prediction, which was not realistic, and likely would have affected the computations for strains in the tendons of the digital flexors. The passive ligament strains, including the accessory ligaments of the digital flexors, depended only on joint angles, and so are more reliable.

Moreover, a question relating to both surface perturbations is whether the horse was conditioned after the first few trials to expect the perturbation, and was prepared for it in advance. It was observed that the first effect of the soft perturbation on joint motions was the decreased elbow flexion at trot and the increased coffin flexion at canter. The first alteration in response to the soft perturbation occurred approximately 0.08s after first ground contact for both trot and canter. Clayton (2001) reported the motor reaction time of horses to be between 110 and 370ms in response to a visual stimulus, with the shorter reaction times corresponding to the most successful horses in competition. However, the reaction time to a tactile stimulus is shorter than for a visual stimulus for humans and monkeys (Godlove *et al.*, 2014; Ng and Chan, 2012). Supposing the same finding would be observed for horses, it is possible the delay observed between the first impact on the soft perturbation and the beginning of the limb response corresponds to a reaction time. This hypothesis is also supported by

the observation that few changes in joint motions were observed during the second stance phase between the baseline and the soft perturbation. Indeed, more differences would be expected to be observed if it was a reflex time. However, it is possible the horses remembered the area of the runway where the surface change occurred and were more attentive, reducing their reaction time to the hardness change.

There were two questions to be answered through this experiment:

(1) how does the horse respond to a ground surface perturbation? And (2), can the horse respond to a ground surface perturbation in the perturbed stance phase, or does the response occur in the following stance phase?

(1) The data reinforce the notion of the presence of a proximal limb spring, and a distal limb spring. Compensations by the shoulder and elbow affected lacertus fibrosus strain in late stance, but were mostly manifest in the intervening swing phase. The response by the distal limb was focused on the coffin joint, which was more flexed in both stance phases after the soft perturbation, but unchanged in either stance phase in response to the hard perturbation. Otherwise, the main effect of both the soft and hard perturbation at canter, and the hard perturbation at trot was a reduction in distal ligament strains. Interestingly, the majority of the increased strains in the distal ligaments occurred in the perturbed stance phase in response to the soft perturbation.

(2) The question was whether the perturbation would cause the horse to prepare for a similar ground surface stiffness in the second stance phase, but then be unprepared for the return of the surface to the regular surface. If, following the hard perturbation, the limb was more compliant in the second stance phase, then the shoulder and elbow should be more flexed. At trot, the shoulder was more flexed and most of the distal ligaments were less strained, but at canter there was no effect. If, following the soft perturbation, the limb was stiffer in the second stance phase, then the joints should be relatively less flexed during mid-stance, but this was not the case. However, the digital flexors were observed to be more strained at both trot and canter, suggesting a response by this muscle group to stiffen the limb, and the coffin joint was more flexed perhaps as a consequence of this tension.

## VII. References

- Bolwell, C. F., Rogers, C. W., Gee, E. K. and McIlwraith, C. W. (2017b) 'Epidemiology of musculoskeletal injury during racing on New Zealand racetracks 2005-2011', *Animals*, 7(8), pp. 62.
- Burn, J. F. (2006) 'Time domain characteristics of hoof-ground interaction at the onset of stance phase', *Equine Veterinary Journal*, 38(7), pp. 657-663.
- Clayton, H. M. (2001) 'Chapter 8, Performance in Equestrian sports', In Back, W. and Clayton, H.M. (eds.) *Equine Locomotion*. London: W. B. Saunders.
- Godlove, J. M., Whaite, E. O. and Batista, A. P. (2014) 'Comparing temporal aspects of visual, tactile, and microstimulation feedback for motor control', *Journal of Neural Engineering*, 11(4).
- Hill, W. T. (2003) 'Survey of injuries in Thoroughbreds at the New York Racing Association tracks', *Clinical Techniques in Equine Practice*, 2(4), pp. 323-328.
- McGuigan, M. P. and Wilson, A. M. (2003) 'The effect of gait and digital flexor muscle activation on limb compliance in the forelimb of the horses *Equus caballus*', *The Journal of Experimental Biology*, 206(Pt8), pp. 1325-1336.
- Ng, A. W. Y. and Chan, A. H. S. 'Finger response times to visual, auditory and tactile modality stimuli'. *Proceedings of the International MultiConference of Engineers and Computer Scientists*, Hong Kong.
- Parkin, T. (2008) 'Epidemiology of racetrack injuries in racehorses', *Veterinary Clinics of North America: Equine Practice*, 24(1), pp. 1-19.
- Perkins, N. R., Reid, S. W. and Morris, R. S. (2004b) 'Profiling the New Zealand Thoroughbred racing industry. 2. Conditions interfering with training and racing', *New Zealand Veterinary Journal*, 53(1), pp. 69-76.
- Peterson, M. L., McIlwraith, C. W. and Reiser, R. F. (2008) 'Development of a system for the in-situ characterisation of Thoroughbred horse racing track surfaces', *Biosystem Engineering*, 101(2), pp. 260-269.
- Pruszynski, J. A., Kurtzer, I. and Scott, S. H. (2008) 'Rapid motor responses are appropriately tuned to the metrics of a visuospatial task', *Journal of Neurophysiology*, 100(1), pp. 224-238.
- Robin, D., Chateau, H., Pacquet, L., Falala, S., Valette, J.-P., Pourcelot, P., Ravary, B., Denoix, J.-M. and Crevier-Denoix, N. (2009) 'Use of a 3D dynamometric horseshoe to assess the effects of an all-weather waxed track and a crushed sand track at high speed trot: Preliminary study', *Equine Veterinary Journal*, 41(3), pp. 253-256.
- Rosanowski, S. M., Chang, Y. M., Stirk, A. J. and Verheyen, K. L. P. (2016) 'Descriptive epidemiology of veterinary events in flat racing Thoroughbreds in Great Britain (2000 to 2013)', *Equine Veterinary Journal*, 49(3), pp. 275-281.
- Setterbo, J. J., Yamaguchi, A., Hubbard, M., Upadhyaya, S. K. and Stover, S. M. (2011) 'Effects of equine racetrack surface type, depth, boundary area, and harrowing on dynamic surface properties measured using a track-testing device in a laboratory setting', *Sports Engineering*, 14(2-4), pp. 119-137.
- Wilson, A. M., McGuigan, M. P., Su, A. and Borgert, A. J. v. d. (2001) 'Horses damp the spring in their step', *Nature* 414, pp. 895-899.

# Chapter 7

## Conclusions

### I. Introduction

The purpose of this thesis was to test how unexpected variations in surface hardness caused by inconsistency in track surface properties affect the motion and loading of the soft tissue structures of the limb, which could lead to an increased risk of musculoskeletal injury.

In Part 1, a musculoskeletal model of the whole equine forelimb was developed from data published in the literature and derived from anatomical measurements. This musculoskeletal model was then used in Part 2 to determine the effects of the perturbations by the ground surface on the limb response and to assess whether the response occurs acutely in the perturbed stance phase or in the next stance phase.

### II. Effect of the perturbation

#### II.A. Statistical model

The statistical model used in this thesis included the horse as a random variable, and the perturbation condition and horse velocity as independent variables. However, no interactions between any of the variables were considered. These choices for the statistical model implied:

- All the horses had the same response to the perturbation conditions
- The gait of all horses was affected similarly by velocity
- The effect of the perturbation and the effect of the velocity were independent

These assumptions could lead to errors in the interpretation of the effect of the perturbations, but it also means that the effects observed in this study were common to all the horses, whatever their daily activities and experiences.

Other independent variables were also tested. All the kinematic data were collected from the right forelimb of the horse from the approach to the perturbation area through to the end of the next stance phase after the perturbation, with the condition that the hoof of this limb landed in the perturbation area. In some trials, the left forelimb hit near the boundary of the perturbation pit before the right (studied) forelimb and for others the right forelimb hit the perturbation pit first. The first limb hitting the perturbation area was initially tested as an independent factor in the statistical models

but that resulted in poorer models, in that the associated AIC (Akaike information criterion) was larger. That suggests there were no differences between the data collected with the left forelimb hitting the perturbation area first and the data with the right forelimb hitting the perturbation first. It could mean the response of the forelimb did not depend on what the other forelimb experienced, at least not in the same stride. Further analysis of the data would be required to determine if the experience of the second forelimb to hit the ground (e.g. the right forelimb hitting the perturbation area) influences the behaviour of the first forelimb to hit the ground during the following stance phase (e.g. the left forelimb hitting the ground for the second stride).

The trial number was also tested in the statistical models but then removed because its inclusion resulted in poorer models (larger AIC). However, the trial number was considered as a continuous variable when it could have been better to use a discrete variable representing a stage when the horse was not expecting the perturbation and a stage when the horse knew where to expect the perturbation. In other words, after the horse is perturbed the first time, does the horse then remember that perturbation on its next approach, and does this affect its response? Raking the ground surface between trials to hide the perturbation area in the runway was done to minimise this expectation, but the horse may well have been expecting a disruption to its passage. Creating such a variable would require further study to determine the number of trials required for the horse to remember the perturbation on its subsequent approach. Moreover, this number would be expected to depend on other parameters, such as the severity of the perturbation and the velocity of the horse. The perturbations employed were minimal and well within the capacity of the horse to accommodate them.

### II.B. Responses to perturbations

The discrete effects of the perturbations have been discussed in the previous chapter.

Little is known about the equine limb's ability to adjust rapidly to acute changes in a surface. We do know that the limb has some potential to behave like a "tuneable spring" in that the muscles of the limb seem to be capable of adjusting the overall limb compliance in response to the stiffness of the surface. The proximal components of the limb spring are predominantly muscular, with some collagenous (passive) contribution and this proximal element is primarily responsible for control of the angular displacement of the elbow and shoulder joints (McGuigan and Wilson, 2003) but changes in compliance of the proximal spring are likely to affect the compensations observed in the distal limb. The distal limb spring is almost entirely collagenous, and although the muscles of the digital flexors can shorten minimally, due to their pennation, their main effect is to preload their tendons, thus stiffening the distal limb for weight bearing. The equine limb changes its length during weight bearing

principally by accommodating hyperextension of the fetlock joint through strain of the flexor tendons, although the proximal limb muscles also have some scope for tuning of the overall limb stiffness (McGuigan and Wilson, 2003). Of the distal limb tendons, the suspensory ligament and superficial digital flexor behave almost entirely passively whereas the deep digital flexor behaves elastically as well as actively shortening its muscular parts for a small amount of concentric digital flexion (Zarucco *et al.*, 2004). Limb stiffening in late swing (in preparation for stance) and in early stance is also accomplished through co-contraction of the extensors with the flexors, which reduces the net moment-generating capacity of all the muscles (Harrison *et al.*, 2012). The planar spring-mass model (eg. Geyer *et al.* (2005)) is reasonably good at predicting centre of mass excursions if limb stiffness and limb angle at contact are known, but random perturbations must interrupt this dynamic relationship. Mathematical modelling of the limb-spring system can simply ignore foot-ground perturbations, and make the spring-mass model look fairly self-stable. However, a more complex model must address locomotion on variable or unstable ground where limb motion during swing and immediately following ground contact must respond to expected and unexpected surface perturbations.

It is useful to think of hoof contact on the ground taking place through three discrete phases; the pre-impact phase (just before contact), the primary impact (where the hoof collides with the ground) and the secondary impact (where the rest of the leg collides with the hoof) (Thomason and Peterson, 2008) and many investigators of riding surfaces fail to attach much importance to the first phase. In the pre-impact phase, only small inertial forces are acting on the hoof, but the limb as a whole is prepared for the landing by widespread co-contraction of muscles (Harrison *et al.*, 2012). The flexors and extensors of the forelimb joints activate in mid- to late swing, and then typically deactivate by mid-stance as the collagenous tissues of the limb support the joints during the “inverted pendulum” motion of the limb over the planted hoof. At canter, deep digital flexor and common digital extensor muscles peak in their activity at the swing-stance transition, while the superficial digital flexor peaks later in mid-stance. The primary impact phase is marked by a small acceleration peak as the lateral heel lands, followed instantly by a large vertical spike as the rest of the hoof collides with the track. The vertical deceleration is faster than the horizontal, and is accompanied by a vibration up the limb (Thomason and Peterson, 2008) which is attenuated by the digital flexors (Wilson *et al.*, 2001). Hardness of the track surface has a significant effect on this phase of the impact, and variability of the large impact spike is high, reflecting some kinematic variation in hoof placement from stride to stride (Gustas *et al.*, 2001; Gustas *et al.*, 2006a). Although the accelerations are large in this first impact phase, the force on the hoof is low (Thomason and Peterson, 2008). In the second impact phase, there is a rapid rise in horizontal braking force as the hoof stops sliding and a rise in the vertical force as the hoof accepts the weight of the limb and superincumbent body. The approximate time course of this phase is 30-50

ms (Gustas *et al.*, 2006a) which is the minimum period of muscle latency, suggesting that the impact characteristics cannot be modulated within a stance phase by voluntary muscle activity (Johnston and Back, 2006). In trotting horses with induced superficial digital flexor tendon lesions, the peak braking forces and braking impulses were reduced in the period following loading, but the braking forces in the first 15% of stance were similar to pre-lameness values (Clayton *et al.*, 2000) suggesting little voluntary control over the early phase of hoof impact.

Notwithstanding the importance of the early stance phase in the loading of the limb, real-time studies of the stability of the equine locomotor system in the period around limb impact with the ground are few. In fowl, the proximal limb musculature is controlled in a feed-forward manner, while the distal limb joints get higher-gain proprioceptive feedback and are therefore highly load-sensitive. During unexpected limb perturbation, the limb retraction by the hip muscles is unaffected despite altered limb loading, while the distal joints switch between spring-like and damping functions (Daley *et al.*, 2007). The multiarticular distal muscles operate, through their long tendons, to accommodate the fast stabilising mechanisms that are controlled by spring-mass dynamics (Biewener and Daley, 2007). Human runners prepare for a perturbation with an increase in limb stiffness and reduction in limb angle in accordance with the predictions of a stable spring-mass system (Grimmer *et al.*, 2008).

However, the latency and time course for this adjustment in equine locomotion is unknown. In humans, spinal reflexes can counter limb perturbations in as little as 20-40 ms, and these are followed by longer latency responses of 50-105 ms (Pruszynski *et al.*, 2008). Given that the stability of the impact phase of the equine hoof on a surface is going to be reliant on the variability of the surface, it would be useful to know how the horse adapts its limb stiffness in response to a perturbation caused by an irregularity in the surface. The horse's distal limb is governed by tendons on its flexor and extensor surfaces, and these are the only active mechanisms through which the horse can respond when the hoof is distracted in any direction. These then impart larger joint reaction forces during stance, and while they may stabilise the distal limb segments, they may also cause large inter-segmental forces that may be deleterious. The stiffening of the limb may also reduce the soft tissues' ability to dampen the impact vibrations. Electromyographic studies indicate clearly that the deep digital flexors are active through the end of swing to late stance and their antagonist, extensor digitorum, is co-active at the end of swing and into the early stance phase (Cheung *et al.*, 1998; Jansen *et al.*, 1992; Tokuriki, 1974; Tokuriki *et al.*, 1999).

The limb response to the perturbation condition was similar between trot and canter for the soft perturbation but different between gaits for the hard perturbation. That could have been due to the severity of the change in stiffness of the surface. The hardness of the perturbation was not measured

but the hardness difference between the baseline and the soft perturbation felt subjectively more severe than the hardness difference between the baseline and the hard perturbation. That could mean the severity of the hardness change between the hard perturbation and the baseline was increased substantially, from trot to canter, resulting to a change in the limb response whereas the hardness change between the soft perturbation and the baseline was severe enough to trigger the same limb response at trot and at canter. However, to test the relationship between severity and responses at trot and canter would require collection of more gait data with different levels of severity of soft and hard perturbation.

### II.C. Comparison to literature

To date, although many studies have evaluated gait on different surfaces, no studies have focused on the limb response to a sudden hardness perturbation. Few have studied the relationships between ground reaction forces and kinematic data. Crevier-Denoix *et al.* (2010) reported that fetlock hyperextension was increased when the ground reaction force was greater. However, in response to the hard perturbation, fetlock hyperextension was decreased during the perturbed stance phase at canter and during the second stance phase at trot; and in response to the soft perturbation, the fetlock hyperextension was decreased during the perturbed stance phase at canter. The limb response observed as a result of the soft perturbation is in agreement with the observation reported by Crevier-Denoix *et al.* (2010), but not the response observed to the hard perturbation. The differences between the observations may mean the horse does not adapt its limb to the hardness of a ground surface in the same way as it adapts its limb to respond to a sudden hardness perturbation.

Most of the soft tissues affected by the perturbation conditions had their maximal strains decreased. The only tissues that had their maximal strain increased by the perturbation condition were the extensor branches of the suspensory ligament over the soft perturbation during the perturbed stance for both trot and canter, and during the second stance phase at canter; the ulnar and radial heads of the deep digital flexor over the soft perturbation at trot during both stance phases; and the lacertus fibrosus at the end of the perturbed stance phase/ beginning of the swing phase over both the soft and hard perturbation at trot. These observations do not agree with earlier findings that the most frequently affected soft tissues by musculoskeletal injury are the superficial digital flexor tendon and the suspensory ligament and less frequently the deep digital flexor tendon, its check ligament and the sesamoidean ligaments (Hill, 2003; Rosanowski *et al.*, 2016). Further studies are required to determine if the differences observed here are due to modelling choices, such as including the proximal sesamoid bones in the segment of another bone, or representing a muscle that has more than one origin and one insertion sites as several independent muscles; or because the changes in these soft tissues

occurred in a later stance phase. Indeed, only the stance phase following the perturbed stance phase of the same forelimb (the right) was studied but some changes could also occur in a later stance phase by delay of reaction or could occur in the stance phase of the other forelimb (the left) following the perturbed stance phase of the right forelimb.

### III. Musculoskeletal model

#### III.A. Segments

Some smaller bones were represented with a contiguous segment (such as the proximal sesamoids at the fetlock with the metacarpus) because their individual movements cannot be measured separately using skin-mounted markers. However, to fully understand the role of these joints and their associated soft tissues in force transmission, it would be important to separate the movement of these smaller bones from the movement of the segment in which they are modelled. This is particularly the case for the proximal sesamoid bones at the fetlock and the strains computed in all the soft tissues having an origin or insertion on them (particularly the suspensory ligament and its extensor branches, and the more distal sesamoidean ligaments). It would also be interesting to determine the consequences on the soft tissues of separating the carpal joint into its separate functional units (radiocarpal joint and midcarpal joint). The strains computed in the suspensory ligaments by the model were overestimated, compared to data reported in the literature. It can also be supposed that the strains of the ligaments and tendons crossing the carpal joints and the interphalangeal joints would be affected. However, it would be complicated to predict if the model was overestimating or underestimating the strains in these tissues because they generally cross several joints, and their strains are then affected by the combined effect of all the joint positions.

#### III.B. Ligament and muscle-tendon units

AnyBody does not permit a muscle or ligament to have more than one origin and one insertion. The muscles and ligaments that did have more than one origin and one insertion were therefore modelled as several muscles or ligaments. The main problem with this requirement is the relationship between the separate heads of the muscles because although the different parts of a muscle or ligament may have a combined action, they are modelled as independent structures. For example, the separate muscle modelling the humeral head of the deep digital flexor may be stretched due to elbow motion while the muscles modelling the radial and ulnar heads of the deep digital flexor are not. Because the separate heads of a muscle are independent, the role of a multi-head muscle may be different from its actual role. This problem could be solved by adding an optimization function in AnyBody model

taking into account that the different heads of a same muscle have to be activated and deactivated at the same moments.

To avoid the tendons going through intermediate bones from their origin to insertion sites, such as the extensor carpi radialis through the carpal bones during carpal flexion, via points were added on the bony surface to force their line-of-action to get around the joints. However, the accuracy of the paths could be improved by determining the position of motionless points on them or by determining the surface geometry around which the paths are going. The line-of-action of the ligaments and muscles are important for the force predictions (Carbone *et al.*, 2015). Indeed, the line-of-action determines the moment that would be created by a muscle; by changing it, the force the muscles have to provide would be modified to compensate the change of line-of-action, which would also affect the load sharing between the muscles.

The database of the properties of all the muscles published is limited. There is a huge gap in the literature on the static tendon and ligament strains when the horse is in a standing position. Further, to accurately model the muscles in the 2- and 3-element Hill model, the maximal contraction speed, maximal isometric force and the relative amount of fast fibres are required. These have not been reported in the literature, and so only estimates are available. This will be the focus of a subsequent study.

### III.C. Joints

In this preliminary test of the model, joint motion was limited to flexion and extension in the anatomical sagittal plane of the individual joints. The number of cameras (six), and the length of the calibrated volume within which we were collecting data precluded collecting data from both sides of the runway, which would have been necessary for accurate detection of motion in the horizontal and frontal planes. The positions of the segments were not constrained in the global reference frame, but were only constrained through their joints, which means that the abduction/adduction and axial rotation of the whole limb was free. That implies that the whole modelled limb might not have had exactly the same orientation as the horse limb on which data were collected. This may have led the model to over- or under-estimate the joint angles. Moreover, joint angles may be affected by skin movement that was not considered in this study. Back (2001) illustrated the difference between the joint motions before and after correcting the skin movement and showed that the effect is the largest around the shoulder due to subcutaneous motion of the scapula, changing even the shape of the curve, and is more and more reduced when moving distally. Because of this effect, it was not possible to compare the shoulder motion against data reported in the literature, and the presence of the saddle would have made correcting scapular skin motion artefact tenuous. However, the elbow motion was

compared and the elbow flexion seemed to be over-estimated only at right lead canter but not at trot or at left lead canter and the elbow extension seemed to be over-estimated only at trot. Skin movement may depend, therefore, on the gait and thus its effect on the joint motions is specific to a gait. Nonetheless, if the angles computed are not the “exact” values, comparison of the differences between the perturbations and the baseline are still viable.

The model could be tested to study the abduction, adduction and axial rotations of the limb but it would need more accurate kinematic data in the frontal and horizontal planes. However, collecting data in all three planes at once would require more than the six cameras used in this study, as we would have needed cameras recording from the opposite side of the runway for a full 3D picture.

### III.D. Scaling

Scaling is absolutely necessary to adapt the model template to a particular horse. In this model, the segments are scaled linearly, with the correct length along the axial dimension of the long bone. However, the factors used in the transverse and cranio-caudal directions were estimated. It could be interesting to develop another scaling function based on bony landmarks. Scaling errors would introduce errors in different elements of the model. Indeed, during the scaling loop, parameters such as tendon and ligament slack lengths might be affected. During the dynamic loop, scaling errors might affect the inertial properties of the segments. The inertial properties define how the segments resist changes in angular motion and are integral to computing the moment of each segment around its proximal joints. An error in the inertial properties of a segment would then affect the moments around the joints and thus would affect the forces developed in the muscles, tendons and ligaments.

Moreover, the model was based on the bony CT images from one horse. Although all horses used in this study were Thoroughbreds whose mass varied from about 450 to 600 kg, scaling the same model over such a large range of mass might introduce errors, and it could be supposed that the distribution of mass across the different segments is not the same between horses. This problem could be fixed by using a scaling function based instead on bony landmarks.

### III.E. Model validation

Validating a model is important as it proves the robustness and power of the model to represent the functions for which it was developed. Nigg and Herzog (2006) proposed three different methods: direct measurements, indirect measurements and trend measurements. The direct measurements consist of comparing the data collected in a limited set of experiments to the data predicted by the model. For example, it would be comparing the joint angles directly measured from the horse to the joint angles modelled based on the marker position collected. The indirect measurement validation is

based on the same idea but compares different data; for example, the force predicted within a muscle to EMG data collected for this muscle, in which case the amplitude of the two signals may not be directly comparable, but the shape of the activation curve might be. Finally, the trend measurement method compares the relationships between facts and results, but is not looking for an agreement of the variables. For example, it would be comparing the measured alterations in joint motions due to ground hardness perturbation to the modelled alterations due to ground hardness perturbation without comparing the joint motions themselves between the measurements and model. This last method is the one that should be used for the model developed, because its use is to understand the relationships between the ground hardness change and the soft tissue behaviours. To evaluate the model, it would require collection of ground reaction force data and electromyographic data for all conditions (baseline, hard perturbation and soft perturbation).

In this study, the preliminary model was validated in Chapter 4 by comparing the modelled data from the baseline sand surface to data reported in the literature. The patterns of joint motions observed were similar within and between horses, which indicates the model is reliable. The profiles of joint movement were similar to other studies reported in the literature, although those studies were run on different surfaces (hard floor, treadmill), without a rider, and at different gait velocities. This notwithstanding, the gross patterns of movement per joint were similar to the data calculated by this model. Given that the kinematic output from the model behaved as expected on the baseline surface, we assume that the data collected over the perturbed surfaces was likewise handled appropriately and accurately depicted the joint motions and concomitant tendon and ligament strains. As this was the first study of its kind, investigating the discrete effects of the limb to surface hardness perturbation, there are no relevant comparisons to be made to other studies in the literature. It is unknown whether the introduction of a surface hardness perturbation could create more skin movement, which would in turn affect the modelled joint angles.

## IV. Conclusion

### IV.A. Hardness perturbation in racetrack

Based on the joint motions, the response delay to the soft perturbation was estimated to be about 0.08s. However, the stance duration was reported to be around 77ms for the forelimb for horses galloping at  $17\text{m}\cdot\text{s}^{-1}$  (Witte *et al.*, 2006). Supposing the response delay observed in this study can be transposed to racing horses, it means horses would be able to react to a hardness change only in the stance phase following the perturbed one. That means two stance phases may cause injuries in the horse limbs, the perturbed one and the one during which the horse responds to the perturbation, especially if the surface has then changed back, or to something else.

However, determining the limb response mechanisms (or its absence) at gallop would require the collection of data at this gait. To clarify one point in the injury mechanism, it would be necessary to determine if a racing horse responds to localized hardness change or if such a localized hardness change happens too fast for the horse to consider it. Indeed, it would allow determination if the horse gets injured because it is not adapting its limb response to the hardness perturbation or if it gets injured because it reacts to the perturbation with a delay and changes its limb compliance when back on the regular surface.

It would also be interesting to determine if a hardness perturbation in a racetrack, that could put a horse at gallop at risk, has a significant effect on gait at trot and/or at canter. If so, it would mean that by studying the limb behaviour of a horse trotting or cantering along the racetrack, it would be possible to test the consistency of the racetrack without putting a horse at risk.

### IV.B. Improving the musculoskeletal model

The first step to improve the model would be to correct the ground reaction force prediction. It would solve several difficulties in studying the limb response to the perturbation. Correcting the ground reaction force prediction would permit to compute the forces within the different muscles and so to study the muscular response of each individual structure. In this way, it would be possible to observe the behaviour of the muscles, and determine their roles by identifying those that respond rapidly to protect the limb over a sudden hardness change and those that respond slowly to adapt the limb to subsequent strides. In addition, it would also permit to compute the forces within the ligaments, which would help to better understand the effect of a sudden change on the passive structures and determine whether they are biologically significant. Finally, it would also allow us to study and determine the role of the tendons of the deep and superficial digital flexors in adapting the equine forelimb response to a sudden hardness change. All these more detailed data on the soft structures would permit a better understanding of the response mechanisms of the equine forelimb, and might give insight about the coordination between muscles and their individual role.

The second step to improve the model would be to complete the soft tissue properties. Collecting data such as the static tendon and ligament strains when the limb is in the standing position would fill a huge gap in the literature.

For future studies, it would be interesting to use bony landmarks to scale the model and the inertial properties of the segments and to use the standardised bony landmarks to position the other segmental markers (used to collect gait data) in the model. That might create a model that would be more accurate and more representative to the live horse from which the gait data were collected.

## Chapter 7 Conclusions

More cameras should be used to collect the data from both lateral and medial sides but also with some cameras more forward and other more backward and at different heights to have more accurate data in all the three anatomical planes of the joints. Accurate data from all planes of motion would allow the investigator to free the constraints on abduction/adduction and axial rotations of the joints and to study them, which would in turn allow the observation of the consequences of the introduction of hardness perturbation on the collateral ligaments as well as on all the muscles and tendons running on the lateral or medial sides of some joints.

This preliminary model of the equine forelimb allowed us to study the changes in joint excursions and tendon and ligament strains. Although improvements are necessary for that preliminary model, it successfully showed its ability to differentiate the horse forelimb response to a sudden hardness change.

## V. References

- Back, W. (2001) 'Chapter 5, Intra-limb coordination: the forelimb and the hind limb', In Back, W. and Clayton, H.M. (eds.) *Equine Locomotion*. London: W. B. Saunders.
- Biewener, A. A. and Daley, M. A. (2007) 'Unsteady locomotion: integrating muscle function with whole body dynamics and neuromuscular control', *Journal of Experimental Biology*, 210(Pt17), pp. 2949-2960.
- Carbone, V., Fluit, R., Pellikaan, P., Krogt, M. M. v. d., Janssen, D., Damsgaard, M., Vigneron, L., Feilkas, T., Koopman, H. F. J. M. and Verdonschot, N. (2015) 'TLEM 2.0 – A comprehensive musculoskeletal geometry dataset for subject-specific modeling of lower extremity', *Journal of Biomechanics*, 48(5), pp. 734-741.
- Cheung, T. K., Warren, L. K., Lawrence, L. M. and Thompson, K. N. (1998) 'Electromyographic activity of the long digital extensor muscle in the exercising Thoroughbred horse', *Equine Veterinary Journal*, 30(3), pp. 251-255.
- Clayton, H. M., Schamhardt, H. C., Willemen, M. A., Lanovaz, J. L. and Colborne, G. R. (2000) 'Kinematics and ground reaction forces in horses with superficial digital flexor tendinitis', *American Journal of Veterinary Research*, 61(2), pp. 191-196.
- Crevier-Denoix, N., Robin, D., Pourcelot, P., Falala, S., Holden, L., Estoup, P., Desquilbet, L., Denoix, J.-M. and Chateau, H. (2010) 'Ground reaction force and kinematic analysis of limb loading on two different beach sand tracks in harness trotters', *Equine Veterinary Journal*, 42(S38), pp. 544-551.
- Daley, M. A., Felix, G. and Biewener, A. A. (2007) 'Running stability is enhanced by a proximo-distal gradient in joint neuromechanical control', *Journal of Experimental Biology*, 210(3), pp. 383-394.
- Geyer, H., Seyfarth, A. and Blickhan, R. (2005) 'Spring-mass running: simple approximate solution and application to gait stability', *Journal of Theoretical Biology*, 232(3), pp. 315-328.
- Grimmer, S., Ernst, M., Günther, M. and Blickhan, R. (2008) 'Running on uneven ground: leg adjustment to vertical steps and self-stability', *Journal of Experimental Biology*, 211(18), pp. 2989-3000.
- Gustas, P., Johnston, C., Roepstorff, L. and Drevemo, S. (2001) 'In vivo transmission of impact shock waves in the distal forelimb of the horse', *Equine Veterinary Journal*, 33(S33), pp. 11-15.
- Gustas, P., Johnston, C., Hedenstrom, U., Roepstorff, L. and Drevemo, S. (2006a) 'A field study on hoof deceleration at impact in Standardbred trotters at various speeds', *Equine and Comparative Exercise Physiology*, 3(3), pp. 161-168.
- Harrison, S. M., Whitton, R. C., King, M., Haussler, K. K., Kawcak, C. E., Stover, S. M. and Pandy, M. G. (2012) 'Forelimb muscle activity during equine locomotion', *The journal of Experimental Biology*, 215(17), pp. 2980-2991.
- Hill, W. T. (2003) 'Survey of injuries in Thoroughbreds at the New York Racing Association tracks', *Clinical Techniques in Equine Practice*, 2(4), pp. 323-328.
- Jansen, M. O., van Raaij, J. A., Van den Bogert, A. J., Schamhardt, H. C. and Hartman, W. (1992) 'Quantitative analysis of computer-averaged electromyographic profiles of intrinsic limb muscles in ponies at the walk', *American Journal of Veterinary Research*, 53(12), pp. 2343-2349.
- Johnston, C. and Back, W. (2006) 'Hoof ground interaction: when biomechanical stimuli challenge the tissues of the distal limb', *Equine Veterinary Journal*, 38(7), pp. 634-641.
- McGuigan, M. P. and Wilson, A. M. (2003) 'The effect of gait and digital flexor muscle activation on limb compliance in the forelimb of the horses *Equus caballus*', *The journal of Experimental Biology*, 206(Pt8), pp. 1325-1336.
- Nigg, B. M. and Herzog, W. (2006) 'Chapter 4, Modelling', In Nigg, B.M. and Herzog, W. (eds.) *Biomechanics of the musculo-skeletal system, Third Edition*: Wiley-Blackwell.

## Chapter 7 Conclusions

- Pruszynski, J. A., Kurtzer, I. and Scott, S. H. (2008) 'Rapid motor responses are appropriately tuned to the metrics of a visuospatial task', *Journal of Neurophysiology*, 100(1), pp. 224-238.
- Rosanowski, S. M., Chang, Y. M., Stirk, A. J. and Verheyen, K. L. P. (2016) 'Descriptive epidemiology of veterinary events in flat racing Thoroughbreds in Great Britain (2000 to 2013)', *Equine Veterinary Journal*, 49(3), pp. 275-281.
- Thomason, J. J. and Peterson, M. L. (2008) 'Biomechanical and mechanical investigations of the hoof-track interface in racing horses', *Veterinary Clinics of North America: Equine Practice*, 24(1), pp. 53-77.
- Tokuriki, M. (1974) 'Electromyographic and joint-mechanical studies in quadrupedal locomotion. 3. Gallop', *Japanese Journal of Veterinary Science*, 36(2), pp. 121-132.
- Tokuriki, M., Ohtsuki, R., Kai, M., Hiraga, A., Oki, H., Miyahara, Y. and Aoki, O. (1999) 'EMG activity of the muscle of the neck and forelimb during different forms of locomotion', *Equine Veterinary Journal*, 31(S30), pp. 231-234.
- Wilson, A. M., McGuigan, M. P., Su, A. and Borgert, A. J. v. d. (2001) 'Horses damp the spring in their step', *Nature* 414, pp. 895-899.
- Witte, T. H., Hirst, C. V. and Wilson, A. M. (2006) 'Effect of speed on stride parameters in racehorses at gallop in field conditions', *The Journal of Experimental Biology*, 209(21), pp. 4389-4397.
- Zarucco, L., Taylor, K. T. and Stover, S. M. (2004) 'Determination of muscle architecture and fiber characteristics of the superficial and deep digital flexor muscles in the forelimbs of adult horses', *American Journal of Veterinary Research*, 65(6), pp. 819-828.

# Appendix: Ligament, muscle and tendon properties

## I. Ligament properties

Table 36 Ligament properties

Tissue		Number of specimens	Elastic modulus (MPa)	Maximal strain	Surface (mm <sup>2</sup> )	Force at maximal strain (N)
Sesamoidean ligaments	Straight	6 (4 left, 2 right)	69 (22)	0.21 (0.02)	53 (12)	732 (102)
	Medial Oblique	6 (4 left, 2 right)	49 (26)	0.42 (0.18)	34 (9)	643 (210)
	Lateral Oblique	6 (4 left, 2 right)	39 (17)	0.33 (0.12)	37 (16)	418 (139)
	Medial collateral	1 (1 left, 0 right)	24	0.42	18	181
	Lateral collateral	1 (1 left, 0 right)	35	0.68	10	235
Elbow collateral ligaments	Lateral	10 (5 left, 5 right)	4 (2)	0.46 (0.10)	302 (70)	555 (204)
	Caudal Medial	10 (5 left, 5 right)	19 (16)	0.52 (0.20)	89 (44)	607 (162)
	Cranial Medial	4 (2 left, 2 right)	141 (79)	0.23 (0.10)	34 (10)	916 (370)
Carpal collateral ligaments	Lateral	11 (6 left, 5 right)	52 (22)	0.26 (0.07)	52 (12)	656 (230)
	Medial	10 (5 left, 5 right)	35 (23)	0.27 (0.09)	84 (31)	736 (513)
Fetlock collateral ligaments	Lateral	10 (5 left, 5 right)	48 (22)	0.43 (0.13)	40 (12)	743 (229)
	Medial	11 (6 left, 5 right)	78 (61)	0.43 (0.12)	38 (17)	1050 (526)
Pastern collateral ligaments	Lateral	8 (4 left, 4 right)	38 (12)	0.34 (0.10)	50 (33)	563 (193)
	Medial	8 (4 left, 4 right)	30 (12)	0.42 (0.20)	59 (31)	629 (115)

## II. Muscle-tendon data

## II.A. Muscle-tendon properties

Table 37 Muscle and tendon properties

Muscle-Tendon	Tendon			Muscle			
	Length (cm)	Thickness (cm)	Width (cm)	Length (cm)	Pennation angle (°)	Bundle Length (cm)	Sarcomere length (µm)
Lateral digital extensor	51	0.1	0.6	27.5	17	3.7	2.32
Common digital extensor	60	0.3	1.1	27.5 (radial head) 30.5 (humeral head)	15 (lower part of the muscle) 10 (upper part of the muscle)	11 (lower part) 8.5 (upper part)	3.08 (radial head) 3.17 (humeral head)
Extensor carpi obliquus	17	0.1	0.8	26	23	1.9	2.56
Extensor carpi radialis	21.5	0.4	2.4	31.5	30	7.8	1.75
Ulnaris lateralis	20	0.8	3 (lower part) 0.8 (upper part)	33	30	1.5	1.69 (cranial) 2.73 (caudal upper) 2.07 (caudal lower)
Flexor carpi radialis	15	0.3	0.8	29	7	7.5	1.97
Flexor carpi ulnaris	2.5	0.7	2.8	38	32	2	1.95 (Humeral head) 2.30 (Ulnar head)
Deep digital flexor	45	1	3 (proximal part) 1.8 (middle part) 3.2 (distal part)	40 (humeral head) 25 (ulnar head) 17 (radial head)	23	7.2	2
Superficial digital flexor	42	1	2.3 (proximal part) 1.8 (middle part) 3.4 (distal part)	39	40	0.8	1.88

## II.B. Muscle-tendon origin and insertion sites

### II.B.1. Lateral digital extensor (LDE)

The LDE has three origin and one insertion sites. The proximal origin is on the lateral side of the humeral epicondyle, the two others are on the radius. The proximal radial origin is on the head of the radius and the second radial origin is a 19-cm band running along the junctions between the radius and the ulna (Figure 37). The insertion site is on the proximal part of the dorsal surface of the proximal phalanx.

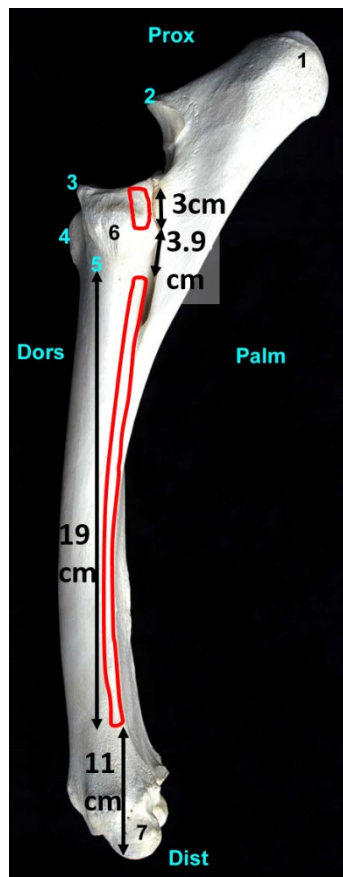


Figure 37 Lateral view of the radius/ulna. Radial origin sites of the LDE

### II.B.2. Common digital extensor (CDE)

The proximal origin of the CDE is located on the lateral side of the humeral epicondyle (Figure 38), the distal origin is on the lateral, proximal part of the radius (Figure 39). The muscle inserts in the distal phalanx.

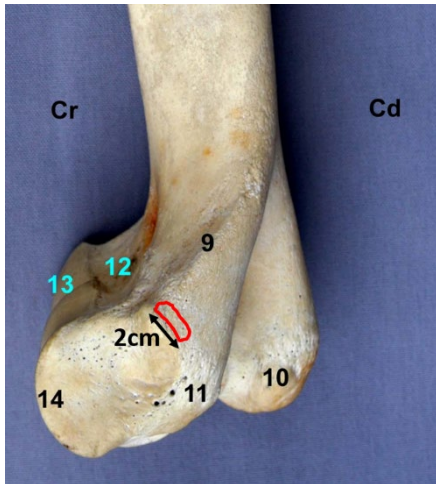


Figure 38 Lateral view of the distal part of the humerus. Humeral origin site of the CDE

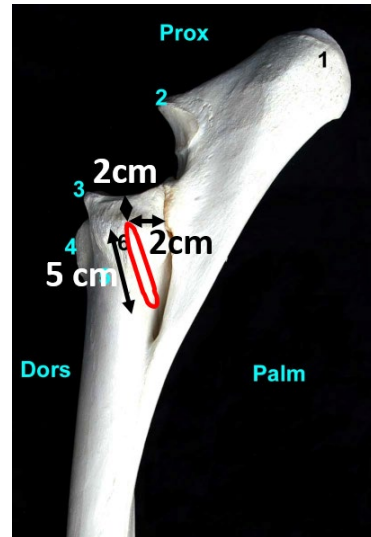


Figure 39 Lateral view of the proximal part of the radius/ulna. Radial origin of the CDE

### II.B.3. Extensor carpi obliquus (ECO)

The origin of the ECO runs along the distal radial origin of the LDE on the lateral side of the radius (Figure 40 and Figure 41). Its insertion site is located on the proximal, lateral part of the lateral splint bone (Figure 42).

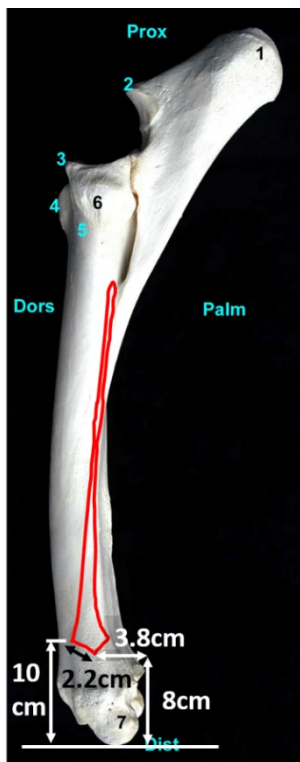


Figure 40 Lateral view of the radius/ulna. Origin site of the ECO

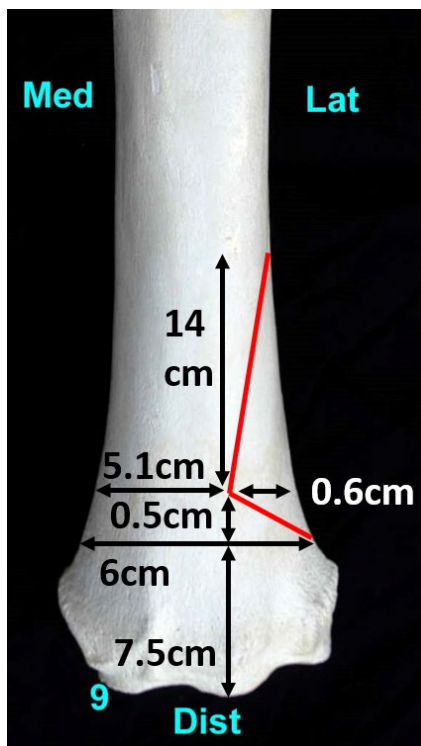


Figure 41 Cranial view of the distal part of the radius. Origin site of the ECO

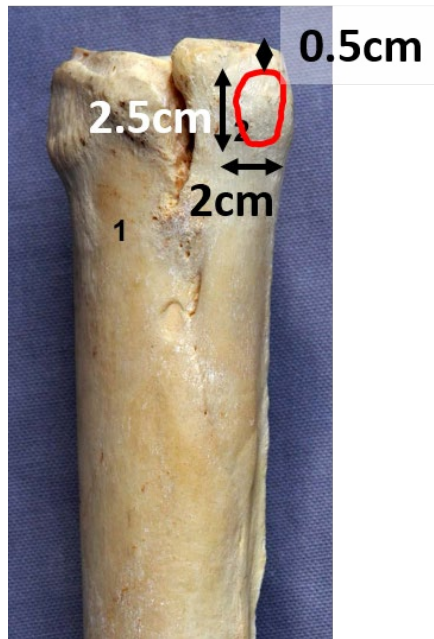


Figure 42 Lateral view of the proximal part of the metacarpus. Insertion site of the ECO

#### II.B.4. Extensor carpi radialis (ECR)

The origin of the ECR is a 7-cm band proximal to the lateral humeral epicondyle (Figure 43). Its insertion is on the dorsomedial tuberosity of the metacarpus.

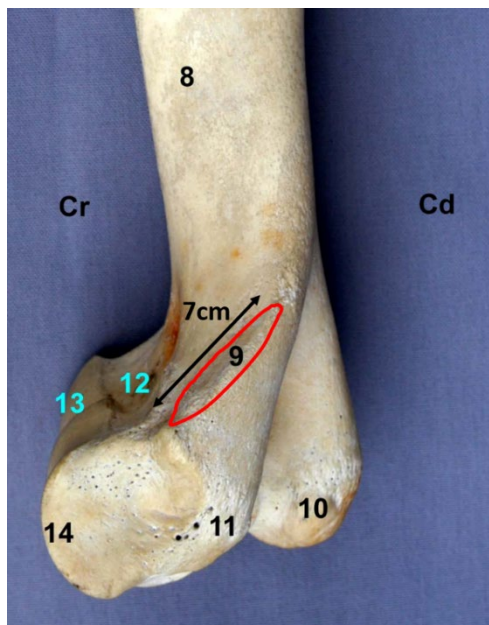
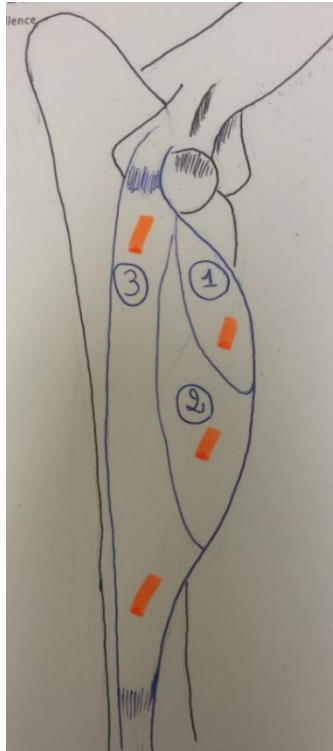


Figure 43 Lateral view of the distal part of the humerus. Humeral origin of the ECR

II.B.5. Ulnaris lateralis (UL)



*Figure 44 Drawing of the UL and the sites of samples used to measure the UL properties (in orange)*

The samples to measure the properties of the UL were taken from the cranial upper and intermediate parts (areas 1 and 2 in Figure 44) and from the caudal upper and lower parts (area 3 in Figure 44).

The insertion site of the UL is located on the upper lateral part of the humeral epicondyle (Figure 45). The insertion sites of the UL are on the accessory carpal bone and on the proximal extremity of the lateral splint bone (Figure 46 and Figure 47).

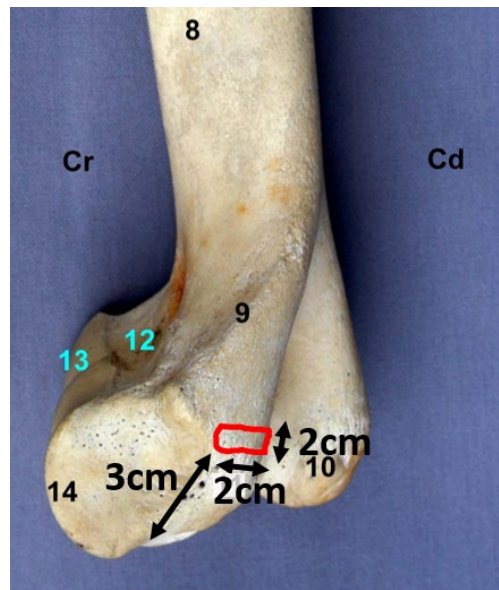


Figure 45 Lateral view of the distal part of the humerus. Origin site of the UL

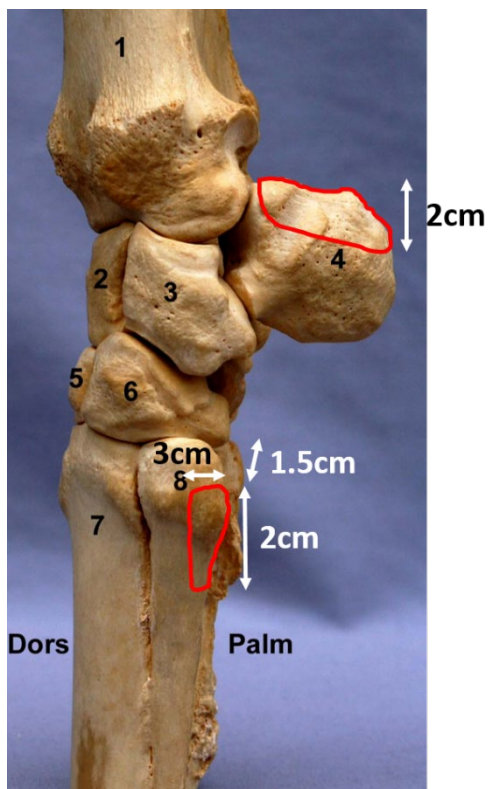


Figure 46 Lateral view of the carpus. Insertion sites of the UL

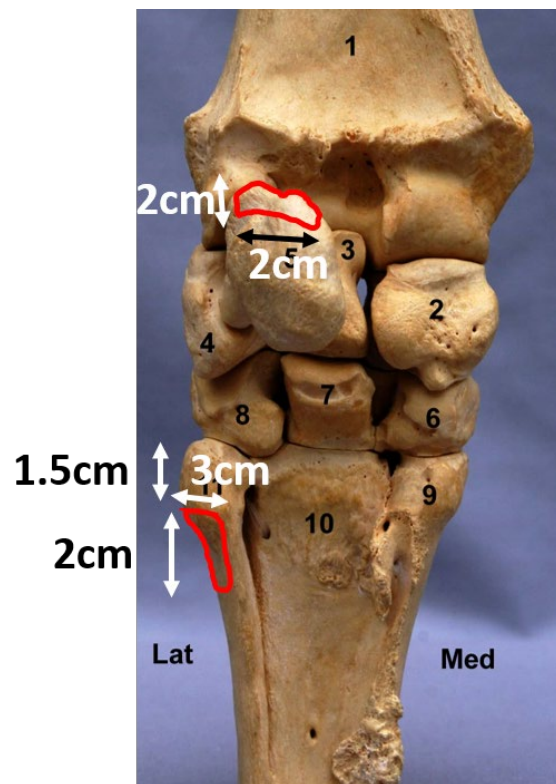


Figure 47 Caudal view of the carpus. Insertion sites of the UL

### II.B.6. Flexor carpi radialis (FCR)

The FCR only has one insertion site, on middle medial humeral epicondyle (Figure 48), and one insertion site, on the proximal extremity of the medial splint bones (Figure 49).

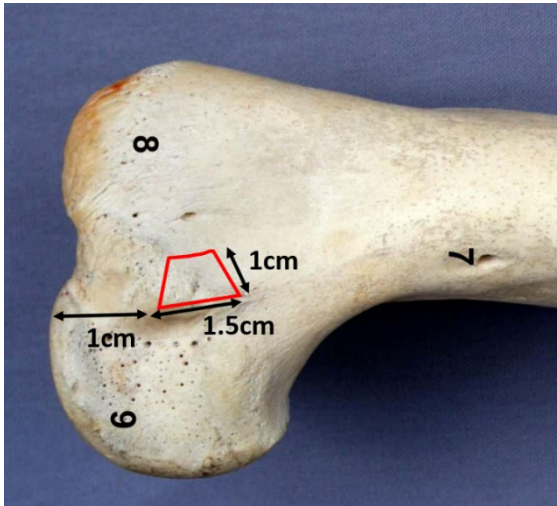


Figure 48 Medial view of the distal part of the humerus.  
Origin site of the FCR

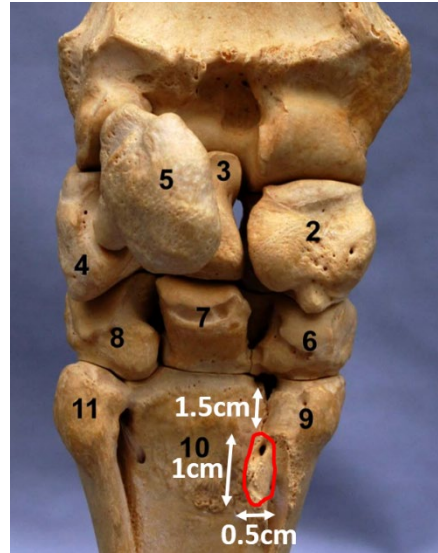


Figure 49 Caudal view of the carpus.  
Insertion site of the FCR

### II.B.7. Flexor carpi ulnaris (FCU)

The FCU has two origin sites, one on the medial epicondyle of the humerus (Figure 50) and the other on the caudal edge of the ulnar olecranon. It has one insertion site on the accessory carpal bone (Figure 51).

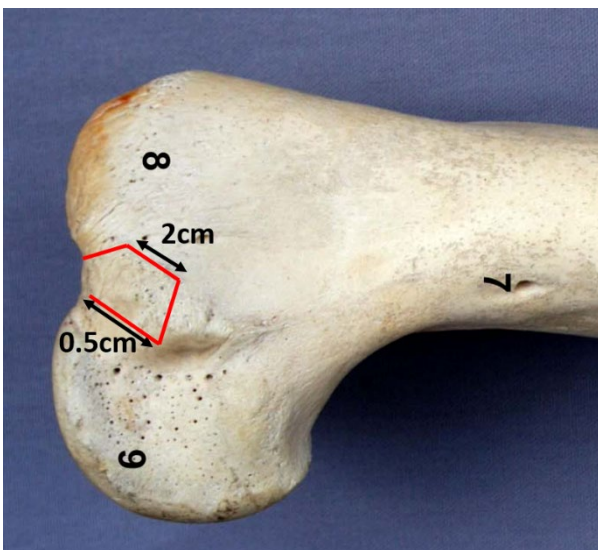


Figure 50 Medial view of the distal part of the humerus.  
Origin site of the FCU

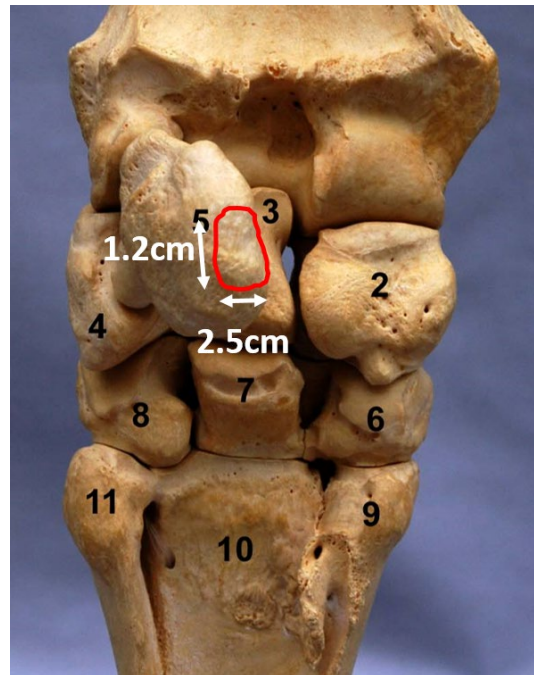


Figure 51 Caudal view of the carpus. Insertion site of the FCU

II.B.8. Deep digital flexor (DDF)

The DDF has three origin sites and one insertion site. The origin sites are the medial, distal, caudal epicondyle of humerus (), a 7-cm band on the distal, caudal part of the radius (), and the medial part of the ulnar olecranon (). The insertion site is on the caudal side of the distal phalanx.

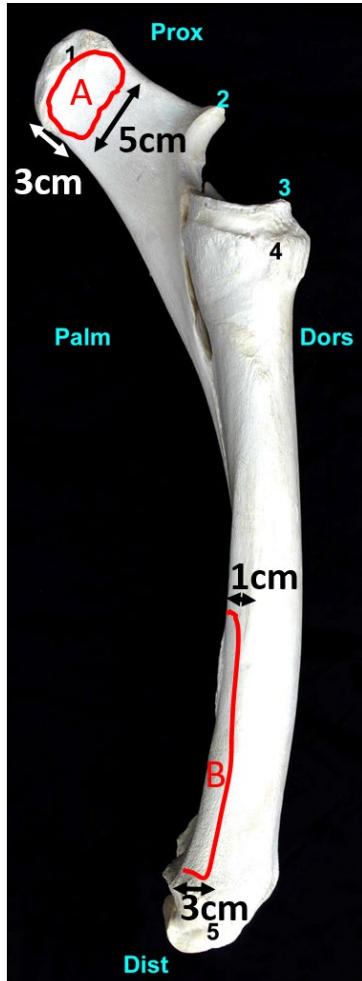


Figure 52 Medial view of the radius/ulna. Radial and ulnar insertion sites of the DDF

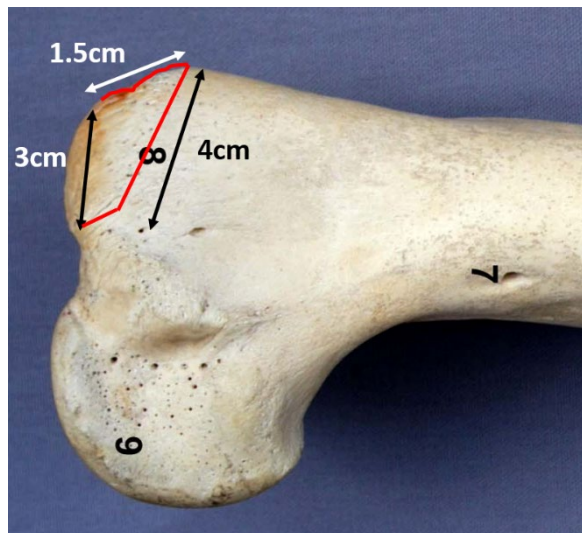
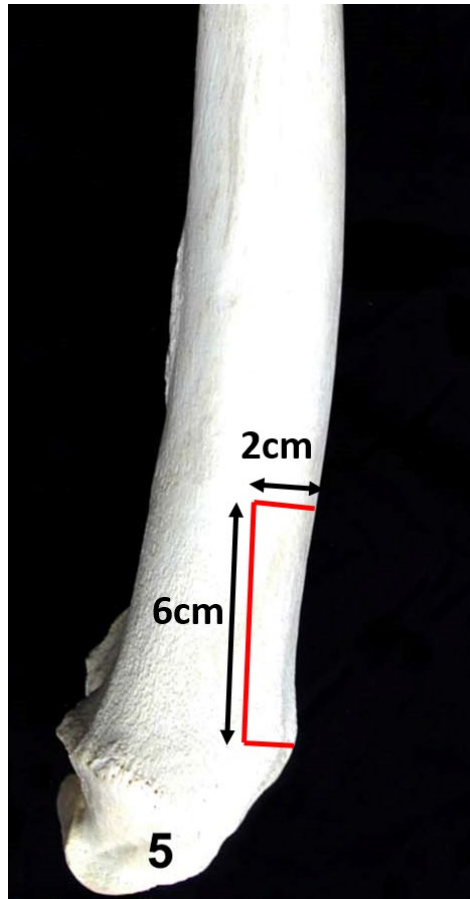


Figure 53 Medial view of the distal part of the humerus. Humeral origin site of the DDF

II.B.9. Superficial digital flexor (SDF)

The SDF has two origin sites and one insertion site. The origin sites are the medial, distal, caudal epicondyle of humerus (the same as the humeral origin of the DDF, Figure 50) and a 6-cm band on the lateral side of radius (). The insertion site is on the caudal side of the proximal phalanx.



*Figure 54 Medial view of the distal part of radius/ulna. Radial origin of the SDF*